Synthesis and application of colloids in soft matter systems

By

Thomas S. Skelhon

A thesis submitted in fulfillment of the requirements for the degree of

Doctor of Philosophy in Chemistry

University of Warwick, Department of Chemistry

October 2013

Table of Contents

Figures

Tables

Acknowledgments

Initially, I have to thank those who have shared the rollercoaster ride of the Ph.D. within the BonLab past and present. Namely Rong, Yunhua, Joe, Imperial Rob, Saif, Rob Young, Alan, Catheline, Gabit, Nick, Tom Ruhland, Florence Gayet, but especially my lab partners in crime Adam and Holly.

I could not have possibly completed the research contained within this thesis without the help of various staff throughout the university including Steve York (physics electron microscopy), Marcus, Lee, Kirk and Rob (mechanical and electrical workshops), Roger Thorpe (dept. of engineering) and Neil Reynolds (WMG). Nick Barker I have to thank for the opportunity for the outreach experience I have thoroughly enjoyed. Also noteworthy is Dr. Fox for his inspiring coffee room chats.

I have to thank the friends who have been an integral part of the fun times I have experienced at Warwick over the years, especially the Glendale Warriors whom have had to endure co-habitation with me.

I'm very grateful to my parents; Louise and Martin, and my brother Jack who have supported me emotionally and financially through my university experience. I just hope that I live up to their expectations as a 'wise investment'!

Finally, my supervisor Stefan Bon deserves a special mention. Stefan has allowed me the opportunities, freedoms and support which have greatly contributed towards a fantastic experience at Warwick over the last 8 years. Although we have seen our differences and at times may have caused some mutual frustration, I can only reserve a deep respect for Stefan; not only as a mentor, supervisor and 'Boss', but also as a friend.

Declaration

I hereby declare that this thesis consists of my own work, with the exception of the collaborative work conducted below:

- Chapter 2 – Janus particle suspensions for ice crystal tests were made in collaboration with Dr. Attyah Al-Zhrani. Ice crystal splat testing of aqueous Janus particle suspensions was carried out by Thomas Congdon and Bibiana Yeo.
- Chapter 4 – Synthesis and optical microscopy of hard-soft Janus particles used for self assembly cluster measurements were carried out by Nathan Peck under my supervision.
- Chapter 5 and 6 – DSC analyses of chocolate emulsion formulations were conducted by Adam Morgan

Any work previously published is referenced at the opening page of each chapter. All work contained herein was conducted in the Department of Chemistry, University of Warwick between September 2009 and September 2013. No material contained in this thesis has been previously submitted for a degree at any other institution.

Signed: Date:

Abstract

We explore two distinct domains in the field of soft matter. The first three experimental chapters concern the synthesis, characterisation and application of Janus particles fabricated by heterogeneous polymerisation techniques. Initially in **Chapter 2** we describe an optimised one pot seeded emulsion polymerisation strategy to render submicron amphiphilic Janus particles exhibiting surface active behaviour which can be tuned by the variation of hydrophilic to hydrophobic lobe volume ratios. These particles have been shown to inhibit ice recrystallisation in aqueous systems. In **Chapter 3** we explore the synthesis of hard-soft Janus particles comprising of respective high and low glass transition temperature lobes. Although the rate of polymerisation is unaffected by available seed particle surface area, particles with multiple soft lobes and secondary nucleation occur below a seed surface area threshold. We additionally demonstrate the ability to fabricate sub-micron hard-soft Janus particles. **Chapter 4** utilises the particles made in the previous chapter as building blocks to fabricate 'colloidal molecules' and colloidosomes. In the former case, cluster morphology of particles is shown to be governed by surface area minimisation of the central soft domain.

The final two experimental chapters explore two different strategies to emulsify water into chocolate whilst retaining the desirable physical characteristics of the confectionery. In **Chapter 5** we utilise colloidal silica and a cationic polyelectrolyte to generate highly stable quiescent Pickering emulsions, allowing up to 50% of the fat content in chocolate to be replaced with water and fruit juice. **Chapter 6** improves upon this work by allowing

the replacement of up to 80% of the fat content in chocolate by the dispersion of aqueous hydrogels within the chocolate fat matrix. In both chapters we characterise the physical properties of the formulations and demonstrate their suitability for use in chocolate confectionery.

Publication List

Skelhon, T. S., Olsson, P. K. A., Morgan, A. R., and Bon, S. A. F., High internal phase Agar hydrogel dispersions in cocoa butter and chocolate as a route towards reducing fat content. *Food and Function*, **2013**, *4*, 1314-1321. **Cover article, Issue 4 p1279**

Skelhon, T. S., Grossiord, N., Morgan, A. R., and Bon, S. A. F., Quiescent water-in-oil Pickering emulsions as a route toward healthier fruit juice infused chocolate confectionery. *Journal of Materials Chemistry*, **2012**, *22*, 19289-19295

Morgan, A. R., Dawson, A., Mckenzie, H. S., Franks, H., Skelhon, T. S., Beanland, R., and Bon, S. A. F., Chemotaxis of Catalytic Silica-Manganese Oxide "Matchstick" Particles, *Materials Horizons*, **2014**, DOI:10.1039/C3MH00003F

Ruhland, T. M., Groschel, A. H., Ballard, N., Skelhon, T. S., Walther, A., Muller, A. H. E., and Bon, S. F. A., Influence of Janus Particle Shape on Their Interfacial Behaviour at Liquid-Liquid Interfaces, *Langmuir*, **2013**, *29* (5), 1388-1394

Morgan, A. R., Ballard, N., Rochford, L. A., Nurumbetov, G., Skelhon, T. S., and Bon, S. A. F., Understanding the multiple orientations of isolated superellipsoidal hematite particles at the oil-water interface, *Soft Matter*, **2013**, *9*, 487-49

Ruhland, T. M., Mckenzie, H. S., Skelhon, T. S., Walther, A., Muller, A. H. E., and Bon, S. A. F., *Under Review*

Al-Zhrani, A. S., Skelhon, T. S., Yeo, B., Deller, R. C., Congdon, T., Gibson, M. I., Bon, S. A. F., Anisotropic Particles Inhibit the Recrystallisation of Ice. *In preparation*

Skelhon, T. S., Peck, N., Olsson, P. K. A., Morgan, A. R., Bon, S. A. F., Synthesis of 'Hard-Soft' polymer Janus particles and their assembly into Colloidal Molecules and Colloidosomes. *In preparation*

Abbreviations

(Cryo) FEG-SEM	(Cryogenic) Field Emission Gun Scanning Electron Microscopy
AFM	Atomic force microscopy
AIBN	Azobisisobutyronitrile
BA	n-Butyl acrylate
DLS	Dynamic Light Scattering
DVB	Divinylbenzene
EGDMA	Ethylene glycol dimethacrylate
FFT	Fast Fourier Transform
HEMA	Hydroxyethyl methacrylate
LCST	Lower critical solution temperature
LVER	Linear Viscoelastic Region
MLGS	Mean Largest Grain Size
NaSS	Sodium Styrene Sulfonate
NIPAM	N-isopropyl acrylamide
pBA	Poly(butyl acrylate)
PGPR	Poly(glycerol) poly(ricinoleate)
pSty	Poly(styrene)
PVP	Poly(vinylpyrrolidone)
TEM	Transmission Electron Microscopy
T_g	Glass transition temperature
X_M	Fractional monomer conversion
XPS	X-ray photoelectron spectroscopy

Chapter 1

Introduction to Soft Matter

Soft condensed matter and *complex fluid* are terms to describe materials which exist neither as a crystalline solid, nor as an ideal liquid, but exhibit behaviour of both extremes, simultaneously. In everyday life, soft matter materials are ubiquitous, and form integral components in building materials (paint), personal care products (toothpaste), food (chocolate) and pharmaceuticals (oral suspensions). The elusive term 'soft matter' can be divided into several more focussed categories, including certain polymers, gels, colloids, surfactants and liquid crystals. Whilst these materials seem to possess little in common, they all exhibit similar physical properties which permit them to be classed as one discipline.

The behaviour of soft matter systems cannot be explained solely by atomic and molecular theory (i.e. microscopic), nor by bulk behaviour (macroscopic), but are explained on an intermediate length scale between nano and micro –meters, so named *mesoscale*. Thermal fluctuations and Brownian motion that occur at scales of k_BT influence soft matter, and therefore the mesoscale components should be considered in a constant state of flux. For example, the random motion of polymer chains in solution or a melt and the Brownian diffusion of colloidal particles in dispersion occur at room temperature. Soft matter components often exhibit the ability to self assemble. These materials can trend towards a state of equilibrium (static self assembly), or assemble upon dissipating energy (dynamic self assembly).[1] The energetic and entropic forces at play in soft matter systems

permit the formation of complex, hierarchical structures and exhibit rich phase behaviour. Non-ideal mechanical behaviour is also a hallmark of complex fluids. A soft matter material response to an applied stress will rarely be either a Newtonian liquid or a Hookean solid. It will instead exhibit complex non-Newtonian and viscoelastic properties, based on interactions occurring on the mesoscale.[2]

1.1 Colloids

Of the soft matter domains, the field of colloids is perhaps the most significant. A colloid is a dispersion of one material within another, first documented by Thomas Graham in 1694.[3,4] Colloids possess a dispersed or discontinuous phase, which consists of finely divided material of approximately 1 nm - 10 µm diameter, in the presence of a surrounding continuous or environment phase. Colloids can be classified by the nature of the continuous and dispersed phases as seen in table 1.1.

		Dispersed Phase		
		Gas	**Liquid**	**Solid**
Continuous Phase	**Gas**	-	Liquid Aerosol	Solid Aerosol
	Liquid	Foam	Emulsion	Sol / suspension
	Solid	Solid Foam	Gel	Solid Sol

Table 1.1 Classification of colloids by the nature of their dispersed and continuous phases

One particular example of a colloid is that of a *polymer colloid*, referring to solid particle suspensions, where the particulate matter is constructed of polymer chains, often prepared by free radical polymerisation. Naturally occurring polymer colloids exist, such

as the milky sap known as latex, tapped from the rubber tree that has been used for centuries by the natives of South America. Polymer colloids can be found both as solid suspension, and almost as an emulsion. In the former case the particle content has a relatively high glass transition temperature (T_g), for instance poly(styrene) with a T_g of +105 °C. Alternatively, if the polymer T_g is low, for instance poly(butyl acrylate) with a T_g of -54 °C, the particle can be treated as a liquid droplet.

One of the key properties of a colloidal dispersion is the vast surface area resulting from the combined contribution of the dispersed phase. For instance, if 1 kg of poly(styrene) is dispersed in to water as 200 nm diameter spheres, the total interfacial area is 28530 m^2. Therefore, the stability of this magnitude of interface is one of the most pertinent issues addressed in colloid science.

1.2 Stability of colloids

Colloidal particles are divided into two categories, *lyophilic* (thermodynamically stable) and *lyophobic* (thermodynamically unstable). Often the continuous phase is aqueous, and we therefore refer to the particles as *hydrophilic* and *hydrophobic* respectively. The former are dispersed easily into a continuous phase forming thermodynamically stable microgel (hydrogel) suspensions. However, the dispersion of hydrophobic particles is thermodynamically disfavoured, creating an interfacial energy which provides a driving force for aggregation and phase separation to reduce the surface area.

Liquid droplet dispersions within a liquid continuous phase, i.e. emulsions, are susceptible to similar effects. However, aggregation of droplets ultimately results in irreversible coalescence, a fate which can also be ascribed to 'soft' deformable particles. Additionally, Ostwald ripening can occur, whereby smaller droplets (with a higher Laplace pressure) are observed to shrink and disappear, in favour of larger droplets.[5] This is caused by the limited dissolution of the dispersed phase into the continuous phase, and therefore transport into the larger droplet with reduced surface area to volume ratio.

Aggregative effects are a result of the Brownian motion, causing particles or droplets of the dispersed phase to collide, which occurs frequently. Although Ostwald ripening does not involve the collision of droplets, the Laplace pressure is proportional to the interfacial tension of the droplet. Therefore colloidal stability depends on how the particles interact upon close proximity (and for the case of Ostwald ripening, the magnitude of the droplet surface tension). If a repulsive force exists, the particles repel each other, forming a kinetically stable dispersion. The potential energy of which, as a function of separation for spherical particles was described by Hamaker,[6] depicted in equation 1.

$$V_A = \frac{-A}{6}\left(\frac{2A^2}{H^2+4aH} + \frac{2a^2}{(H+2a)^2} + \frac{ln\, H^2+4aH}{(H+2a)^2}\right) \quad (1)$$

Where V_A, a and H represents the van der Waals attractive potential, particle radius and interparticle separation respectively. A represents the Hamaker constant, determined by the polarisability and density of the atoms within the particles. This expanded expression

takes into account the self attraction of the continuous (liquid) phase. A repulsive force to counteract this attraction and therefore provide colloidal stability can be applied in two primary ways.

1.2.1 Electrostatic stabilisation

In an aqueous or polar continuous phase, static repulsions arising from surface charges present on the particle surface provide sufficient resistance to aggregation. The surface charges induce the formation of an electrical double layer, a local increase in counterions around the particle which consists of an inner *Stern layer* where the counter ions are tightly bound to the surface and an outer more diffuse layer, bounded by the *slipping plane*. An expression for the electric potential (V_R) arising from the double layer can be expressed as in equation 2 as a function of surface electric potential V_s, interparticle distance from surface H and characteristic thickness of the diffuse layer (Debye length), κ.

$$V_R = V_s e^{(-\kappa H)} \qquad (2)$$

The hydrodynamic radius of a particle includes this layer, and its stability can be measured by dynamic light scattering and electrophoretic mobility respectively, as described in Appendix A.

The DLVO theory developed independently by Derjaguin and Landau in 1941,[7] and Verwey and Overbeek in 1948,[8] comprehensively explains the combination of both the

van der Waals and Coulombic forces at play between particles with overlapping double layers. Upon interaction of the double layers, a locally higher concentration of solute ions exist, thereby increasing the free energy of the system. In order to balance the osmotic pressure arising from this electrochemical potential, solvent molecules diffuse to this area to re-equilibrate, therefore driving particles apart. Therefore combining the van der Waals attraction potential (V_A) and Coulombic repulsive potential (V_R) as equation 3 gives an expression for the total potential (V_t).

$$V_t = V_A + V_R \tag{3}$$

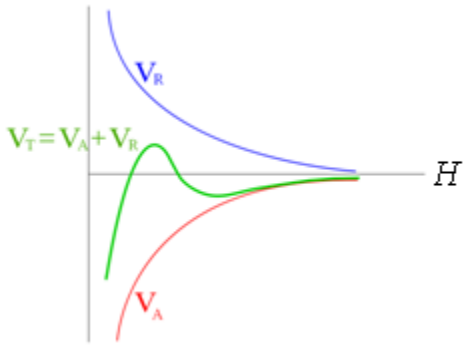

Figure 1.1 Schematic of repulsive (V_R), attractive (V_A) and combined total (V_t) potentials arising from the respective Columbic and van der Waals interactions between two negatively charged particles in water over interparticle separation (H)

The total potential can be plotted as a function of spherical particle separation, represented in figure 1.1 as two negatively charged particles in water. Attractive forces dominate at small and large particle separations, which can give rise to reversible flocculation[9] at the secondary minimum. The primary minimum is considered deep enough that particles at this separation are considered irreversibly bound. However, repulsive forces overrule any attractive potentials at extremely small (Born) and

intermediate (electrical double layer) distances, thereby providing colloidal stability in the latter case.

1.2.2 Steric stabilisation

Van der Waarden in 1950 first observed the stabilisation of carbon black particles by long chain aliphatics in a low dielectric solvent.[10] Almost 20 years later, Napper,[11–15] fully quantified the effect of steric stabilisation involving the adsorption of long chain non-ionic polymers onto a particle surface. Steric stabilisers can be referred to as protective colloids and usually possess an affinity to the continuous phase. The mechanism of repulsion arises from two factors: (1) the entropic compression of the polymer chains upon particle-particle contact and (2) the increase in osmotic pressure arising from the locally high concentration of polymer chains between particles. Osmotic pressure repulsion and entropic chain repulsion are expressed in equations 4 and 5 respectively.

$$V_{Osm} = \frac{4\pi a}{V}(Ø^2)(0.5-\chi)\left(\delta-\frac{H}{2}\right)^2 \quad (4)$$

$$V_{VR} = \left(\frac{2\pi a}{M_W}\phi_p L^2 \rho_p\right)\left(\frac{H}{L} ln\left(\frac{H}{L}\left(\frac{3-H/L}{2}\right)^2\right) - 6\ln\left(\frac{3-H/L}{2}\right) + 3\left(1+\frac{H}{L}\right)\right) \quad (5)$$

Where V, $Ø$, χ, δ, ρ represent molar volume, effective volume fraction of polymer, adsorbed layer thickness, Flory-Huggins interaction parameter and density respectively.

The interaction parameter can be estimated by use of the Hildebrand or Hansen solubility parameters δ_s and δ_p as seen in equation 6.

$$\chi = \frac{V_{seg}(\delta_s - \delta_p)^2}{RT} \quad (6)$$

In this expression V_{seg}, R and T represent actual volume of a polymer segment, universal gas constant and temperature respectively. The Hansen solubility parameters predict the mutual miscibilities of one material within another based on molecular interactions.

Steric stabilisation is effective both in non-aqueous and aqueous systems, or where ionic strength and pH of the continuous phase may suppress electrostatic double layer (i.e. negligible zeta potential). It is commonly used in industrial processes as an effective anti-caking or sedimentation agent which can improve film formation properties and provides the primary stabilisation mechanism in dispersion polymerisation systems.

Electrostatic and steric stabilisation can be used in conjunction as a hybrid stabilisation system, either in the form of a charged particle surface possessing non-ionic polymer hairs or the use of ionic polyelectrolyte polymer chains.

1.3 Heterogeneous polymerisation techniques

There are several classes of heterogeneous polymerisation techniques, that combined, allow the synthesis of a wide range of polymer colloid particle sizes, using many different monomers. Heterogeneous polymerisations are more complex than

homogeneous systems owing to the compartmentalisation effects between phases and kinetics of polymerisation, particle nucleation and growth.

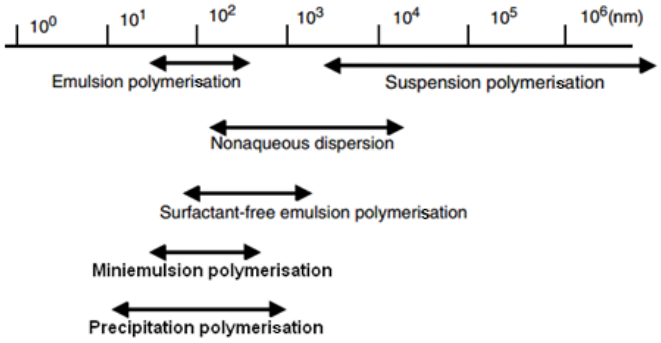

Figure 1.2 The particle size ranges possible from common heterogeneous polymerisation techniques

The five main classes of heterogeneous polymerisation are emulsion, dispersion, mini-emulsion, precipitation and suspension. The particle size range accessible by each technique is pictured in figure 1.2 above. A comprehensive description is ascribed to techniques deployed in this thesis with a brief outline given to other techniques.

1.3.1 Emulsion polymerisation

Of the heterogeneous polymerisation systems available, emulsion polymerisation is the most studied and exploited industrially. It is a highly versatile technique able to synthesise particles of between 10-700 nm diameter. One of the most attractive attributes of emulsion polymerisation is ability to use water as the continuous phase for a wide range of monomer systems.

An emulsion polymerisation starts with monomers which are sparingly soluble in an aqueous continuous phase which also hosts the vast majority of initiating species and

emulsifier, if used. Thermal or redox initiation is generally used to start an emulsion polymerisation; however more exotic methods such as electromagnetic[16] and ultrasonic radiation[17] have been reported. Some monomers, known as *surfmers* possess stabilisation qualities which are grafted into the polymer chains, and present on the particle surface providing colloidal stability.

The progression of an emulsion polymerisation can be divided into 3 distinct stages.

During *Interval I,* the reaction mixture is continually agitated to generate monomer droplets and ensure monomer saturation of the continuous phase. Upon initiation, the limited concentration of monomer dissolved in the continuous phase begin to propagate using radicals generated to form continuous phase soluble oligoradicals. Initially, particle formation was believed to occur following a micellar nucleation pathway described by Smith and Ewart.[18] According to this theory, micelles present in the continuous phase resulting from being above the critical micellar concentration (CMC) of surfactant stabilises monomer. The entry of an oligoradical into a micelle forms a new particle owing to the rapid polymerisation of monomers within the micelle. Oligoradical entry into the monomer droplets is very unlikely due to their large size and therefore low surface area of monomer droplet available for entry. Following the Smith-Ewart theory, *Interval I* ends when the concentration of surfactant drops below the CMC, stopping the formation of any new particles, and instead surfactant molecule adsorption onto pre-existing polymer particles prevails.

However, it was soon discovered that in other monomer systems, the surfactant concentration had little overall effect on particle number and that stable particles could easily be formed without surfactant entirely.[19] This ultimately led to the alternative homogenous nucleation model[20–24] developed by Hansen, Ugelstad, Fitch and Tsai (HUFT theory) which describe the growth of oligomeric radicals in the continuous phase until a critical chain length solubility threshold J_{crit}, above which the juvenile chain collapses into a primary particle. Depending on the stability of these particles and the availability of emulsifying species, the primary particles coagulate until the particle surface is sufficiently stabilised. *Interval I* ends in this case when no new particles form. These events are summarised schematically in figure 1.3

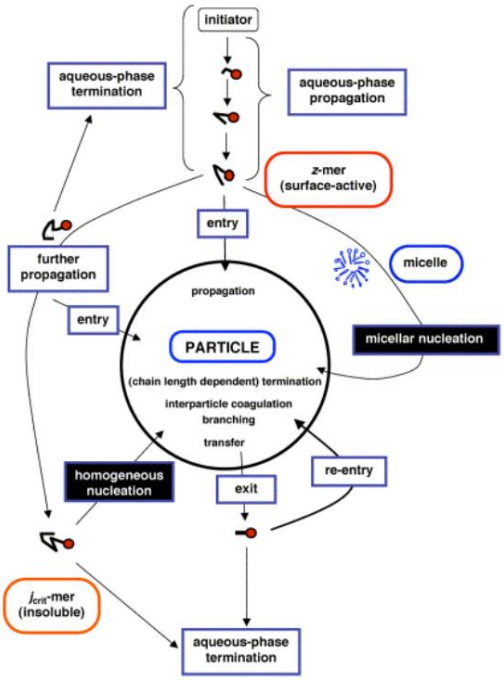

Figure 1.3 Possible events occurring during the initial stages of an emulsion polymerisation from a radical perspective, reproduced from Gilbert *et al.*[25]

Interval II is defined by a constant polymerisation rate. The monomer consumed within the growing particles is replenished by diffusion from the monomer droplets, through the continuous phase and into the growing particles. At this stage, the particles can accommodate only one radical. The compartmentalised radicals cannot react with radicals in other particles, leading to an elevated polymerisation rate compared with bulk and solution polymerisations. Entry of a second radical into the particle terminates the polymerisation within the particle, only to be re-started upon the entry of a further third radical. As such, a growing particle has an average of 0.5 radicals during *Interval II*; however, this number can be lower due to radical exit into the continuous phase or higher in the case of large or high viscosity particles. This is known as *zero-one* kinetics and was quantitatively theorised by Smith and Ewart.[18] It is worth noting that a deviation from *zero-one* kinetics can occur with larger particles (greater than 60 nm for styrene). Due to an increased size, the particle can accommodate more than one propagating radical without termination, leading to *pseudo-bulk* kinetics as seen in *Interval III*.

When the monomer droplets have been exhausted, the polymerisation enters *Interval III* and the rate of polymerisation slows due to the decreasing concentration of monomer in the particles. At this point, monomer content in the continuous phase is also depleted and leads to very high conversions in emulsion polymerisations. In some cases, the increased viscosity due to lack of monomer inside the particles can permit more than one radical (*pseudo-bulk*). As such, the number average radicals per particle increases leading to a substantial increase in polymerisation rate and decrease in termination during *Interval III* named *Trommsdorff-Norrish* effect.[26]

1.3.2 Dispersion polymerisation

Dispersion polymerisation provides a highly convenient and reliable method to make polymeric particles between 0.1 - 15 μm diameter. Micron sized particles are utilised in a variety of commercial applications including column packing materials, toners, instrument calibration standards, components in LCD displays and biomedical assays.[27–29]

Prior to the widespread application of dispersion polymerisation; first developed in the 1960's by ICI,[30] the synthesis of micron sized particles was troublesome owing to the intermediate size range lying between particle sizes readily obtained by emulsion (10 - 700 nm) and suspension (50 - 1000 μm) polymerisation. Seeded emulsion polymerisation,[31] two stage swelling systems[32] and the dynamic swelling method[33] have successfully been developed as alternative routes to fabricate monodisperse micron sized particles.

Typically, a dispersed polymerisation system begins as a homogeneous mixture of monomer, solvent, steric stabiliser and initiator.[34] The solvent is often a non-aqueous solvent, such as methanol or ethanol. The monomer employed is soluble in the solvent, but upon polymerisation above a critical chain length, the oligomer becomes insoluble in the reaction medium and collapses into a primary particle.

Colloidal stability of the particles is imparted from the polymeric stabiliser which chemisorbs (grafts) and/or physisorbs upon the formation of the unstable primary

particles thereby providing a steric barrier against coagulation. The most common stabilisers deployed for conventional dispersion polymerisation are poly(vinyl pyrrolidone), hydroxylpropylcellulose (and related cellulose esters), poly(acrylic acid), poly(methacrylic acid) and poly(vinyl alcohol).[27,35,36] However, as the polymeric stabiliser presents on the outer surface of the particle, functionality can be imparted to the particle dispersions through the stabiliser. As a result, Tseng *et al*. used various co-stabilisers to manufacture particles with hydroxyl, carboxyl, amide and silane surface functionalities.[37]

Until fairly recently, successful crosslinking in dispersion polymerisations has been difficult to control. Crosslinking agents such as divinylbenzene cannot be added in batch to styrenic polymerisations above 0.6 wt% as this invariably causes coagulation due to the high sensitive nature of the nucleation stage in dispersive polymerisation systems.[37] However, recent reports of using EGDMA, seeded dispersion or semi-batch methods incorporating co-monomers after the nucleation stage have allowed crosslinking.[38–40]

Mechanism of dispersion polymerisation

Dispersion polymerisation is believed to proceed according to aggregative and coagulative nucleation theories,[41] derived from the homogenous nucleation theory[20] whereby the key step in defining particle number of the system is upon formation of sterically stabilised particles.[42]

Prior to initiation, the components of the polymerisation form a homogenous solution. After initiation, polymer chains grow in solution until a critical length at the threshold of their solubility (molecular weight of the polymer is directly proportional to solubility). These chains collapse into unstable primary particles which rapidly coalesce to a point at which they become sterically stabilised with sufficient polymeric stabiliser chains covering the particle surface. This is referred to as 'critical point'. Beyond this, no further particles develop. Any nuclei or primary particles formed in the solvent phase after critical point are captured by the particles. Polymerisation proceeds inside the particles until monomer source is exhausted. This process is depicted in figure 1.4.

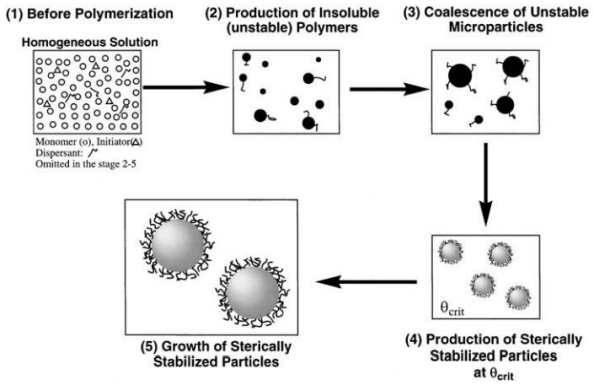

Figure 1.4 A schematic model for the particle nucleation and growth of sterically stabilised particles in dispersion polymerisation. Reproduced from Kawaguchi[43]

Additional events can occur in a dispersive system including micellar nucleation and radical transfer to the polymeric stabiliser. These events are summarised in figure 1.5 below.

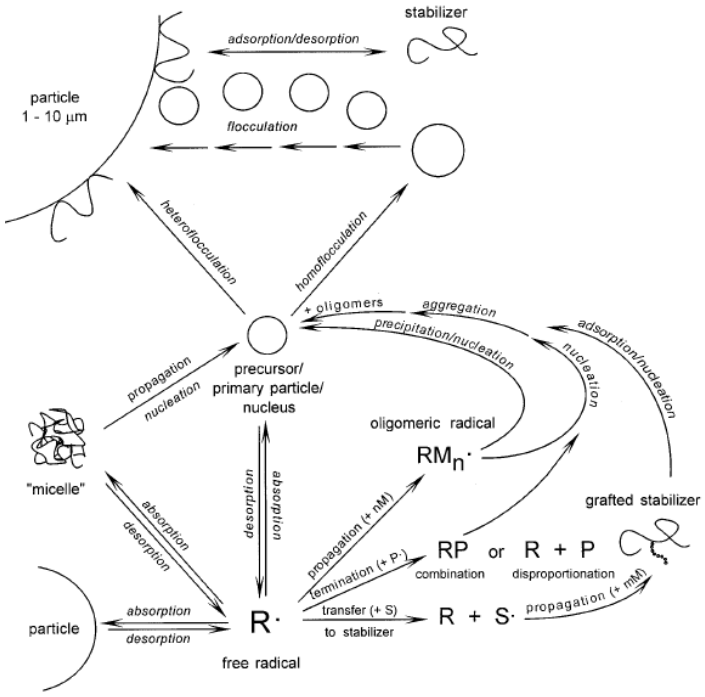

Figure 1.5 Schematic representation of mechanisms involved in free radical dispersion polymerisation

Control over particle properties

Size control of the resulting latex can be tuned by altering reaction parameters. Varying monomer concentration, polymer-solvent miscibility, polymeric stabiliser concentration and stabiliser molecular weight can have a profound effect on particle size, but also make this type of heterogeneous polymerisation system sensitive to minor changes in reaction parameters.[44] Accordingly, a comprehensive model has been developed to predict particle core radius based on the reaction parameters which has been proven to correlate well with experimentally observed values.[45]

1.3.3 Suspension polymerisation

Conceptually the simplest heterogeneous polymerisation, whereby the monomer is insoluble in the continuous phase and the initiator is soluble in the monomer. The reaction mixture is agitated to form monomer droplets, stabilised by the presence of a surfactant to restrict coalescence. Polymerisation occurs within the droplets leading to a relative polydisperse size distribution similar to the monomer emulsion. Typical size range 2 μm – 1 mm diameter

1.3.4 Precipitation polymerisation

Similar to dispersion polymerisation by the fact that the initial reaction mixture is homogeneous, however, particles do not swell with monomer. This is usually due to the high degree of crosslinking or monomer-polymer incompatibility as in the cases of polymerisation of divinylbenzene and acrylonitrile respectively. Particle growth is attributed to the precipitation of oligomeric chains onto the particle surface, often impairing a rough topology to the particles. Typical size range: 10 nm – 1000 nm diameter.

1.3.5 Miniemulsion polymerisation

A stable emulsion of insoluble monomer in a water continuous phase is first generated by a source of high shear, often an ultrasonicator. High amounts of surfactant and the use of a hydrophobic agent (such as hexadecane) restrict coalescence and Ostwald ripening. The initiator is water soluble and radicals are captured by the emulsified monomer droplets

during initiation, leading to polymerisation within the droplets. Typical size range 10 nm - 500 nm diameter.

Two types of heterogeneous polymerisations that generate polymer colloids are used extensively in this thesis to manufacture a specific class of particles so named Janus particles. An introduction to the field of 'Janus particles' and the wide range of synthetic techniques used to manufacture them is given below. A more comprehensive introduction to particular synthetic routes and applications of Janus particles is explored in the relevant chapter.

1.4 Janus particles

First popularised in the scientific community by de Gennes in his 1991 Nobel prize lecture,[46] Janus, the Roman god depicted with two faces; one looking into the past and one, the future, has been used to describe a class of colloidal particles which possess morphological and / or chemical heterogeneity, imparting unique anisotropic character. Recently, this topic has seen much attention, giving rise to a whole plethora of particle architecture and functionality. Therefore, there is potential for these particles to deployed in a range of applications such as Pickering stabilisers for emulsions[47–49] and emulsion polymerisation;[50] in optics and displays,[51] biosensors[52] and medical imaging.[53–55] Many different fabrication techniques have been developed to prepare Janus particles as outlined below.[56]

1.4.1 Toposelective surface modification

One of the most simple and intuitive methods to fabricate Janus particles involves the partial surface modification of one hemisphere of a spherical colloid, without altering the other. This has been demonstrated effectively by several routes. In particular by embedding in a film,[57] gel trapping[58] and embedding in a photo resist layer[59] prior to chemical treatment of the unprotected hemisphere.

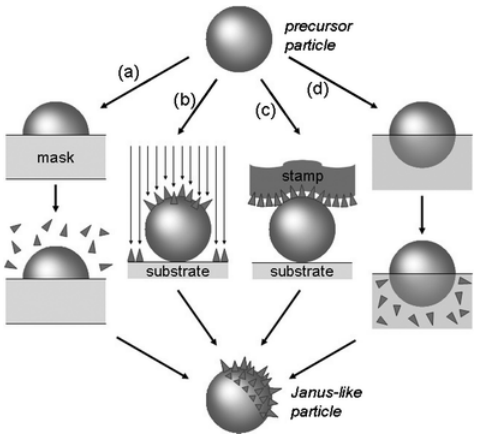

Figure 1.6 Schematic depicting the variety of different methods to manufacture Janus particles by toposelective surface modification. (a) embedding in a film and treating exposed side, (b) directional flux of material, (c) microcontact printing, (d) partial contact with reactive media[56]

Additionally, other methods of toposelective surface modification including subjecting particles to a directional flux,[60] microcontact printing[61] and partial contact with reactive media; adsorption to both a plane[62] (i.e. Langmuir trough) and curved interface[63] (i.e. emulsion) have been reported to render colloids with anisotropic surface chemistry (figure 1.6). It is only the final example however, using emulsion based systems that

provides route to manufacturing particles by toposelective surface modification in bulk quantities.

1.4.2 Template directed assembly

A different approach involves the assembly of colloidal precursor particles using the external influence of a template. By using lithography, 1-D and 2-D dimensional templates can define the morphology of the assembled cluster through geometric confinement before annealing the particles together.[64] Examples of which are displayed in figure 1.7(a).

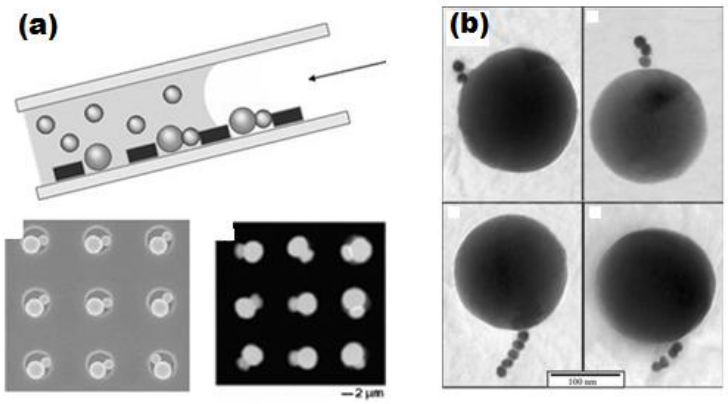

Figure 1.7 (a) Use of templates to geometrically confine particles of different size and (b) assembly of gold nanoparticles onto silica particles by deposition through a microporous membrane to render Janus particles

Microporous membranes have also been used as templates to attach single or chains of gold nanoparticles onto aminated silica particles, rendering a 'snowman' or 'tadpole' structure as seen in figure 1.7(b).[65] Despite the great range of structures and high precision of fabrication of Janus particles available by this route, the low yield and relatively high cost does present an issue for commercialisation.

1.4.3 Controlled surface nucleation

The controlled growth of a particle nucleated from the surface of a seed particle to render 'snowman', 'acorn' and 'dumbbell' shaped particles has been achieved by using inorganic and metallic particles.[66–68] Typically precursor particles are synthesised, providing a nucleation site for oxidised/reduced ions in solution to grow a second lobe. The particles formed are generally 10-50 nm diameter and are very sensitive to reaction conditions, making reproducibility challenging. Hybrid polymer-inorganic Janus particles have also been generated through emulsion polymerisation of styrenic monomers in the presence of inorganic silica seeds. Initially, the seeds are treated to promote partially positive interactions with the growing oligoradicals in solution, thereby nucleating and growing lobes off the silica particle.[69] The number and shape of the lobes nucleated off one particle can be controlled by varying diameter and concentration of silica seeds[70] and by varying the surface modification density.[71] The hybrid polymer-inorganic synthetic technique gave rise to a complex array of shapes which have recently been referred to as colloidal molecules, and are further discussed in chapter 4. Finally, very few examples of wholly polymeric Janus particles fabricated by surface nucleation have been reported. Wang *et al.* present a single example of this type; the growth of a poly(butyl acrylate) lobe off poly(styrene) precursor particles to render fully polymeric hard-soft Janus particles.[72]

1.4.4 Microfluidics

Microfluidic devices provide a powerful technique to manufacture Janus particles on the micrometre scale. Spherical chemically anisotropic Janus particles can be made through jetting two monomers into a co-flow device before post-polymerisation as seen in figure 1.8(a). Varying flow rates changes respective hemispherical ratio and can form ternary particles.[73] Using a co-flow technique, many variations of Janus particles have been demonstrated including magnetic,[74] hydrophilic-hydrophobic via double emulsion[75] and hydrogel-colloidal particle aggregate hybrids.[76] Although generally confined to the micrometre scale, biphasic electrified jetting has also been used to obtain Janus droplets of nanoscale dimensions.[77]

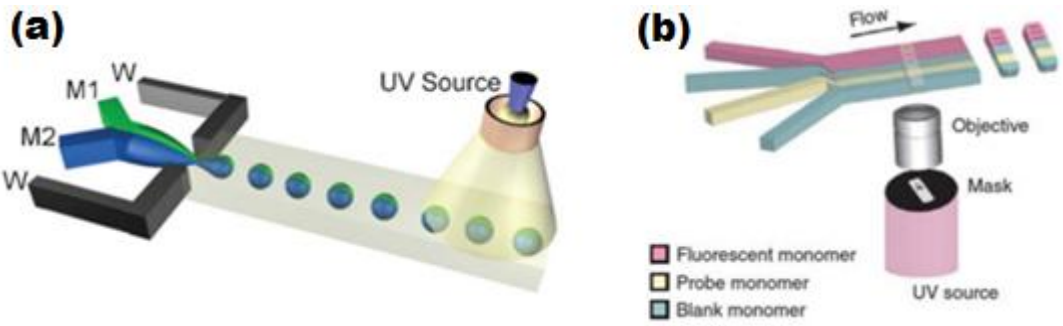

Figure 1.8 (a) Microfluidic co-flow jetting device forming hemispherical Janus monomer droplets which are polymerised by a UV source.[73] (b) Quadruple co-flow device using a mask and UV source to pattern highly complex Janus particles for medical diagnostics[52]

One particular example demonstrates the versatility of microfluidics as a route to Janus particles. Doyle *et al.* demonstrated by using a quadruple co-flow device, mask and UV source, that highly chemical and morphological anisotropic particles could be generated with very high precision as depicted in figure 1.8(b).[52] However, ultimately,

microfluidics do suffer from high scalability issues, limiting its use commercially to high-end biomedical screening and drug delivery.

1.4.5 Phase separation phenomena

A final method to render Janus particles is through phase separation, the formation of a secondary entity from a 'seed' particle. This has been achieved in both inorganic and polymeric systems. Core-shell inorganic particles have been demonstrated to phase separate as a result of a chemical reaction with one of the components. Silver particles with a silica shell lead to the formation of secondary silver lobe in the presence of molecular iodine, a strong oxidising agent (figure 1.9).[78] Metastable FePt core CdS shell particles were shown to phase separate upon heating due to the incompatibility of the FePt and CdS lattice.[79]

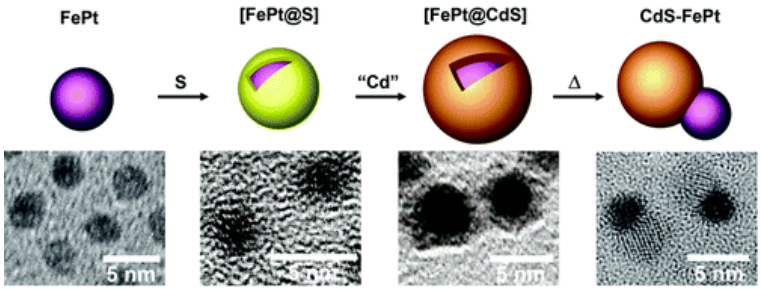

Figure 1.9 Phase separation of a metastable FePt core from a CdS shell upon heating. An example of synthesising Janus particles from inorganic phase separation[78]

Phase separation in polymer colloid systems was first fully characterised by El Aasser and co-workers.[80,81] In these examples, a crosslinked polymer latex, made by emulsion polymerisation was swollen with further styrene was observed to phase separate upon heating to render a second polymer lobe on the side of the particle. This particular

synthetic route towards Janus particle synthesis is attractive owing to the ability to conduct reactions in bulk, using relatively inexpensive and simple experimental techniques.

1.5 Chocolate: from a colloidal perspective

In the latter part of this thesis, we investigate the replacement of fat content in chocolate with water by use of Pickering stabilised emulsions (chapter 5) and hydrogel dispersions (chapter 6); therefore a background of chocolate formulation and properties from a colloidal perspective is given below.

Chocolate is one of the many real-life examples of food colloids which, like most colloidal systems rely on the interplay of forces at the *mesoscale* to produce the desired *macroscopic* eating qualities it possesses. Chocolate is a complex material, which when molten can be described as a multiphase fluid dispersion of solid non-fat particles comprising mainly of sugar crystals and cocoa solids in a fat continuous phase. The fat phase is generally a mixture of cocoa butter and milk fats. The composition ratio of these major components varies between formulations, whereby white chocolate contains no cocoa solids and a large quantity of cocoa and milk fats, whereas dark chocolate can contain over 70% cocoa solids (by weight) and little fat. Aside from taste, the major 'eating quality' of chocolate arises from its texture upon consumption, a desirable *macroscopic* behaviour that the consumer benefits from. In addition there are a wide variety of chocolate confectionery products available, from traditional 'tablet' blocks to more complex products which incorporate other components such as air bubbles, biscuit,

liquid and solid centres. Therefore a variety of manufacturing approaches are employed, of which many will require the flowability of chocolate component of the product to be tuned to allow practical manufacture. Both consumption texture and flow of chocolate during processing are physical properties, governed by colloidal interactions.

1.5.1 Rheology of chocolate

The flow behaviour of molten chocolate is of high importance for chocolate manufacturers due to the reasons given above. Viscosity alone is insufficient to describe the flow characteristics of chocolate, due to its more complex rheological properties. Instead, it can be described as a pseudoplastic fluid, whereby a certain shear force is required to initiate flow, so named *yield stress*. Once flowing, the chocolate then adopts a non-Newtonian flow profile where viscosity is proportional to applied shear force, so named *plastic viscosity*. These two components are combined in the form of the Casson equation,[82] used widely in industry to characterise the rheology of chocolate. This model is described in depth in chapter 6, part 3.9. The effect of yield stress is important in terms of shape retention of the formulation.

Figure 1.10 (left) misshapen enrobed chocolate products with 'feet' resulting from insufficient yield stress. (right) Effect of yield stress on coating chocolate biscuits. Note the result of a too high yield stress[83]

As shown in figure 1.10; a high yield stress is required for products with decorative markings, and a low yield stress is required for thin coatings of chocolate over biscuits. Plastic viscosity is an important factor in the thickness of chocolate coatings, whereby a lower viscosity results in thinner coatings. In aerated products, viscosity affects the bubble size within the chocolate matrix (figure 1.11). Furthermore, higher viscosity chocolate requires increased pumping costs.

Figure 1.11 Effect of plastic viscosity of chocolate on bubble size in aerated products[83]

The rheological properties of molten chocolate are affected by several major factors; particle size of cocoa and sugar solids, fat content and emulsifier content. In the first instance it is important to note that the upper size limit for particle size in chocolate formulations is approximately 30 µm diameter. Above this 'mouthfeel' threshold, the tongue perceives a gritty sensation which is unpleasant for the consumer. Therefore the conching and milling process during chocolate manufacture reduces overall particle size to below this diameter.[83] The size distribution of the particulate matter has a profound effect on the yield stress of the chocolate formulation. As seen in figure 1.12, while plastic viscosity is relatively unaffected by particle size, there is a significant increase in yield stress upon decreasing size distribution.[84]

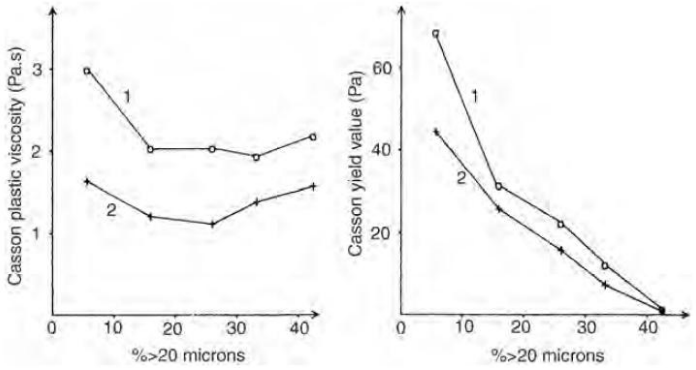

Figure 1.12 Influence of particle size distribution on Casson plastic viscosity and yield stress of chocolate. (1) 30% fat; (2) 32% fat[84]

This effect arises from the increased surface area of solid particulate as a result of the milling. The additional surface area requires more coating by the fat component of the chocolate, bringing particles closer together, eventually forming a loose network of solid particles. A greater force is needed to break up this network and induce flow, hence a greater yield value. Therefore while smaller particle distributions give an enhanced mouthfeel sensation, an undesired increase in yield stress may arise. This can be counteracted by the addition of more fat.

Fat content influences both the plastic viscosity and yield stress of chocolate formulations as seen in figure 1.13. The increase of fat content up to a threshold of 36% significantly affects the plastic viscosity due to the additional free flowing fat that lubricates the solid particles, and is more pronounced in formulations with a finer particle size distribution. Yield stress is also decreased as the distance between particles which form networks resistive to initial flow are increased with a higher fat content.[84]

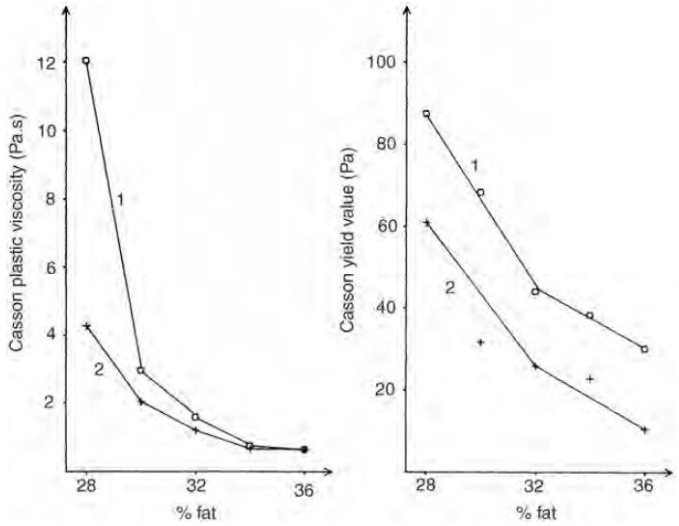

Figure 1.13 Influence of fat content on Casson plastic viscosity and yield value of chocolate. Fine (1) and coarse (2) particulate size distributions[84]

The use of emulsifiers as additives to chocolate formulations is commonplace in the confectionery industry. Emulsifiers are used essentially as lubricants for the solid particulates within the liquid fat matrix. Soy bean lecithin and polyglycerol polyricinoleate (PGPR) are the two most common used emulsifiers, and are often used in conjunction for optimal flow performance.[85] These compounds work by adsorbing to the surface of the sugar and cocoa solid particles, thereby preventing agglomeration of the solid components and reducing the friction drag between the solid and liquid phases through a reduced interfacial tension. This gives a smoother and creamier texture associated with a higher cocoa butter content, without actually adding further cocoa butter. As emulsifiers are both cheaper, and more effective by concentration at reducing viscosity than cocoa butter, the use of emulsifiers gives major economic benefit to manufacturers.

1.5.2 Moisture in chocolate

The rheology and textural qualities of chocolate are additionally affected by the presence of water in the final product. The addition of a small quantity of water into chocolate results in a dramatic and undesirable increase in viscosity. This occurs due to the softening of the hard sugar crystals into semi soft gels which ultimately form a floc network in the formulation, causing the viscosity increase. Associated with this, the formulation can attain a gritty texture owing to the formation of large aggregates of sugar particles. During conventional chocolate production, the manufacturer will aim to remove as much water content as possible during conching as for every 0.3 wt% of water left in the formulation, approximately 1 wt% of additional fat content is required to be added to mitigate the detrimental effect of the moisture. The addition of a significant quantity of water (ca. 20 wt%), will reduce overall viscosity due to the complete dissolution of sugar into the water phase. However, this inevitably results in phase separation between the fat and aqueous phase.[83]

There are culinary examples where water can successfully be incorporated into a chocolate formulation. The emulsification of cream, (an oil-in-water emulsion itself) into molten chocolate results in the formation of a water-in-oil emulsion of water droplets within the chocolate fat matrix. This emulsion is stabilised by naturally occurring compounds in the milk (i.e. lecithin) and chocolate and compartmentalises the water from the fat and sugar particles. Although the resulting formulation, known as a *ganache* does not suffer from a viscosity increase or gritty sensation, the product experiences a vast

reduction in elastic modulus (i.e. loss of mechanical stiffness), and will not set. With this in mind, the addition of water into chocolate formulations to provide a benefit to consumers and chocolate manufacturers alike presents an interesting challenge in the field of soft matter.

1.6 Scope and outline

This thesis explores two distinct areas in the field of soft condensed matter. Both parts are however, intrinsically linked through the behaviour they exhibit, and the theory applied to characterise material fabrication and their properties.

The first part, incorporating Chapters 2, 3, and 4 involves the fabrication of polymer colloid Janus particles through various heterogeneous polymerisation systems. These particles are characterised and investigated for their use in commercial applications.

The second part, incorporating Chapters 5 and 6 explore two distinct methods to reach the same aim; the ability to reduce the fat content in chocolate through emulsification of water into the chocolate fat matrix without a detriment to the textural and mechanical properties of the final product.

In **Chapter 2**, the synthesis of Janus particles of sub-micron dimensions are synthesised by a one pot seeded emulsion polymerisation. We demonstrate how the size and respective lobe size of these particles can be tuned. The interfacial behaviour of these particles is investigated and their effectiveness as ice crystal growth inhibitors explored.

In **Chapter 3** we discuss the synthesis of both nano- and micron scale 'hard-soft' biphasic Janus particles by seeded dispersion polymerisation of a 'soft' low T_g monomer butyl acrylate in the presence of poly(styrene) seed particles.

The self-assembly behaviour of these 'hard-soft' particles into 'colloidal molecules' and colloidosomes are discussed in **Chapter 4.** Using interfacial energy minimisation as a driving force, the self-assembled particles assume a low energy conformation, supported by computer simulations. When agitated with air, the particles are observed to adhere to the liquid-gas interface, forming stable colloidosomes with interesting textured topology.

Chapter 5 discusses the Pickering stabilisation of fruit juice in oil emulsions with inorganic nanoparticles as a route to reducing the fat content in chocolate formulations. The synergistic effect of chitosan and colloidal silica on emulsion properties is explored through sunflower oil, cocoa butter and ultimately chocolate.

In an alternative approach, a method of dispersing a high volume of micron sized aqueous hydrogels throughout oil, cocoa butter and chocolate is explored as another route to reducing the fat content of chocolate in **Chapter 6**.

1.7 References

(1) Whitesides, G. M.; Grzybowski, B. *Science* **2002**, *295*, 2418–2421.

(2) Jones, R. A. L. *Soft Condensed Matter*; 1st ed.; Oxford University Press: Oxford, 2002; pp. 1–21.

(3) Graham, T. *Journal of the Chemical Society* **1864**, *17*, 318–327.

(4) Graham, T. *Journal of the Chemical Society* **1864**, *17*, 368–371.

(5) Ostwald, W. *Lehrbuch der Allgemeinen Chemie*; 2nd ed.; Engelmann: Leipzig, 1896.

(6) Hamaker, H. C. *Physica* **1937**, *4*, 1058–1072.

(7) Deryagin, B.; Landau, L. *Acta Physicochimica U.R.S.S.* **1941**, *14*, 633–662.

(8) Verwey, E. J. W.; Overbeek, J. T. G. *Theory of the Stability of Lyophobic Colloids*; Elsevier Pub. Co., 1948; p. 216.

(9) Overbeek, J. T. G. *Journal of Colloid and Interface Science* **1977**, *58*, 408–422.

(10) Van der Waarden, M. *Journal of Colloid Science* **1950**, *5*, 317–325.

(11) Napper, D. H. *Journal of Colloid and Interface Science* **1969**, *29*, 168–170.

(12) Napper, D. H. *Journal of Colloid and Interface Science* **1970**, *33*, 384–392.

(13) Napper, D. H. *Journal of Colloid and Interface Science* **1970**, *32*, 106–114.

(14) Napper, D. H. *Journal of Colloid and Interface Science* **1977**, *58*, 390–407.

(15) Napper, D. H.; Netschey, A. *Journal of Colloid and Interface Science* **1971**, *37*, 528–535.

(16) Vanderhoff, J. W. Method for carrying out chemical reactions with microwave energy. U.S. Patent 3,432,413, 11 March, March 11, 1969.

(17) Biggs, S.; Grieser, F. *Macromolecules* **1995**, *28*, 4877–4882.

(18) Smith, W. V.; Ewart, R. H. *The Journal of Chemical Physics* **1948**, *16*, 592–600.

(19) Goodall, A. R.; Wilkinson, M. C.; Hearn, J. *Journal of Polymer Science: Polymer Chemistry Edition* **1977**, *15*, 2193–2218.

(20) Fitch, R. M.; Tsai, C. H. *Polymer Colloids*; Plenum Press: New York, 1973; p. 73.

(21) Hansen, F. K.; Ugelstad, J. *Journal of Polymer Science: Polymer Chemistry Edition* **1978**, *16*, 1953–1979.

(22) Hansen, F. K.; Ugelstad, J. *Journal of Polymer Science: Polymer Chemistry Edition* **1979**, *17*, 3033–3045.

(23) Hansen, F. K.; Ugelstad, J. *Journal of Polymer Science: Polymer Chemistry Edition* **1979**, *17*, 3047–3067.

(24) Hansen, F. K.; Ugelstad, J. *Journal of Polymer Science: Polymer Chemistry Edition* **1979**, *17*, 3069–3082.

(25) Thickett, S. C.; Gilbert, R. G. *Polymer* **2007**, *48*, 6965–6991.

(26) Flory, P. J. In *Principles of Free Radical Polymerisation*; Cornell University Press: New York, 1953; pp. 125–129.

(27) Ober, C. K.; Lok, K. P. Dispersion polymerisation process for toner compositions. U.S. Patent 4,617,249, October 14, 1986.

(28) Ugelstad, J.; Berge, A.; Ellingsen, T.; Schmid, R.; Nilsen, T.-N.; Mørk, P. C.; Stenstad, P.; Hornes, E.; Olsvik, Ø. *Progress in Polymer Science* **1992**, *17*, 87–161.

(29) Poehlein, G. W.; Ottewill, R. H.; Goodwin, J. W. *Science and Technology of Polymer Colloids: Preparation and reaction engineering*; Nijhoff, 1983.

(30) Barrett, K. E. J. *British Polymer Journal* **1973**, *5*, 259–271.

(31) Ugelstad, J.; Mórk, P. C.; Kaggerud, K. H.; Ellingsen, T.; Berge, A. *Advances in Colloid and Interface Science* **1980**, *13*, 101–140.

(32) Ugelstad, J. *Die Makromolekulare Chemie* **1978**, *179*, 815–817.

(33) Okubo, M.; Shiozaki, M.; Tsujihiro, M.; Tsukuda, Y. *Colloid and Polymer Science* **1991**, *269*, 222–226.

(34) Slomkowski, S.; Alemán, J. V.; Gilbert, R. G.; Hess, M.; Horie, K.; Jones, R. G.; Kubisa, P.; Meisel, I.; Mormann, W.; Penczek, S.; Stepto, R. F. T. *Pure and Applied Chemistry* **2011**, *83*, 2229–2259.

(35) Lok, K. P.; Ober, C. K. *Canadian Journal of Chemistry* **1985**, *63*, 209–216.

(36) Almog, Y.; Reich, S.; Levy, M. *British Polymer Journal* **1982**, *14*, 131–136.

(37) Tseng, C. M.; Lu, Y. Y.; El-Aasser, M. S.; Vanderhoff, J. W. *Journal of Polymer Science Part A: Polymer Chemistry* **1986**, *24*, 2995–3007.

(38) Song, J.-S.; Tronc, F.; Winnik, M. A. *Journal of the American Chemical Society* **2004**, *126*, 6562–6563.

(39) Song, J.-S.; Winnik, M. A. *Macromolecules* **2005**, *38*, 8300–8307.

(40) Peng, B.; Wee, E.; Imhof, A.; Blaaderen, A. *Langmuir* **2012**, *28*, 6776–6785.

(41) Feeney, P. J.; Napper, D. H.; Gilbert, R. G. *Macromolecules* **1987**, *20*, 2922–2930.

(42) Gilbert, R. G. *Emulsion Polymerisation: A Mechanistic Approach*; 1st ed.; Academic Press: London, 1995.

(43) Kawaguchi, S. *Advances in Polymer Science* **2005**, 299–328.

(44) Paine, A. J.; Luymes, W.; McNulty, J. *Macromolecules* **1990**, *23*, 3104–3109.

(45) Kawaguchi, S.; Winnik, M. A.; Ito, K. *Macromolecules* **1995**, *28*, 1159–1166.

(46) De Gennes, P.-G. *Angewandte Chemie* **1992**, *31*, 842–845.

(47) Takahara, Y. K.; Ikeda, S.; Ishino, S.; Tachi, K.; Ikeue, K.; Sakata, T.; Hasegawa, T.; Mori, H.; Matsumura, M.; Ohtani, B. *Journal of the American Chemical Society* **2005**, *127*, 6271–6275.

(48) Perro, A.; Meunier, F.; Schmitt, V.; Ravaine, S. *Colloids and Surfaces A: Physicochemical and Engineering Aspects* **2009**, *332*, 57–62.

(49) Teo, B. M.; Suh, S. K.; Hatton, T. A.; Ashokkumar, M.; Grieser, F. *Langmuir* **2011**, *27*, 30–33.

(50) Walther, A.; Hoffmann, M.; Müller, A. H. E. *Angewandte Chemie* **2008**, *47*, 711–714.

(51) McConnell, M. D.; Kraeutler, M. J.; Yang, S.; Composto, R. J. *Nano letters* **2010**, *10*, 603–609.

(52) Pregibon, D. C.; Toner, M.; Doyle, P. S. *Science* **2007**, *315*, 1393–1396.

(53) Selvan, S. T.; Patra, P. K.; Ang, C. Y.; Ying, J. Y. *Angewandte Chemie* **2007**, *46*, 2448–2452.

(54) Jiang, J.; Gu, H.; Shao, H.; Devlin, E.; Papaefthymiou, G. C.; Ying, J. Y. *Advanced Materials* **2008**, *20*, 4403–4407.

(55) Hu, S.-H.; Gao, X. *Journal of the American Chemical Society* **2010**, *132*, 7234–7237.

(56) Perro, A.; Reculusa, S.; Ravaine, S.; Bourgeat-Lami, E.; Duguet, E. *Journal of Materials Chemistry* **2005**, *15*, 3745–3760.

(57) Casagrande, C.; Fabre, P.; Raphaël, E.; Veyssié, M. *Europhysics Letters* **1989**, *9*, 251–255.

(58) Paunov, V. N.; Cayre, O. J. *Advanced Materials* **2004**, *16*, 788–791.

(59) Bao, Z.; Chen, L.; Weldon, M.; Chandross, E.; Cherniavskaya, O.; Dai, Y.; Tok, J. B.-H. *Chemistry of Materials* **2002**, *14*, 24–26.

(60) Takei, H.; Shimizu, N. *Langmuir* **1997**, *13*, 1865–1868.

(61) Cayre, O.; Paunov, V. N.; Velev, O. D. *Chemical Communications* **2003**, 2296–2297.

(62) Fujimoto, K.; Nakahama, K.; Shidara, M.; Kawaguchi, H. *Langmuir* **1999**, *15*, 4630–4635.

(63) Gu, H.; Yang, Z.; Gao, J.; Chang, C. K.; Xu, B. *Journal of the American Chemical Society* **2005**, *127*, 34–35.

(64) Xia, Y.; Yin, Y.; Lu, Y.; McLellan, J. *Advanced Functional Materials* **2003**, *13*, 907–918.

(65) Nagle, L.; Fitzmaurice, D. *Advanced Materials* **2003**, *15*, 933–935.

(66) Yu, H.; Chen, M.; Rice, P. M.; Wang, S. X.; White, R. L.; Sun, S. *Nano letters* **2005**, *5*, 379–382.

(67) Gao, X.; Yu, L.; MacCuspie, R.; Matsui, H. *Advanced Materials* **2005**, *17*, 426–429.

(68) Teranishi, T.; Inoue, Y.; Nakaya, M.; Oumi, Y.; Sano, T. *Journal of the American Chemical Society* **2004**, *126*, 9914–9915.

(69) Reculusa, S.; Poncet-Legrand, C.; Ravaine, S.; Mingotaud, C.; Duguet, E.; Bourgeat-Lami, E. *Chemistry of Materials* **2002**, *14*, 2354–2359.

(70) Duguet, E.; Reculusa, S.; Perro, A.; Poncet-Legrand, C.; Ravaine, S.; Bourgeat-Lami, E.; Mingotaud, C. *MRS Proceedings* **2011**, *847*, EE1.1.

(71) Reculusa, S.; Poncet-Legrand, C.; Perro, A.; Duguet, E.; Bourgeat-Lami, E.; Mingotaud, C.; Ravaine, S. *Chemistry of Materials* **2005**, *17*, 3338–3344.

(72) Wang, D.; Dimonie, V. L.; Sudol, E. D.; El-Aasser, M. S. *Journal of Applied Polymer Science* **2002**, *84*, 2710–2720.

(73) Nie, Z.; Li, W.; Seo, M.; Xu, S.; Kumacheva, E. *Journal of the American Chemical Society* **2006**, *128*, 9408–9412.

(74) Kim, S.-H.; Sim, J. Y.; Lim, J.-M.; Yang, S.-M. *Angewandte Chemie* **2010**, *49*, 3786–3790.

(75) Chen, C.-H.; Shah, R. K.; Abate, A. R.; Weitz, D. A. *Langmuir* **2009**, *25*, 4320–4323.

(76) Shah, R. K.; Kim, J.-W.; Weitz, D. A. *Advanced Materials* **2009**, *21*, 1949–1953.

(77) Roh, K.; Martin, D. C.; Lahann, J. *Nature materials* **2005**, *4*, 759–763.

(78) Mulvaney, P.; Giersig, M.; Ung, T.; Liz-Marzán, L. M. *Advanced Materials* **1997**, *9*, 570–575.

(79) Gu, H.; Zheng, R.; Zhang, X.; Xu, B. *Journal of the American Chemical Society* **2004**, *126*, 5664–5665.

(80) Sheu, H. R.; El-Aasser, M. S.; Vanderhoff, J. W. *Journal of Polymer Science Part A: Polymer Chemistry* **1990**, *28*, 653–667.

(81) Sheu, H. R.; Vanderhoff, J. W. *Journal of Polymer Science Part A: Polymer Chemistry* **1990**, *28*, 629–651.

(82) Casson, N. In *Rheology of Dispersed Systems*; Mill, C. C., Ed.; Pergamon Press: New York, 1959; p. 84.

(83) Beckett, S. T. *The Science of Chocolate*; 2nd ed.; RSC Publishing: Cambridge, 2008.

(84) Chevalley, J. In *Industrial Chocolate Manufacture and Use*; Beckett, S. T., Ed.; Blackwell Publishing Ltd: Oxford, UK, 1999.

(85) Schantz, B.; Rohm, H. *LWT - Food Science and Technology* **2005**, *38*, 41–45.

Chapter 2

Synthesis and interfacial properties of amphiphilic Janus particles and their use as ice crystal inhibitors*

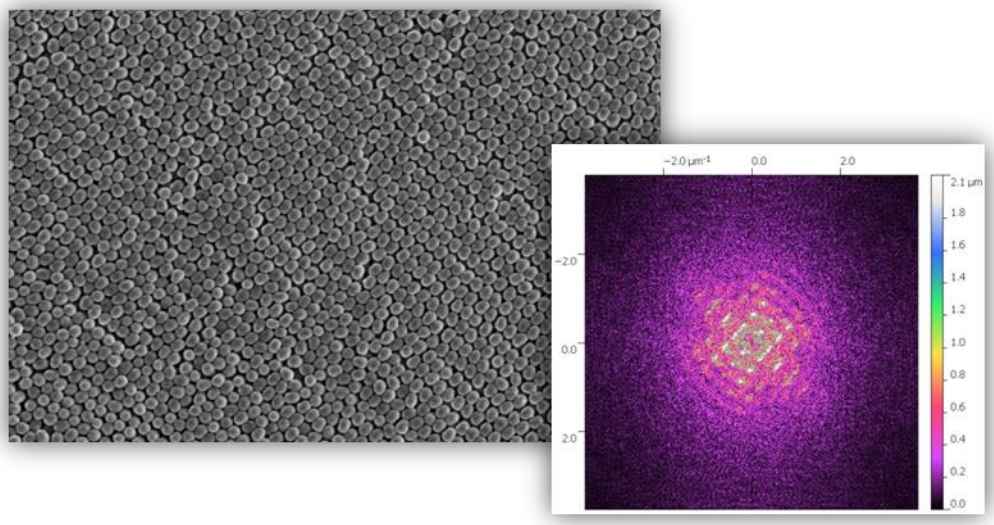

2.1. Abstract

In this chapter we describe the one-pot synthesis of amphiphilic sub-micron sized Janus particles through a seeded-swelling emulsion polymerisation strategy and their use as ice crystal inhibitors. Hydrophilic co-monomer 2-hydroxyethyl methacrylate is used to synthesise seed particles with a hydrophilic surface, enabling the phase separation of a well defined hydrophobic polystyrene lobe. The relative lobe sizes can be tuned by the mass variation of monomers used during the synthesis. Submicron amphiphilic Janus particles of varying hydrophilic: hydrophobic ratios were found to exhibit surface active

* Part of this work is published elsewhere: *Use of Synthetic Janus Particles for preventing or reducing crystal growth.* S.A.F. Bon and M. I. Gibson, Patent No. **WO 2013/050773**

behaviour by adsorbing to liquid-liquid interfaces and reducing surface energy, the variation of which dependent on hydrophilic : hydrophobic lobe size ratio. Additionally, the Janus particles adopted a range of packing conformations depending on the concentration of particles in convectively drying suspensions. Similar to our amphiphilic Janus particles, naturally occuring ice crystal inhibitors proteins and macromolecules possess hydrophilic and hydrophobic moieties. As such we investigate the ability for Janus particles to inhibit ice crystal growth. Ultimately, the Janus particles were found to arrest crystal growth with a larger particle hydrophobic : hydrophilic ratio proving more effective at ice recrystallisation inhibition. As such, these particles have the potential to be used as anti-freeze agents in a range of applications.

2.2. Introduction

Ice crystal growth inhibition is an area of significant interest due to the commercial and medical implications of effective inhibitor compounds. The process of freezing and thawing can be detrimental in aqueous systems subjected to sub-zero (degrees Celcius) temperatures. Intercellular and intracellular ice crystal growth cause rupture and localised high concentration of electrolytes in living tissue, posing difficulties in the cryo-preservation of organs.[1,2] Growing ice fronts exclude particulates from the crystal matrix thereby causing aggregation of colloidal particles between crystal grains.[3] 'Soft' i.e. low T_g aqueous colloidal dispersions such as paint formulations are especially sensitive to freezing. Upon re-crystallisation, frozen food products such as ice cream attain a 'grainy' texture attributed to the increased crystal size.[4]

Many organisms which survive in sub-zero conditions manufacture antifreeze (glyco-) proteins[5] which serve to prevent the nucleation and growth of ice crystals when dispersed in aqueous conditions. Several approaches have been undertaken to gain insight as to how these biomacromolecules retard ice crystal growth. Proteins possessing antifreeze efficacy in organisms, are often identified, isolated and expressed as in the case of *Lolium Perenne*.[6] Alternatively, simple macromolecules with antifreeze activity for example poly(vinyl alcohol) are chemically and structurally varied,[7–9] or total synthesis of peptide-based analogues[10,11] are used in crystal inhibition studies.

The vast majority of studies into mechanism of inhibition focus on the molecular scale, attempting to elucidate 'molecular recognition'[12] of the additive with the growing ice front, or disruption of the growing front in the supercooled melt. One common theme amongst all anti-freeze (glyco-)proteins studied at the molecular scale is the presence of both hydrophilic and hydrophobic moieties, revealing an amphiphilic structure.[7] Generally speaking, in the case of antifreeze proteins, the hydrophobic moieties are thought to interact with the ice, whilst the hydrophilic component faces the supercooled melt.[13] However, there are examples of inorganic antifreeze compounds which are thought to complex with the ice through hydrophilic hydrogen bonding interactions leaving the hydrophobic face exposed.[14]

A generally accepted theory for ice recrystallisation inhibition and freezing point depression resulting from foreign bodies and impurities derives from the Kelvin (Gibbs-Thomson) Effect. If a growing ice grain encounters an impurity, it can either migrate

alongside the growing ice front, or leave the particle behind. In either case, a curved interface is formed. As a result of the Kelvin effect, crystal growth on to a curved interface is unfavourable as a result of the curvature. It can be noted that total coverage of the interface with the impurity is not required for effective ice crystal inhibition. According to Raymond and deVries; crystal growth can be halted when the average spacing between the adsorbed impurities is equal or less than twice the critical radius of curvature.[15]

Amphiphilic sub-micron Janus particles have been shown to experimentally[16] and theoretically[17] interact and assemble at liquid-liquid interfaces according to their respective chemical and morphological anisotropy. In this vein, we investigate the use of amphiphilic Janus particles as mesoscale analogues of molecular antifreeze compounds.

From a commercial perspective, the manufacture of Janus particles for this purpose must be easily scalable, economically viable, non-toxic and conform to the relevant regulations that permit their use in applications such as foodstuffs and coatings formulations. Therefore, of the range of synthetic methods available to manufacture amphiphilic particles, waterborne heterogeneous polymerisation such as emulsion polymerisation presents an attractive option.

2.2.1 Emulsion polymerisation

Emulsion polymerisation has proven to be a versatile tool in the fabrication of submicron-sized polymer colloids with intriguing variations in the chemical

composition and morphology of the particles. Examples include, core-shell[18,19], armoured[20,21], hairy[22], and hollow[23] polymer particles which can lead to innovative applications in products such as impact modifiers[24] pressure sensitive adhesives[25], colloidal surfactants[26], and opacifiers[27] in coatings respectively. One pursuit in the fabrication of these types of structurally more complex particles is to develop straightforward and scalable emulsion polymerisation protocols which require a minimum of reaction and purification steps.

2.2.2 Synthesis of submicron Janus particles

Our interest lies in the fabrication of peanut- or dumbbell-shaped colloids, exhibiting an amphiphilic Janus-type character. By this we mean that the two lobes possess opposing chemical characteristics with respect to wettability of their dispersion medium. One synthetic route toward dumbbell polymer colloids by emulsion polymerisation was pioneered by El-Aasser and coworkers[28,29] who made elegant use of the phenomenon of contraction of crosslinked elastic polymer networks upon elevation of temperature. In essence heating up lightly crosslinked poly(styrene) microspheres swollen with styrene monomer and an oil-soluble radical initiator resulted in the formation of a monomer protrusion. A local higher rate of polymerisation within the protrusion further accentuates the newly developed shape through diffusion of monomer. The process of phase separation by this means is explained by the theory of entropic phase separation which is described below.

2.2.3 Thermodynamics of entropic phase separation

Swelling of a crosslinked seed particle in a monomer solution can be explained theoretically by the combination of three thermodynamic factors: free energy of monomer and polymer mixing (ΔG_m), interfacial energy between particle surface and continuous medium (ΔG_t), and the energy component as a result of an elastic retractile force (ΔG_{el}) arising from the crosslink density of the particle (expressed in equation 1). These three factors define the equilibrium between concentration of monomer in the particle and the continuous phase.

$$\Delta G_{mp} = \Delta G_{el} + \Delta G_t + \Delta G_m \quad (1)$$

By substituting the Flory-Huggins mixing expression[30] for (ΔG_m), Flory-Rehner equation[31] for (ΔG_{el}) and the Morton equation[32] for (ΔG_t), we get an expression which can be evaluated qualitatively as shown in equation 2. *R* is the ideal gas constant, *T* system temperature, *N* is number of polymer chains per molar volume of polymer V_p. V_m is molar volume of monomer, γ particle water interfacial tension, *a* is radius of the swollen polymer particle, χ_{mp} is the Flory monomer-polymer interaction parameter.

$$[\Delta G_{mp} = RTNV_m (V_p{}^{1/3} - \tfrac{1}{2}V_p) + 2V_m\gamma/a + RT[ln(1-V_p) + V_p + \chi_{mp}.V_p{}^2] \quad (2)$$

From this expression, it is possible to see which factors promote or disfavour particle swelling. These factors have been summarised in figure 2.1. For instance, low T and γ and a favourable χ_{mp} mixing parameter energetically promotes swelling.

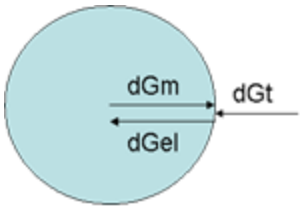

	Arises From	Contribution	Depends on
Mixing Force ΔG_m	Absorption of Monomer	(-) Promotes Expansion	Vp, j, χ_{mp}
Elastic Retractile ΔG_{el}	Contraction of stretched network	(+) Restrains Expansion	N, T
Interfacial Tension ΔG_t	Increase of Surface Area	(+) Restrains Expansion	r, γ

Figure 2.1 Schematic and table summarising the effect of three major thermodynamic forces on the swelling of a particle

Based on the factors indicated above, the particle will swell to equilibrium size i.e. $\Delta G_{m,p} = 0$. Phase separation of the equilibrated swollen particle can be induced by exploiting the thermal dependence of the elastic retractile force component (ΔG_{el}). Upon heating, ΔG_{el} provides an overwhelming elastic retraction force, causing the particle to rapidly de-swell. This force arises from the thermal energy provided to relax the elongated polymer chains resulting from the swelling step. Such a rapid de-swelling can cause a singular monomer protrusion to breach the particle surface, the morphology of which is dominated by the wettability of the monomer to the polymer.

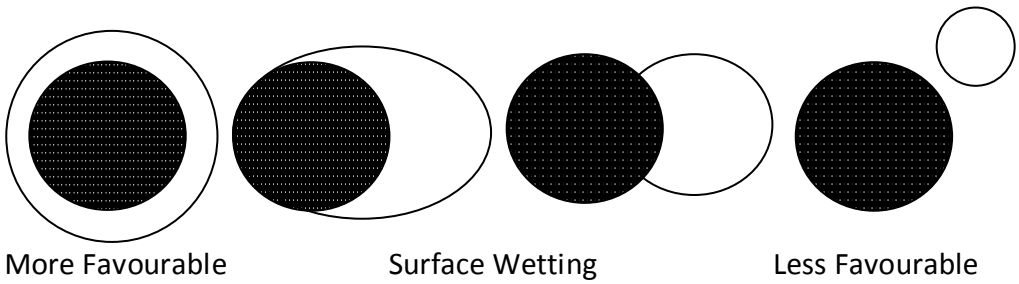

Figure 2.2 Schematic indicating the range of morphology possible depending on differences of surface wettability between the monomer and seed polymer

Figure 2.2 graphically depicts the range of morphology one can expect depending on the surface wettability of the monomer to polymer. The interfacial energy difference between the two extremes of wettability can be expressed as shown in equation 3 where γ_{mw}, γ_{pm} and γ_{pw} represent the monomer-water, polymer-monomer and polymer-water interfacial tensions respectively.

$$E = 4\pi\,\gamma_{mw}\,[(a_p2 - a_m2) + (\gamma_{pm} - \gamma_{pw})a_p2] \quad (3)$$

If the monomer favourably wets the particle surface, a core-shell type particle is formed, whereas complete non-wetting of the particle surface causes the monomer to be expelled from the droplet resulting in separate droplet formation in the continuous phase. Based on the interfacial energies between the two polymers and the continuous phase, Waters developed a model to predict the surface morphology of composite latex particles.[33] In this study, the surface energies of each interface, between a 'hydrophilic' and 'hydrophobic' polymer and the interfacial energy between each of these polymers and the continuous phase water was considered as a function of volume fraction to yield total interfacial energy of the system. Minimisation calculations of these total interfacial energies yield the most thermodynamically favourable particle morphology ranging from (inverted) core shell to particle expulsion. In addition, the model considered non-deformable and deformable polymers, inferring the ability to calculate morphologies of 'soft' composite particles.

2.2.4 Entropic phase separation as a route to dumbbell colloids

This approach has become a popular route toward synthesis of dumbbell colloids owing to the ability to tune particle morphology through the chemical properties of the reagents.

Mock *et al.* exploited this synthetic procedure through several seeded polymerisations of a highly crosslinked (18 wt% DVB w/r to monomers) emulsion polymerisation seed. A hydrophilic corona was polymerised around the seed latex before swelling which increased the contact angle between extruded monomer and polymer surface, resulting in a more defined secondary lobe, whilst still permitting optimum swelling of the core with monomer.[34] Weitz *et al.* employed a similar strategy to fabricate larger 5 μm diameter Janus particles by seeded emulsion polymerisations indicating the ability to scale up particle size by an order of magnitude. Fabricating particles of this size allowed the kinetics of the phase separation to be observed by optical microscopy, disclosing the fact that a phase separation occurs only the in the first 100 seconds of thermal treatment, thereafter, the growth of the new lobe is driven by the migration of monomer into the newly formed lobe.[35] Furthermore, dimer and trimer particles fabricated in successive seed emulsion polymerisations are possible if the crosslinking content of the respective monomer lobes is varied, an example of controlling ΔG_{el} through crosslinking co-monomer concentration.[36]

A variety of shapes and chemical compositions of anisotropic Janus particles have been fabricated by entropic phase separation. Mu *et al.* swelled polystyrene microspheres with a mixture of toluene and 4-vinyl pyridine to render a series of Janus particles, their

morphology depending on the ratio of toluene and 4-vinyl pyridine[37]. Hydrogel-polystyrene Janus particles have been demonstrated by swelling polystyrene microspheres with toluene and N-isopropylacrylamide to render thermally responsive Janus particles owing to the LCST of p(NIPAM).[38] In an example using an alternative to styrene as the seed particle monomer, Pan *et al.* swelled a poly(vinylidene fluoride) latex with styrene composite latex particles.[39] Finally, a seeded emulsion polymerisation of bis-acrylamide crosslinked poly(NIPAM) has been demonstrated to form a homogeneous hydrophilic layer over the entire Janus particle resulting in isotropic chemistry on an anisotropic morphology.[40]

These examples indicate that seeded emulsion polymerisation, exploiting the entropic phase separation technique is a flexible and versatile method to generate polymeric Janus particles of tuneable size, geometry and chemical anisotropy. However, many of these examples require multistep reactions separated by purification and dialysis steps. If particles of this type are to find a use in commercial applications, a simple optimised synthetic procedure needs to be developed. As such we investigate an optimised synthetic procedure to fabricate amphiphilic Janus particles on a bulk scale before characterising their interfacial properties and their effectiveness at inhibiting ice crystal growth.

2.3. Results and discussion

2.3.1 One pot synthesis of amphiphilic Janus particles

Following the route of entropic phase separation of polymer colloid particles manufactured by emulsion polymerisation, the first step is to develop a seed particle that fulfils the requirements of the phase separation thermodynamics. By this we mean that the seed particle must be adequately crosslinked and possess a surface chemistry distinctly more hydrophilic from that of the secondary lobe (which will be hydrophobic). For this reason we investigate an emulsion polymerisation system incorporating non-ionic monomer 2-hydroxyethyl methacrylate (HEMA), anionic monomer sodium styrene sulfonate (NaSS), styrene and crosslinking agent divinylbenzene (DVB).

Seed particles synthesis

Poly(styrene) based seed particles were fabricated through a surfactant free emulsion polymerisation. As aforementioned, a hydrophilic layer on the surface of the seed particle accentuates the definition of the phase separated hydrophobic monomer lobe as a result of the significant difference in surface tension between the phases. Many literature examples graft the hydrophilic polymer[34,35,38] or inorganic[41] layer onto the un-functionalised poly(styrene) seed particle via an additional reaction step. We negate the need for this step by incorporating the hydrophilic co-monomer 2-hydroxyethyl methacrylate (HEMA) into the seed particle co-polymerisation alongside the anionic co-monomer sodium styrene sulfonate. The *ab initio* emulsion co-polymerisation of styrene and HEMA has been reported to fabricate particles with a high degree of p(HEMA) on the surface as determined by XPS[42] and AFM[43] techniques. However, the use of HEMA in a styrene emulsion polymerisation as a sole co-monomer in absence of surfactant has been reported to possess a weak nucleation ability, generating larger particles of up to

600 nm diameter.[44] Therefore an anionic sulfonate functionalised styrene monomer (sodium styrene sulfonate at 0.5 wt% w/r to monomers) was employed as charge stabiliser, with 0.5 wt% w/r to styrene reported to reduce particle size from 500 – 1000 nm to 150 - 400 nm.[45] In addition, the overall polymerisation rate was shown to increase in accordance to the addition of a small quantity of NaSS into a styrene emulsion polymerisation.[46] Unlike molecular surfactants which are physisorbed to the particle surface, sodium styrene sulfonate is polymerised into the particle polymer matrix and presents mostly on the particle surface providing robust charge stabilisation, without the risk of desorption.[44] This charged surface provides another part of the colloidal stabilisation that allows for stable phase separation of a hydrophobic lobe.

In order to fulfil the elastic retractile force component (ΔG_{el}) that allows thermally induced phase separation; 1 wt% (w/w w/r to total monomer content) of divinylbenzene (DVB) crosslinking agent was incorporated into the polymerisation. This concentration has been proven to provide reliable swelling and subsequent phase separation by our group and others.[28,47]

We therefore investigated the quaternary emulsion polymerisation of styrene, divinyl benzene, sodium styrene sulfonate and hydroxyethyl methacrylate in batch conditions at 2 wt% total monomer content (w/r to continuous phase). As p(HEMA) has been reported to present mostly on the particle surface, 1 wt% w/r to total monomer was deemed sufficient to render a hydrophilic surface, as excessive concentrations have been shown to induce secondary nucleation.[44] The emulsion polymerisations were conducted in a single jacketed reactor with overhead stirrer, initiated using potassium persulfate

(0.5 wt% w/r to monomers) by heating the reaction mixture to 70 °C using a recirculation bath. An additional emulsion polymerisation without HEMA was conducted for comparison. The polymerisations were followed kinetically by extracting aliquots of the aqueous phase at set time intervals and analysing by dynamic light scattering and conversion by gravimetry (as seen in figure 2.3). The resulting particle suspensions were dialysed against deionised water for 14 days, changing the water regularly before measuring particle size, zeta potential and analysis by scanning electron microscopy.

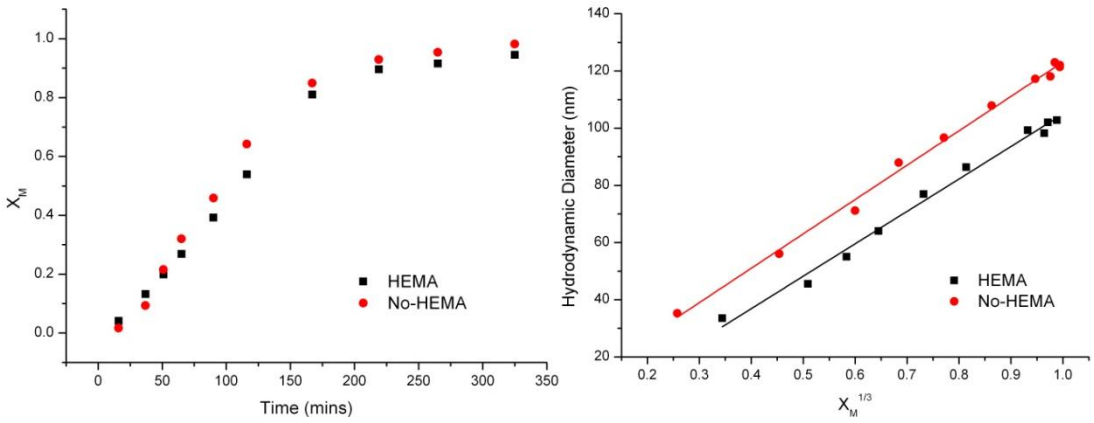

Figure 2.3 (left) Conversion plots and (right) particle hydrodynamic diameter as a function of (conversion)$^{1/3}$ for the seed emulsion polymerisation with and without HEMA co-monomer. Lines indicate fitted linear functions (expt. TS500)

In terms of kinetics, it can be seen from figure 2.3 (left) that the emulsion polymerisation with HEMA has slightly a faster polymerisation rate during the first 60 minutes / 20% conversion. After which, the non-HEMA reaction gains an increased rate and overtakes the HEMA containing emulsion polymerisation. It can also be noticed that the HEMA conversion profile takes on a more linear profile up to 80% conversion

compared with the non-HEMA reaction. Figure 2.3 (right) reveals a linear particle growth profile when plotted as a function of (conversion)$^{1/3}$. This indicates a short nucelation period without the formation of secondary nucleation, which is in accordance with the observed DLS and FEG-SEM data reported below.

Qin *et al.* report that during the poly(styrene-co-HEMA) emulsion polymerisation, chain growth falls into two domains, poly(styrene) rich and p(HEMA) rich. Owing to the hydrophilic nature of HEMA, mostly consumed in the early stages of the polymerisation, forms small hydrogel particles of 40-60 nm. Due to osmotic pressure, styrene swells these initial p(HEMA) particles and polymerises within.[48] Therefore, the more linear conversion profile for polymerisations containing HEMA can be ascribed to a 'core-shell' particle growth mechanism where monomer diffusion into the particle is in competition with polymerisation rate as discussed by Chen *et al.* for the kinetics of styrene-co-HEMA emulsion polymerisations.[49]

Phase separation of p(HEMA) and p(Sty) domains occurs within the swollen low viscosity particles causing the more hydrophilic p(HEMA) domains to present on the particle surface. We can see that a 1 wt% (w/r to total monomer) loading of HEMA in the seed emulsion co-polymerisation is clearly sufficient to render a visible hydrophilic layer onto the seed particle. When dispersed in aqueous media, the pHEMA swells to a hydrogel, hence the crinkled appearance arises from the dehydration of the p(HEMA) corona upon drying for SEM analysis. Figure 2.4 depicts the topological difference between particles containing p(HEMA) (figure 2.4 top), and particles synthesised in

absence of HEMA (figure 2.4 bottom). The literature reports that XPS analysis of poly(styrene-co-HEMA-co-NaSS) emulsion polymerisations reveal that the particle surface is enriched with ~10 % and ~40% p(NaSS) and p(HEMA) respectively when 0.4 and 0.6 wt% of the monomers are used.[44] In terms of overall particle size difference between poly(styrene) seed particles with and without HEMA as seen in figure 2.4 (top left), a slightly larger particle size can be seen in the absence of HEMA. This could be attributed to a higher number of particles formed in the case of HEMA, thereby reducing overall particle size.

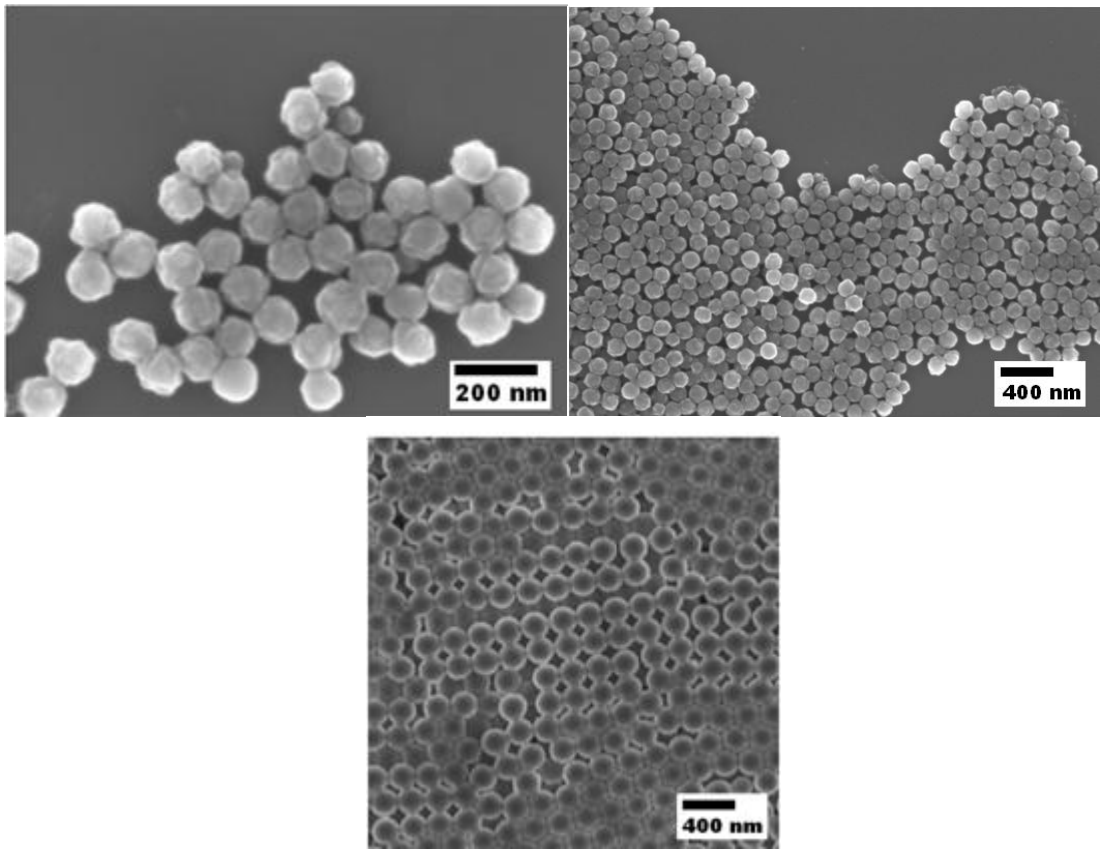

Figure 2.4 (Top)FEG-SEM micrographs of Janus seed particles with HEMA corona (TS255-Seed). (Bottom) FEG-SEM micrographs of Janus seed particles without p(HEMA) (TS166)

Hydrodynamic diameter (fig. 2.5 top right), PDI (fig. 2.5 bottom left) and zeta potential (fig. 2.5 bottom right) measurements of several latexes over a range of ionic strengths were analysed to ascertain how the addition of HEMA affected the colloidal properties of the seed product. In addition, identical seed particle latex (with HEMA) made at the higher polymerisation temperature of 80 °C has been added to see if polymerisation temperature affects the surface properties of the seed latex. Increasing reaction temperature incites negligible difference in terms of size, polydispersity and colloidal stability. However, the addition of HEMA has significant implications on colloidal stability.

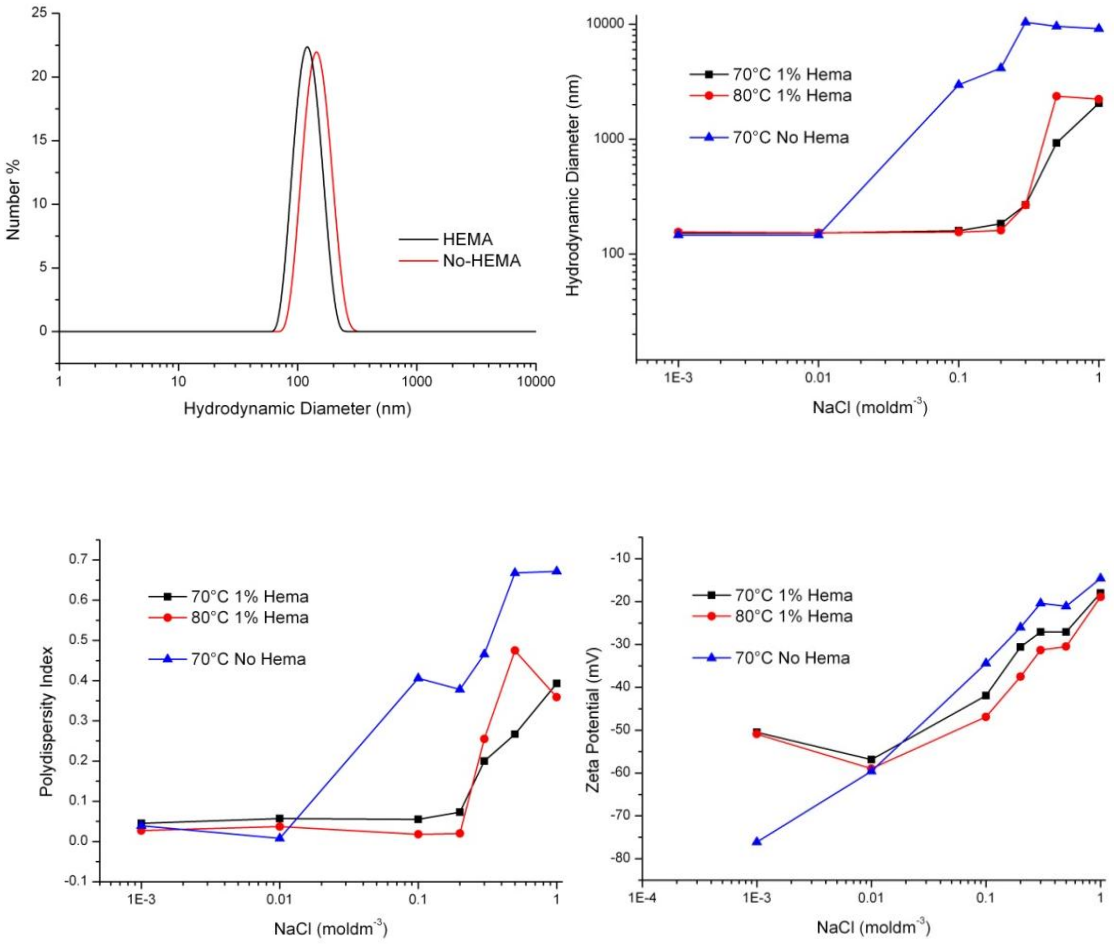

Figure 2.5 (Top left) Number average size distribution for poly(styrene) seed particles with and without HEMA (TS500). Hydrodynamic radii (Top right) Polydispersity indices (Bottom left) and Zeta potentials (Bottom right) of seed particles plotted over a range of salt concentrations measured by dynamic light scattering. (70°C – TS500, 80°C – TS255 Seed)

In the absence of HEMA, the zeta potential at low salt concentration is considerably more negative than the latexes with p(HEMA). At higher salt concentrations, there is negligible difference between latexes with and without the HEMA co-monomer. At low salt concentrations i.e. 10^{-3} M NaCl, the hydrated p(HEMA) corona screens part of the negative surface charge brought about by the sodium styrene sulfonate polymer on the particle surface causing the less negative zeta potential in latexes with p(HEMA). At higher salt concentrations i.e. $>10^{-2}$ M NaCl, the anionic charge is suppressed by the salt, more so than the presence of the HEMA corona.

In terms of hydrodynamic diameter and polydispersity index, the difference in colloidal stability between latexes with and without HEMA is far more pronounced. In the absence of HEMA, the measured hydrodynamic diameter vastly increases due to coagulation of the latex at salt concentrations above $1x10^{-2}$ M. However, the latexes incorporating HEMA start to coagulate at $2x10^{-1}$ M NaCl. This resistance to flocculation at higher salt concentrations can be attributed to the presence of a steric barrier formed by the hydration of the p(HEMA) chains on the surface of the polystyrene latex. We can therefore confirm that the presence of p(HEMA) on the particle surface has been confirmed both by scanning electron microscopy and by use of dynamic light scattering in solutions of varying salt content.

2.3.2 Swelling and phase separation polymerisation

We then investigated the use of these hydrophilic particles in swelling and entropic phase separation reactions without prior purification. This was accomplished by injecting the second stage polymerisation components to the completed reaction mixture from the seed emulsion polymerisation.

In a typical procedure, immediately after the initial polymerisation, without opening the reactor, the seed latex is rapidly cooled to room temperature and the second stage styrene and AIBN thermal initiator solution is injected and degassed. The mixture is maintained at room temperature and stirred for 120 minutes before re-heating to thermal initiation temperature of the AIBN at 70 ℃. This temperature is maintained for 12 hours to allow full conversion of the second phase. We investigated the addition of three different ratios of monomer with respect to the initial polymer seed mass: 0.8:1, 1.25:1 and 2.25:1. By this we mean that of an initial charge of 4 g of seed particles, 3.2 g, 5 g and 9 g of styrene (containing 1 wt% AIBN w/w w/r to styrene) was added to the reactor. The conversion of the second phase was followed by gravimetric analysis of samples extracted at set time intervals as depicted in figure 2.6.

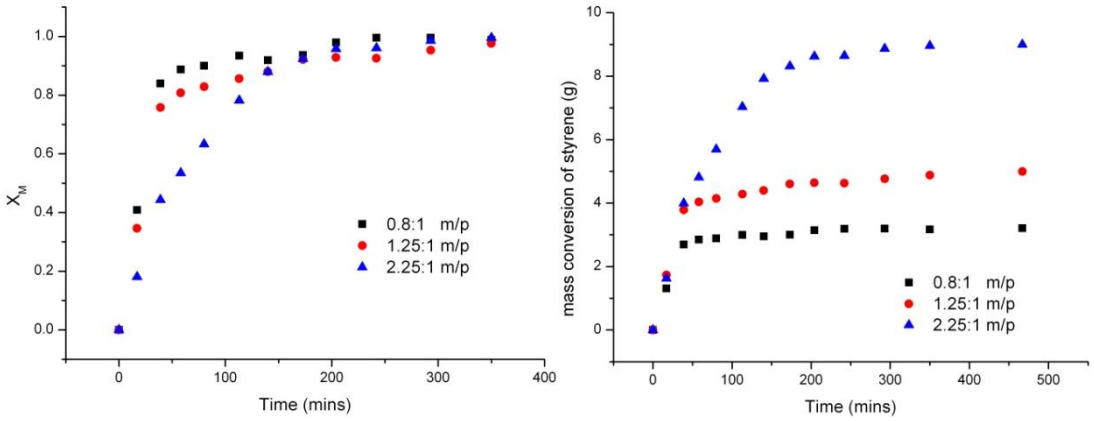

Figure 2.6 Fractional conversion (left) and mass conversion (right) of the seeded emulsion polymerisations as a function of time for three ratios of added monomer to seed polymer mass ratios(TS520)

The conversion profiles indicated in figure 2.8 indicate that the rate of seeded emulsion polymerisation is constant in each case, therefore the addition of more monomer increases the time to reach full conversion.

By using FEG-SEM, the morphology of the resulting Janus particles can be observed as seen in figure 2.7. In the micrograph, each particle has formed into a dumbbell morphology arising from the phase separation of poly(styrene) during the entropic phase separation step. It is possible to make out the crinkled seed particle lobe and the smooth second stage poly(styrene) lobe on each particle.

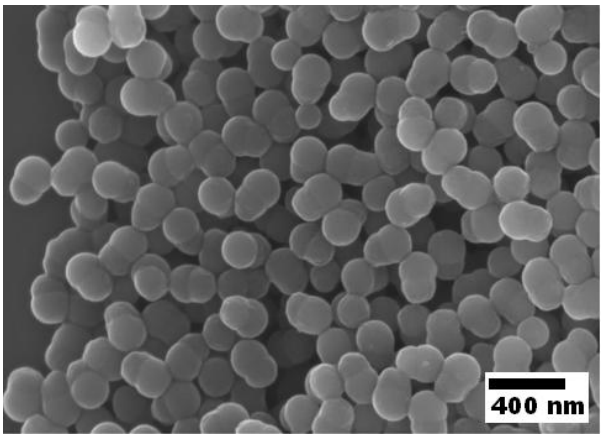

Figure 2.7 FEG-SEM image of amphiphilic Janus particles with 3:1 monomer : polymer ratio (TS255D)

The swelling kinetics of a seed latex is dependent on two major factors; 1) transport of monomer through the continuous phase to the particle surface and 2) diffusion into the particle. Providing sufficient shear force in the system to keep the continuous phase saturated with monomer, transport is relatively fast, on the timescale of minutes.[50] Monomer diffusion into a polymer particle, especially crosslinked, can be slow in comparison.[51] This is due to the 'dry' non solvated nature of a polymer latex. In previous literature examples of entropic phase separation, seed latexes are often purified, resulting in a completely non-solvated particle core. Accordingly, swelling the latex with monomer requires 10-24 hours before equilibrium swelling is reached.

In our system, we found that swelling time could be reduced to 120 minutes whilst still rendering Janus particles of desired geometry. We attribute this due to negating the purification step and commencing swelling immediately after seed particle synthesis. A plausible explanation for the successful reduction in swelling time is due to the presence of monomer and short chain soluble polymer chains solvating the seed particle polymer

chains at the end of the initial polymerisation. This 'plasticisation' effect is lost if the seed latex is purified.

Control of lobe size

We investigated the effect of varying the mass ratio of monomer to polymer seed phase in an attempt to tune the relative lobe sizes. Monomer : polymer mass ratios, from now on noted as m/p ratios of 1:1, 2:1 and 3:1 were employed. For instance, to fabricate particles with a 3:1 m/p ratio based on an initial styrene-co-NaSS charge of 4 g, 12 g of styrene containing 1 wt% AIBN (w/r to monomer) would be charged into a reactor containing a hydrophilic seed particle latex of 2 wt% total solids content before degassing, stirring at room temperature for 2 hours then heating to 70 °C. The subsequent Janus particles for each ratio were imaged by FEG-SEM and can be seen in figure 2.8.

1:1

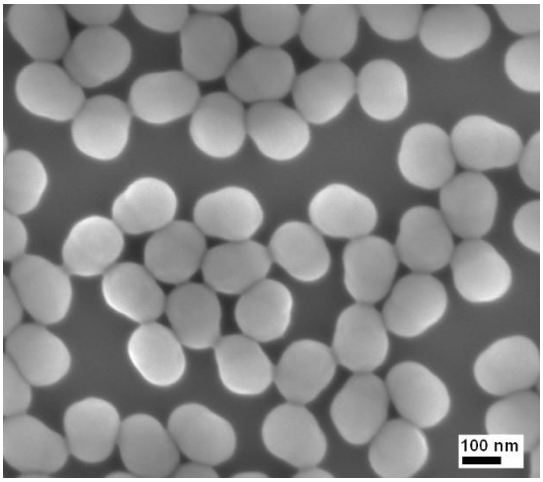

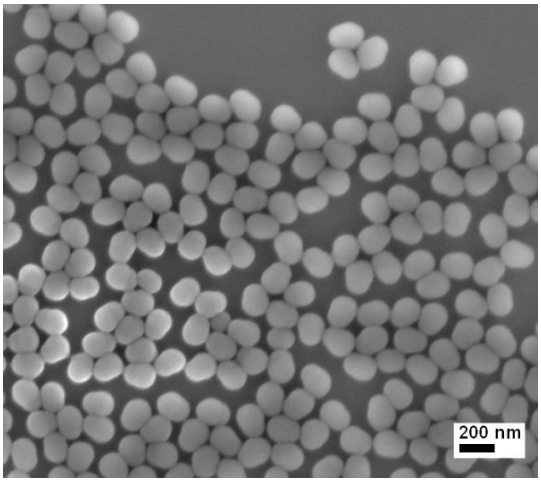

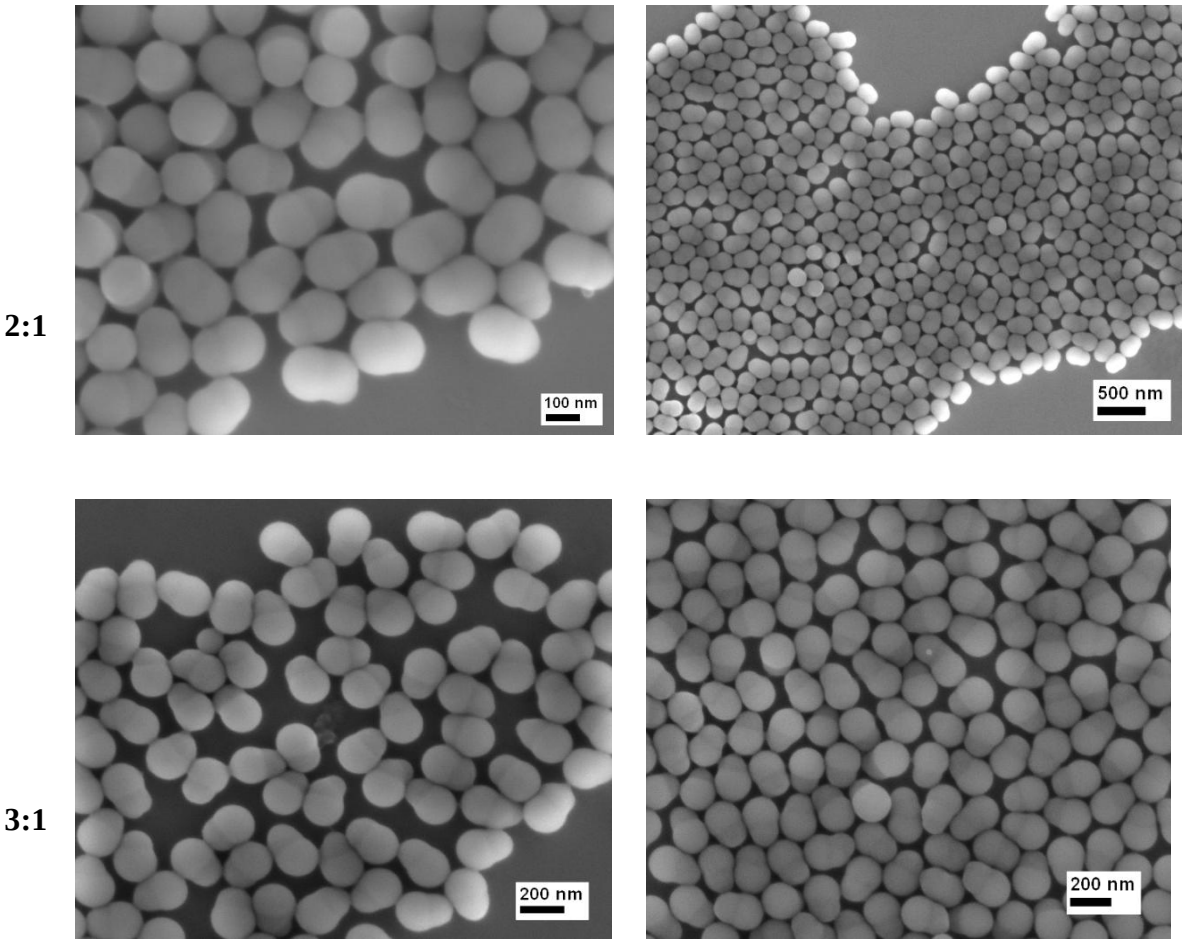

Figure 2.8 FEG-SEM images of Janus particles, including high magnification at different m/p ratios as indicated on the left (1:1 – TSGN-1-1, 2:1 – TSGN-2-1, 3:1 – TSGN-3-1)

Characterisation of size for each ratio was determined by DLS and by quantitative analysis of SEM images. The latter was accomplished by modelling particles as two spherical caps as depicted in figure 2.9. From the dimensions obtained by SEM image analysis, volume and diameter of each lobe was calculated through equations 4 and 5 before plotting in figure 2.10(right).

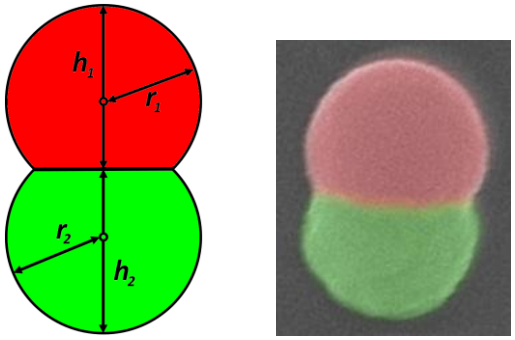

$$V = \frac{\pi h^2}{3}(3a - h) \quad (4)$$

$$a = \frac{r^2 + h^2}{h^2} \quad (5)$$

Figure 2.9 Schematic and high resolution fake colour FEG-SEM image of a Janus particle (TS255D) depicting the dimensions measured for spherical cap size evaluation, the function of which is expressed on the right

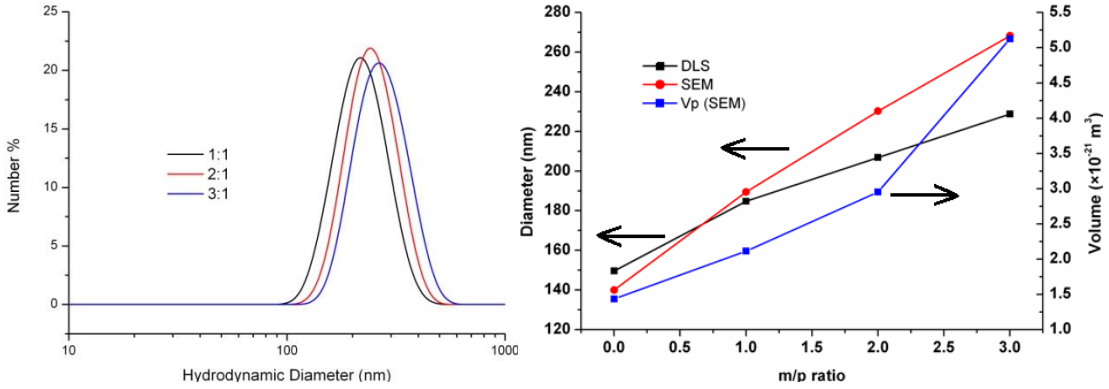

Figure 2.10 (left) Hydrodynamic Diameter size distribution for the 3 ratios of Janus particles (right) Diameter as measured by dynamic light scattering (DLS) and by measurement of the longest axis by (SEM) using samples (1:1 – TSGN-1-1, 2:1 – TSGN-2-1, 3:1 – TSGN-3-1). Using the image analysis in fig. 2.12, volume of the particles is plotted (V_p) – all as a function of monomer:polymer ratio

As monomer to polymer ratio increases, the particle size increases accordingly. Although the DLS result acknowledges this increase, as seen in figure 2.10, it is not accurate due to the limitation of the instrument to assume spherical morphology. Therefore SEM image analysis was undertaken to correctly evaluate Janus particle size.

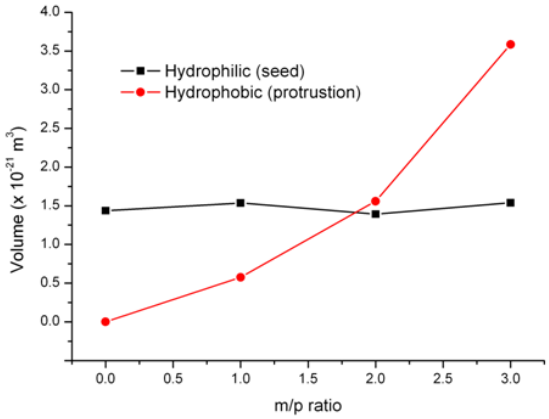

Figure 2.11 Volume of respective hydrophilic and hydrophobic lobes on Janus particles at different m/p ratios (0:1 – TS255-Seed, 1:1 – TSGN-1-1, 2:1 – TSGN-2-1, 3:1 – TSGN-3-1) based on SEM image analysis from fig. 2.12

The volume of the respective lobe sizes for each m/p ratio, including seed particles is plotted in figure 2.11. The volume of the seed particle barely changes regardless of swelling amount, leading to the conclusion that little second phase monomer remains in the primary particle after the thermal entropic phase separation and polymerisation. Additionally, the volume of the hydrophobic lobe for each ratio is lower than expected when compared with the mass of monomer introduced in the second phase. A plausible explanation for this, taking in account the high conversion (>95%) and absence of secondary nucleation is the growth of oligomeric chains in the continuous phase. The presence of sodium styrene sulfonate in the reaction mixture promotes oligomeric chain growth. Alternatively, owing to the low solids content of the reaction, it is possible that a significant fraction of second stage monomer is lost through evaporation during the degassing and polymerisation stage, part of which is exacerbated by the large headspace in the reactors used. However, similar disparities between expected and observed second phase volume in methyl methacrylate swollen poly(methyl methacrylate) particles have been noted by Butterworth.[52] In this example, despite working at a higher solids content

of 40 wt% and reducing monomer loss through alternative degassing techniques, an unexplained loss of volume in the extruded polymer lobe is observed. This disparity is found to reduce with increasing m/p ratios. Regardless of the volume disparity, hydrophobic lobe growth is consistent with the addition of second phase monomer without affecting the size of the seed particle.

Colloidal stability of Janus particles with varying lobe sizes

The size and colloidal stability of Janus particles were measured as a function of solvent ionic strength in the same manner as the seed particles described above. Dilute aqueous suspensions of Janus particles were analysed by dynamic light scattering in a range of salt concentrations. Figure 2.12 indicates the hydrodynamic diameter and polydispersity index measured by dynamic light scattering over a range of concentrations of sodium chloride. PDI and hydrodynamic radius remain constant until 0.1 M NaCl, after which both PDI and radius increase drastically indicating colloidal instability and flocculation. A closer inspection reveals that above 0.1 M NaCl, the highest hydrophobic : hydrophilic ratio is the most colloidally unstable. We can therefore deduce that the hydrophilic seed particle provides the major component of the colloidal stability through the p(NaSS) and p(HEMA) present on the surface, whilst the hydrophobic lobe contributes very little towards the colloidal stability of the system.

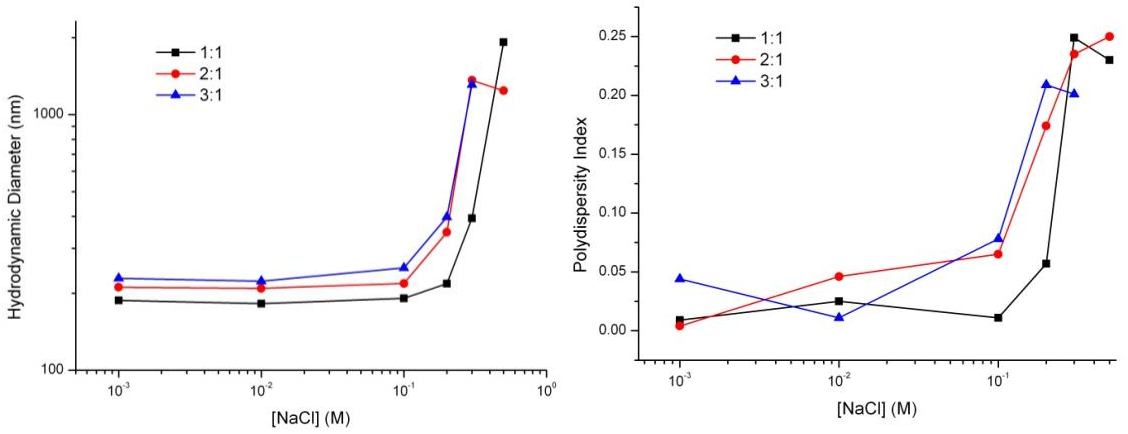

Figure 2.12 Janus particles of varying m/p ratios (1:1 – TSGN-1-1, 2:1 – TSGN-2-1, 3:1 – TSGN-3-1) plotted as (left) hydrodynamic diameter and (right) PDI, both as a function of salt concentration as determined by DLS

Zeta potential measurements over a range of concentrations as plotted in figure 2.13 indicate that all three lobe ratios are stable to a similar magnitude and are equally affected by the salt effect of double layer compression. Zeta potential measurements taken in deionised water at pH 5.5 show a small decrease in electrophoretic mobility for increasing hydrophobic lobe size.

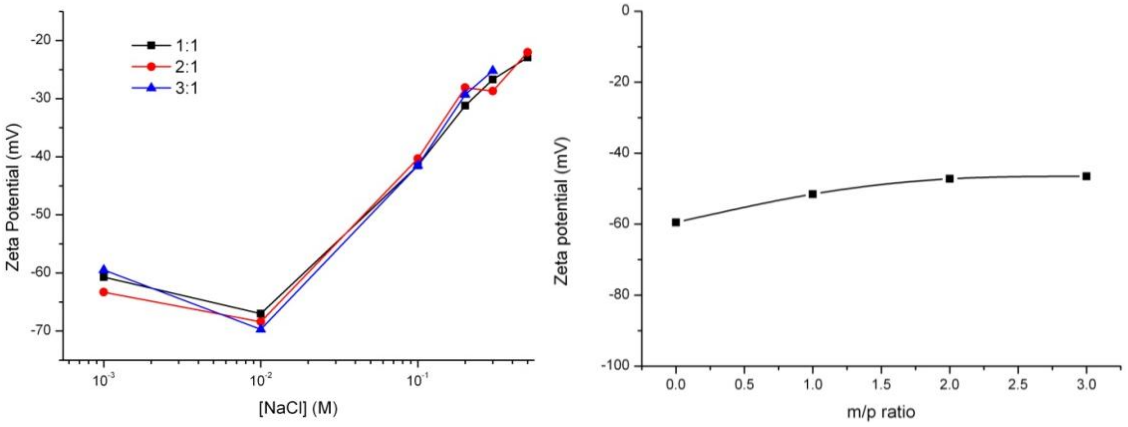

Figure 2.13 (left) Zeta potentials of Janus particles of varying m/p ratios (1:1 – TSGN-1-1, 2:1 – TSGN-2-1, 3:1 – TSGN-3-1) plotted as a function of salt concentration (right) zeta potential as a function of m/p ratio measured in deionised water at pH 5.5

An interesting point to note are the small differences in zeta potential between the particles of varying m/p ratio as seen in figure 2.13. It is expected that particles with an increasing hydrophobic lobe volume (i.e greater m:p ratio) would possess a far lower zeta potential as the hydrophilic lobe provides the sole electrostatic stabilisation for the particle. In addtion we would expect the newly formed hydrophobic lobes of the Janus particles to coalesce during polymerisation or flocculate if no stabilisation were imparted. This leads us to believe that some stabilisation is imparted to the hydrophobic lobe during particle synthesis. During seed particle polymerisation, the use of hydrophilic monomers HEMA and NaSS result in the formation of water soluble oligomers. As these are not removed through a cleaning process after the seed particle polymerisation, these oligomers can plausibly act as a surfactant by adsorbing to the hydrophobic poly(styrene) second phase, thereby providing a degree of colloidal stability. Whilst this provides a beneficial stabilisation contribution, a disadvantage is the reduced particle amphiphilicity.

2.3.3 Limitation of solids content

We investigated upscaling the seeded polymerisation system to achieve a higher total solids content which would be a desirable requirement if these Janus particles were to be manufactured commercially. Typically, seed particle emulsion polymerisations are run at 2 wt% solids content, leading to a total of 4, 6 and 8 wt% total solids for 1:1, 2:1 and 3:1 m/p ratios respectively. To improve synthetic yield, suitable for commercial application, we attempted to increase the monomer loading to accept up to 30 wt% total solids content. Above 20 wt% we observed the presence of dimers, trimers and tetramers for all three ratios investigated. Scanning electron micrographs of particles

from a 30 wt% seeded emulsion polymerisation at 2:1 m/p ratio can be seen in figure 2.14.

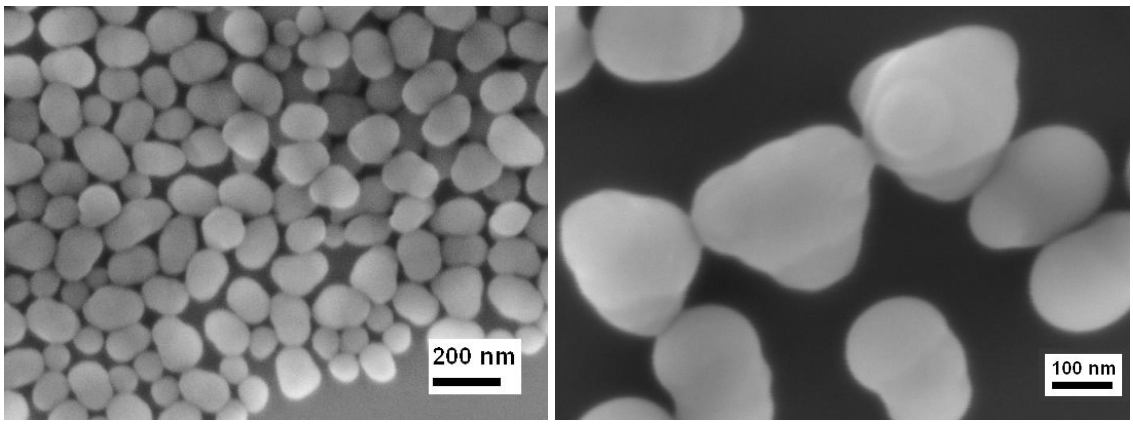

Figure 2.14 FEG-SEM images of a Janus particles synthesised at 30 wt% solids content with a 2:1 m/p ratio (TSGN-30wt)

The formation of these higher order particles is thought to be a result of coalescence during the start of the second polymerisation. During the early stages of the second polymerisation, the newly formed secondary lobe is plasticised as a result of the high monomer concentration within, resulting in a 'soft' lobe well above the polystyrene glass transition temperature. Due to the surfactant free nature of the polymerisation system, the soft lobes possess little colloidal stability. In higher solids content systems, these soft lobes collide and coagulate as there is no repulsive barrier. This can give rise to dimers, trimers, tetramers and higher ordered structures. The structures we obtained are similar to the 'colloidal molecules' obtained by van Blaaderen and coworkers when purposefully phase separating liquid monomer protrusions from crosslinked polystyrene latex particles and subsequently coalescing these particles together.[53] The coalescence in their case resulted from the monomer protrusion coalescing with any solid surface due

to the lack of stabilisation. This provides a reasonable explanation for the formation of dimers, trimers and tetramers in our system at higher solids contents.

2.3.4 Physical properties of Janus particles

Liquid-liquid interfacial behaviour

The surface active behaviour of our amphiphilic Janus particles at liquid-liquid interfaces was investigated by use of droplet shape analysis. Specifically we are interested to see if the particles adsorb to liquid-liquid interfaces, and how the difference of hydrophilic and hydrophobic lobe size ratio affects the contribution to interfacial energy once adsorbed. In order to characterise this behaviour, dialysed Janus particles were dispersed into an aqueous phase (0.1 wt%) which was in turn used to form a droplet within a hexadecane phase. The free energy at a clean hexadecane oil interface (53.3 mNm^{-1})[54] provides a large driving force for dispersed surface active particulates to adsorb on to the interface in order to reduce the surface free energy. We observed an interfacial tension value of 43.49 mNm^{-1} for the pure water-hexadecance interface (without particles) utilising hexadecane of 99% purity.

The profile of suspended aqueous Janus particle suspensions within an organic phase allows the interfacial tension to be measured by the Young-Laplace equation as described elsewhere[55] and explained in Appendix A. Measuring this value at intervals affords the change in interfacial tension as a function of time. Each measurement was repeated three times before averaging for each m/p ratio.

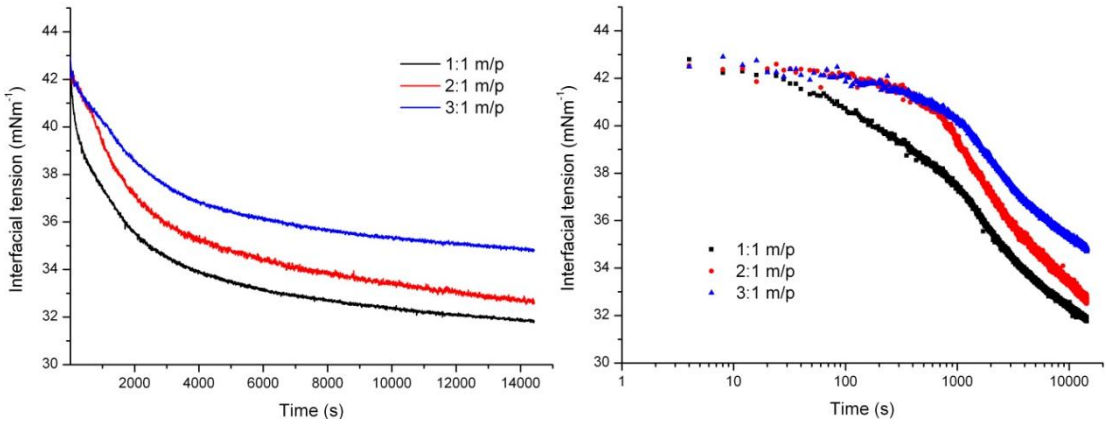

Figure 2.15 Interfacial tension as a function of time for a droplet of 0.1 wt% aqueous suspensions of Janus particles suspended in hexadecane as measured by droplet shape analysis. Three m/p ratios of particles (1:1 – TSGN-1-1, 2:1 – TSGN-2-1, 3:1 – TSGN-3-1) were measured. (left) linear scale, (right) logarithmic scale

Initially, for all samples, upon the formation of the droplet in the organic phase, interfacial tension drops rapidly owing to instantaneous absorption of Janus particles at the interface, depicted in figure 2.15 (left). As the exposed oil/water interface decreases, particle adsorption rate slows, trending towards a plateau value. The equilibrium interfacial tension attained by the system is affected by the hydrophobic : hydrophilic ratios of the Janus particles. Particles with the least hydrophobic content achieve the lowest surface free energy. Increasing the hydrophobic lobe ratio causes an increase in equilibrium interfacial tension. As the hydrophobic lobe size increases, although there is a slight increase in the displaced oil-water interface (reducing interfacial tension), the surface area from the hydrophobic hemisphere contributes a larger positive free energy (increasing interfacial tension).

When the temporal axis is presented logarithmically as in figure 2.15 (right), it is possible to see several transitions at approximately T = 2000 s whereby the rate of

change of interfacial tension suddenly alters. Transitions of this nature have been reported by our collaborators[16] who observed transitions when using polydisperse Janus 'discs' as solid stabilisers in similar experimental systems. The reasoning behind this effect pointed towards the rearrangement of discs at the liquid-liquid interface to optimise the packing efficiency. It could be possible for the Janus particles in our system to adopt a more efficient packing arrangement in correlation to this transition. In order to confirm a transition of this nature, visual representations of particles at an interface are required.

2.3.5 Crystalline behaviour of Janus particles

Owing to the interfacially active behaviour observed by the particle suspensions in the liquid-liquid system, we undertook experiments to visualise the condensed assembly of Janus particles at an interface or substrate. A simple method in order to accomplish this was to observe the arrangement of Janus particles dried onto a solid substrate, enabling the visualisation of particles by electron microscopy.

To investigate the assembly behaviour at flat interfaces, dilute aqueous solutions (0.01 wt%) of amphiphilic Janus particles were convectively assembled on to silicon wafers through a controlled drying process. Spherical latex particles are well known to spontaneously crystallise into 2-D and 3-D lattices, when appropriately monodisperse, usually adopting a hexagonal packing configuration; the most spatially efficient.

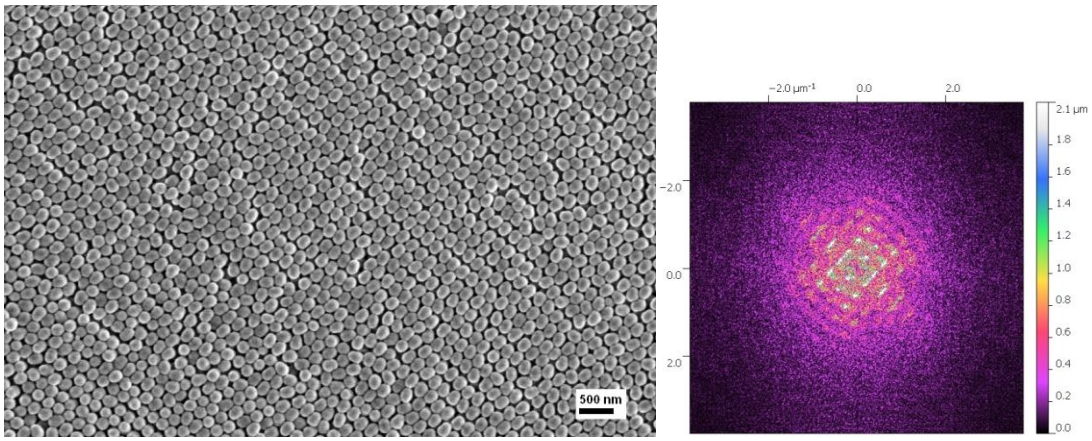

Figure 2.16 (l) FEG-SEM image of convectively assembled Janus particles of 2:1 m/p ratio. (r) Fast Fourier Transform analysis of the FEG-SEM image (TSGN-2-1)

All three hydrophilic : hydrophobic Janus particle ratios (1:1 – TSGN-1-1, 2:1 – TSGN-2-1, 3:1 – TSGN-3-1) were tested for any difference in packing behaviour, however all were observed to adopt similar crystalline packing arrangements, therefore one example is discussed here. Imaging of the silicon wafer under dry-SEM conditions revealed that the amphiphilic Janus particles adopted a crystalline packing arrangement with many crystal grains extending over several microns. Fast Fourier Transform (FFT) of this image indicates a clear spot pattern confirming an oblique lattice structure (figure 2.16). Many of the crystal grains are oriented in the direction of drying, whereby the hydrodynamic capillary force applied to the anisotropic particle aligns it longitudinally.

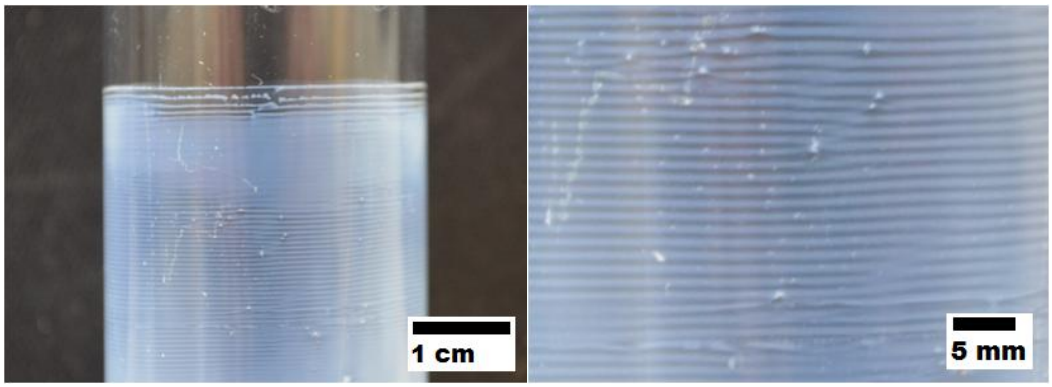

Figure 2.17 Photograph (l) and close up (r) of strata caused by drying effects on glass tube substrate during thermally assisted convective assembly of Janus particles (TSGN-2-1)

We observed the presence of 'pinning lines' on the sample, causing stratification of the crystalline arrays as seen in figure 2.17. At the drying pinning lines, the receding edge of the droplet in a drying system is halted by the favourable interactions with the surface, eventually when the air-water surface tension overcomes this interaction, the receding line moves rapidly to relax this force. This results in areas with high to low concentrations of solid particulate. Scanning electron microscopy was used to image the orientation of particles across these pinning lines. An overview of the particles across the pinning line by FEG-SEM is depicted in figure 2.18. A range of packing orders can be seen across the image, corresponding to the change in particulate concentration. These regions are marked A – D and their natural delineations are marked. The solid concentration is lowest at A, and increases to D. The drying direction is seen to proceed from right to left i.e. A to D in figure 2.18. The concentration gradient is dependent on the distance from the pinning line. Close to the pinning line (i.e. at region A), the droplet height is very small, allowing only a monolayer to form, whereas at distances further from the pinning line, the droplet height is larger, allowing the particles to orient out of

plane (region C) and ultimately form a bilayer (region D). This phenomena has been quantified by Perelaer *et al.*[56] when observing the respective positions of trimodal sized particles at the pinning line. It was found that smaller particles packed closer to the pinning line than larger particles which were restricted by droplet height. Higher magnification images of these regions were analysed to determine packing arrangements as seen in figure 2.19.

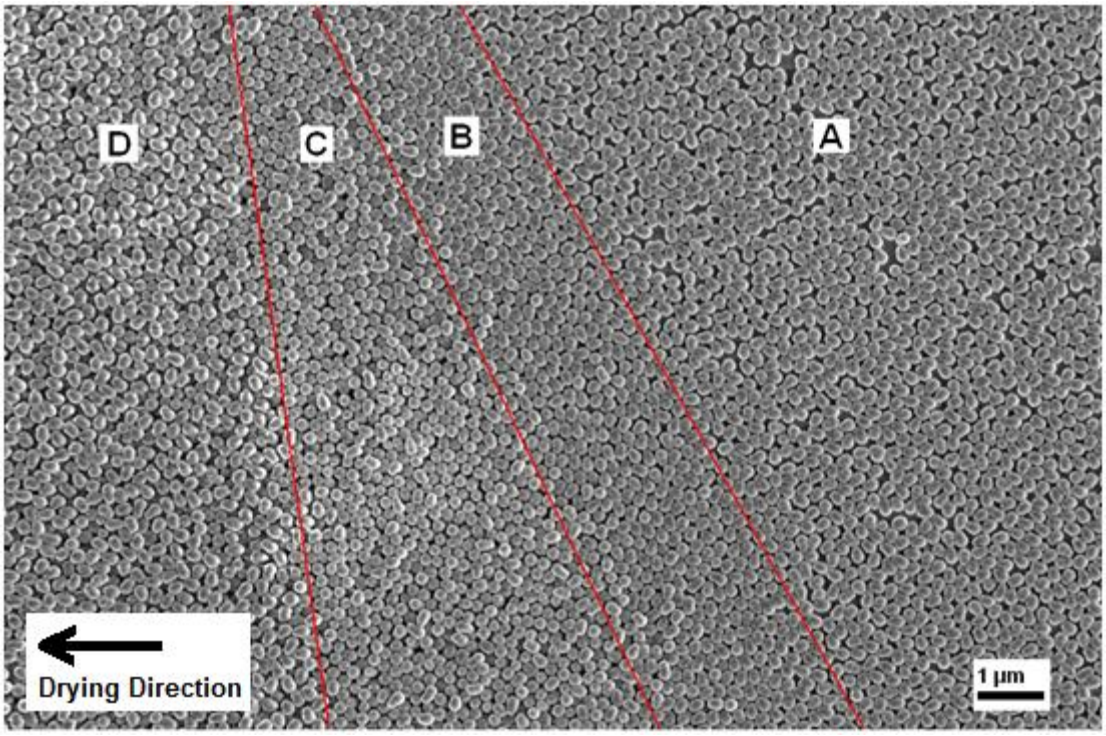

Figure 2.18 FEG-SEM image across a pinning line region of convectively assembled Janus particles (TSGN-2-1) on a silica substrate. Areas of different packing arrangements are indicated and delineated by red lines. The drying direction, i.e. direction of receeding droplet is indicated in the bottom left hand corner.

Areas of lower solid concentration as in region A there exists little structural order. The fast Fourier transform of this region mirrors this with no defined spot pattern. At region B, an oblique lattice is formed with all particles lying down in phase, a clear spot pattern is visible on the FFT for this region. As the concentration increases (C), in order to pack

the monolayer more efficiently, an out of plane configuration with hexagonal packing is formed. Further increasing the concentration causes a bi-layer to form. Particles are visible on two levels. This attains little structural order, both in the image and FFT.

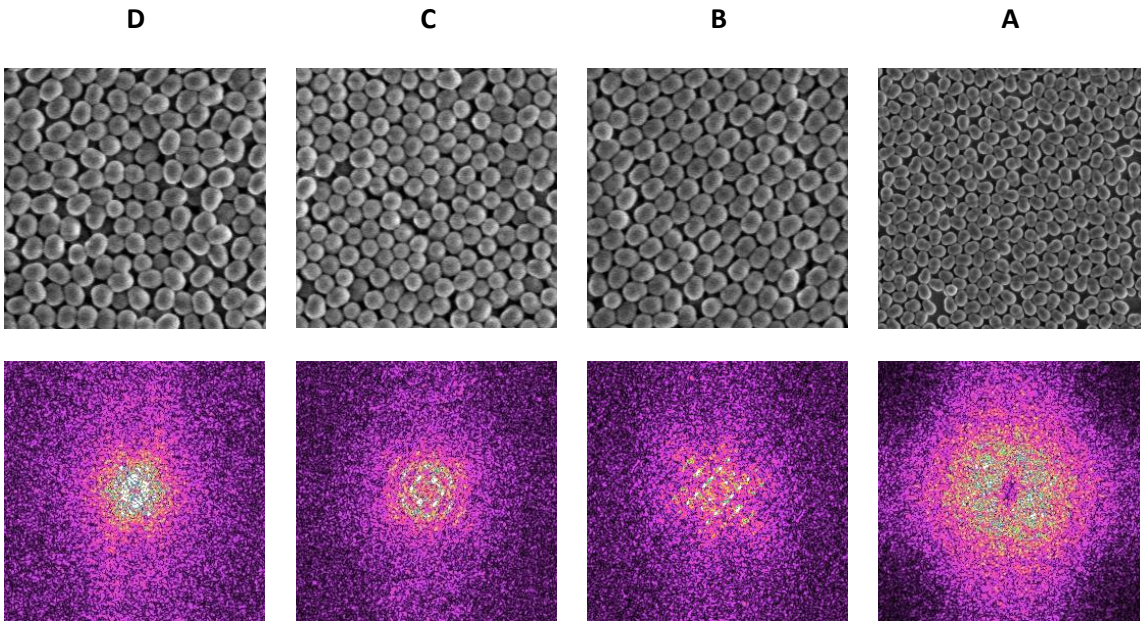

Figure 2.19 High magnification FEG-SEM images of the areas in fig. 2.18 with different packing orders, with associated FFT analysis below each image

As such we can infer that several packing configurations of the particles can occur depending on the concentration of the solution. Particles will alter packing configurations to mediate the solids concentration with the entropy required for higher packing efficiencies, i.e. from amorphous (A), oblique (B), to hexagonal (C), until an ordered monolayer is unsustainable, thereby forming an amorphous bilayer (D). This analysis correlates to the phase transitions observed during oil/water interfacial tension measurements and therefore a change in packing order could be a plausible reason for the effect. Results of a similar nature utilising Janus particles an order of magnitude larger were reported showing a linear dependence of layer thickness with respect to

particle concentration.[57] In another example, Janus particles possessing a silicate shell[41] on the hydrophilic lobe have been demonstrated to manufacture 3-D colloidal crystals with remarkable control have under the influence of an external electrical field.[58]

2.3.6 Foam stabilisation using Janus particles

In order to verify the presence of amphiphilic Janus particles at fluid interfaces, we analysed the structure of a foam generated by the incorporation of air into an aqueous suspension of Janus particles (TS255D), . Cryogenic scanning electron microscopy was used to image water/air foam stabilised solely by amphiphilic Janus particles. Dilute aqueous suspensions (1.0 wt%) of Janus particles were handshaken to generate a coarse foam, which in turn was rapidly frozen in liquid nitrogen prior to imaging under cryogenic conditions. Large spherical and elliptical air bubbles are clearly seen throughout the sample as seen in figure 2.20 and 2.21(r)

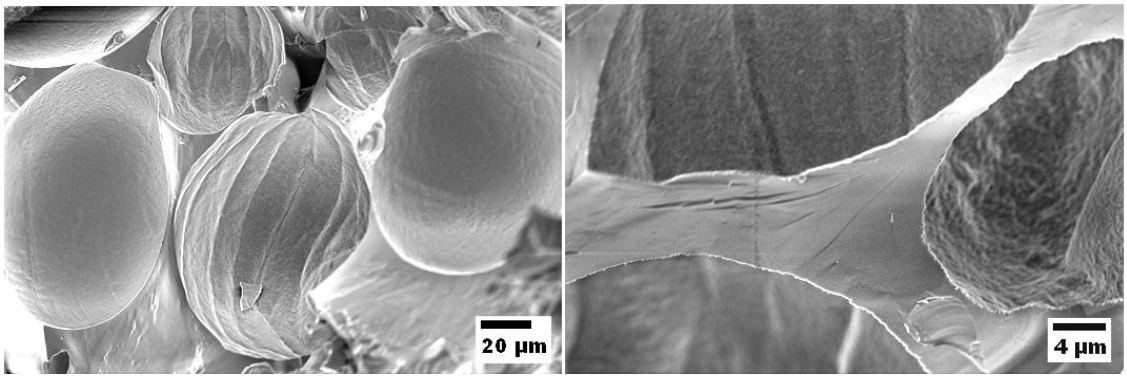

Figure 2.20 Cryo-SEM images of an aqueous foam stabilised by Janus particles (TS-255D). (l) a collection of bubbles in close proximity, note the bucking of the bubble caused by jamming of particles at the air-water interface. (r) Plateau-Rayleigh junction between three bubbles

Some bubbles reveal 'creases' formed during the freezing process as the air cooled, quickly reducing interfacial area. These creases indicate that the interface buckles rather than 'eject' particles to counter the reduction in interfacial area, giving an insight to the large energetic barrier to remove particles.

Higher magnification of the air/liquid interface reveals complete interfacial coverage by the particles as seen in figure 2.21(l). It is interesting to note that particles are not observed protruding from the bulk ice. The regular small blemishes on the ice surface are ice recrystallisation artifacts.

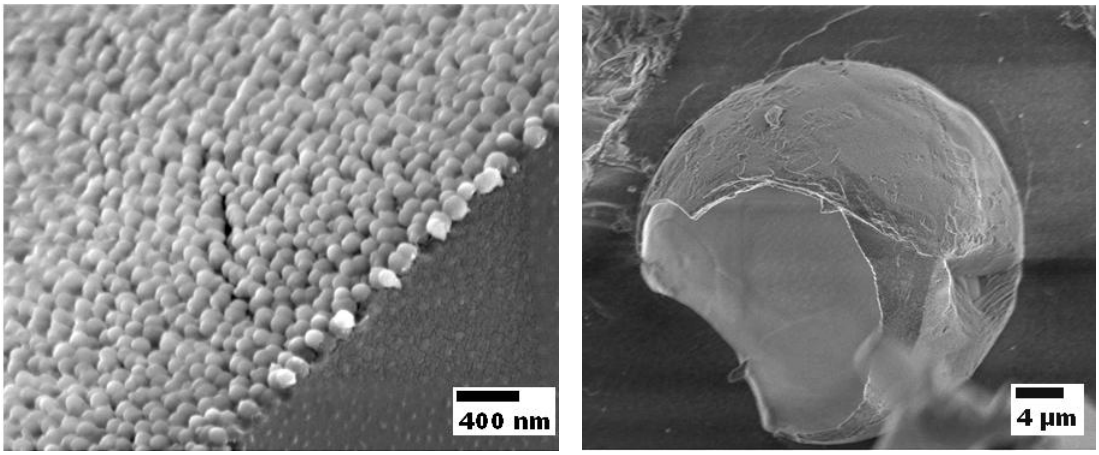

Figure 2.21 Cryo-SEM images of (l) close-up of the air-water interface revealing the location of the Janus particles (TS255D). (r) A bubble stabilised by Janus particles on both interfaces, enclosing a thin water film

It is not possible to comment upon the orientation of the particles based on this imaging technique due to the sublimation process which removes ice from the surface of the sample and therefore interferes with the orientation of the particles when ice in the interstitial sites is removed. However, we can confirm that the particles preferentially

absorb to the interface rather than reside in the bulk solution and require a very large force for removal i.e. the droplet would rather buckle than eject particles.

2.3.7 Ice crystal inhibition of Janus particles

Following from the concept that amphiphilic proteins and macromolecules exhibit ice crystal inhibition efficacy, we investigate the use of hydrophilic-hydrophobic Janus particles as biomimetic analogues for this purpose, as depicted schematically in figure 2.22. This is supported by the observed surface activity of the Janus particles and the observation of their presence in large concentrations at the air-water interface in a cryogenically frozen foam as discussed above.

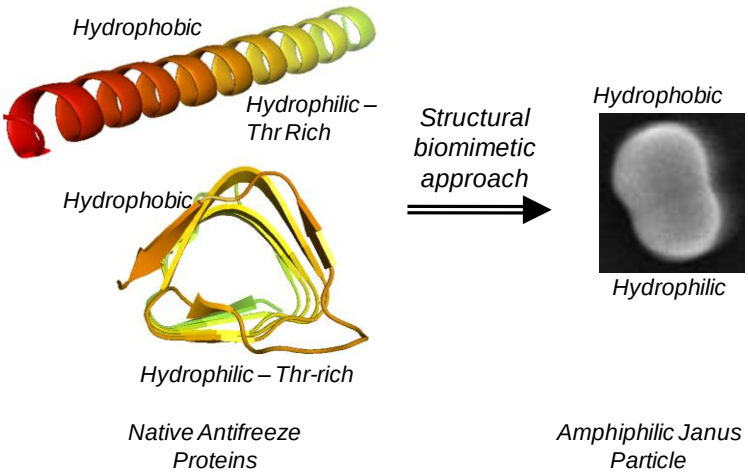

Figure 2.22 Schematic indicating how native antifreeze proteins assemble into quaternary amphiphilic structures and our bio-mimetic approach using polymeric Janus particles. SEM image from sample TS255D

Initially, a range of Janus particles with varying hydrophilic-hydrophobic ratios were fabricated in a similar synthetic procedure as outlined above. Pure aqueous suspensions of these particles at known concentrations were analysed for their ability to arrest ice crystal growth by means of a splat test assay. FEG-SEM images of these particles

alongside their hydrophobic volume and surface area percentage can be seen in figure 2.23. At this stage, it is more practical to quantify the hydrophilic : hydrophobic ratio in terms of percentage.

The splat test assay is a simple method to observe the recrystallisation of ice. A single droplet of the aqueous particle suspension is deposited onto a stage cooled to -50 °C from a height of 50 cm. The resulting droplet freezes quickly forming a wafer approximately 1 cm in diameter and 20 µm thick. Annealing of the wafer occurs at -6 °C over a period of 30 minutes, after which the ice crystals were imaged by optical microscopy to determine the mean largest grain size (MLGS).

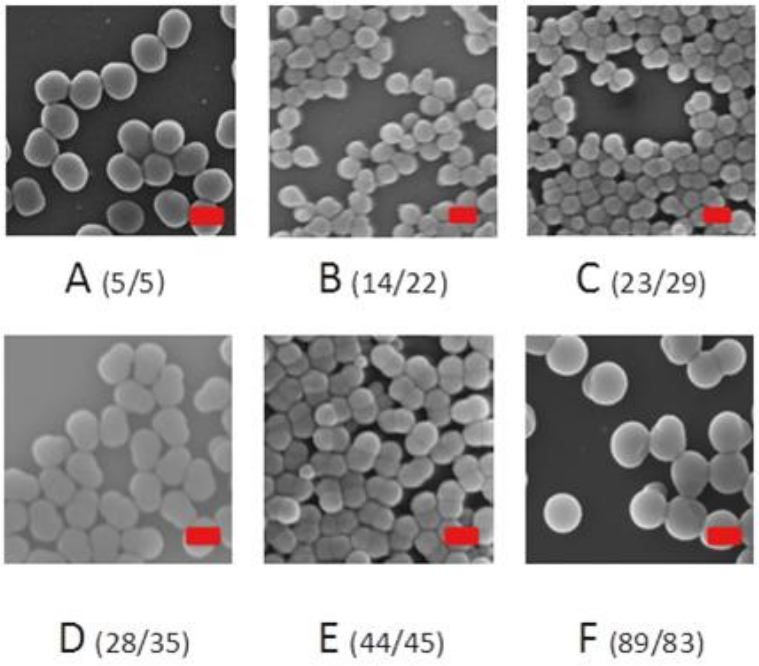

Figure 2.23 A range of Janus particles with varying hydrophilic: hydrophilic lobe ratios. (A: TSPS-24, B: TSSW 110, C: TSSW 219, D: TSSW 300, E: TSSW 298, F: TSSW 291) Numbers below each image represent volume and surface area % of hydrophobic parts respectively. These particles were used in the splat test assay Scale bars are 200 nm

The results of the splat test assay are presented in figure 2.24. Particles with increasing hydrophobic volume % exhibit the best ice crystal growth inhibition compared with Janus particles of less hydrophobic content. Additionally, there appears to be a maximum efficacy that the particles possess, that despite increasing particle concentration, results in a plateau of activity.

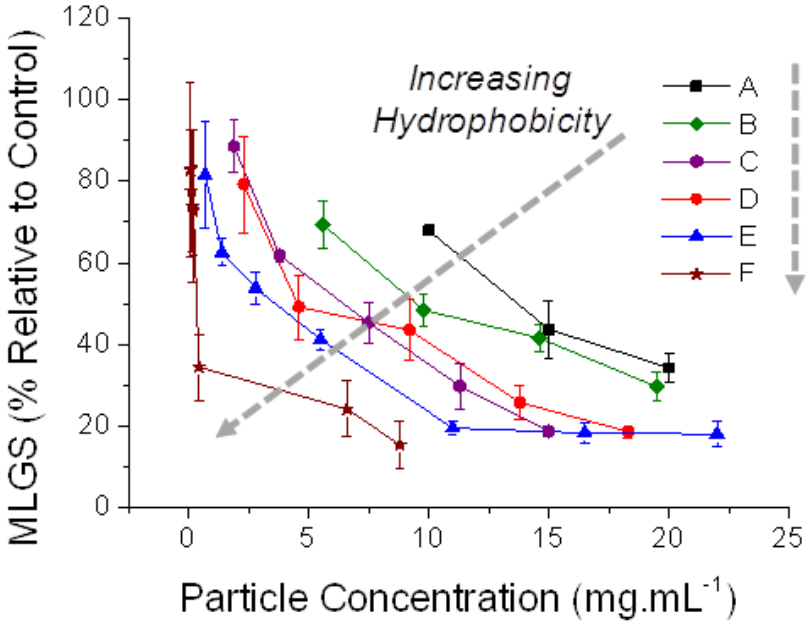

Figure 2.24 Results of the splat test assay with mean largest grain size (MLGS) plotted as a function of suspension concentration for a range of hydrophilic:hydrophobic ratios presented in figure 2.23

A plausible explanation for the increased efficacy at higher hydrophobic ratios is the magnitude of induced ice grain front curvature that the particle induces. Increasing the curvature of the ice grain front creates a larger exposed surface area and ultimately a decrease in freezing point owing to the Gibbs-Thompson effect. However, this is speculative until the direct observation of a particle at a growing ice front is studied.

When comparing efficacy of ice crystal inhibition of Janus particles compared with that of naturally occurring antifreeze proteins. The most active particle; sample 'F' with 89 vol% hydrophobicity completely arrested ice crystal growth at approximately 8 mg/mL solids concentration, whereas the hyperactive antifreeze protein from *Lolium perenne* inhibits ice grow at concentrations of 10 μg/mL.[6] Although the antifreeze protein exhibits a greater efficacy at ice crystal inhibition than our Janus particles, important factors to consider are the much higher costs associated with the bulk production of proteins compared with particles fabricated by emulsion polymerisation. In addition, our particles are more robust to extremes of environment conditions including pH and temperature which may well denature the anti-freeze protein.

2.4 Conclusions

We demonstrate a one-pot seeded emulsion polymerisation system to manufacture amphiphilic Janus particles on a bulk scale with the ability to tune relative hydrophilic : hydrophobic ratios. Despite being able to manufacture Janus particles in a significantly shorter timescale than other reported methods, the reaction yield is limited to 20 wt% total solids content owing to coagulation. However, the amphiphilic particles possess an affinity to adsorb to interfaces, as demonstrated by cryogenic electron microscopy and droplet shape analysis. These results indicate that the interfacial tension can be tuned by the variation of m/p ratio. The particles were also discovered to assume different packing geometries based on suspension concentration, explaining kinetic transitions observed in droplet shape analysis. Splat assay testing revealed that amphiphilic Janus particles are not as effective at ice crystal inhibition at equivalent concentrations to

naturally occurring antifreeze proteins. However, this disparity is offset by the significantly reduced manufacturing costs and resistance to extreme conditions that Janus particles possess over their protein counterparts. The ice crystal inhibition efficacy of the particles shows a dependence on hydrophilic : hydrophobic ratio, with the most hydrophobic exhibiting the greatest effect. Therefore, these particles have potential 'anti-freeze' applications in products sensitive to ice crystal growth provided that the manufacturing process is optimised to yield a higher solids content.

2.5 Experimental

2.5.1 Materials

Styrene (ReagentPlus, 99%), Divinylbenzene (mixture of *m* and *p* isomers, 80%), 2-Hydroxyethylmethacrylate (97%), Sodium 4-vinylbenzenesulfonate (90%) Poly (ethylene glycol) methacrylate (average M_n 500 $gmol^{-1}$), hexadecane (*ReagentPlus,* 99%) all supplied by Sigma Aldrich, UK. Azobisisobutyronitrile (97%, supplied by VWR, UK). Potassium Persulfate, (puriss 99%, Fluka, UK) were used as supplied. Monomers were filtered through a basic alumina column to remove inhibitors. Deionised water was filtered and purified to 18 $M\Omega cm^{-1}$.

2.5.2 Equipment

Electron microscopy

(Cryogenic) Scanning Electron Microscopy analyses were carried out using a Zeiss Supra 55-VP Field Emission Gun Scanning Electron Microscope with a Gatan Alto 2500 cryo transfer system and a Gatan C1002 liquid nitrogen cold stage.

'Dry'-SEM: Dilute aqueous dispersions of particles were cast on to silicon wafer and allowed to dry in ambient conditions. Wafer was adhered to aluminium stub with a double sided carbon tab and then carbon coated using carbon evaporator for 4 seconds. The prepared sample was imaged at 3 kV under high vacuum conditions.

'Cryo'-SEM: Dilute foam suspension was drawn into a brass rivet and cooled in liquid nitrogen. Samples were fractured by cold scalpel to reveal clean surface. After, sample was heated to −90 °C under high vacuum for 10 minutes to remove contaminant ice through sublimation followed by platinum sputter target coating in an argon atmosphere (20 seconds, 10 mA). Imaging was undertaken at −120 °C using a 3 kV accelerating voltage with a gold anti-contaminator at −189 °C.

Dynamic light scattering

Malvern instruments Zetasizer ZS, (Malvern, UK). Dilute 1 mL aqueous dispersions of particles were dispensed into plastic cuvettes and thermally equilibrated to 25 °C prior to the measurement of 3 sets of measurements, each of 10 subruns using a 173° backscattering angle.

Convective assembly

Janus particles as purified by dialysis were dispersed by ultrasound into 18 $M\Omega cm^{-1}$ deionised water at 0.01, 0.1 and 1 wt% solids content. Pristine slivers of silicon water placed diagonally in open topped vials were submerged with the dilute suspensions and placed into a high precision temperature controlled oven at 60 °C and left undisturbed until oven humidity returned to ambient. Silicon wafers were removed, carbon coated by 3 x 2 second cycles of the carbon evaporator before imaging in dry SEM conditions at 3

kV. Images were processed in ImageJ[59] before using open source image analysis software Gwyddion[60] to compute FFT.

Droplet shape analyser

Using a DSA-100 with peltier controlled temperature stage (Kruss, Germany), dilute suspensions of Janus particles were prepared in 18 $M\Omega cm^{-1}$ deionised water pre saturated in hexadecane. A single 10 µL pendant droplet was formed from a 1.83 µm diameter flat-top needle in hexane pre saturated with water and thermally stabilised at 25 °C in a sealed peltier humidity chamber. T_0 was set to droplet formation in the organic phase. DSA software captured an image once every 5 seconds for 16000 seconds using axisymmetric profile analysis to compute interfacial tension recorded as a function of time based on predefined interfacial tension values for hexadecane/water surface free energy being input.

Splat test assay

An Olympus CX41 microscope equipped with a UIS-2 20x/0.45/∞/0-2/FN22 lens (Olympus Ltd., Southend on sea, UK) and a Canon EOS 500D SLR digital camera were used to obtain all images. For cryomicroscopy a nanolitre osmometer (Otago Osmometers Ltd, Dunedin, New Zealand) was used to provide a constant annealing temperature. Determination of ice crystal inhibition activity was achieved using a modified "splat" assay. A 10 µL droplet of the analyte solution in saline solution ([NaCl] = 0.5 $mg.mL^{-1}$ was expelled at a fixed height of 2 m onto a glass coverslip placed upon a pre-cooled (CO_2(s)) aluminium plate. This was immediately transferred onto the pre-cooled microscope stage (-6 °C) and left to anneal for 30 minutes.

Photographs of the wafer were taken at both 0 and 30 minutes through crossed polarisers. A large number of the ice crystals (>30) were then measured to find the largest grain size dimension along any axis. The average largest value from 3 individual photographs was calculated to give the mean largest grain size (MLGS). Reported errors are the coefficient of variation (standard deviation/mean) from a minimum of 3 individual data sets. Values are reported as the MLGS relative to that obtained for PBS alone.

2.5.3 Emulsion polymerisation

Seed particle synthesis

Deionised water and 4-vinylbenzenesulfonate was charged to a 250 mL single jacketed reactor (Radleys Reactor Duo, overhead mechanical blade type PTFE coated stirrer at 250 rpm and Julbo heater recirculator) and purged with nitrogen stirring for 45 mins prior to the addition of the remaining monomers (see table 2.1). Degassing was continued for a further 15 minutes prior to heating to polymerisation temperature (70 or 80 °C), when thermally stable, potassium persulfate (1 wt % w/r to monomer) dissolved in 1 mL degassed deionised water is injected into the system. Polymerisation ensues for 6 hours. In order to measure kinetics, 2 mL aliquots of the continuous phase were extracted from the reactor periodically, cooled on ice and aerated to quench polymerisation before analysis by gravimetry and dynamic light scattering.

Seed Emulsion Polymerisation	Mass
Water	96 g
Styrene	3.88 g
Divinylbenzene	0.04 g
2-Hydroxyethyl methacrylate	0.05 g
Sodium styrene sulfonate	0.02 g
Potassium Persulfate	0.05 g

Table 2.1 List of chemicals required to render seed particle latex

Swelling step

After allocated polymerisation time, the seed latex is rapidly cooled to room temperature and charged with an AIBN, styrene and divinylbenzene solution according to table 2.2. After a further 15 minute nitrogen purge, reactor is sealed, and stirred for 120 minutes at 25 °C to swell particles. Following the swelling period, reactor is heated to 70 °C for 8 hours.

Seeded Polymerisation	1:1	2:1	3:1
Styrene	3.96 g	7.92 g	11.88 g
AIBN	0.04 g	0.08 g	0.12 g

Table 2.2 List of chemicals required for seeded emulsion polymerisation with different m/p ratios

Reaction kinetics

In both seed particle and seeded emulsion polymerisations, reaction kinetics were followed by gravimetry and particle size analysis. In a typical procedure, 2 mL aliquots

of continuous phase were extracted from the reaction vessel at fixed time intervals and cooled on ice. Conversion was ascertained gravimetrically, alongside evolution of particle size by DLS.

2.6 References

(1) Fowler, A.; Toner, M. *Annals of the New York Academy of Sciences* **2005**, *1066*, 119–135.

(2) Han, B.; Bischof, J. C. *Cryobiology* **2004**, *48*, 8–21.

(3) Colard, C. A. L.; Cave, R. A.; Grossiord, N.; Covington, J. A.; Bon, S. A. F. *Advanced Materials* **2009**, *21*, 2894–2898.

(4) Griffith, M.; Ewart, K. V. *Biotechnology Advances* **1995**, *13*, 375–402.

(5) Harding, M. M.; Anderberg, P. I.; Haymet, A. D. J. *European journal of biochemistry* **2003**, *270*, 1381–1392.

(6) Sidebottom, C.; Buckley, S.; Pudney, P.; Twigg, S.; Jarman, C.; Holt, C.; Telford, J.; McArthur, A.; Worrall, D.; Hubbard, R.; Lillford, P. *Nature* **2000**, *406*, 256–256.

(7) Gibson, M. I. *Polymer Chemistry* **2010**, *1*, 1141–1152.

(8) Gibson, M. I.; Barker, C. A.; Spain, S. G.; Albertin, L.; Cameron, N. R. *Biomacromolecules* **2009**, *10*, 328–333.

(9) Congdon, T.; Notman, R.; Gibson, M. I. *Biomacromolecules* **2013**, *14*, 1578–1586.

(10) Tam, R. Y.; Rowley, C. N.; Petrov, I.; Zhang, T.; Afagh, N. A.; Woo, T. K.; Ben, R. N. *Journal of the American Chemical Society* **2009**, *131*, 15745–53.

(11) Tachibana, Y.; Fletcher, G. L.; Fujitani, N.; Tsuda, S.; Monde, K.; Nishimura, S.-I. *Angewandte Chemie* **2004**, *43*, 856–862.

(12) Mizrahy, O.; Bar-Dolev, M.; Guy, S.; Braslavsky, I. *PloS one* **2013**, *8*, e59540.

(13) Sönnichsen, F. D.; DeLuca, C. I.; Davies, P. L.; Sykes, B. D. *Structure* **1996**, *4*, 1325–1337.

(14) Deville, S.; Viazzi, C.; Guizard, C. *Langmuir* **2012**, *28*, 14892–14898.

(15) Raymond, J. a; DeVries, a L. *Proceedings of the National Academy of Sciences* **1977**, *74*, 2589–2593.

(16) Ruhland, T. M.; Gröschel, A. H.; Ballard, N.; Skelhon, T. S.; Walther, A.; Müller, A. H. E.; Bon, S. A. F. *Langmuir* **2013**, *29*, 1388–1394.

(17) Park, B. J.; Lee, D. *ACS nano* **2012**, *6*, 782–790.

(18) Granciot, R.; Williams, D. J.; Engineering, C. *Polymer* **1970**, *8*, 2617–2629.

(19) Hughes, L. J.; Brown, G. L. *Journal of Applied Polymer Science* **1961**, *5*, 580–588.

(20) Colver, P. J.; Colard, C. a L.; Bon, S. A. F. *Journal of the American Chemical Society* **2008**, *130*, 16850–16851.

(21) Teixeira, R. F. A.; McKenzie, H. S.; Boyd, A. A.; Bon, S. A. F. *Macromolecules* **2011**, *44*, 7415–7422.

(22) Min, K.; Gao, H.; Yoon, J. A.; Wu, W.; Kowalewski, T.; Matyjaszewski, K. *Macromolecules* **2009**, *42*, 1597–1603.

(23) McDonald, C. J.; Devon, M. J. *Advances in colloid and interface science* **2002**, *99*, 181–213.

(24) Qian, J. Y.; Pearson, R. A.; Dimonie, V. L.; El-Aasser, M. S. *Journal of Applied Polymer Science* **1995**, *58*, 439–448.

(25) Wang, T.; Colver, P. J.; Bon, S. A. F.; Keddie, J. L. *Soft Matter* **2009**, *5*, 3842–3849.

(26) Fujii, S.; Mochizuki, M.; Aono, K.; Hamasaki, S.; Murakami, R.; Nakamura, Y. *Langmuir* **2011**, *27*, 12902–12909.

(27) Kowalski, A.; Vogel, M.; Blankenship, R. M. Multistage polymer particles, aqueous dispersions of these particles, films, compositions for coating and/or impregnating, multistage polymers and their use. European Patent 0022633 A3, January 21, 1981.

(28) Sheu, H. R.; El-Aasser, M. S.; Vanderhoff, J. W. *Journal of Polymer Science Part A: Polymer Chemistry* **1990**, *28*, 653–667.

(29) Sheu, H. R.; Vanderhoff, J. W. *Journal of Polymer Science Part A: Polymer Chemistry* **1990**, *28*, 629–651.

(30) Flory, P. J. *The Journal of Chemical Physics* **1941**, *9*, 660–660.

(31) Flory, P. J.; Rehner, J. *The Journal of Chemical Physics* **1943**, *11*, 521–527.

(32) Morton, M.; Kaizerman, S.; Altier, M. W. *Journal of Colloid Science* **1954**, *9*, 300–312.

(33) Waters, J. A. *Colloids and Surfaces A* **1993**, *83*, 167–174.

(34) Mock, E.; Bruyn, H. De; Hawkett, B.; Gilbert, R. *Langmuir* **2006**, 4037–4043.

(35) Kim, J.; Larsen, R. J.; Weitz, D. A. *Synthesis* **2006**, 14374–14377.

(36) Kim, J.-W.; Larsen, R. J.; Weitz, D. A. *Advanced Materials* **2007**, *19*, 2005–2009.

(37) Yang, M.; Wang, G.; Ma, H. *Chemical communications* **2011**, *47*, 911–913.

(38) Mock, E. B.; Zukoski, C. F. *Langmuir* **2010**, *26*, 13747–13750.

(39) Pan, M.; Yang, L.; Guan, B.; Lu, M.; Zhong, G.; Zhu, L. *Soft Matter* **2011**, *7*, 11187–11193.

(40) Chu, F.; Siebenbürger, M.; Polzer, F.; Stolze, C.; Kaiser, J.; Hoffmann, M.; Heptner, N.; Dzubiella, J.; Drechsler, M.; Lu, Y.; Ballauff, M. *Macromolecular rapid communications* **2012**, 1–7.

(41) Park, J.-G.; Forster, J. D.; Dufresne, E. R. *Journal of the American Chemical Society* **2010**, *132*, 5960–5961.

(42) Okubo, M.; Yamamoto, Y.; Kamei, S. *Colloid & Polymer Science* **1989**, *267*, 861–865.

(43) Okubo, M.; Suzuki, T.; Fukuhara, Y. *Colloid and Polymer Science* **2003**, *281*, 569–574.

(44) Xu, X.-J.; Siow, K.-S.; Wong, M.-K.; Gan, L.-M. *Journal of Polymer Science Part A* **2001**, *39*, 1634–1645.

(45) Goodall, A. R.; Wilkinson, M. C.; Hearn, J. *Journal of Polymer Science: Polymer Chemistry Edition* **1977**, *15*, 2193–2218.

(46) Kim, J. H.; Chainey, M.; El-Aasser, M. S.; Vanderhoff, J. W. *Journal of Polymer Science Part A* **1992**, *30*, 171–183.

(47) Al Zahrini, A. Ph.D. Thesis, University of Warwick, 2011.

(48) Qin, D.; Lian, G.; Qin, S.; Ford, W. T. *Langmuir* **2010**, *26*, 6256–61.

(49) Chen, S.-A.; Chang, H.-S. *Journal of Polymer Science Part A: Polymer Chemistry* **1990**, *28*, 2547–2561.

(50) Gilbert, R. G. *Emulsion Polymerization: A Mechanistic Approach*; 1st ed.; Academic Press: London, 1995.

(51) Van der Zeeuw, E. A.; Sagis, L. M. C.; Koper, G. J. M. *Macromolecules* **1996**, *29*, 801–803.

(52) Butterworth, S. Ph.D. Thesis, University of Manchester, 2013.

(53) Kraft, D. J.; Vlug, W. S.; Van Kats, C. M.; Van Blaaderen, A.; Imhof, A.; Kegel, W. K. *Journal of the American Chemical Society* **2009**, *131*, 1182–1186.

(54) Wu, D.; Hornof, V. *Chemical Engineering Communications* **1999**, *172*, 85–106.

(55) Kutuzov, S.; He, J.; Tangirala, R.; Emrick, T.; Russell, T. P.; Böker, A. *Physical chemistry chemical physics* **2007**, *9*, 6351–6358.

(56) Perelaer, J.; Smith, P. J.; Hendriks, C. E.; Van den Berg, A. M. J.; Schubert, U. S. *Soft Matter* **2008**, *4*, 1072–1078.

(57) Hosein, I. D.; Liddell, C. M. *Langmuir* **2007**, *23*, 10479–10485.

(58) Forster, J. D.; Park, J.-G.; Mittal, M.; Noh, H.; Schreck, C. F.; O'Hern, C. S.; Cao, H.; Furst, E. M.; Dufresne, E. R. *ACS nano* **2011**, *5*, 6695–700.

(59) Schneider, C. A.; Rasband, W. S.; Eliceiri, K. W. *Nature Methods* **2012**, *9*, 671–675.

(60) Nečas, D.; Klapetek, P. *Central European Journal of Physics* **2011**, *10*, 181–188.

Chapter 3

Synthesis of 'hard-soft' Janus particles by seeded dispersion polymerisation

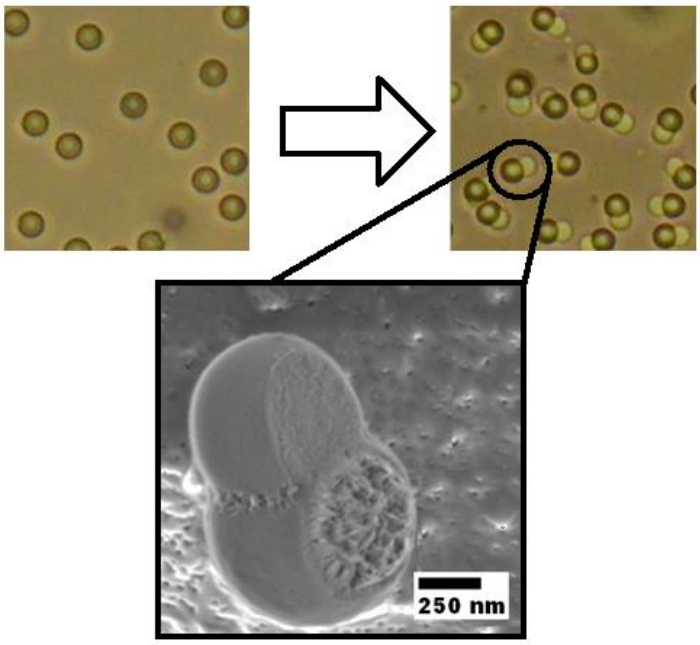

3.1 Abstract

This chapter concerns the synthesis of 'hard-soft' bi-phasic Janus particles with distinct lobes of 'soft' poly(*n*-butyl acrylate) and 'hard' poly(styrene) by a seeded dispersion polymerisation of butyl acrylate in the presence of poly(styrene) seed particles. Surface nucleation by capture of the oligoradicals onto the surface of the seed particles hereby forming a distinct new polymer phase is found to be the formation. The total available poly(styrene) seed surface area plays a significant role in the size and number of poly(butyl acrylate) lobes grown off a single particle. At particularly low values for the surface area, we observe the formation of multi-lobe particles. We show that our

synthesis method can be transferred to the sub-micron domain by using seed particles of 200 nm in diameter. It is thought our hard-soft Janus particles will have potential applications in the field of directional adhesion and wet deposition onto substrates by using the 'soft' phase as an adhesive patch.

3.2 Introduction

3.2.1 'Hard-soft' Janus particles

In the previous chapter we demonstrated how seeded emulsion polymerisation was used effectively to manufacture amphiphilic Janus particles using a technique pioneered by Sheu *et al.*[1,2] This is one of many examples of anisotropic Janus particles made via seeded emulsion polymerisation demonstrating its highly versatile nature. Despite the recent focus on *amphiphilic* Janus particles; there is scope towards the investigation of particles with alternative chemical and functional properties.

In particular we are interested in dumbbell shaped Janus particles possessing distinctive high and low glass transition temperature lobes respectively, so named 'hard-soft' Janus particles. Owing to wide differences of material behaviour at each 'end' of the particle; the ability for one lobe to deform under ambient conditions whilst the other remains a robust and solid entity presents an attractive research direction in the field of Janus particles. As the soft lobe can deform and coalesce on contact with a substrate, it could be seen as an adhesive patch. Therefore, Janus particles of this morphology possess directional adhesion whilst leaving the hard phase surface chemistry exposed. This improves upon the existing unidirectional adhesion and total surface coverage of hard-

soft core-shell counterparts. As such, 'hard-soft' Janus particles have been investigated in the field of wet deposition for hair care applications utilising the soft phase for adhesion and hard phase to impart functions beneficial to consumer experience.[3] In order to manufacture particles of this geometry, a seeded emulsion polymerisation system would seem an obvious choice.

3.2.2 Synthesis of hard-soft Janus by seeded emulsion polymerisation

During the 1980's, several groups reported the anomalous particle morphologies obtained when conducting emulsion polymerisations of acrylate monomers in the presence of seed particles. In particular, the emulsion polymerisation of styrene in the presence of a butyl acrylate seed particles[4–6] or inversely, the emulsion polymerisation of poly(butyl acrylate) in the presence of poly(styrene) seed particles.[7–9] The homo-polymers of styrene and butyl acrylate possess widely varying glass transition temperatures of +105 °C[10] and -54 °C[11] respectively. Therefore composite core-shell latex particles of these polymers, either possessing a hard (high T_g) core and soft (low T_g) shell or inversely a soft core and hard shell find applications as strengthening agents[12] and impact modifiers[13] in films, coatings and adhesives. However, instead of the formation of a core-shell morphology, many resultant seeded polymerisation particles additionally exhibited anomalous morphology in the form of 'raspberry', 'half-moon'[6] and 'dumbbell'[5] shaped morphologies. This effect is ascribed to 'phase separation' whereby seed particles swollen with the secondary monomer phase separate within the particle into distinct polymer and a secondary polymer domain upon polymerisation. This arises from the development of polymer/polymer incompatibility over the course of the reaction. In order to mediate the new interfacial tension formed within the particle, the morphology changes to minimise

this energy. The deciding factor between the observed geometries relies on the relative surface tensions between the two polymer phases, and the interfacial tension between each polymer and the continuous phase.[14] The surface charge arising from surfactants[6] and initiator residues[15] at surface of the particles also influences these surface energies and plays a role in deciding particle morphology. As a result, prediction of particle morphology is challenging and highly sensitive to a variety of experimental factors when attempting to make structured particles by seeded emulsion polymerisation of incompatible polymers.

Using a different approach of seeded emulsion polymerisation: entropic phase separation of a secondary compatible 'soft' polymer lobe from a crosslinked polymer matrix has been attempted using N-isopropylacrylamide (NIPAM) and poly(styrene) seed particles by Mock *et al.*[16] In order to aid the phase separation of NIPAM from poly(styrene), the seed particles are swollen with NIPAM and toluene. Upon heating, the toluene and NIPAM phase separate and propagates in the extruded droplet. However, high resolution scanning electron micrographs of these particles reveal that the p(NIPAM) protrusion is not well defined and that much of the p(NIPAM) has encapsulated the seed particle due to the soft hydrophilic nature of the p(NIPAM) enveloping the hydrophobic poly(styrene) seed over time.

Essentially, seeded emulsion polymerisation is a challenging technique as a route to synthesise controlled Janus particle structures and many problems arise from the swelling of the seed particles with the secondary monomer. Additionally, emulsion

polymerisations are also limited by size whereby particles exceeding 1 µm in diameter are challenging to manufacture, unless successive seeded emulsion polymerisations are used, requiring multiple polymerisation steps to form a batch of micron sized particles. Often micron-sized structured particles are desired in certain applications. For instance functionalised poly(styrene-co-divinylbenzene) particles used in ion exchange[17] or protein recovery chromatographic applications.[18]

Other methods have been proven to manufacture larger micron sized structured particles, including the emulsion polymerisation of a seed particle made by dispersion polymerisation[19] and the dynamic swelling method.[20,21] An effective route towards anisotropic polymeric particles is seeded dispersion polymerisation.

3.2.3 Seeded dispersion polymerisation

Seeded dispersion polymerisation has been used effectively to synthesise particles of varying morphology. One of the motivating factors for synthesising Janus particles by this method is the lack of swelling of the seed particles. In a dispersion polymerisation system, the monomers are completely soluble in the continuous phase and generally do not swell the seed particles. This eliminates problems arising from the phase separation within seed particles. Additionally, the non-aqueous environment of the continuous phase also reduces the influence of charged residues from surfactants, initiators or charged co-monomers on final particle morphology. Instead, hydrophobicity of the continuous phase plays a role on particle geometry: As depicted in figure 3.1(a); Fujibayashi and co workers[22] demonstrate an impressive example of how seeded dispersion polymerisations of 2-ethylhexylmethacrylate in the presence of poly(styrene) seed particles and various

organic hydrocarbon solvents can yield a variety of particle morphologies at different polymer conversions. In figure 3.1(b), Okubo *et al.*[23] fabricate 'snowman' shaped particles through the seeded dispersion polymerisation of butyl methacrylate with micron sized poly(styrene) seeds. Interestingly particles with a single 'lobe' were generated with smaller seed particles of 1.28 μm diameter, whereas 'confetti' particles possessing multiple lobes from single seed particle were found to form when a larger seed particle of 2.67 μm diameter was used. This difference in morphology was attributed to the absorption of multiple radical oligomers onto larger particles. Figure 3.1(c) depicts 'raspberry' textured spherical particles synthesised through a seeded dispersion polymerisation of methyl methacrylate with a poly(methyl methacrylate) seed particle dispersion reported by Shi *et al.*[24] In this case, the formation mechanism of the textured surface was found to be kinetically controlled. After heating the textured particles in their native reaction solvent of methanol, the particles were found to attain a smooth spherical surface. Therefore, the textured surface was proposed to have been formed by the capture of oligomeric radicals on the particle surface which in turn underwent propagation from the adsorption of MMA from the continuous phase.

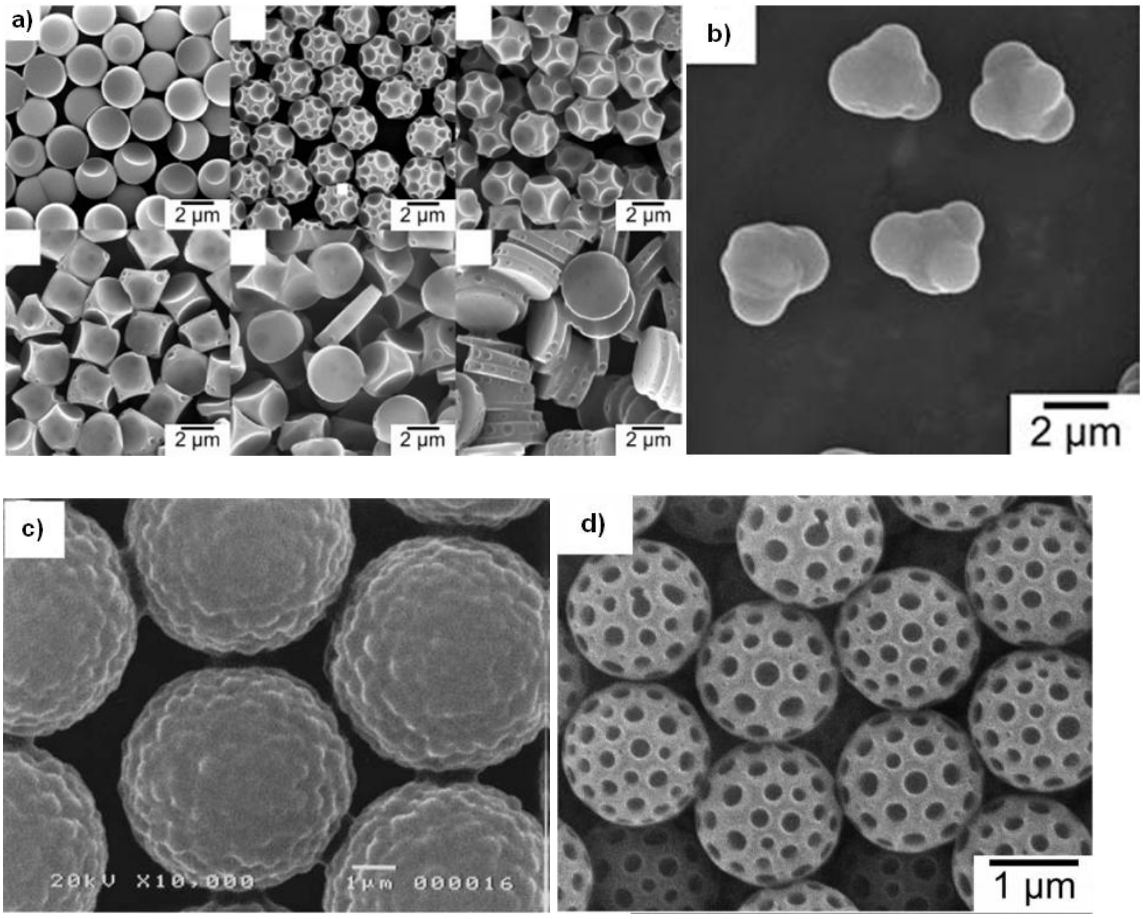

Figure 3.1 (a) seeded dispersion polymerisation of 2-Ethylhexyl methacrylate in the presence of poly(styrene) seed particles and various organic solvents.[22] **(b)** seeded dispersion polymerisation of BMA in the presence of poly(styrene) seed particles.[23] **(c)** Seeded dispersion polymerisation of MMA with p(MMA) seeds.[24] **(d)** seeded dispersion polymerisation of BMA in the presence of poly(styrene-co-styrene sulfonate) and dodecane[25]

In a further example, Fujibayashi *et al.*[25] conducted a seeded dispersion polymerisation of butyl methacrylate in the presence of a poly(styrene-co-sodium styrene sulfonate) seed particles and dodecane droplets. Post polymerisation, the dodecane was evaporated leaving dimples in the surface of the micron sized particles as seen in figure 3.1(d) to resemble 'golf balls'.

In a non-seeded dispersion polymerisation, the final particle size can be controlled by altering the reaction parameters such as monomer and surfactant concentration as well as the relative hydrophobicity of the solution phase.[26] Seeded dispersion polymerisations are equally affected by these factors, and can induce changes in morphology. For instance the various shapes demonstrated by Fujibayashi *et al.*[22] in figure 3.1(a) were manufactured by altering the hydrophobicity of the solution phase. Alternatively the pore size of the 'golf-ball' particles depicted in figure 3.1(d) is controlled by the concentration of co-solvent dodecane present during the polymerisation.[25] Therefore final particle size and morphology can be tuned in seeded dispersion techniques.

3.2.4 Synthesis of hard-soft Janus by seeded dispersion polymerisation

As aforementioned, styrene and butyl acrylate have widely varying glass transition temperatures. They have also been proven to successfully polymerise in dispersive conditions to render monodisperse particles of micron dimensions.[26,27] Therefore, both monomers are ideal for our purpose. Incorporating these two monomers, one study investigates the seeded dispersion polymerisation of butyl acrylate and styrene in the presence of poly(butyl acrylate), poly(styrene) and poly(butyl acrylate-co-styrene) seed particles, manufacturing particles of varied geometries and compositions.[28]

In one particular example of this work, the seeded dispersion polymerisation of butyl acrylate in the presence of a poly(styrene) seed under alcoholic conditions using poly(vinyl pyrrolidone) as a protective colloid rendered biphasic micron sized 'Janus' particles consisting of a singular poly(butyl acrylate) lobe grown off poly(styrene) seed

particles, an example of which can be seen in figure 3.2. The surface of poly(styrene) seed particles grafted with a layer of steric surfactant provide the locus of nucleation for butyl acrylate.

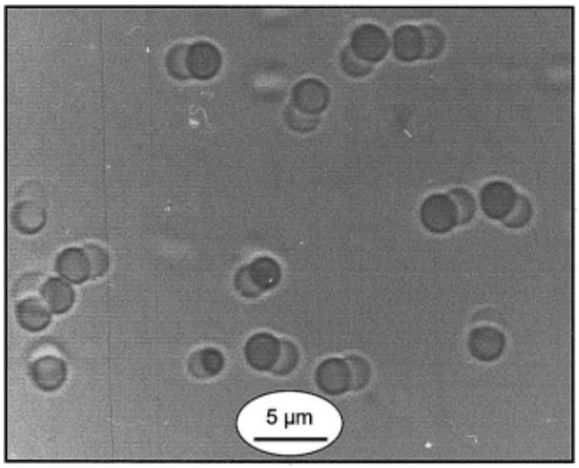

Figure 3.2 Optical micrograph of poly(styrene)/poly(butyl acrylate) Janus particles reported by Wang *et al.*[28]

This example demonstrates an ideal route to form particles of our desired geometry and properties. However, this work was briefly reported, detailing only the observation of particle geometry (figure 3.2) and fails to discuss the formation mechanism and effect of seed particle concentration on the reaction kinetics and particle morphology. As such, we aim to further investigate the mechanism and kinetics of this seeded dispersion polymerisation system and intend to develop it to allow tuning of particle and respective lobe size. Additionally, we explore an adaptation of this polymerisation system to enable the synthesis of sub-micron hard-soft Janus particles.

3.3 Results and discussion

3.3.1 Synthesis of micron sized hard-soft Janus particles

The synthetic procedure to fabricate 'hard-soft' Janus particles involves a two-step reaction. Micron sized poly(styrene) seed particles are made initially through a dispersion polymerisation in methanol. After this a seeded dispersion polymerisation of butyl acrylate in the presence of these seed particles in a methanol-water medium renders a singular lobe of poly(butyl acrylate) on the surface of the poly(styrene) seed particle.

Initially polystyrene seed particles were synthesised via a dispersion polymerisation procedure[26] in methanol to make spherical particles of 2.5 µm average diameter and a monodisperse size distribution. A typical procedure involves the batch addition of styrene, poly(vinyl pyrrolidone) K90 (PVP, 360,000 $gmol^{-1}$) as protective colloid, thermal radical initiator AIBN and methanol as the continuous phase into a sealed, stirred reaction flask. The PVP content was fixed at 5.5 wt% w/r to styrene, AIBN 1 wt% w/r to styrene and a monomer content of 26 wt% w/r to methanol. The reaction mixture was purged with nitrogen before initiation by heating to 70 ℃. After conducting the polymerisation for 24 hours, the dispersion was cleaned by centrifugation at 7882 *g* for 10 minutes and re-dispersed into fresh methanol to remove excess PVP in the continuous phase. The remaining solids content, deemed mostly PVP, in the continuous phase after polymerisation was found to be 3.21 wt% as determined by gravimetric analysis of the first supernatant from centrifugation purification. Final monomer conversions of seed particle dispersion polymerisations exceeded 95% as determined by gravimetry before

centrifugation. The supernatant after the first sedimentation of seed latex was transparent indicating the absence of sub 500 nm diameter secondary nucleated particles given the speed and duration of centrifugation. The resulting particles can be seen optically in figure 3.3 alongside the laser scattering analysis in methanol revealing a monomodal size distribution.

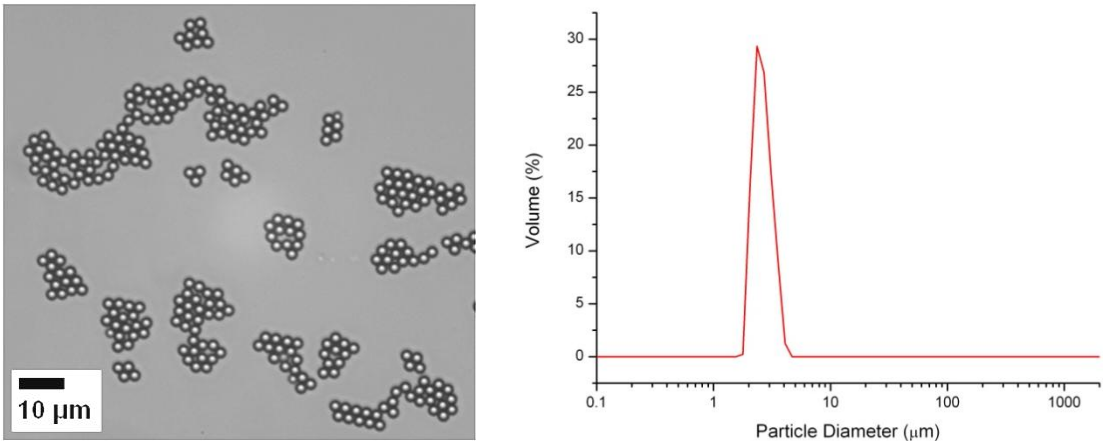

Figure 3.3 (left) optical micrograph of 2.5 µm diameter poly(styrene) seed particles. (right) Laser scattering analysis of the seed particles in methanol (TSNP03)

In order to form the secondary 'soft' lobe, a seeded dispersion polymerisation was undertaken in the presence of micron sized polystyrene seed particles made in the procedure outlined above. This was conducted in batch by addition of cleaned seed particle dispersion, PVP K90 surfactant, butyl acrylate and AIBN in a 90:10 (w/w) methanol-water medium. Methanol is used specifically in this reaction as longer chain alcohols are good solvents for poly(butyl acrylate). In these reactions, the PVP content was reduced to 2 wt% w/r to butyl acrylate. This was to promote the growth of poly(butyl acrylate) particles off the polystyrene seed particles rather than provide sufficient steric stabilisation for the growth of poly(butyl acrylate) as separate particles. Butyl acrylate concentration was fixed at 10 wt% (w/w) with respect to total liquid content, with 1 wt%

AIBN (w/w) with respect to butyl acrylate deployed as thermal initiator. In one example, the seed particle mass was equal to the butyl acrylate mass charged to the reaction (i.e. both 10 wt% of total reaction components). These particles immediately prior to reaction (left), and the resultant particles after the seeded dispersion polymerisation (right) can be seen in figure 3.4. In the latter case note the darker sphere represents the poly(styrene) seed particle, and the lighter part represents the newly formed poly(butyl acrylate) lobe.

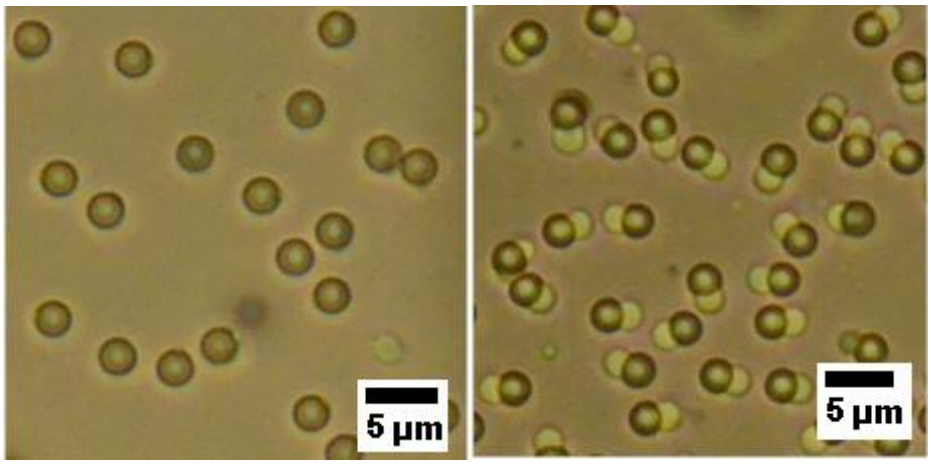

Figure 3.4 Optical micrograph of poly(styrene) seed particles (TSNP03) (left) and 'hard-soft' Janus particles (TS502-seeded) (right). In the right image; the darker sphere represents the more dense poly(styrene) seed, whereas the lighter part represents the poly(butyl acrylate) lobe. Note also the light patches in the centre of the poly(styrene) lobes are an optical arifact. The smaller particles observed in the right hand image is p(BA) secondary nucleation

To allow high resolution observation of the hard-soft Janus particles without deformation of the soft phase, cryogenic scanning electron microscopy was used to image particles at -120 °C as depicted in figure 3.5. The freeze-fracture preparation process for cryo-SEM has split a particle down the centre, revealing the inner structure. In both images, the larger lobe is the poly(styrene) seed particle with the smaller lobe representing the poly(butyl acrylate) phase.

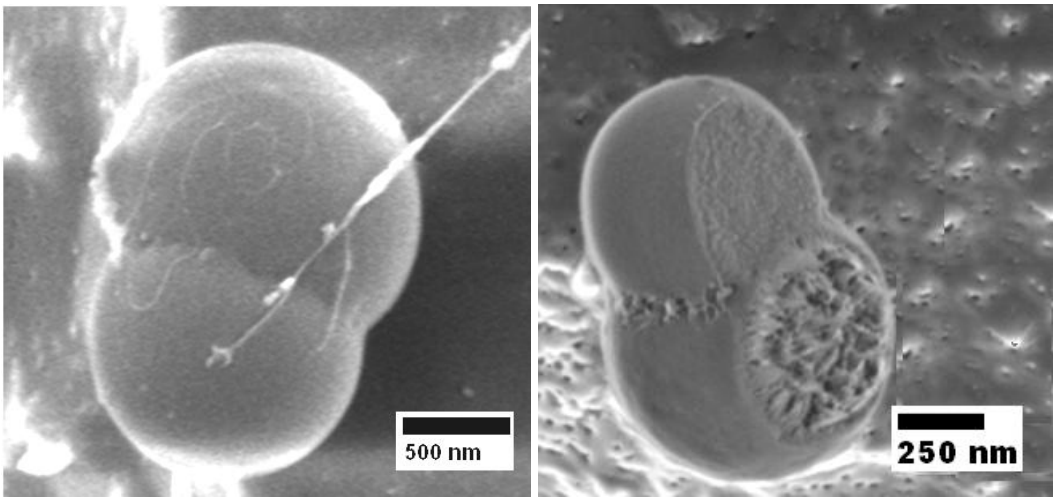

Figure 3.5 Cryogenic scanning electron micrographs of hard-soft Janus particles. (l) a whole particle, (r) a cross-section through a particle. In both images the larger lobe represents the poly(styrene) core particle (TS405-1)

The cross-sectional slice through the Janus particle seen in figure 3.5(r) indicates two distinct parts to the particle, seen by the differences in surface roughness across the fracture plane. There appears to be a clear delineation between the two phases indicating that no swelling and subsequent polymerisation has occurred, ruling out entropic phase separation from within the particle. We may therefore attribute the formation mechanism of the second pBA lobe to the capture of oligomeric radicals from the solution phase onto the particle surface during the initial stage of the seeded dispersion polymerisation, where it further propagates to form a lobe. Similar examples of anisotropic particles formed dispersive systems have acknowledged this formation mechanism.[23,24] If this is the case, we should expect the number of lobes on a particle to be dependent on the total seed surface area available to nucleate from.

3.3.2 Seeded dispersion polymerisation of butyl acrylate in the presence of polystyrene seed particles at varying concentrations

A series of seeded dispersion polymerisations of butyl acrylate in the presence of a varied quantity of seed particles were performed in order to investigate the influence of seed particle concentration, i.e. the total seed surface area; on the polymerisation kinetics and growth of the poly butyl acrylate lobe from the seed particles. Five polymerisations of butyl acrylate (10 wt% w/w) with a range of seed particle concentrations outlined below in table 3.1 were conducted in a methanol : water medium (90:10 w/w) using AIBN as thermal initiator and PVP-K90 as a protective colloid (1 wt% and 2 wt% w/r to BA respectively). One dispersion polymerisation of butyl acrylate was conducted in absence of seed particles for comparison. All reactions were conducted *ab initio*, being degassed for 15 minutes prior to heating to 70 °C by submerging in a pre-heated oil bath. Aliquots of reaction mixture were extracted at set time intervals, analysed by optical microscopy, and gravimetry for polymer conversion. Final monomer conversions of all seeded particle dispersion polymerisations exceeded 90% as determined by gravimetry. Less than 0.75 wt% solids content were found in the continuous phase after gravity separation of continuous from particle phase in all seeded dispersion polymerisations.

[Mass] of dried Seed particles	[Number] of Seed Particles	[Surface Area] of seed particles	Reference
0 g/L	0 /L	0 m^2/L	TS502-non
20.92 g/L	2.17 x 10^{12} /L	46 m^2/L	TS471-3
27.88 g/L	4.23 x 10^{12} /L	83 m^2/L	TS471-1
90.50 g/L	9.37 x 10^{12} /L	199 m^2/L	TS502-seeded
203.66 g/L	2.11 x 10^{13} /L	448 m^2/L	TS471-2

Table 3.1 Concentrations by mass, number and surface area of the seed particle quantities used in the seeded dispersion polymerisations

Polymerisation kinetics

Monomer conversion data (X_M) obtained from the gravimetric analysis of the seeded dispersion polymerisations (plotted as a function of time in figure 3.6(l) was applied to a free radical polymerisation rate equation, taking into account initiator decomposition. The rate equation in this case is expressed in equation 1 and plotted in figure 3.6(r).

A first order relationship exists between monomer concentration and polymerisation rate, except at the start of the reaction where an induction period can be seen. This is attributed to the reaction reaching thermal equilibrium. The rate of polymerisation is relatively unaffected by the presence of polystyrene seed at all concentrations of seed particles. However, the non-seeded polymerisation is seen to progress at a slightly elevated rate in comparison to the seeded polymerisations during the first 150 minutes of the reaction.

$$-\ln(1-X_M) = 2k_p\sqrt{\frac{f[I]_o}{k_d k_t}}\,(1-\sqrt{e^{-k_d t}}) \qquad (1)$$

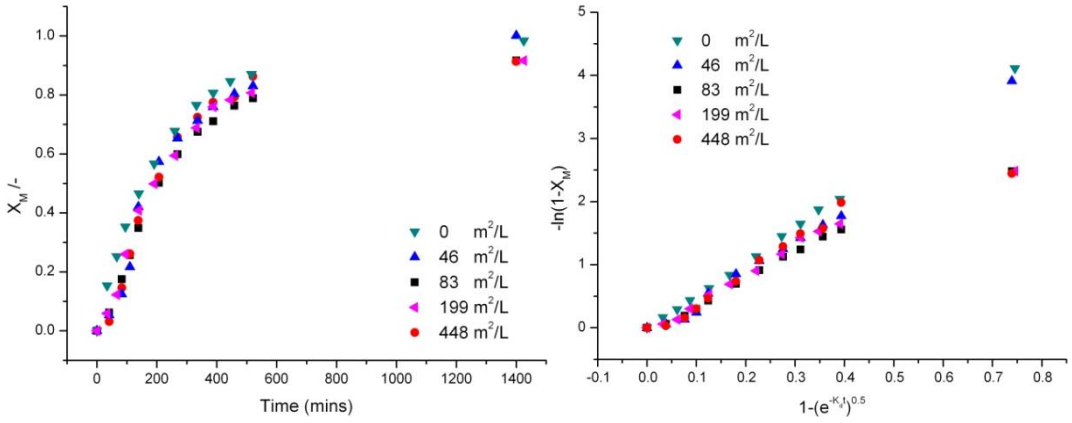

Figure 3.6 (l) Conversion as a function of time for the seeded dispersion polymerisations at various seed particle concentrations – given as seed surface area concentration. (r) First order kinetic plot taking into account initiator decomposition of the seeded dispersion polymerisations

The elevated polymerisation rate for the non-seeded polymerisation arises from the dependence of solution polymerisation kinetics during the early stages of the polymerisation on initiator concentration. The seed particles absorb some of the radicals causing a temporary depression in polymerisation rate. However, once the reaction progresses into the latter heterogeneous phase, i.e. polymerisation ensues within the pBA lobes, rate is not influenced by initiator concentration in the continuous phase.[29]

In comparison of our observations with that of previously reported literature, we find that our results conflict with that of the kinetics of seeded dispersion polymerisations of MMA in the presence of micron sized pMMA seeds.[30] In the pMMA system, the initial polymerisation rate was observed to be higher by a factor of 1.3 compared with an identical non-seeded reaction. We attribute this disparity to the fact that a far higher monomer/polymer mass ratio (28:1) was employed in the pMMA system (compared to

the 4:1 mass ratio used in our highest BA containing reaction), and an overall higher starting concentration of monomer in the continuous phase which has been shown to increase initial polymerisation rate. Conversely, Perro *et al.* report that emulsion polymerisation rate of styrene in the presence of silica seeds in manufacturing hybrid colloidal Janus particles by surface nucleation is not affected by the presence of seed particles in accordance with our observations.[31]

Particle Growth kinetics

Optical micrographs of the seeded dispersion polymerisations were taken at set intervals throughout the polymerisation. An example set of optical micrographs imaging the growth of a secondary lobe of poly(butyl acrylate) can be seen in figure 3.7. Based on these images, quantitative measurements regarding the evolution of lobe volume as the reaction progresses were taken to analyse particle growth kinetics.

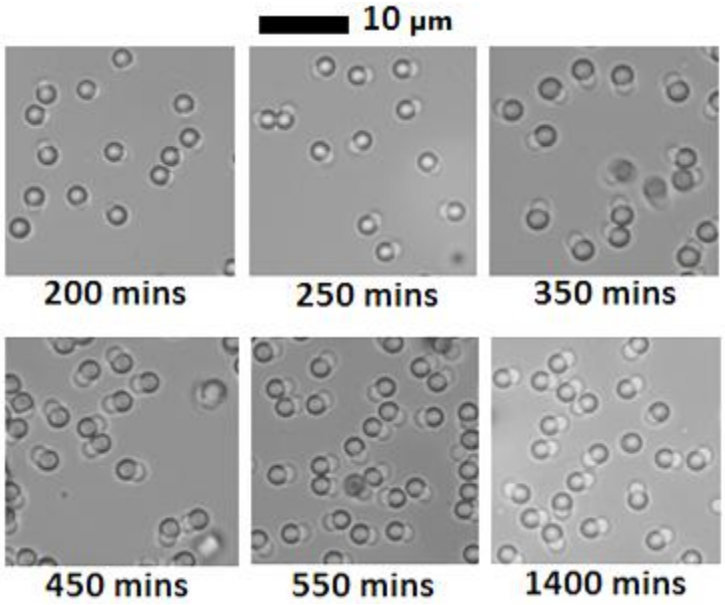

Figure 3.7 Optical micrographs of particles during a seeded dispersion polymerisation of BA in the presence of polystyrene seed particles (199 m^2/L)

The volume of the growing poly(butyl acrylate) lobe was modelled as a spherical cap, whereby the pBA lobe was treated as a hemisphere of a sphere. Taking the height of the lobe (h) and radius (a), displayed in figure 3.8, volume can be calculated following equation 2 where r is calculated using equation 3 It is worth noting that one assumption taken in this measurement is that the area of contact between the poly(styrene) and poly(butyl acrylate) lobe is treated as planar rather than a 3-D curved surface.

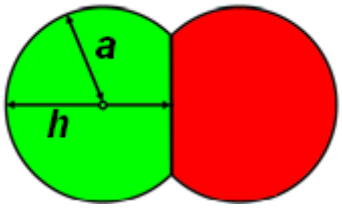

Figure 3.8 Schematic of the measurements taken to calculate volume of the poly(butyl acrylate lobe) (green) growing off a polystyrene seed particle (red)

$$V = \frac{\pi h^2}{3}(3a - h) \quad (2)$$

$$a = \frac{r^2 + h^2}{h^2} \quad (3)$$

Despite the relatively negligible effect that seed particle concentration has on the rate of polymerisation, its influence on lobe volume is far more significant. Values of the calculated volume for the poly(butyl acrylate) lobes are plotted as a function of monomer conversion in each reaction as depicted in figure 3.9.

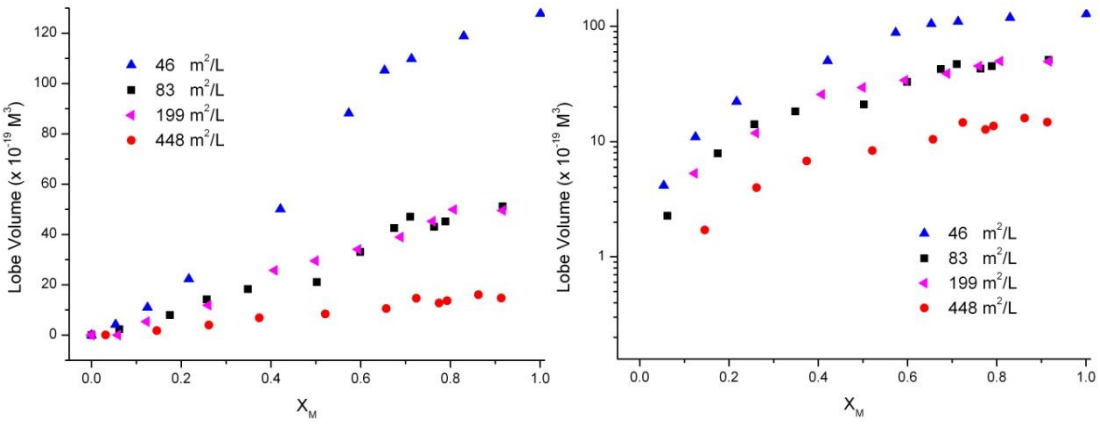

Figure 3.9 Calculated lobe volume based on optical micrographs as a function of monomer conversion during seeded dispersion polymerisations with linear (left) and logarithmic (right) y-axes respectively

As the monomer concentration in each reaction is equivalent, yet the number of seed particles is varied, an increase in lobe volume for lower seed particle concentrations is expected. Indeed this general trend is seen in figure 3.9. However the lobe growth profile for the polymerisation conducted with 83 m^2/L seed surface area overlaps with that of the polymerisation for 199 m^2/L seed surface area. It would be expected that the profile for 83 m^2/L should exceed that of 199 m^2/L. In addition, the observed lobe volume of the pBA lobes for the lowest seed surface area reactions of 46 and 83 m^2/L do not reach the expected volume based on the mass of monomer at the set seed particle concentration, as expressed in equation 4. Where lobe volume (V_{lobe}) is a product of mass of butyl acrylate (M_{BA}), density of poly(butyl acrylate) (ρ_{pBA}), divided by the number of seed particles (N_p).

$$V_{lobe} = \frac{M_{BA}\rho_{pBA}}{N_p} \quad (4)$$

Optical micrographs of the final particle dispersions reveal why these disparities are observed for the reactions at lower seed surface area as seen in figure 3.10. The polymerisations containing the highest seed surface area reveal monodisperse poly(styrene) seed particles, each possessing one lobe of poly(butyl acrylate). However, the lowest seed surface area polymerisations of 46 and 83 m^2/L indicate the presence of a large quantity of secondary nucleation. In addition some poly(styrene) seed particles possessing more than one pBA lobe can be seen.

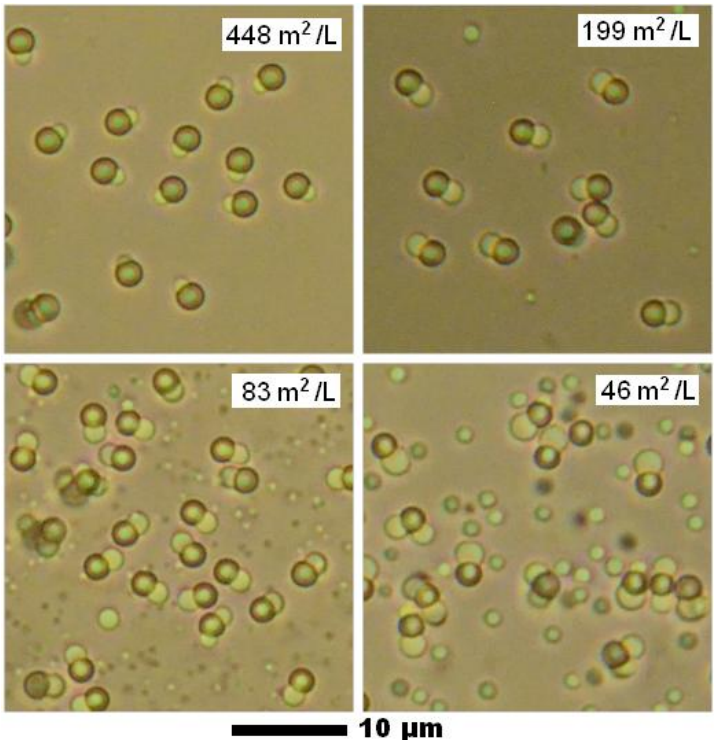

Figure 3.10 Optical micrographs of final seed particle dispersions after 24 hours polymerisation time for each of the seeded dispersion polymerisations. The seed surface area for each reaction is indicated on the micrographs

The growth of the pBA lobes can be calculated as a function of conversion to allow the expected lobe volume based on monomer mass charged to the system and seed particle concentration (expressed in equation 5) to be compared with experimentally observed

values of volume. When pBA lobe volume fraction is measured as a function of conversion, a linear dependence can be seen for all reactions as shown in figure 3.11(l). Lobe volume fraction is calculated by dividing the observed lobe volume during the polymerisation by the final measured lobe size. Fitting the dependence of all reaction profiles in figure 3.10(l) yields a linear function which can in turn be used to calculate expected lobe volume growth as a function of conversion.

$$V_{expected} = \frac{X_M K}{N_p} \tag{5}$$

$$K = 1.17$$

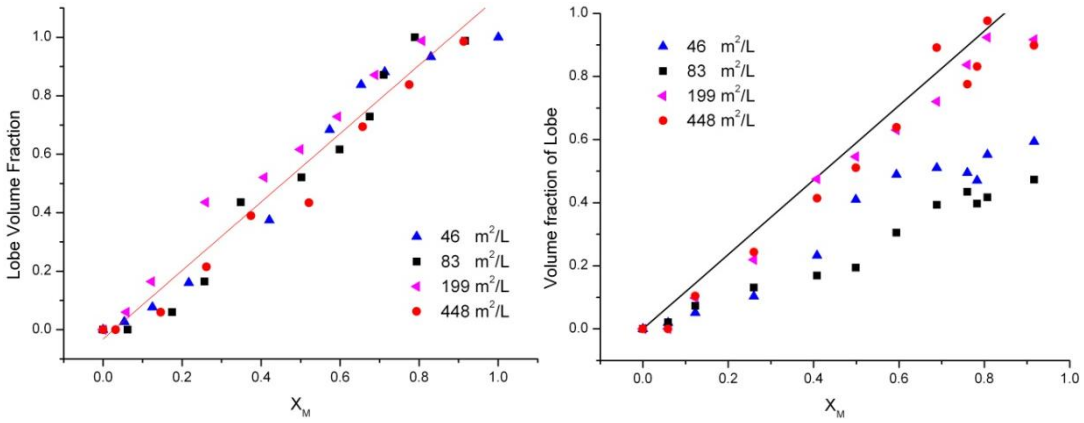

Figure 3.11 (l) Observed lobe volume (expressed as a fraction of final lobe volume) as a function of conversion. Red line represents a linear fit of $y = mx$ for all reactions whereby $m = 1.17$. (r) Measured lobe volume fractions normalised against expected lobe volume as a function of conversion. Black line represents the theoretical fractional growth profile for the reactions based on conversion data

The expected linear volume growth and the observed values for lobe growth are plotted in figure 3.11(r). From this it can be seen that seeded dispersion polymerisations not

affected by secondary nucleation (199 and 448 m^2/L seed surface area) show a consistent fit with the expected linear volume growth profile. The polymerisations incorporating a lower seed surface area deviate significantly from the linear growth curve as a result of secondary nucleation.

The presence of secondary nucleation and multiple lobe formation in samples with low seed surface area gives an insight into the particle formation mechanism for the seeded dispersion polymerisation. All dispersion polymerisations start as a homogeneous solution whereby homogenous nucleation occurs in the continuous phase. In our case of seeded dispersion polymerisations, as the oligoradicals grow towards a critical threshold size, they may be captured by the surface of a seed particle and commence nucleation on the surface of the seed particle. In reactions with high concentrations of seed particles, there is a large surface area available for capture. However when the available seed surface area is too low, capture by a seed particle surface may not occur before the oligoradical reaches a critical threshold size and precipitates out into a secondary primary particle. In the seeded dispersion polymerisation with the lowest seed surface area (46 m^2/L, the volume of secondary nucleated pBA particles has been measured optically and plotted alongside lobe volume in figure 3.12. The secondary nucleation is present from the early stages of the reaction, i.e. at 10% conversion.

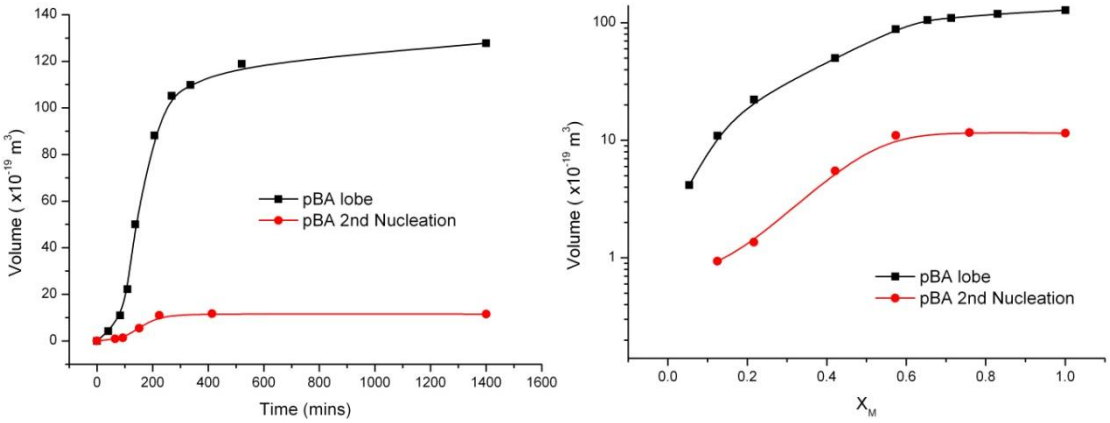

Figure 3.12 Linear volume as a function of time (left) Logarithmic volume versus conversion (right) for a seeded dispersion polymerisation at 46 m^2/L seed surface area for both lobe size and size of secondary nucleation

Alternatively, several oligoradicals may be captured by a particle surface and propagate separately without coalescing forming particles with multiple soft lobes. Both of these phenomena are observed in seeded dispersion polymerisations with a reduced seed surface area. This poses a number of questions however. How can several propagating pBA particles reside on a single seed particle without coalescing? How will two lobes on a particle affect the individual growth of the lobes rather than a single propagating lobe? To answer these questions, optical microscopy analyses of particle dispersions with multiple lobes were conducted.

Hard-soft Janus particles with multiple lobes

In order to quantify the prevalence of seed particles possessing multiple lobes, populations of particles in each of the seeded dispersion reactions of varying seed surface area were counted for particles with multiple lobes, with over 150 particles being counted per sample particle dispersion. The results are presented in table 3.2.

Seed surface area	Particles with multiple lobes in population
448 m^2/L	2.60 %
199 m^2/L	7.04 %
83 m^2/L	7.54 %
46 m^2/L	35.74 %

Table 3.2 Percentage of particles with multiple pBA lobes for each seeded dispersion polymerisation

As expected, the number population of particles with multiple lobes increases as the seed surface area available to nucleate from decreases. This observation correlates with results reported from the seeded emulsion polymerisation of styrene in the presence of silica seed particles, whereby varying the surface area of silica seed in the reaction determines the number of poly(styrene) lobes grown off a single seed particle.[31] In this example the total seed surface area in the reaction was varied by altering seed particle size, therefore larger seed particles would reliably accommodate more poly(styrene) nodules, allowing the controlled nucleation of up to 6 lobes, and in extreme cases; many lobes with the final particle resembling a raspberry structure.[31–33] However, in contrast to these works, our system is susceptible to secondary nucleation, therefore preventing controlled nucleation of a larger number of pBA lobes at consistent volume.

Multi-lobe Janus particles were seen to adopt a variety of angle separation between the pBA lobes as seen in figure 3.10 (46 m^2/L). To investigate this observation a seed particle dispersion with a high quantity of multi-lobe particles (46 m^2/L) was analysed by measuring the angles between the centre of the pBA lobes and the central poly(styrene) core. The measurement is depicted in figure 3.13(l). As an example, a particle with lobes at either end in a linear geometry would give an angle of 180°. A population of 75 multi-

lobe particles were analysed in this manner and a histogram of the results can be seen in figure 3.13(r).

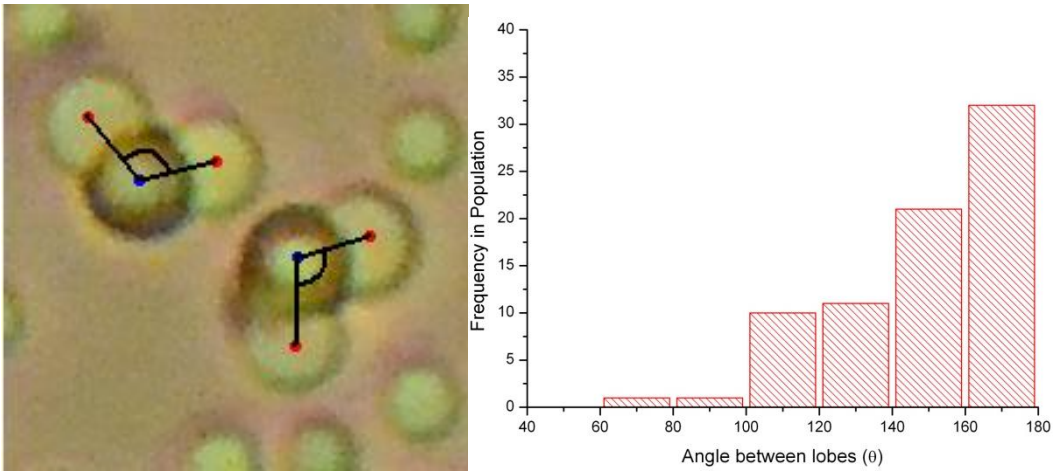

Figure 3.13 (l) Optical micrograph of multi-lobe particles overlaid with the angle measured between the centre of the two pBA. (r) Histogram of 75 measured angles between the pBA cores (46 m^2/L: TS471-3)

Evidently, higher populations of multi-lobe particles are found with an increased angle of separation. This population dependence on lobe angle could arise from the coalescence of lobes at low angles of separation. Two lobes nucleated 90° apart may well coalesce during the reaction as the lobes grow and come into contact. The probability of this occurring decreases with increasing angle of separation. Seven days after synthesis, the multi-lobed particles were reanalysed by optical microscopy (figure 3.14) and found to have shown little difference in morphology or number population (with respect to single lobed particles). This would suggest that the poly(butyl acrylate) lobes are somewhat grafted to the surface of the poly(styrene) seed particle, otherwise we would expect the multi-lobe particles to migrate into a single lobe to minimise unfavourable interfacial

energies between the pBA and pSty surface, and equally to minimise the pBA – continuous phase interfacial tension.

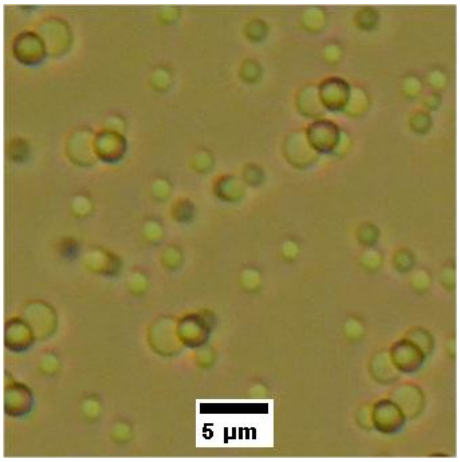

Figure 3.14 Optical micrograph of multi-lobe particles 7 days after synthesis indicating little change in particle morphology (46 m^2/L: TS471-3)

When comparing the volume of pBA lobes on Janus particles with single lobes with that of multi-lobe particles, it was found that single lobes possessed a greater volume than individual lobes on a multi-lobe particle. A quantitative measurement was undertaken to investigate this observation (figure 3.15(r)). The volume of pBA lobes on a set of 10 Janus particles with two lobes were separately measured, added and averaged. This data is plotted alongside the average volume of a pBA lobe on a single lobed particle, seen in figure 3.15(l).

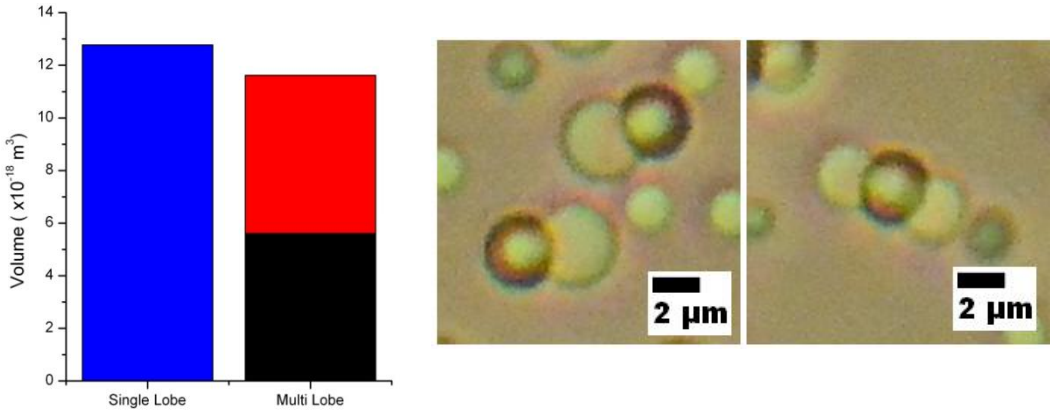

Figure 3.15 (l) Average volume of pBA lobe for a single lobed particle (blue) and the averaged volume of each lobe of a seed particle possessing two pBA lobes. The red and black each represent the average volume of each lobe on the multi-lobe particle. (r) Optical micrographs indicating the volume difference between lobes on single and multi-lobe particles (sample 46 m^2/L: TS471-3)

Individual pBA lobes on multi-lobe particles were found to vary widely in size. However, the combined volume of pBA phases on a multi-lobe particle are approximately equivalent to the pBA volume of a single lobed particle. This indicates that each seed particle can only grow a limited volume of pBA from the surface, regardless of the number of lobes it nucleates. It would be expected that every lobe grows to a consistent size at the same rate, as observed for single-lobed particles. The range of pBA lobe sizes seen in multi-lobes particle points towards a heterocoagulation formation mechanism, whereby a *precipitated* oligomer is adsorbed onto the surface of the particle. A plausible explanation for the consistent net volume of pBA from multi-lobe particles compared with single lobed counterparts could arise from the local concentration of monomers and oligoradicals found in the continuous phase in the immediate vicinity of the particles. In the close proximity of another growing pBA lobe, a local depression of monomer and oligoradicals may be found, as two pBA lobes will possess a significantly higher surface

area than a single lobe of the same volume. This could pay a role of inhibiting lobe growth by diffusion limitation.

Involvement of seed particles in the seeded dispersion polymerisation

Finally, in order to verify that the seed particles have little involvement in the seeded dispersion polymerisation by way of swelling and polymerisation from within the particle, the seed particle diameters for each seed surface area reaction was monitored as the polymerisation progressed.

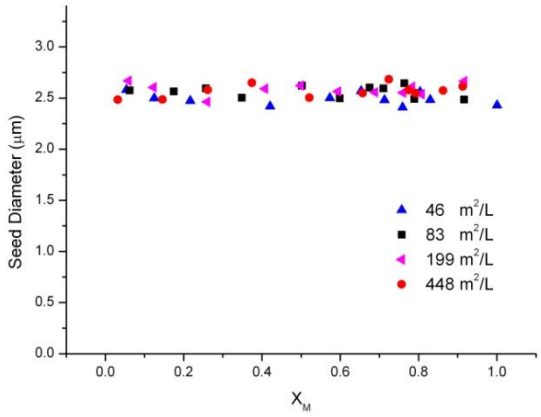

Figure 3.16 Poly(styrene) seed particle diameters measured by optical microscopy as a function of polymer conversion for each of the seeded dispersion polymerisations at varying seed surface area

As seen in figure 3.16, very little change in seed diameter occurs over the course of the polymerisation, regardless of seed particle concentration thereby ruling out swelling and subsequent polymerisation within the seed particles. This observation mirrors the cryo-SEM analysis whereby clear delineation between the pSty and pBA phases could be seen.

3.3.3 Synthesis of sub-micron hard-soft Janus particles

The synthesis of micron sized 'hard-soft' Janus particles is simple through dispersion polymerisation as demonstrated above, however the lower size limit of reliable monodisperse dispersion polymerisation is approximately 1 µm. As aforementioned, the synthesis of hard-soft Janus particles through seeded emulsion polymerisation has proved difficult. We therefore investigate an extension of the seeded dispersion polymerisation to synthesise particles of sub-micron dimensions. In order to accomplish this, we require a sub-micron seed particle with the same surface properties as the larger micron sized system. Du *et al.* report an emulsion polymerisation procedure to render sub-micron poly(styrene) latex particles stabilised by PVP, thereby presenting an ideal route to fabricate the seed particles.[34]

A waterborne emulsion polymerisation to render a sub-micron polystyrene latex of approximately 200 nm diameter using PVP-K30 (40,000 $gmol^{-1}$) was conducted. Most waterborne emulsion polymerisations exploit the use of electrostatic surfactants to control colloidal stability and particle size. However, as the resulting particles are redispersed into an organic solvent for the secondary polymerisation, PVP was used instead. In a typical procedure, styrene, PVP K30 and water were charged to a single jacketed 250 mL reactor with the styrene content fixed at 10 wt% total solids content. The amount of steric surfactant PVP-K30 added was set at 7.5 wt% w/r to styrene to fabricate a latex of approximately 200 nm diameter.[34] Thermal initiator potassium persulfate was used to initiate the reaction at 70 °C for 24 hours. The seed polymerisation was followed both by

gravimetry and dynamic light scattering, as such, the particle growth and polymerisation kinetics data can be found plotted in figure 3.17(r).

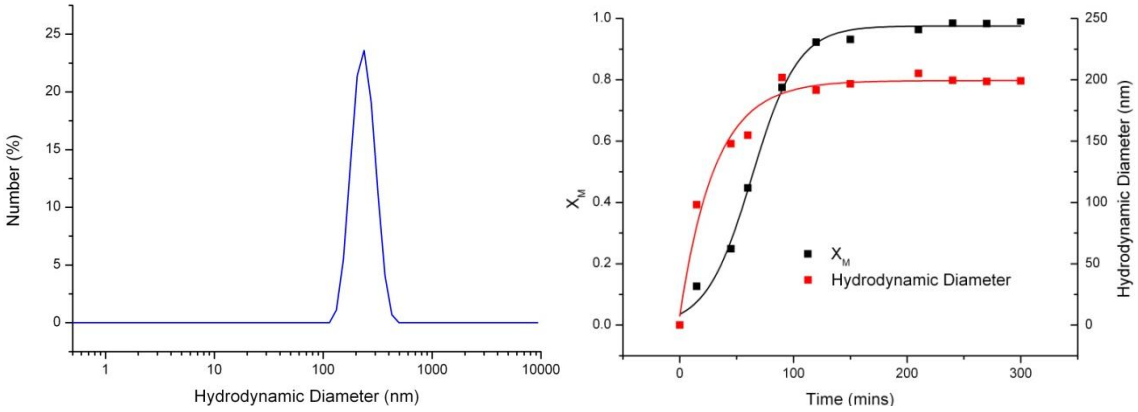

Figure 3.17 (l) Size distribution of the sub-micron poly(styrene) seed latex as measured by dynamic light scattering. (TSNP108) (r) Conversion and hydrodynamic diameter (DLS) as a function of time for the styrene emulsion polymerisation to synthesise the sub-micron seed latex

The resulting poly(styrene) latex particles were analysed by both FEG-SEM and by DLS. As seen from the micrographs in figure 3.18 and dynamic light scattering data plotted in figure 3.17(l); the result is a monodisperse poly(styrene) latex with a 200 nm diameter (by number average). The use of PVP-K30 as a steric stabiliser ensures a layer of stabiliser on the surface of the particles which acts as a favourable nucleation site for the subsequent seeded dispersion polymerisation in the same manner as the larger micron sized particles.

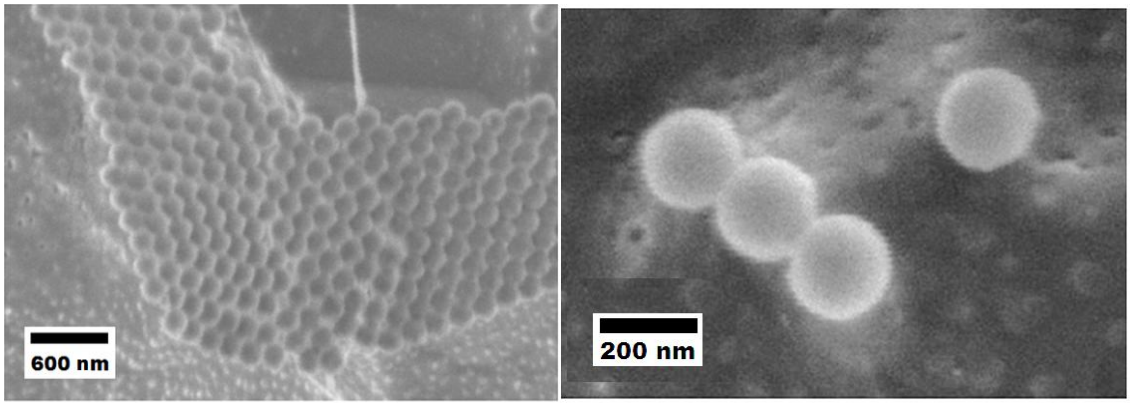

Figure 3.18 (l) Cryo-SEM image of the submicron poly(styrene) seed particles (r) high magnification of the same particles (TSPOsty240)

Prior to the seeded dispersion polymerisations, the waterborne latex was dialysed against methanol until dispersed in a pure methanol environment. After which the dispersion is cleaned of any remaining PVP by repeated centrifugation cycles in methanol. Owing to the size of the particles, suspensions would remain colloidally stable against sedimentation for prolonged periods extending over months.

A similar strategy to the seeded dispersion polymerisations involving micron sized poly(styrene) particles was applied to nucleate and grow a secondary lobe of pBA from the surface of the sub-micron seed particles. The purified poly(styrene) seed particle latex was charged to a round bottom flask in a 90% methanol 10% water (w/w) environment with butyl acrylate (0.5 wt% w/w) using PVP-K30 (2 wt% w/r to butyl acrylate) as a steric stabiliser. Owing to the seed surface area dependence of the polymerisation, the seed particle concentration was reduced to match the seed surface area per litre with that studied in the micron sized system. This effectively reduced seed solid content from 10 to 1.05 wt% (w/w). The measured seed surface area after preparation of the experiment was

calculated at 246 m^2/L. Throughout the reaction, aliquots of reaction mixture were extracted from the reaction and analysed for conversion gravimetrically, analysed by dynamic light scattering and cryogenic scanning electron microscopy, as can be seen in figure 3.19.

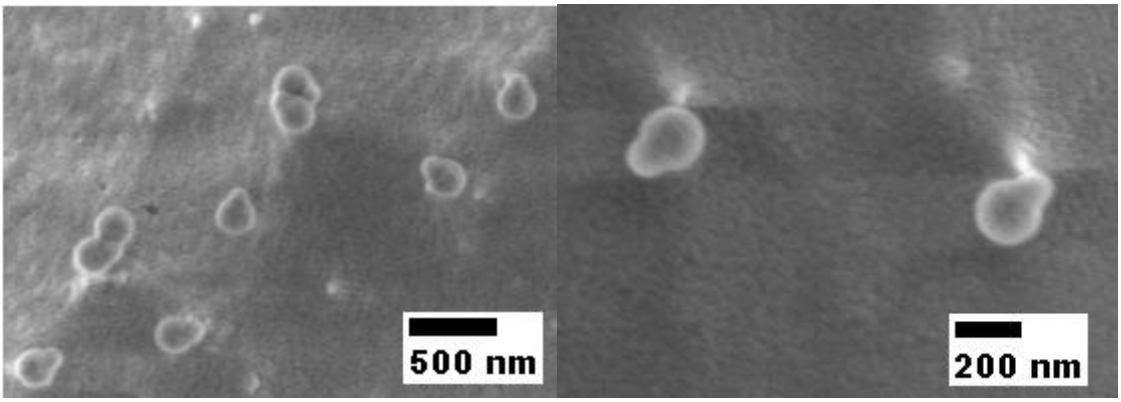

Figure 3.19 High magnification cryo-SEM images of submicron hard-soft Janus particles (TSNP110)

Cryo-SEM images reveal the characteristic dumbbell morphology of Janus particles. Half the mass of butyl acrylate was added in comparison to the mass of seed particles for this reaction. Clearly, the larger sphere is the poly(styrene) seed with a smaller lobe of poly(butyl acrylate) grown from it.

In terms of kinetics; the monomer conversion as a function of time can be seen in figure 3.20(l) alongside the number averaged hydrodynamic diameter for the resultant Janus particles (figure 3.20 (r). The seed particle size distribution has been plotted for comparison.

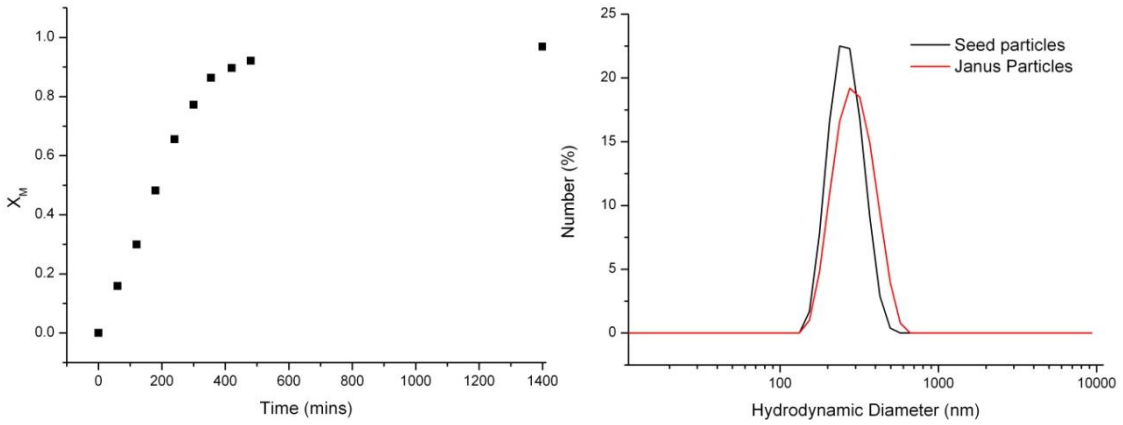

Figure 3.20 (l) BA monomer conversion as a function of time for a seeded dispersion polymerisation of BA in the presence of submicron poly(styrene) seed particles. (TSNP110) (r) Particle size distribution data of the resultant Janus particles after seeded dispersion polymerisation (TSNP110) and the poly(styrene) seed particles prior to polymerisation (TSNP108)

The conversion-time data for the seeded dispersion polymerisation indicates a similar reaction profile to that of the micron sized seeded dispersion polymerisation, reaching high conversion over 24 hours of reaction time. Comparison of the particle size distributions of the seed particles and final Janus particles (figure 3.20(r)) reveal a minor increase in hydrodynamic diameter and slight broadening of polydispersity towards larger particles. However, according to this data, no aggregates or coagulation have formed resulting from the reaction. A closer analysis of the volume averaged hydrodynamic diameter of particles by dynamic light scattering was conducted during the dispersion polymerisation with peak values are plotted as a function of conversion in figure 3.21.

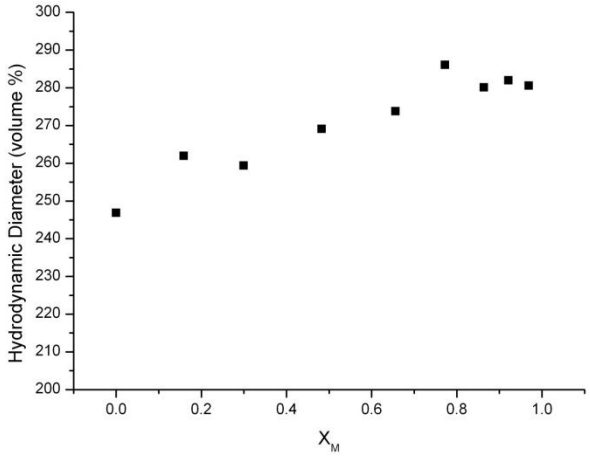

Figure 3.21 Volume averaged hydrodynamic diameter as a function of conversion for Janus particle samples extracted during the seeded dispersion polymerisation of TSNP110

An increase in particle size from the initial volume weighted seed diameter of 250 nm can be seen during the polymerisation up to a final value of approximately 280 nm in a similar manner to the results seen in for the micron sized seeded dispersion polymerisations. Due to the limitation of dynamic light scattering to assume spherical geometry on anisotropic particles, we cannot quantitatively comment on the increase in hydrodynamic diameter as a function of conversion.

3.4 Conclusions

We demonstrate a reliable method to fabricate 'hard-soft' Janus particles by a two-step seeded dispersion polymerisation. By various optical and kinetic analyses we find that the rate of polymerisation during the seeded dispersion polymerisation of butyl acrylate in the presence of poly(styrene) seed particles is unaffected by the concentration of seed particles. However, a profound effect on the volume and number of pBA lobes per seed particle is observed. A low seed surface area concentration results in the formation of

multi-lobed particles and significant secondary nucleation. As a result of this work, the optimum parameters for synthesising 'hard-soft' Janus particles can be found, without undesired effects such as secondary nucleation and multi-lobed particles. Additionally we translate the synthetic procedure to allow the formation of sub-micron scale 'hard-soft' particles verified by cryo-SEM, therefore opening the range of accessible size for these particles from nano to micron scale. With a robust synthetic technique to fabricate 'hard-soft' Janus particles we may engage in research to exploit the anisotropic directional properties of these particles in fields such as wet deposition and self assembly.

3.5 Experimental

3.5.1 Materials

Styrene (ReagentPlus, 99%), *N*-butyl acrylate (>99%), poly(vinyl pyrrolidone) (PVP-K90, 360,000 $gmol^{-1}$ and K30, 40,000$gmol^{-1}$), all supplied by Sigma Aldrich, UK. Azobisisobutyronitrile (97%), Ethanol (absolute AR), Methanol (AR), all supplied by VWR, UK. were used as supplied. Monomers were filtered through a basic alumina column to remove inhibitor before use. Deionised water was filtered and purified to 18 $M\Omega cm^{-1}$.

3.5.2 Equipment

Particle sizing measurements of micron sized colloids were undertaken using a Mastersizer 2000 (Malvern Instruments, Malvern, UK). Dilute particle suspensions in methanol were introduced using the µP dispersion unit. Laser was aligned to optimum transmission intensity and a background spectrum collected to eliminate any

contaminants presenting in the final data. Dilute suspensions of 1 wt% were introduced drop wise by submerged syringe until 5% laser obscuration was reached. A 30 second sampling time across the entire measurement range from 2 nm – 2 mm was conducted three times before averaging to yield final results.

Dynamic light scattering measurements were conducted using a Malvern instruments Zetasizer ZS, (Malvern, UK). Dilute 1 mL dispersions of particles in methanol were dispensed into plastic cuvettes and thermally equilibrated to 25 ℃ for 2 minutes prior to measurement of 3 sets of measurements, each of 10 sub runs using 183° backscattering angle. Values for number (%) and volume (%) as a function of hydrodynamic diameter were used.

Particles dispersions were imaged on a Leica DM2500M in bright field transmission mode using a Nikon D5100 camera.

Cryogenic Scanning Electron Microscopy analyses were carried out using a Zeiss Supra 55-VP Field Emission Gun Scanning Electron Microscope with a Gatan Alto 2500 cryo transfer system and a Gatan C1002 Liquid Nitrogen cold stage. Dilute aqueous suspensions (1 wt% w/v) of particles were drawn into a brass rivet and cooled in liquid nitrogen. Samples were heated to −95 ℃ under high vacuum for 15 minutes to remove contaminant ice through sublimation followed by platinum sputter target coating in an argon atmosphere (25 seconds, 10 mA). Imaging was undertaken at −120 °C using a 1.5 kV accelerating voltage with a gold anti-contaminator at −189 ℃.

All image analysis was conducted using open source software ImageJ (NIH, US).[35]

3.5.3 Dispersion polymerisation

Synthesis of micron sized seed particles

All components in table 3.3 were charged to a 250 mL round bottom flask prior to stirring and nitrogen purge for 40 minutes. After which, the flask was heated to 70 °C for 24 hours whilst under stirring and slight nitrogen overpressure. Resulting particle dispersions were centrifuged and redispersed in methanol three times before analysis by optical microscopy and laser scattering (Mastersizer).

Seeded dispersion polymerisations

Cleaned seed particle dispersions of 11 wt% solids content were charged to a round bottom flask alongside all other components in table 3.3, stirred and purged with nitrogen for 20 minutes prior to sealing and heating at 70 °C for 24 hours.

Components	2.5 µm Seed Particles (TSNP03)	Seeded dispersion polymerisation (TS502-seeded)
Styrene	25.0 g	-
AIBN	0.25 g	0.1 g
PVP-K90	1.50 g	0.03 g
Methanol	70.0 g	17.3g
n-butyl acrylate	-	3.00 g
water	-	5.70 g
Seed particle suspension	-	27.0 g

Table 3.3 List of chemicals required for poly(styrene) seed particle synthesis

Kinetic experiments

For kinetic experiments, a varied quantity of 2.5 µm seed particles diameter as verified by optical microscopy and laser scattering were charged to a round bottom flask

alongside the other reagents in table 3.4. Reaction mixtures were then stirred and purged with nitrogen for 20 minutes prior to sealing and heating at 70 °C for 24 hours. During the polymerisation aliquots of 2 mL were extracted at set time periods, aerated with oxygen and cooled on ice to quench polymerisation before measuring conversion gravimetrically and imaging by optical microscopy.

Reagents	Mass	Reference
2.5 µm pSty seed particles	0 g	TS502-non
	10 g	TS471-2
	5 g	TS502-seeded
	2.5 g	TS471-1
	1.25 g	TS471-3
PVP-K90	0.10 g	
Methanol	40.5g	
n-butyl acrylate	5.00g	
Water	4.50 g	
AIBN	0.05 g	

Table 3.4 List of reagents used in the kinetic seeded dispersion polymerisation experiments

Synthesis of submicron hard-soft Janus particles

All components in table 3.5 except potassium persulfate were charged to a 250 mL single jacketed glass reactor vessel fitted with a PTFE overhead stirrer with propeller blade (Radleys reactor duo). The contents were purged with nitrogen for 45 minutes whilst stirring at 180 rpm prior to sealing with slight nitrogen overpressure. Reactor was then heated to 70 °C by a recirculation heat bath (Julabo), when thermal equilibrium was

attained, potassium persulfate in 5 mL degassed, deionised water was charged to the reactor. Polymerisation ensued for 24 hours before cooling to room temperature and dialysis against methanol using a cellulose dialysis membrane. Dialysis ensued for 7 days, changing solvent once per 24 hours. Excess PVP-K30 was removed afterwards by 3 centrifugation cycles at 7882 *g* for 60 minutes. The supernatant was disposed, and the pellet re-dispersed in methanol. Gravimetry was used to ascertain accurate solids content of the purified seed dispersion.

Dispersion Polymerisation	Mass
Deionised Water	200 g
PVP-K30	1.50 g
Styrene	20.0 g
Potassium Persulfate	0.30 g

Table 3.5 List of chemicals required for submicron poly(styrene) seed particles by emulsion polymerisation (TSNP108)

Seeded dispersion polymerisation in the presence of submicron seed particles

Reagents described in table 3.6 below were charged to a 50 mL round bottom flask fitted with magnetic follower and rubber septum. The contents of the flask were purged with nitrogen for 20 minutes prior to sealing. Reactions were then heated to 70 °C (thermostated oil bath, Heidolf) for 24 hours. During the polymerisation aliquots of 2 mL were extracted at set time periods, aerated with oxygen and cooled on ice to quench polymerisation before measuring conversion gravimetrically and size analysis by DLS.

Seeded dispersion polymerisation	Mass
Methanol	22.5 g
Water	7.00 g
Poly(styrene) seed latex (12.27 wt% solid content)	5.00 g
Butyl Acrylate	0.35 g
PVP K30/K90	0.013 g
AIBN	0.05 g

Table 3.6 List of chemicals required for seeded dispersion polymerisations in the presence of sub-micron poly(styrene) seed particles (TSNP110)

3.6 References

(1) Sheu, H. R.; El-Aasser, M. S.; Vanderhoff, J. W. *Journal of Polymer Science Part A: Polymer Chemistry* **1990**, *28*, 653–667.

(2) Sheu, H. R.; Vanderhoff, J. W. *Journal of Polymer Science Part A: Polymer Chemistry* **1990**, *28*, 629–651.

(3) Ballard, N. Ph.D. Thesis, University of Warwick, 2012.

(4) Okubo, M.; Katsuta, Y.; Matsumoto, T. *Journal of Polymer Science Part C* **1982**, *20*, 45–51.

(5) Min, T. I.; Klein, A.; El-Aasser, M. S.; Vanderhoff, J. W. *Journal of Polymer Science Part A* **1983**, *21*, 2845–2861.

(6) Chen, Y.-C.; Dimonie, V.; El-Aasser, M. S. *Journal of Applied Polymer Science* **1991**, *42*, 1049–1063.

(7) Okubo, M.; Murakami, Y.; Fujiwara, T. *Colloid & Polymer Science* **1996**, *274*, 520–524.

(8) Okubo, M.; Fujiwara, T.; Yamaguchi, A. *Colloid & Polymer Science* **1998**, *276*, 186–189.

(9) Okubo, M.; Kanaida, K.; Matsumoto, T. *Colloid & Polymer Science* **1987**, *265*, 876–881.

(10) Rieger, J. *Journal of Thermal Analysis* **1996**, *46*, 965–972.

(11) París, R.; De la Fuente, J. L. *Journal of Polymer Science Part B* **2007**, *45*, 1845–1855.

(12) Becu-Longuet, L.; Bonnet, A.; Pichot, C.; Sautereau, H.; Maazouz, A. *Journal of Applied Polymer Science* **1999**, *72*, 849–858.

(13) Brady, A. J.; Keskkula, H.; Paul, D. R. *Polymer* **1994**, *35*, 3665–3672.

(14) Sundberg, D. C.; Casassa, A. P.; Pantazopoulos, J.; Muscato, M. R.; Kronberg, B.; Berg, J. *Journal of Applied Polymer Science* **1990**, *41*, 1425–1442.

(15) Cook, D. G.; Rudin, A.; Plumtree, A. *Journal of Applied Polymer Science* **1992**, *46*, 1387–1393.

(16) Mock, E. B.; Zukoski, C. F. *Langmuir* **2010**, *26*, 13747–13750.

(17) Ugelstad, J.; Söderberg, L.; Berge, A.; Bergström, J. *Nature* **1983**, *303*, 95–96.

(18) Ellingsen, T.; Aune, O.; Ugelstad, J.; Hagen, S. *Journal of Chromatography A* **1990**, *535*, 147–161.

(19) Shen, S.; El-Aasser, M. S.; Dimonie, V. L.; Vanderhoff, J. W.; Sudol, E. D. *Journal of Polymer Science Part A* **1991**, *29*, 857–867.

(20) Okubo, M.; Yamashita, T.; Suzuki, T.; Shimizu, T. *Colloid & Polymer Science* **1997**, *275*, 288–292.

(21) Okubo, M.; Minami, H. *Colloid & Polymer Science* **1996**, *274*, 433–438.

(22) Fujibayashi, T.; Okubo, M. *Langmuir* **2007**, *23*, 7958–7962.

(23) Okubo, M.; Fujibayashi, T.; Yamada, M.; Minami, H. *Colloid and Polymer Science* **2005**, *283*, 1041–1045.

(24) Shi, S.; Zhou, L.; Wang, T.; Bian, L.; Tang, Y.; Kuroda, S. *Journal of Applied Polymer Science* **2011**, *120*, 501–508.

(25) Fujibayashi, T.; Komatsu, Y.; Konishi, N.; Yamori, H.; Okubo, M. *Industrial & Engineering Chemistry Research* **2008**, *47*, 6445–6449.

(26) Paine, A. J.; Luymes, W.; McNulty, J. *Macromolecules* **1990**, *23*, 3104–3109.

(27) Wang, D.; Dimonie, V. L.; Sudol, E. D.; El-Aasser, M. S. *Journal of Applied Polymer Science* **2002**, *84*, 2692–2709.

(28) Wang, D.; Dimonie, V. L.; Sudol, E. D.; El-Aasser, M. S. *Journal of Applied Polymer Science* **2002**, *84*, 2710–2720.

(29) Jiang, S.; Sudol, E. D.; Dimonie, V. L.; El-Aasser, M. S. *Macromolecules* **2007**, *40*, 4910–4916.

(30) Jiang, S.; Sudol, E. D.; Dimonie, V. L.; El-Aasser, M. S. *Journal of Polymer Science Part A* **2008**, *46*, 3638–3647.

(31) Perro, A.; Reculusa, S.; Bourgeat-Lami, E.; Duguet, E.; Ravaine, S. *Colloids and Surfaces A* **2006**, *284–285*, 78–83.

(32) Reculusa, S.; Poncet-Legrand, C.; Perro, A.; Duguet, E.; Bourgeat-Lami, E.; Mingotaud, C.; Ravaine, S. *Chemistry of Materials* **2005**, *17*, 3338–3344.

(33) Perro, A.; Duguet, E.; Lambert, O.; Taveau, J.-C.; Bourgeat-Lami, E.; Ravaine, S. *Angewandte Chemie* **2009**, *48*, 361–5.

(34) Du, X.; He, J. *Journal of Applied Polymer Science* **2008**, *108*, 1755–1760.

(35) Schneider, C. A.; Rasband, W. S.; Eliceiri, K. W. *Nature Methods* **2012**, *9*, 671–675.

Chapter 4

Hierarchical self-assembly of 'hard-soft' Janus particles into colloidal molecules and larger supracolloidal structures

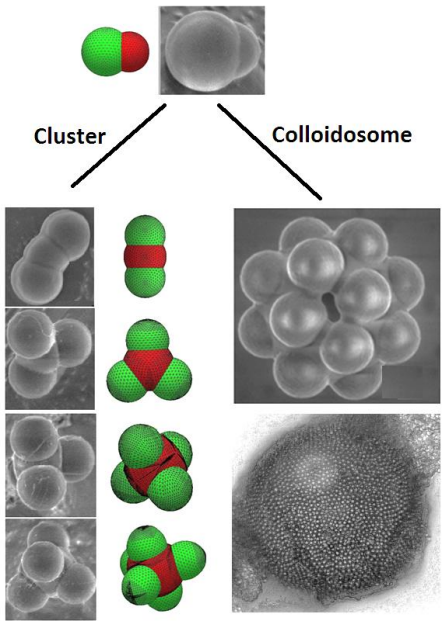

4.1 Abstract

We report the self-assembly of 'hard-soft' micron-sized Janus particles as synthesised in chapter 3 into clusters in aqueous media. The assembly process is induced by the desorption of polymeric stabiliser, poly(vinyl pyrrolidone). Upon contact through collision and coalescence of the soft polymeric lobes, the newly formed clusters adopt a minimised surface area to volume ratio hereby forming distinct microscopic supracolloidal analogues of simple molecular valance shell electron pair repulsion spacefill structures. The effect of shear force and surfactant concentration on the rate of

cluster formation is measured, indicating a strong dependence of increasing flocculation rate upon higher applied shear force and reduction of surfactant concentration. To explain this behaviour, colloidal stability of our particle suspensions were calculated theoretically, comparing the difference of interaction potential between particles with and without an adsorbed steric surfactant. Simulations of expected cluster morphology, compared with those obtained from visual cryo-SEM analysis support the mechanism of assembly driven by surface area minimisation in the case of soft-soft interactions. Altering the soft lobe size with respect to the hard lobe indicates a moderate effect on number of primary particles per cluster. Additionally, higher order structures of clusters containing a number of primary particles exceeding what is possible for a 'solid' core cluster are observed, indicating the formation of 'hollow' structures. As such, we investigate the formation of suprastructures using a high number of 'hard-soft' Janus particles and verify their effective stabilisation of gas bubbles.

4.2 Introduction

Nature possesses the ability to construct complex functional materials from the most basic building blocks, for instance the assembly of molecules from atomic subunits. Following this strategy, there is huge potential in fabricating advanced structures utilising a 'bottom-up' approach. The ability to fabricate materials from a defined set of simple components in a scalable bulk system would find many applications in areas such as photonics[1,2] drug delivery, nano/micro scale electronic devices and structured catalysts.[3]

4.2.1 Colloidal molecules

'Colloidal Molecules' a term coined by van Blaaderen in 2003[4] describes the formation of supracolloidal structures that resemble the configuration of atoms in molecules both in angular arrangement and respective lobe size to that of VSEPR spacefill geometries. There has recently been a surge of interest in this area with various fabrication methods being reported in the literature which can be divided into three main areas: (1) controlled phase separation, (2) controlled surface nucleation, and (3) controlled clustering.

4.2.2 Colloidal clusters from controlled phase separation

The first area involves the total synthesis of colloidal molecules thereby avoiding an 'assembly' step and is possible through phase separation of a protrusion from a core entity. Various inorganic core-shell nanoparticles have been shown to forcefully phase separate under applied reaction conditions.[5–7] This was first reported by Giersig *et al.*[8] when treating silica coated silver nanoparticles with molecular iodine. In less than 20 minutes, a singular lobe of silver iodide nucleates on the surface of the nanoparticles. However, most phase separation reactions form simple 'snowman' or 'dumbbell' type biphasic particles. The same can be said for the majority of the various polymer phase separation routes. Both phase separation by solvent evaporation[9,10] and seeded heterogeneous polymerisations of polymer seed particles (emulsion[11–13] and dispersion[14]) can render 'colloidal molecules', most of which present as biphasic particles. These bi-phasic particles are often referred to as Janus particles and are discussed in the introduction. Although multiple simultaneous protrusions in emulsion[15] and dispersion[16] polymerisations have been reported, these are seldom configurationally controlled and

uniform. Weitz *et al*.[17] extended the approach of a seeded emulsion polymerisation route to render more complex monodisperse dimers, trimers and tetramers based on multiple entropic phase separations,[11] as seen in figure 4.1a.

4.2.3 Colloidal clusters from controlled surface nucleation

Controlled surface nucleation and growth presents a route to more complex architectures than phase separation, with higher order geometries possible. There are many examples of epitaxial growth of hard inorganic systems,[18] growing up to eight lobes off a singular particle.[19] The controlled nucleation of up to 8 poly(styrene) lobes from silica particles has also been documented,[20,21] as shown in fig 4.1b & c.

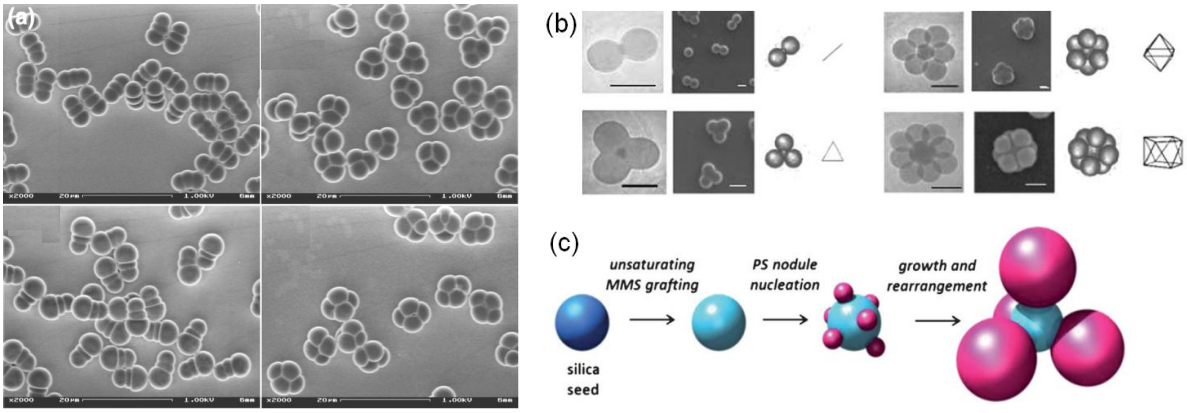

Figure 4.1 (a) entropic phase separation to grow dimers, trimers and tetramers.[17] (b) & (c) growth of hybrid poly(styrene)-silica colloidal molecules[20,21]

4.2.4 Colloidal clusters from controlled clustering

The third area to fabricate colloidal molecules involves the controlled clustering of 'building-block' particles. Directed assembly of spherical particles into 'colloidal

molecules' was first reported by Manorahan *et al.*[22] and provides an elegant example of how particle confinement in an evaporating droplet can be used to control size and shape of colloidal clusters from a monodisperse seed latex (fig. 4.2a). Energy minimisation of the prevailing van der Waals attractions between the uncharged spheres resulted in cluster geometries analogous to the most efficient packing conformation predicted mathematically. This technique was extended to assemble bi-disperse mixtures of polystyrene latex and inorganic nanoparticles (figure 4.2b).[23] The larger microspheres assemble initially upon evaporation of the emulsion droplet, with the smaller inorganic particles assembling around the larger structure upon the drying of the droplet meniscus between the microspheres. Additionally, the geometric confinement of spherical colloids on 2-D templates has been reported, with a myriad of cluster morphologies fabricated through the use of differing sizes of colloids and template shape (see figure 4.2c).[24,25]

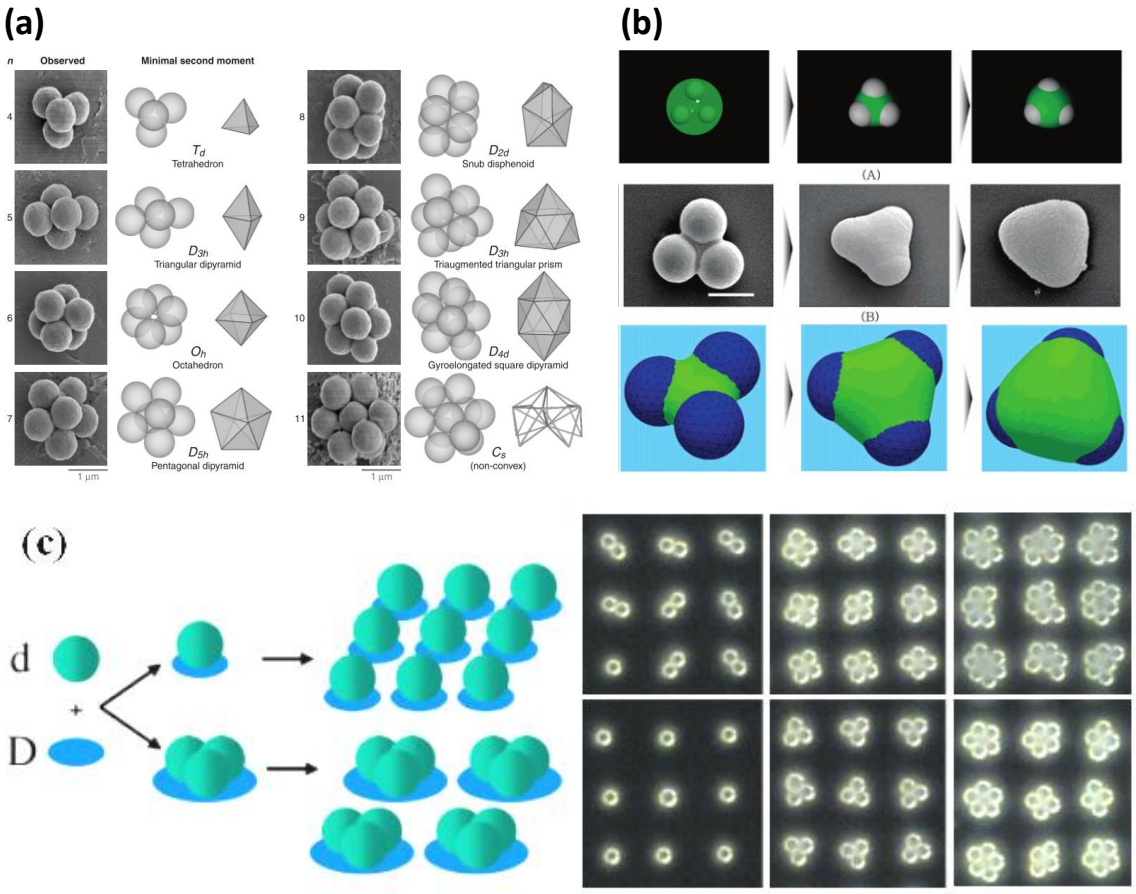

Figure 4.2 (a) Spherical cluster formation by evaporating droplet assembly and sinstering[22] (b) Evaporating droplet assembly of a binary colloidal system[23] (c) Geometric confinement of spherical colloids on 2-D circular templates of varying size to render clusters from 1 -6 primary particles[25]

However, there are limitations to using isotropic spherical particles, as these suffer from uniform particle-particle interactions, often relying on an external force (such as templating) in order to assemble into complex structures. On the other hand, molecular building blocks possess the ability to forge specific and directional interactions. A simple example of this is hydrogen bonding in water and acetic acid, as depicted in figure 4.3. Therefore furnishing colloidal particles with chemical or morphological anisotropy provides the specificity and directionality to allow complex assembly.

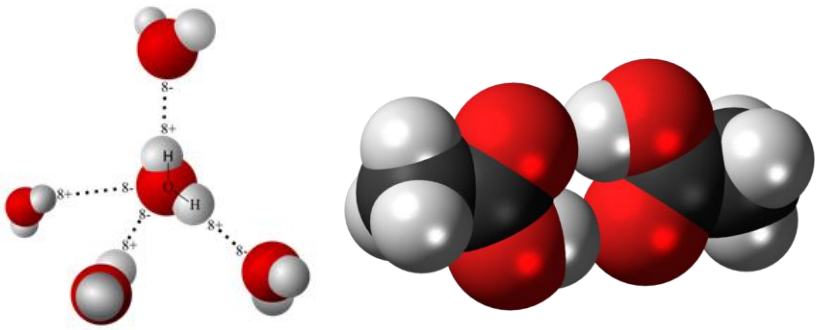

Figure 4.3 Spacefill models of hydrogen bonding in (left) water and (right) acetic acid dimers, illustrating the specificity and directionality of molecular assembly

4.2.5 Anisotropic colloidal assembly

Many techniques of controlling particle assembly through anisotropic elements on particles, such as patches or protrusions, have been reported. Kim *et al.*[26] exploited the use of flat hydrophobic domains on otherwise hydrophilic surface treated polystyrene particles to direct self assembly of polystyrene beads into dimers and trimers (figure 4.4a). The exposed hydrophobic face in an aqueous environment gives rise to an unfavourable interfacial energy. This interfacial energy provides the driving force for the spontaneous site specific assembly of these particles into dimers. The addition of isotropic surfactant treated spheres, allows the formation of trimers.

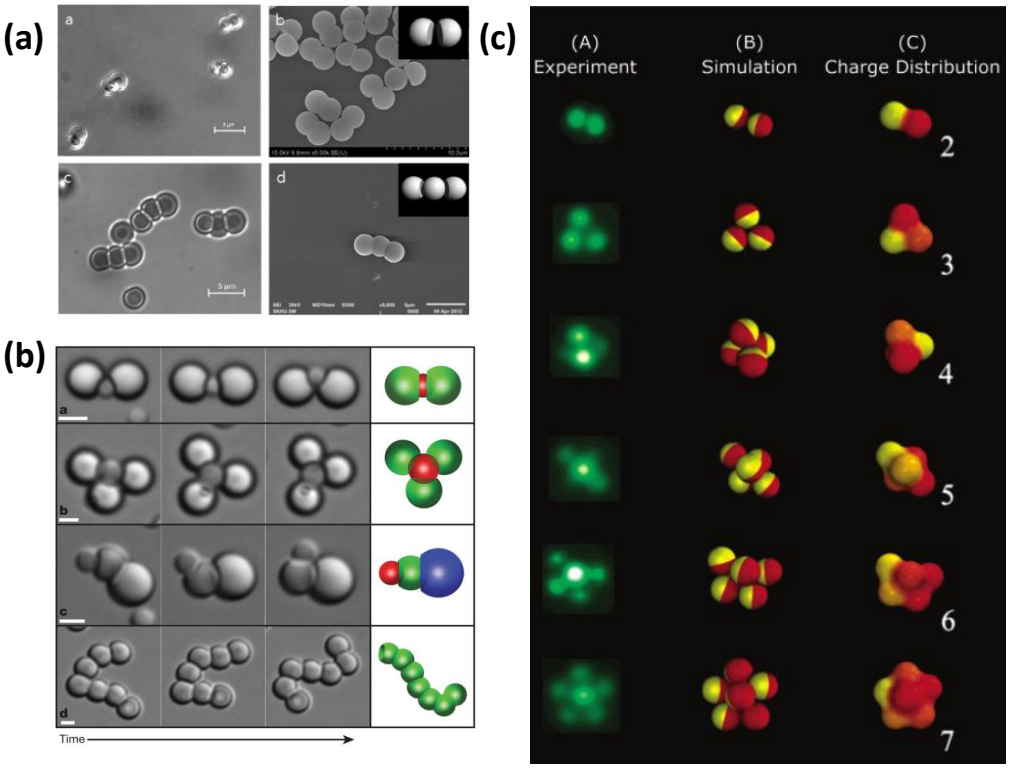

Figure 4.4 (a) hydrophilic polystyrene particles with hydrophobic domains assemble into dimers and trimers driven by the ability to reduce unfavourable interfacial tension arising from the exposed hydrophobic domain.[26] (b) 'Lock and Key' Colloids, using depletion interaction to only allow assembly when the magnitude of interaction is strong enough, i.e. when particles fit snugly into the recess of a larger dimple..[27] (c) Chemically anisotropic spherical Janus particles adopt specific geometries when flocculated in salt solutions based on energy minimisation of the polarised hemispheres[28]

In an elegant advancement, Sacanna *et al.*[27] developed particles with dimples that could participate in site selective interactions. As seen in figure 4.4b, spheres of a specific size interact and assemble within a dimple of a larger particle. This assembly is driven by depletion attraction, using polyethylene imine as a depletion flocculant. The quantity of flocculant is tuned to only allow interaction when sufficient surface area contact is large enough, i.e. only in the lock and key configuration. Therefore, when a range of particles

with varying size are used, only specific assemblies can occur, so named 'lock and key' colloids.

Chemical rather than morphological anisotropy has also been used to assemble spherical Janus particles possessing chemically different hemispheres into clusters.[29] Hong *et al.* synthesised amphiphilic particles with hydrophilic and respective hydrophobic hemispheres. On increasing ionic strength, Janus particles within the suspension are observed to cluster, with the cluster size proportional to salt concentrations.[30] Similarly, particles with an anisotropic distribution of surface charge over the two hemispheres,[28] with zwitterionic activity allowed assembly driven both by van der Waals attractions, and optimisation of the electrostatic interactions with the surface charge of nearby particles giving rise to cluster conformations deviating from equivalent clusters of uncharged spheres (fig 4.4c). Whilst these examples exhibit excellent high fidelity 'Janus character' i.e. well defined 'faces', the fabrication of these particles is hard to scale up.

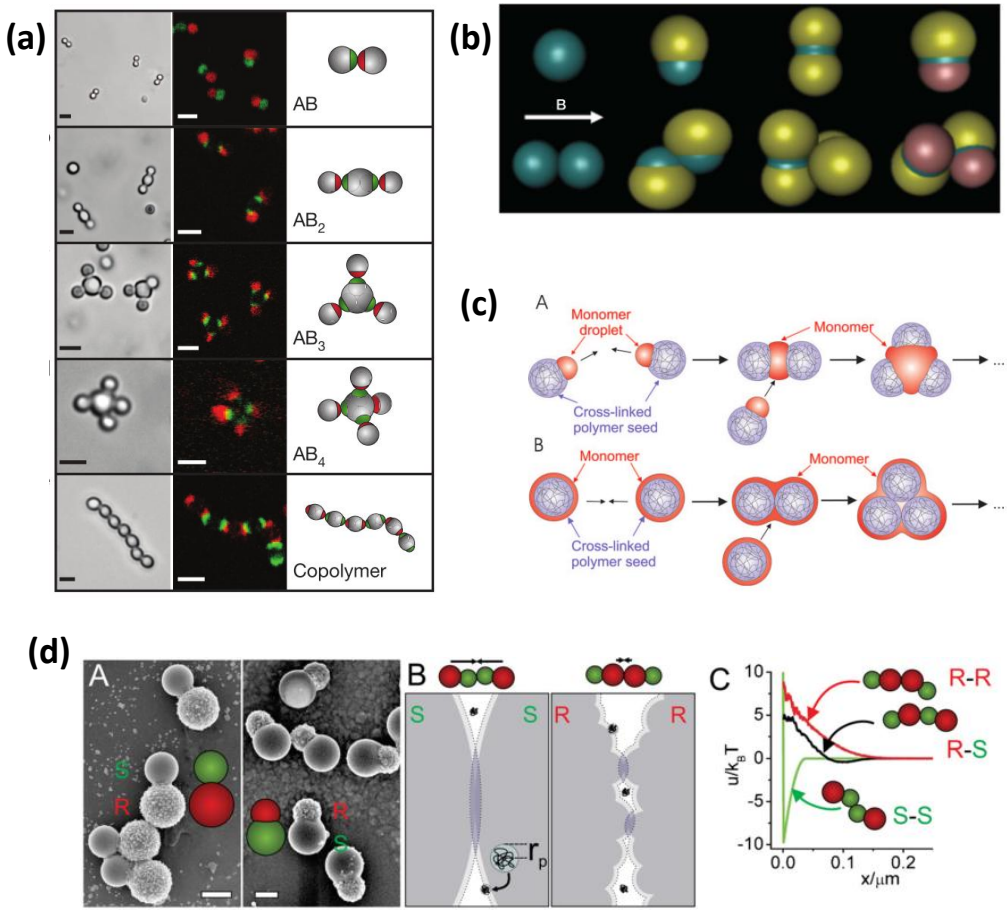

Figure 4.5 (a) Using complimentary DNA binding to selectively control assembly[31] (b) Janus particles incorporating magnetic ferrofluid in one of the lobes assemble in magnetic fields[32] (c) entropic phase separation of a monomer protrusion from a seed particle is a non-stabilised site for assembly into clusters[33] (d) Janus particles use surface roughness anisotropy to direct assembly[34]

Complimentary DNA binding between particles has also been exploited to incorporate selectivity of interaction between particles, thereby paving the way for the assembly of more complex structures (fig 4.5a).[31]

Non-spherical biphasic 'dumbbell' particles are a convenient route to both chemical and geometric directionality. Dumbbell particles with a magnetic ferrofluid lobe assemble

into clusters and chains whilst being subjected to a magnetic field (fig. 4.5b).[32] The conformation of which is a competition between magnetic attraction and steric hindrance. Anisotropic dumbbell particles featuring a 'rough' and 'smooth' phase aggregate into clusters, whereby only the 'smooth' lobes of the particles interact, the 'hard' phases providing a sterically repulsive force against aggregation (fig 4.5d).[34] Despite showing good control of selective interactions to form regular clusters, most of these techniques exploit reversible interactions, whereby application of sufficient shear or a change in ionic strength would cause disintegration of the cluster.

Kraft *et al.*[33] manufacture clusters which are permanently bonded together. Initially a multistep entropic phase separation emulsion polymerisation technique to forms a liquid monomer protrusion from a crosslinked polystyrene seed. The unstabilised monomer protrusions coalesce into 'colloidal molecules' whilst under stirring their morphology governed by the minimisation of exposed monomer interface. In order to lock the conformation, the coalesced monomer core is polymerised. The process is depicted schematically in fig. 4.5c. This example can be seen as a combination of phase separation and controlled clustering. The initial phase separation renders a simple anisotropic Janus particle to provide directionality, which then participates in an assembly step to render clusters of controlled geometry.

By taking inspiration from the advantages of methods described above, we investigate a different approach towards fabricating colloidal clusters. As the previous examples have shown, particle anisotropy provides a source of directionality, leading to specific

interactions between particles, and is therefore a desirable quality. However, many of these interactions are weak and rely on precise tuning of solution conditions. Whilst Kraft and co-workers overcome weak interactions by a post-polymerisation step locking the conformation of the cluster into a polymer matrix, we feel that this can be improved upon by combining the coalescence and 'locking' in one step.

It is our aim to manufacture anisotropic particles which do not require an external templating force in order to aggregate into clusters of controlled morphology. Instead, aggregation is initiated by a simple stimulus and the conformation of these aggregates is locked upon contact without the need for additional reaction steps.

In chapter 3 we discuss the synthesis of micron sized 'hard-soft' Janus particles by the seeded dispersion polymerisation of butyl acrylate in the presence of polystyrene seed particles. The resulting particles are 'dumbbell' shaped with lobes of distinct glass transition temperature; -54 °C for the poly(*n*-butyl acrylate) and +105 °C for the poly(styrene) lobe. A steric stabiliser, that is PVP, is used to impart colloidal stability to these particles whilst in an aqueous dispersed phase. We investigate the aggregation of hard-soft Janus particles upon the removal of the steric barrier and the resulting morphology. The idea being that the soft components of the Janus particles contact and coalesce into clusters of controlled geometry.

4.3 Results and discussion

4.3.1 Dilution as a route to particle flocculation

It is known in dispersion polymerisation, that a steric stabiliser employed to impart stability against particle flocculation and coalescence can be chemisorbed (through grafting) and physisorbed on to the particle surface.[35,36] Initially, flocculation measurements were carried on hard poly(styrene) microspheres synthesised using a steric stabiliser to observe the effect of dilution on colloidal stability in stirred conditions. The idea was to investigate whether dilution is a viable method for inducing particle flocculation through the assumption that steric stabiliser desorbs upon dilution in aqueous media. Polystyrene spheres of 2 µm diameter used in this study were synthesised by dispersion polymerisation in ethanol, using poly(vinyl pyrrolidone) (360,000 $gmol^{-1}$, PVP K90) as a steric stabiliser, and represent the seed particles used to manufacture hard-soft Janus particles.

Time lapse laser scattering measurements of diluted suspensions of purified 2 µm diameter microsphere suspensions were conducted in a Mastersizer 2000 with Hydro S dispersion unit (Malvern Instruments, UK). This setup provides a closed controlled stirred environment allowing periodic measurement of particle size distribution though laser scattering. A purified polystyrene microsphere suspension was introduced into the flow cell and diluted to 0.4 gL^{-1} prior to ultrasonic treatment for 2 minutes using the instrument ultrasonic probe at 100% intensity to disperse any aggregates. Size distribution analyses were conducted at 20 minute intervals over 400 minutes whilst the flow cell was subjected to stirring at 1750 rpm. In a control measurement following an

identical protocol, purified microsphere suspensions were dispersed into an aqueous PVP K90 solution, whereby the concentration of PVP matches that of the reaction conditions used to synthesise the Janus particles (2 wt% w/r to polymer). The results for these analyses can be seen plotted in figure 4.6a for pure water and 4.6b for PVP solution as dispersed phase.

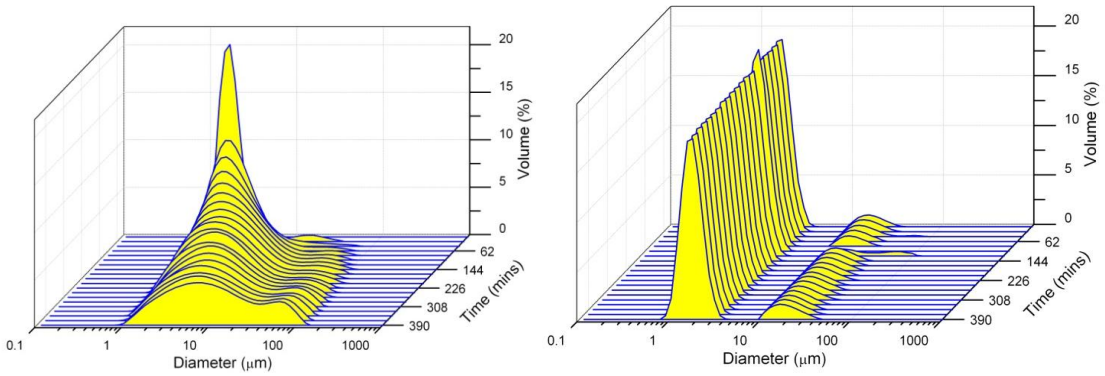

Figure 4.6 Collated Time lapse laser diffraction measurements of PS microspheres (TS408C) in pure water (left) and aqueous PVP-K90 solution (right). Note the smaller secondary peak arises from a small quantity of undispersed aggregate present from the start of the measurement

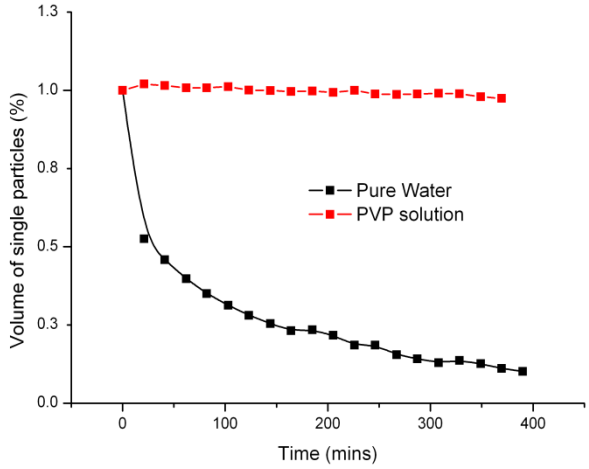

Figure 4.7 Volume fractions of particles (TS408C) measured at 2 μm diameter during the laser scattering measurements (figure 4.6) as a function of time for particle suspensions in pure water and PVP solution

It is clear to see from the figures that particle suspensions without added polymeric stabiliser flocculated over time, whereas microsphere suspensions with stabiliser present

in the medium were stable against any long term flocculation, despite the shear conditions experienced within the flow cell. Whilst the primary particle peak at 2 µm diameter remains constant throughout the measurement period in the presence of polymeric stabiliser, the absence of stabiliser results in a gradual shift upwards in diameter. Values for volume at 2 µm diameter were plotted as a function of time for both the pure water and PVP-K90 solution time lapse measurement, as seen in figure 4.7. This represents the relative concentrations of singular microsphere particles, and indicates that in the presence of PVP, no decline in singular particle number occurs. However an exponential decay of singular particle volume is seen in the absence of PVP. Kraft *et al.* theorised the increase in cluster size as a function of time in their system which involved the coalescence of monomer droplets on the surface of solid particles whilst under the influence of stirring.[33] Additionally, this sample becomes more polydisperse as the number of primary particles in a cluster varies.

These results indicate that colloidal stability is lost upon dilution and particles become susceptible to aggregation when sheared. This is attributed to the desorption of PVP from the particle surface as a result of dilution in water and is supported by the observation that dilute particle suspensions in a PVP solution do not aggregate under shear. Moving forward in our investigation, we can use the dilution effect to induce flocculation.

4.3.2 Flocculation kinetics of hard-soft Janus particles

Based on the microsphere flocculation results, the rate of flocculation of hard-soft Janus particles by turbidity was investigated. We employed a technique to measure singular

Janus particle concentration as a function of time whilst under the influence of a constant mixing force. Chapter 3 outlines the full synthetic procedure to synthesise hard-soft Janus particles. In this experiment, we used particles of equal lobe size (1:1 pSty:pBA) 2 µm in width at the widest point, and 3.5 µm length across the longest axis. Particles were purified by repeated gravity sedimentation and redispersion in deionised water to desorb PVP from particle surface. Centrifugation is not used in the purification stage as this leads to particle fusion on sedimentation. 10 mL of 0.2 gL^{-1} dilute suspensions of Janus particles in deionised water were sealed in 15 mL glass vials before fixing to a rotor of fixed radius. The vials were then rotated at a fixed speed during which the particles coagulated, causing a decrease in turbidity. The experimental setup is depicted schematically in appendix B.

Temporal decrease of turbidity was measured by spectrophotometric absorbance at 540 nm and back calculated through a calibration curve of known primary particle concentration as a function of absorbance (appendix B) to yield a quantitative decrease in singular particle concentration. The results of this experiment are plotted in figure 4.8(l).

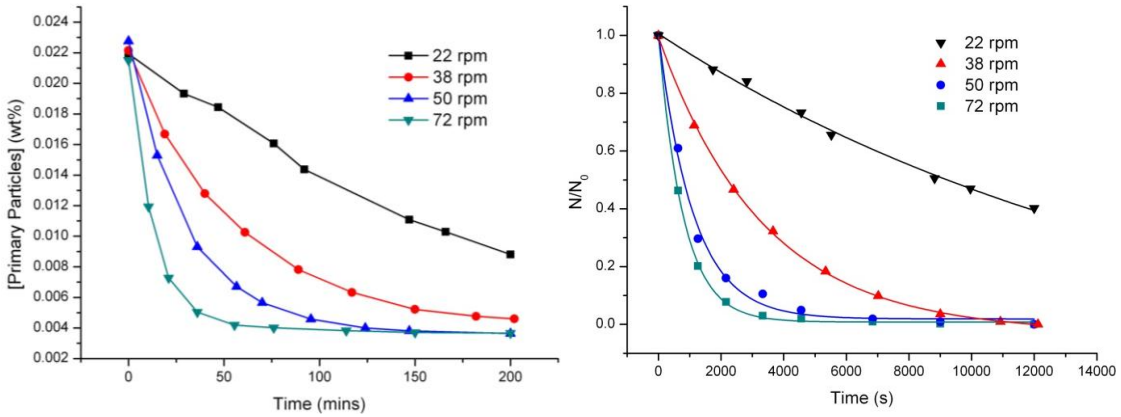

Figure 4.8 (Left) Primary particle (TS450) concentration as a function of time over a range of mixing forces. (Right) Fitting the Smoluchowski orthokinetic flocculation equation (Eqn. 1) to the turbidity decay data

We can see the rate of flocculation is proportional to shear force, and exhibits an exponential decay profile. This data fits a simple derivation of Smulochowski's orthokinetic flocculation well as shown in equation (1) and plotted in figure 4.8(r). The decrease in initial particle number $\frac{N}{N_0}$ exponentially decays with respect to $\bar{G}$ (mixing force), α (collision efficiency), Ω (volume fraction of colloids) and t time, whereby collision efficiency is the fraction of successful aggregations upon particle collision. In our system, the volume fraction of polymer is and collision efficiency is assumed to be constant.

The mixing intensity component (equation 2) is derived from Camp-Stein equation[37] that defines shear force by power dissipation (P) into the system, i.e. rotation speed.

$$\ln \frac{N}{N_0} = -\left(\frac{4}{\pi}\right) \alpha \Omega \bar{G} t \qquad (1)$$

$$\bar{G} = \sqrt{\left[\frac{P}{V \cdot \mu}\right]} \qquad (2)$$

In a similar battery of experiments to ascertain the contribution of PVP in the continuous phase towards restricting flocculation, we measured turbidity of dilute suspensions of particles at fixed rotor speed of 32 rpm, with various concentrations of PVP dispersed into the aqueous phase. The results of these measurements are plotted in fig 4.9.

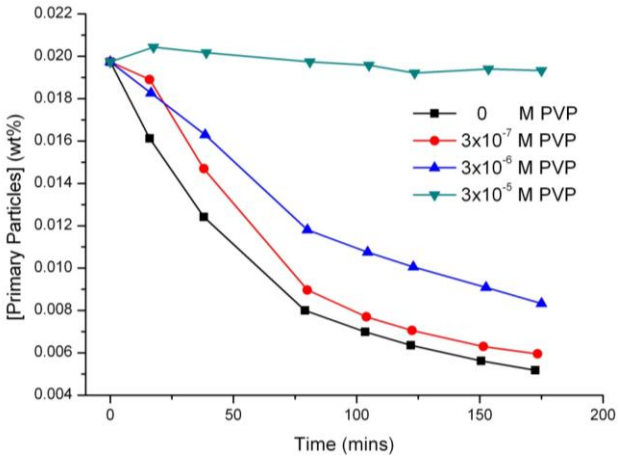

Figure 4.9 Primary Particle concentration as a function of time for a range of PVP-K90 concentrations in the continuous phase, as measured by turbidity (TS449)

Without any added PVP to the solution, the particles flocculated rapidly as expected. However, upon the addition of PVP to the suspension, flocculation rate was slowed, until at $3x10^{-5}$ $moldm^{-3}$, flocculation was completely arrested for the duration of the experiment. Previous studies have calculated the monolayer adsorption isotherms of PVP on to nano-scale poly(styrene) latexes. Kellaway and Nijab[38] quote the saturation adsorption of PVP-K90 on to a polystyrene latex as 30 mg/m^2. This equates to $4.8x10^{-8}$ $moldm^{-3}$ in our system depicted in figure 4.9, which is approximately 3 orders of magnitude lower than the concentration of PVP we require in our system to halt flocculation. It has been noted that PVP adsorbs to a poly(styrene) surface with loops and tails extended out into solution, especially at higher molecular weights (i.e. above 44,000 $gmol^{-1}$), rather than adsorb in monolayer trains.[35] Therefore, we can attribute some of the disparity between our observed concentration of PVP with that of the theoretical total monolayer coverage. Equally, our study focuses on the colloidal stability of micron sized particles whilst under a shear force, compared with the literature examples of nano-sized poly(styrene) latexes under no shear force. Van der Waals attractions between particles in

our case are far stronger than nanoscale particles. Therefore there are higher magnitude attractive forces between the particles in our system. Clearly, full monolayer surface coverage of PVP-K90 is not sufficient to overcome these attractive forces and therefore the PVP dispersed within the aqueous phase plays a role in the stabilisation of the particles, plausibly in the form of depletion stabilisation. One could argue that adsorption of high molecular weight PVP onto the particle interface occurs over longer timescales than the duration of the experiment. However Smith *et al.* determined that the adsorption process of high molecular weight PVP-K90 onto polystyrene spheres occurs rapidly within 5 minutes.[35] An alternative reason may partly be due to the increased viscosity of the system as a result of PVP addition which in turn reduces the mixing force $\bar{G}$ at fixed rotation speed and volume (see equation 1).

4.3.3 Modelling colloidal stability of a sterically stabilised particle dispersion

This reliance of uncharged particles on a steric barrier provided by an external polymer or 'protective colloid' can be quantified theoretically by considering several factors; the van der Waals attraction between two spheres, attractive or repulsive electrostatic surface charge component and 'non-DLVO' steric repulsion from an adsorbed polymer layer. Due to the absence of charged components in the system, contribution of the electrostatic component is negligible. The van der Waals attractive potential V_A is calculated according to Hamaker interaction (see equation 3) taking the Hamaker constant (A) for polystyrene-polystyrene in water medium as 9.25×10^{-21}. *a* and *H* represent particle radius and surface separation respectively.[39] The steric repulsion component based on the Flory Huggins lattice mixing model accounts only for the osmotic pressure contribution alone,

as seen in equation 4. V represents molar volume of solvent, Ø the effective volume fraction of polymer, based on experimentally determined polymer surface coverage.[35] This value is taken as the three dimensional volume that the PVP occupies at the surface and includes the contribution from loops and tails, by taking into account the adsorbed layer thickness. χ is the Flory-Huggins interaction parameter for PVP and water (taken as 0.48), δ is the adsorbed polymer layer thickness, again determined experimentally as 15 nm.[35,38] Combination of both the attractive and repulsive components based on the parameters of our microsphere suspension yields a net potential as seen in fig. 4.10(left). At our given particle radius of 1 μm, the potential is mildly attractive until $H = 2\delta$ (30 nm), where an overwhelming steric repulsion stops flocculation. It is therefore plausible that an excess to monolayer coverage of PVP is required to overcome the mildly attractive zone. If however, the steric barrier is completely removed, i.e. total desorption of the PVP layer in our system, a large attractive potential promotes flocculation as seen in fig. 4.10(right).

$$V_A = \frac{-A}{6}\left(\frac{2A^2}{H^2+4aH} + \frac{2a^2}{(H+2a)^2} + \frac{ln\, H^2+4aH}{(H+2a)^2}\right) \quad (3)$$

$$Vs = \frac{4\pi a}{V}(\emptyset^2)(0.5-\chi)\left(\delta - \frac{H}{2}\right)^2 \quad (4)$$

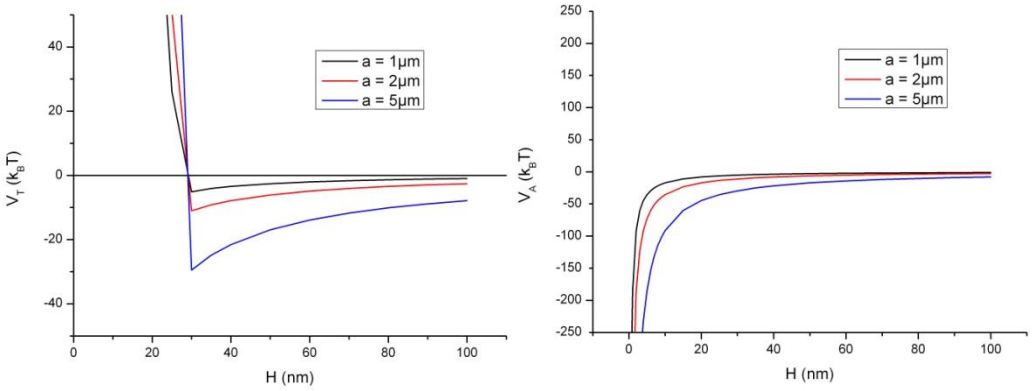

Figure 4.10 Energetic interaction potentials of spherical colloids of varying diameter over a range of inter-particle separations with (left) and without (right**)** the presence of PVP-K90 steric stabiliser

4.3.4 Cluster formation of hard-soft particles

Perhaps the most important part of this investigation involves the visualisation of the particle clusters after flocculation of the Janus particles. For this we synthesised a batch of Janus particles, 0.5:1 pBA/pSty lobe ratio, 2 μm length and 1.5 μm width (across respective axis), defined by optical and scanning electron microscopy analysis seen in figure 4.11.

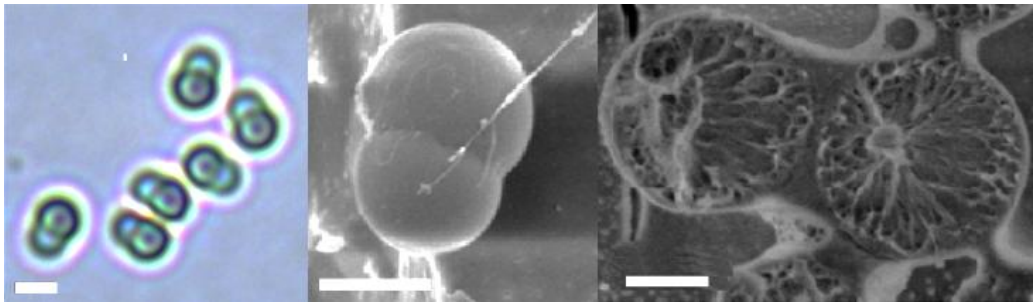

Figure 4.11 Optical (left) and Cryogenic Scanning Electron (centre) micrographs of 0.5:1 pBA:pSty Janus particles (TS405-1), including a freeze-fractured slice through two coalesced particles (right) The larger, darker spheres are the pSty seed with the smaller, lighter lobes representing the pBA lobe. Scale bars 2 μm, 1 μm and 500 nm respectively

In accordance with the other experiments in this chapter, the particles were permitted to sediment and the solvent replaced by deionised water three times. The dilute suspensions of 0.1 wt% solids were hand shaken for 30 seconds by hand to provide the shear force necessary for cluster formation. The cluster suspension was then visualised by optical microscopy and cryo-SEM.

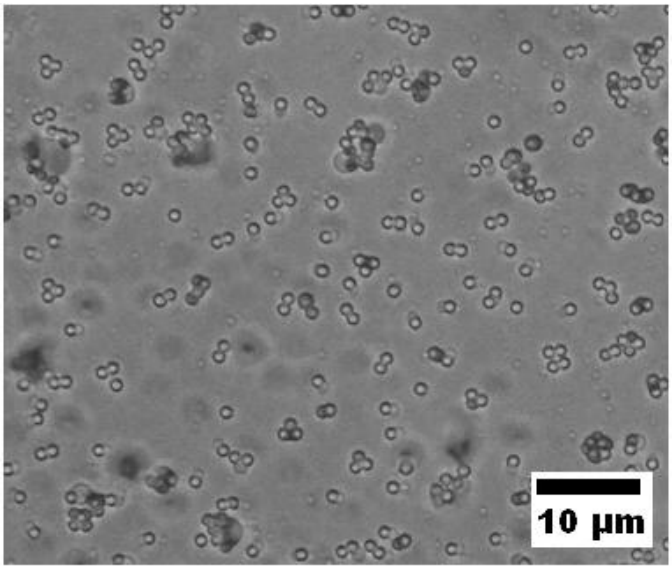

Figure 4.12 Optical micrograph of a typical Janus particle suspension (TS502-seeded) after PVP removal, whereby desorption of the PVP from the particles has led to irreversible flocculation

From the micrograph, many cluster geometries can be seen. The cluster morphology is governed by the orientation of particles upon collision resulting in four possible interaction regimes; hard-hard, hard-soft, soft-soft and simultaneous hard-soft. These interactions are depicted schematically in figure 4.13. Note that the angle of collision can vary.

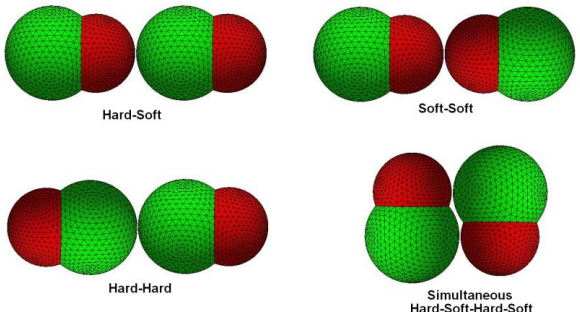

Figure 4.13. Schematic of possible collision arrangements for two Janus particles. Green lobe represents the hard poly(styrene)

Interaction by the first regime whereby a hard lobe of one Janus particle collides with a soft lobe of another, results in a wide range of cluster morphology with little control or regularity. Interaction between two hard lobes of Janus particles is reversible as no coalescence occurs, and easily broken by the application of shear, i.e. agitation or ultrasound. This is demonstrated in the initial flocculation measurements involving hard polystyrene spheres, whereby sonication of the suspension breaks apart any flocs. Particles can also align side by side, giving rise to simultaneous contact between two particles involving four lobes. One particle can approach the other at a varying angle range of 180°. However, this interaction is less likely to occur compared to the other collision regimes. Finally, the most interesting interaction is between two or more soft lobes, especially when visualised under Cryo-SEM and optical microscopy. The left two columns of figure 4.14 depict 5 clusters with 1 – 5 primary particles (N_p) imaged from a single sample of cluster suspension prepared in the manner described above.

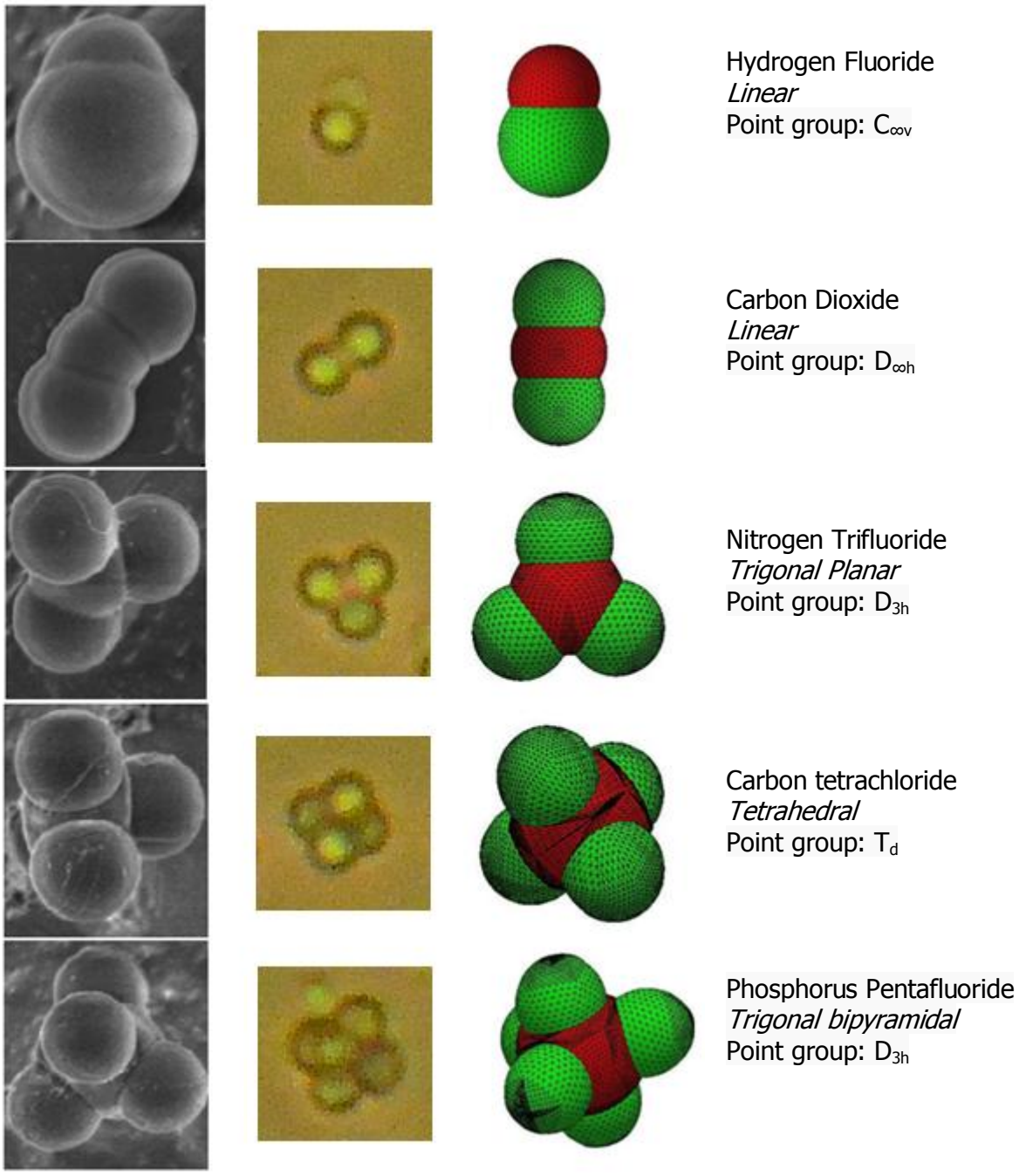

Figure 4.14 (left) High resolution Cryo-SEM images of clusters N_p 1 – 5 coupled with the optical micrograph images of clusters in suspension (centre) – (TS405-1) Respective graphical surface energy minimisation simulation from Surface Evolver, green indicates the 'hard' poly(styrene) phase, red indicates the 'soft' poly(butyl acrylate) phase. (right) Examples of simple molecules with analogous VSEPR spacefill geometries

The most striking aspect of these images is that all of these structures bear a significant mesoscale resemblance to valence shell electron pair repulsion (VSEPR) spacefill models for simple molecules. As outlined in the introduction to this chapter, the synthesis of particles with analogous morphologies and their comparison with molecular systems has been reported by several other groups[20–22,29] and correlate with the mathematically derived lowest energy conformations presented by Battye *et al.*[40] We believe that the reduction of interfacial tension for the soft deformable core is the driving force behind rearrangement into these regular structures. Upon collisions of soft lobes, often a larger surface area of poly(butyl acrylate) will exist than which is favourable. Due to absence of surfactant in the system, this surface area will contribute to a significant unfavourable interfacial tension. Accordingly, the soft component will deform to expose the minimum unfavourable surface area, and therefore form the most efficient geometries as seen in the electron microscopy images.

4.3.5 Surface energy simulations of clusters

To test this theory we conducted surface energy minimisation simulations to model the morphology of particle aggregates from 1 - 5 primary particles upon a soft-soft interaction. Simulation software 'Surface evolver'[41] was used to graphically predict the geometry of particle clusters based on the reduction of interfacial tension of the exposed surfaces. The simulation was built with a set number of coarse primary Janus particles in contact through a central soft domain. The volume of the respective lobes were constrained, forcing the system to adopt the most energetically favourable surface energy conformation within the set volume. The wetting of the hard and soft phase is also pinned to limit the formation of core shell structures whereby the soft phase envelops the

hard phase as this is not observed to occur in the experimental system. The graphical outputs from the simulations can be seen in fig 4.14(centre), presented next to the cryo-SEM images for the purpose of comparison. The simulation data obtained from the surface energy minimisation show a consistent agreement with the morphologies from the cryo-SEM images, indicating that surface energy minimisation is indeed the driving force behind the controlled geometry we observe experimentally.

4.3.6 Statistical distribution of primary particles per cluster

We investigated the effect of increasing the soft pBA lobe size in relation to the poly(styrene) seed particles to see if lobe size ratio affected the number distribution of primary particles found in clusters. A seeded dispersion polymerisation of BA in the presence of poly(styrene) seed particles was conducted in an analogous manner as described in chapter 3. Seed particles of 2 μm diameter at a solids content of 10 wt% in a 90:10 methanol: water (w/w) medium were used. At two intervals during the polymerisation, aliquots of particles were removed and quenched to stop further polymerisation. This provided three samples of hard-soft Janus particles with varying soft: hard ratios, derived from the same seed particle dispersion. Each sample was analysed for conversion and observed by optical microscope. Based on the optical micrographs, accurate lobe volumes were determined, as seen in figure 4.15 alongside polymerisation conversion values.

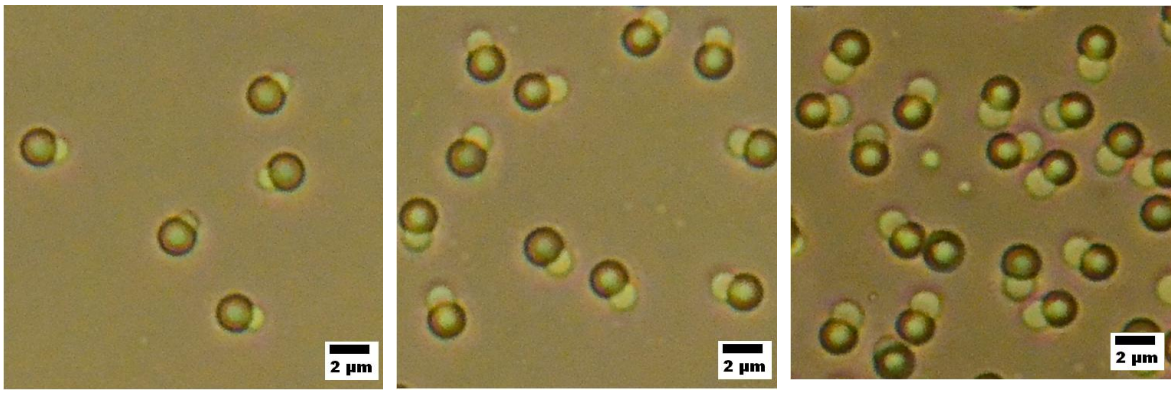

26% Conversion	50% Conversion	91% Conversion
pBA Volume: 1.18 x 10^{-18} m^3	pBA Volume: 2.95 x 10^{-18} m^3	pBA Volume: 4.95 x 10^{-18} m^3

Seed Particle Volume: 9.31 x 10^{-18} m^3

Figure 4.15 Optical micrographs of hard-soft particles (TSNP18) used in cluster counting study, with conversion value at time of sample extraction and pBA lobe volume. Seed particle volume is included for reference

To remove residual monomers and promote the desorption of PVP to allow cluster formation, the particle suspensions were diluted to 0.1 wt% with methanol and allowed to sediment by gravity. The supernatant was replaced with a 50:50 methanol : water (v/v) media and particles redispersed by gentle swirling. This process was repeated once more using deionised water. The three suspensions were then hand shaken for 30 seconds to promote cluster formation, and imaged under an optical microscope. A minimum of 100 clusters containing 2 – 5 primary particles in each sample were counted from several images. Population distributions for these clusters are plotted in figure 4.16. The number fraction is the number of clusters with *x* primary particles as a fraction of the total number of clusters counted (with 2 - 5 primary particles) in a sample.

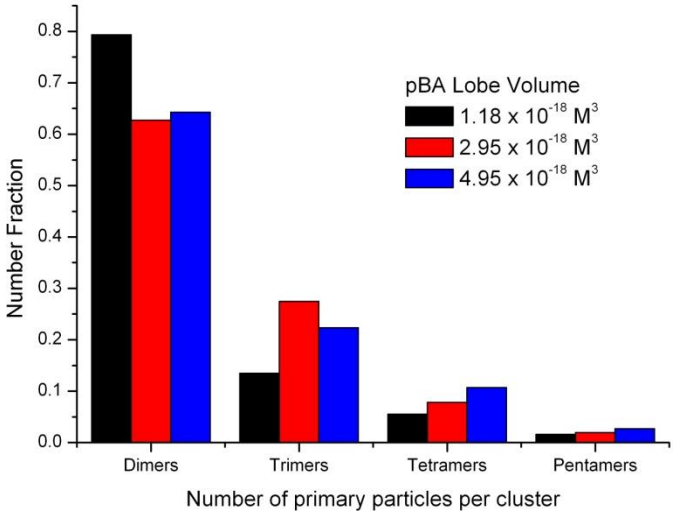

Figure 4.16 Populations of clusters containing 2-5 primary particles for hard soft Janus particles (TSNP08) of three different soft lobe volumes

Clearly in all three samples, clusters containing two primary particles, i.e. dimers, are the most prevalent followed by trimers, tetramers and pentamers respectively. This is logical as once a dimer is formed there is reduced available soft surface area for further particles to adhere to the cluster. This trend continues as the primary particle number per cluster increases. Interestingly, the size of the pBA lobe appears to have a small influence on the cluster size distribution. Upon increasing the size of the pBA lobe, higher populations of clusters with more primary particles are formed relative to other pBA lobe sizes. For instance, the smallest lobe size of 1.18 x 10^{-18} m^3 forms more dimers. The intermediate lobe size of 2.95 x 10^{-18} m^3 forms more trimers, and the largest pBA lobe size of 4.95 x 10^{-19} m^3 forms the most tetramers and pentamers respectively. This effect is plausibly due to the magnitude of soft pBA surface area available for the primary particles to adhere to. As the surface area increases, more primary particles can contribute to the cluster, indicating a degree of geometric constraint arising from the hard poly(styrene) seed particles.

4.3.7 Higher order structures

In addition to clusters containing a small number of primary particles, many aqueous cluster suspensions indicated the presence of higher order structures. These structures consisted of numerous primary particles surrounding a hollow or solid core as evidenced by electron and optical microscopy, forming so called 'colloidosomes' as seen in figure 4.17. Colloidosomes are defined as capsules built from the assembly of smaller colloidal particles and often require a sintering/locking step to lock the structure and seal it. This led us to believe that a secondary assembly mechanism for our system exists.

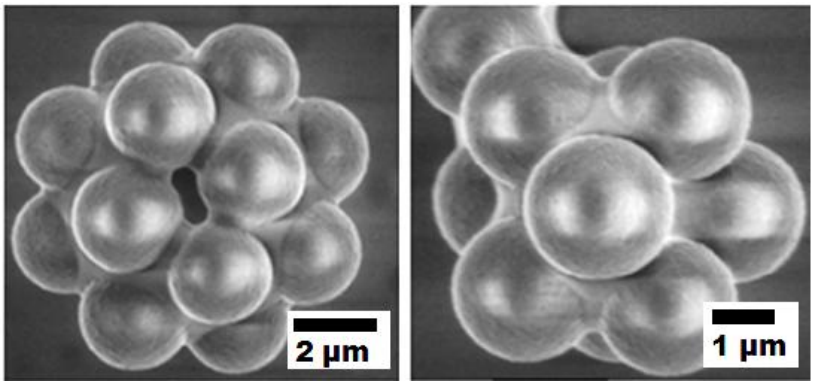

Figure 4.17 Dry FEG-SEM images of higher order clusters (using particles TS405-1)

Figure 4.18 shows several examples of colloidosomes obtained from 0.5:1 soft-hard ratio suspensions by both optical and cryo scanning electron microscopy. From the SEM images it is possible to see that the soft pBA phase of the Janus particles have coalesced, effectively embedding the hard poly(styrene) particles in a soft elastic pBA matrix. The number of primary Janus particle constituents of the colloidosome exceeds the maximum number possible for a cluster possessing a central core and therefore means that Janus particles can coalesce in a 2D planar manner over curved surface, such as a bubble to form a colloidosome. Theoretically, chemically isotropic Janus particles have been shown

to preferentially lie tilted or 'flat' at an interface, therefore maximising the displaced interfacial area.[42] This orientation allows the coalescence of the pBA lobes between the particles in a planar manner.

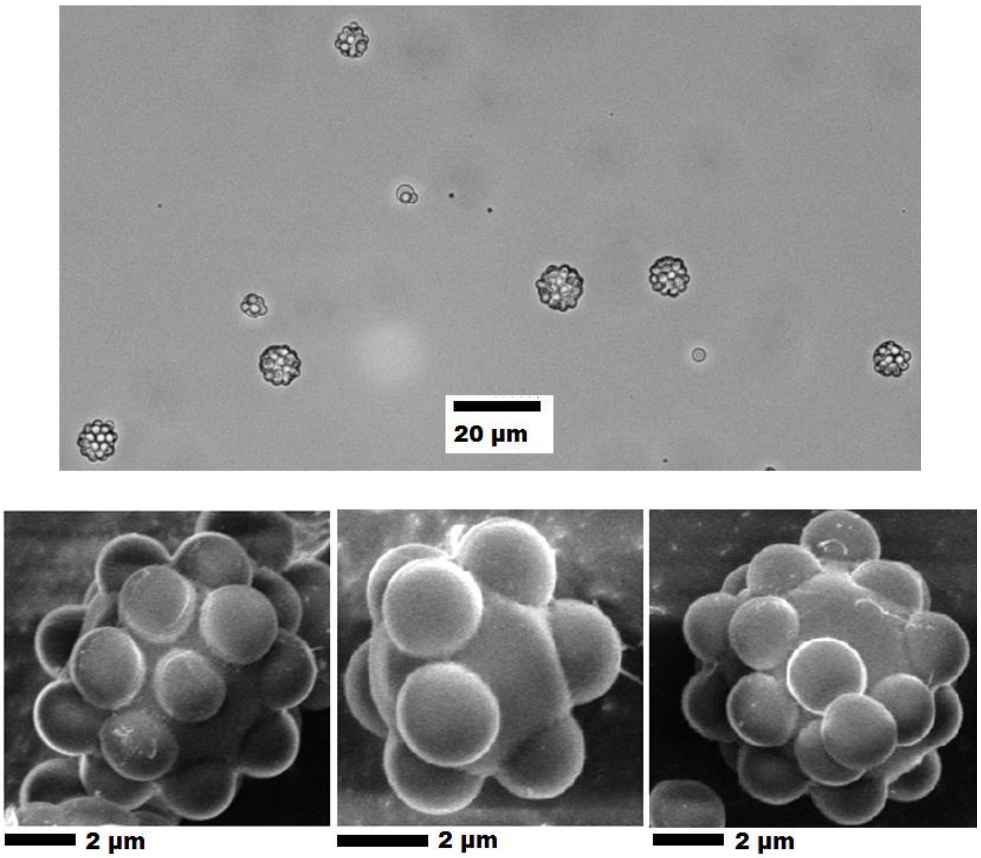

Figure 4.18 (Top) Optical microscope image of higher order particle clusters. (Bottom) Cryo FEG-SEM images of higher order clusters (using particles TS405-1)

4.3.8 Particle stabilised bubbles

To further investigate self assembly at 2D curved interfaces, hollow colloidosomes were made through the assembly of 'hard-soft' Janus particles at a bubble interface. A dilute 0.1 wt% aqueous suspension of 0.5:1 pBA/pSty lobe ratio, 2 µm length and 1.5 µm width (across respective axis) purified Janus particles was shaken vigorously in a manner which aerated the suspension promoting the adsorption of the particles to the air-water interface

of bubbles, forming a particle stabilised foam. The foam was diluted into water, allowing individual and collections of bubbles to be imaged under an optical microscope. Owing to the large z-height of the bubbles, and the use of a high magnification objective, a stack of images at varying focal planes were focus stacked using imageJ software to render images with a large depth of field at high magnification. A set of individual bubbles stabilised by Janus particles can be seen in figure 4.19.

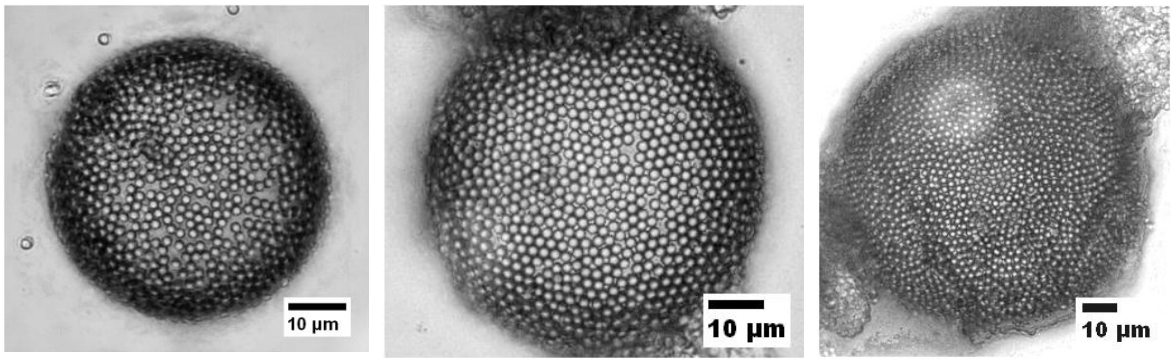

Figure 4.19 Z-stacked optical microscopy image of single bubbles stabilised by hard-soft Janus particles (TS405-1)

Close inspection of the colloidosome surface reveals several features. Despite incomplete coverage of the bubble surface, the particle stabilised bubbles are appear resistant to coalescence despite close proximity to other bubbles (as in fig 4.20).

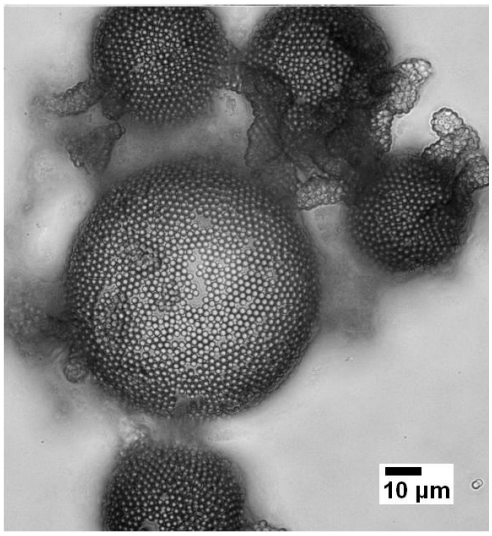

Figure 4.20 Z-stacked optical microscopy image of 5 bubbles of various size in close proximity stabilised by hard-soft Janus particles (TS405-1)

The densely packed particle domains on the bubbles self assemble into a hexagonal close pack configuration, this can be seen in the centre of the bubble in figure 4.21 where large areas of particles form tight hexagonal close packed areas.

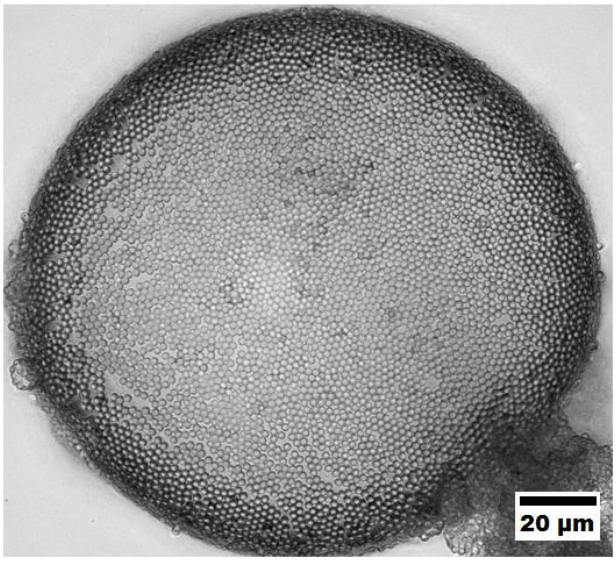

Figure 4.21 Optical micrograph of a large bubble stabilised by Janus particles (TS405-1) with clear hexagonal close pack domains

From the scanning electron microscopy analysis of colloidosomes (figs. 4.17 and 4.18(bottom), and theoretically[42] it was noted that the hard-soft particles can lie horizontally across the interface and coalesce in a 2-D planar manner. In the ideal case of complete coverage, this allows the formation of colloidosomes which are hermetically sealed by the coalescence of the soft component. This negates the need for a mechanism to seal the interstitial areas between particles such as sintering,[43] required in other examples of colloidosome fabrication. The colloidosome suspension was re-imaged 24 hours after formation. The bubbles are stable for an extended period of time, and have attained complete surface coverage as seen in figure 4.22.

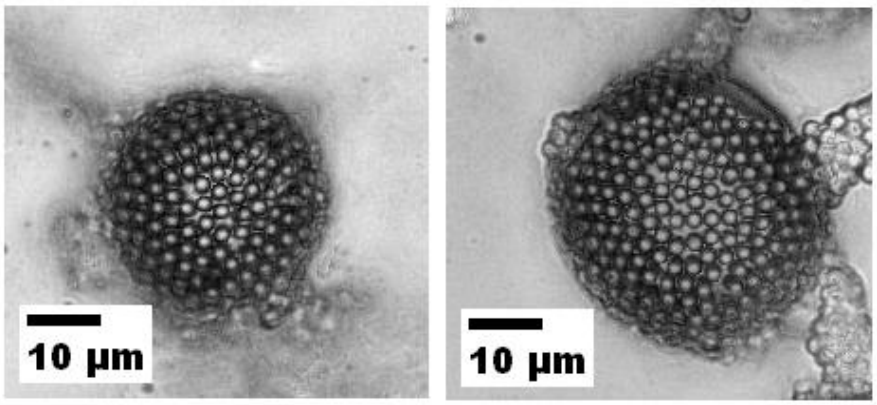

Figure 4.22 Z-stacked optical micrographs of Janus particle colloidosomes 24 hours after formation (using particles TS405-1)

This is expected behaviour for Pickering stabilised bubbles which allow gas diffusion and shrinkage until the particles jam on the surface as a result of decreased interfacial area. At this point particle stabilised droplets and bubbles tend to buckle or adopt a non-spherical shape, maintaining surface area with decreasing volume, exhibiting solid like interfacial behaviour.[44] However, we note very spherical or only slightly aspherical structures upon full coverage. We attribute this behaviour to two effects. Firstly, as the soft component

films forms along the interface, it is plausible that the colloidosome becomes hermetically sealed, leaving no permeation site and therefore the internal pressure is not further reduced by gas diffusion out of the structure. Secondly, the size of the particles are large compared to the curvature of the interface, resulting in a robust shell, resistant to buckling.

4.4 Conclusions

The flocculation of hard-soft Janus particles for the purpose of self assembly into colloidal clusters was investigated. Initial flocculation kinetics of model 'hard' polystyrene microspheres then 'hard-soft' Janus particles revealed that upon dilution, the particles were liable to flocculation, the rate of which proportional to mixing intensity and concentration of PVP in the aqueous phase. We therefore concluded that aggregation is triggered by desorption of steric stabiliser. Upon visual inspection of the colloidal clusters, we found 4 possible interaction regimes whereby particles could contact in a hard-hard, hard-soft, simultaneous hard-soft and soft-soft manner. The latter regime renders controlled aggregation into clusters of which morphology is governed by the deformation of the coalesced soft phase, energetically driven by surface energy minimisation. Interfacial energy simulations of analogous particle clusters provide a good agreement to the experimentally obtained images. Upon quantitative analysis of cluster suspensions, dimers were most commonly formed, with a decreasing trend of number population for successively higher numbers of primary particles per cluster. However, varying the soft : hard lobe ratio has a small influence on the cluster size. Larger soft phase ratios of Janus particles lead to increased populations of larger clusters. This technique to produce clusters is limited by the inability to control the cluster size

distribution and the occurrence of hard-soft interactions leading to uncontrolled cluster morphology. Additionally, hard-soft Janus particles were observed to coalesce over a 2D curved planar air-water interface to form colloidosomes templated around gas bubbles. The use of these particles allows the formation of colloidosomes without a further sintering or chemical process to seal the interstitial sites and retains the textured anisotropic surface typical of a colloidosome.

4.5. Experimental

4.5.1 Materials

Styrene (ReagentPlus, 99%), *N*-butyl acrylate (>99%), poly(vinyl pyrrolidone) (PVP-K90, 360,000 $gmol^{-1}$), all supplied by Sigma Aldrich, UK. Azobisisobutyronitrile (97%), ethanol (absolute AR), methanol (AR), all supplied by VWR, UK. were used as supplied. Monomers were filtered through a basic alumina column to remove inhibitor before use. Deionised water was filtered and purified to 18 $M\Omega cm^{-1}$.

4.5.2 Equipment

Laser diffraction measurements

Bulk particle sizing measurements were undertaken using a Mastersizer 2000 (Malvern Instruments, Malvern, UK). Dilute aqueous particle suspensions were introduced using the Hydro S dispersion unit. Time lapse measurements of 400 minute duration, sampling every 20 minutes were undertaken in a closed system using degassed tap water in ambient conditions stirring at 1750 rpm. The laser was aligned to optimum transmission intensity and a background spectrum collected to eliminate any contaminants presenting

in the final data. Dilute suspensions of 1 wt% were introduced drop wise by submerged syringe to ensure no premature flocculation or bubble introduction until 5% laser obscuration was reached. A 30 s ultrasonic cycle to remove any bubbles and break apart any flocs was run before the measurement ensued. Concentration of particulate was fixed at 0.040% (v/v) with respect to total media volume, as determined by Mastersizer instrumentation.

Turbidity measurements

Hard-Soft Janus particles of 1:1 pSty/pBA ratio, 2 µm diameter were synthesised in a seeded dispersion polymerisation procedure as outlined in chapter 3, purified, and diluted in pure water or PVP-K90 solutions to 0.2 g/L particulate content. 10 mL of these suspensions were sealed in a glass vial and mounted into a Model 777 Microarray Oven (SciGene, California, USA) before rotating at a set speed under ambienttemperature conditions. Periodically, samples from the vials were measured for absorbance at 540 nm using a UV/Vis Spectrophotometer. A calibration curve of known primary particle concentration was measured to back calculate primary particle concentration from absorbance.

Optical microscopy

Particles were imaged on a Leica DM2500M using a Nikon D5100 camera. Focus stacked images were generated using an extended depth of field plugin for imageJ.[45]

Electron microscopy

Cryogenic Scanning Electron Microscopy analyses were carried out using a Zeiss Supra 55-VP Field Emission Gun Scanning Electron Microscope with a Gatan Alto 2500 cryo transfer system and a Gatan C1002 Liquid Nitrogen cold stage. Dilute aqueous suspensions of particles were drawn into a brass rivet and cooled in liquid nitrogen. Samples were heated to −90 °C under high vacuum for 10 minutes to remove contaminant ice through sublimation followed by platinum sputter target coating in an argon atmosphere (20 seconds, 10 mA). Imaging was undertaken at −120 °C using a 3 kV accelerating voltage with a gold anti-contaminator at −189 °C. Image analysis was conducted with ImageJ software (NIH, US)

Simulations of cluster formations

Surface Evolver (Ken Brakke)[41] was used to graphically depict the lowest surface energy morphology of volume constrained Janus particle clusters of $1 < n > 5$. Simulations were built on coarse Janus particles consisting of two separate domains. At the start of the simulation, the particles were in contact by a central domain. Depending on the number of primary particles and desired hard : soft lobe ratio, the separate lobes and central soft domain volume ratio was constrained to the desired parameter. The simulation was then iterated, refined and further iterated until the difference in interfacial energy between the last two iterations was negligible.

4.5.3 Cluster Synthesis

Hard-soft Janus particle synthesis

Poly(styrene) microsphere suspensions and hard-soft Janus particles were synthesised as described in chapter 3, part 3.5.2 (Dispersion Polymerisation) to generate hard-soft Janus particles of 0.5:1 and 1:1 pBA: pSty volume ratios.

Cluster formation

Alcoholic suspensions of Hard-Soft particles were sedimented by gravity before replacement of an equal volume of supernatant with deionised water. Settled particles were re-suspended in fresh media by gentle swirling. This process was repeated twice more before dilution to 0.1 wt% (w/w) solids content in deionised water. After which agitation by handshaking for 30 seconds was used to generate clusters.

Cluster counting measurements

A seeded dispersion polymerisation of BA in the presence of pSty seed particles was conducted in an analogous manner to that described in chapter 3, part 3.5.2 (Dispersion Polymerisation). During the polymerisation, 8 mL aliquots of reaction mixture were withdrawn from the reaction flask at 95 and 191 minutes into the seeded dispersion polymerisation and cooled on ice to quench polymerisation. The remainder of the reaction was heated for a total of 1425 minutes. All three samples were analysed by gravimetry and optical microscopy before diluting to 0.1 wt% (w/w) solids content with methanol before allowing suspensions to sediment by gravity. The supernatant was then replaced with an equivalent volume of 50:50 methanol: water (v/v) before gently swirling

to redisperse particles. This process was repeated once more using fresh water instead. To induce cluster formation, each suspension was hand shaken for 30 seconds and imaged under an optical microscope. Populations of clusters containing 2-5 primary particles were counted using ImageJ software, recording over 100 clusters for each sample over 3 micrographs per sample.

Particle stabilised foams

10 mL of an aqueous suspension of purified hard-soft particles at 0.1 wt% (w/w) was hand shaken in a 15 mL vial in the presence of air as to thoroughly aerate the suspension. The remaining foam layer was carefully re suspended in fresh deionised water prior to imaging.

4.6. References

(1) Subramanian, G.; Manoharan, V. N.; Thorne, J. D.; Pine, D. J. *Advanced Materials* **1999**, *11*, 1261–1265.

(2) Vlasov, Y. a; Bo, X. Z.; Sturm, J. C.; Norris, D. J. *Nature* **2001**, *414*, 289–293.

(3) Ozin, G. a.; Hou, K.; Lotsch, B. V.; Cademartiri, L.; Puzzo, D. P.; Scotognella, F.; Ghadimi, A.; Thomson, J. *Materials Today* **2009**, *12*, 12–23.

(4) Blaaderen, A. Van *Science* **2003**, *301*, 470–471.

(5) Liz-Marzan, L. M.; Giersig, M.; Mulvaney, P. *Chemical Communications* **1996**, 731–732.

(6) Gu, H.; Zheng, R.; Zhang, X.; Xu, B. *Journal of the American Chemical Society* **2004**, *126*, 5664–5665.

(7) Kwon, K.-W.; Shim, M. *Journal of the American Chemical Society* **2005**, *127*, 10269–10275.

(8) Mulvaney, P.; Giersig, M.; Ung, T.; Liz-Marzán, L. M. *Advanced Materials* **1997**, *9*, 570–575.

(9) Saito, N.; Nakatsuru, R.; Kagari, Y.; Okubo, M. *Langmuir* **2007**, *23*, 11506–11512.

(10) Tanaka, T.; Nakatsuru, R.; Kagari, Y.; Saito, N.; Okubo, M. *Langmuir* **2008**, *24*, 12267–11271.

(11) Sheu, H. R.; El-Aasser, M. S.; Vanderhoff, J. W. *Journal of Polymer Science Part A* **1990**, *28*, 653–667.

(12) Kim, J.-W.; Lee, D.; Shum, H. C.; Weitz, D. A. *Advanced Materials* **2008**, *20*, 3239–3243.

(13) Park, J.-G.; Forster, J. D.; Dufresne, E. R. *Journal of the American Chemical Society* **2010**, *132*, 5960–5961.

(14) Wang, D.; Dimonie, V. L.; Sudol, E. D.; El-Aasser, M. S. *Journal of Applied Polymer Science* **2002**, *84*, 2710–2720.

(15) Sheu, H. R.; Vanderhoff, J. W. *Polymer* **1990**, *28*, 629–651.

(16) Okubo, M.; Fujibayashi, T.; Yamada, M.; Minami, H. *Colloid and Polymer Science* **2005**, *283*, 1041–1045.

(17) Kim, J.-W.; Larsen, R. J.; Weitz, D. A. *Advanced Materials* **2007**, *19*, 2005–2009.

(18) Yu, H.; Chen, M.; Rice, P. M.; Wang, S. X.; White, R. L.; Sun, S. *Nano letters* **2005**, *5*, 379–382.

(19) Zeng, J.; Huang, J.; Liu, C.; Wu, C. H.; Lin, Y.; Wang, X.; Zhang, S.; Hou, J.; Xia, Y. *Advanced Materials* **2010**, *22*, 1936–1940.

(20) Perro, A.; Duguet, E.; Lambert, O.; Taveau, J.-C.; Bourgeat-Lami, E.; Ravaine, S. *Angewandte Chemie* **2009**, *121*, 367–371.

(21) Désert, A.; Chaduc, I.; Fouilloux, S.; Taveau, J.-C.; Lambert, O.; Lansalot, M.; Bourgeat-Lami, E.; Thill, A.; Spalla, O.; Ravaine, S.; Duguet, E. *Polymer Chemistry* **2012**, *3*, 1130–1132.

(22) Manoharan, V. N.; Elsesser, M. T.; Pine, D. J. *Science* **2003**, *301*, 483–487.

(23) Cho, Y.-S.; Yi, G.-R.; Lim, J.-M.; Kim, S.-H.; Manoharan, V. N.; Pine, D. J.; Yang, S.-M. *Journal of the American Chemical Society* **2005**, *127*, 15968–15975.

(24) Xia, Y.; Yin, Y.; Lu, Y.; McLellan, J. *Advanced Functional Materials* **2003**, *13*, 907–918.

(25) Lee, I.; Zheng, H.; Rubner, M. F.; Hammond, P. T. *Advanced Materials* **2002**, *14*, 572–577.

(26) Kim, S.-H.; Hollingsworth, A. D.; Sacanna, S.; Chang, S.-J.; Lee, G.; Pine, D. J.; Yi, G.-R. *Journal of the American Chemical Society* **2012**, *134*, 16115–16118.

(27) Sacanna, S.; Irvine, W. T. M.; Chaikin, P. M.; Pine, D. J. *Nature* **2010**, *464*, 575–578.

(28) Hong, L.; Cacciuto, A.; Luijten, E.; Granick, S. *Nano letters* **2006**, *6*, 2510–2514.

(29) Jiang, S.; Chen, Q.; Tripathy, M.; Luijten, E.; Schweizer, K. S.; Granick, S. *Advanced materials* **2010**, *22*, 1060–1071.

(30) Hong, L.; Cacciuto, A.; Luijten, E.; Granick, S. *Langmuir* **2008**, *24*, 621–625.

(31) Wang, Y.; Wang, Y.; Breed, D. R.; Manoharan, V. N.; Feng, L.; Hollingsworth, A. D.; Weck, M.; Pine, D. J. *Nature* **2012**, *490*, 51–55.

(32) Zerrouki, D.; Baudry, J.; Pine, D.; Chaikin, P.; Bibette, J. *Nature* **2008**, *455*, 380–382.

(33) Kraft, D. J.; Vlug, W. S.; van Kats, C. M.; van Blaaderen, A.; Imhof, A.; Kegel, W. K. *Journal of the American Chemical Society* **2009**, *131*, 1182–1186.

(34) Kraft, D. J.; Ni, R.; Smallenburg, F.; Hermes, M.; Yoon, K.; Weitz, D. a; van Blaaderen, A.; Groenewold, J.; Dijkstra, M.; Kegel, W. K. *Proceedings of the National Academy of Sciences* **2012**, *109*, 10787–10792.

(35) Smith, J. N.; Meadows, J.; Williams, P. A. *Langmuir* **1996**, *12*, 3773–3778.

(36) Fantoni, R.; Salari, J. W. O.; Klumperman, B. *Physical Review E* **2012**, *85*, 61404.

(37) Camp, T. R.; Stein, P. C. *Journal of the Boston Society of Civil Engineers* **1943**, *85*, 219–237.

(38) Kellaway, I. W.; Najib, N. M. *International Journal of Pharmaceutics* **1980**, *6*, 285–294.

(39) Hamaker, H. C. *Physica* **1937**, *4*, 1058–1072.

(40) Battye, R. A.; Gibbons, G. W.; Rychenkova, P.; Sutcliffe, P. M. *Journal of Mathematical Physics* **2003**, *44*, 3532–3542.

(41) Brakke, K. A. *Experimental Mathematics* **1992**, *1*, 141–165.

(42) Park, B. J.; Lee, D. *ACS nano* **2012**, *6*, 782–790.

(43) Dinsmore, A. D.; Hsu, M. F.; Nikolaides, M. G.; Marquez, M.; Bausch, A. R.; Weitz, D. A. *Science* **2002**, *298*, 1006–1009.

(44) Datta, S. S.; Shum, H. C.; Weitz, D. A. *Langmuir* **2010**, *26*, 18612–18616.

(45) Forster, B.; Van De Ville, D.; Berent, J.; Sage, D.; Unser, M. *Microscopy Research and Technique* **2004**, *65*, 33–42.

Chapter 5

Water-in-oil Pickering stabilised emulsions for confectionery formulations*


RSC | Advancing the Chemical Sciences

Publishing Platform | ChemSpider | MyRSC |

chemistryworld

HOME NEWS OPINIONS FEATURES REGULARS JOBS PODCASTS

RESEARCH BUSINESS NEWS AND ANALYSIS

Fruit juice infused chocolate to reduce fat consumption

5 September 2012 Elinor Hughes

From left to right: Team members Tom Skelhon, Adam Morgan and Stefan Bon © University of Warwick

5.1 Abstract

The over consumption of junk foods such as chocolate in today's society is a growing problem. Therefore we investigate the replacement of up to 50 wt% of the fat content in chocolate formulations using water or fruit juice to reduce the calorie content of chocolate, whilst retaining its desirable eating qualities. We utilise a synergistic polyelectrolyte and Pickering stabilisation strategy incorporating the natural biopolymer chitosan and fumed silica particles to generate water in oil emulsions stable against

* Parts of this chapter have been published elsewhere: Thomas S. Skelhon, Nadia Grossiord, Adam R. Morgan and Stefan A. F. Bon, Quiescent water-in-oil Pickering emulsions as a route toward healthier fruit juice infused chocolate confectionary. *J. Mater. Chem.*, **2012**, *22*, 19289-95

coalescence. The non-adsorbed silica is shown to form a colloidal gel in the oil phase providing the system with a yield stress, hereby giving it a gel-like and thus quiescent behaviour. The emulsions are stable throughout the processing conditions required for chocolate manufacture and we ultimately demonstrate formulations possessing the same desired cocoa butter crystal structure for milk, dark and white chocolate as well as cocoa butter, as determined by DSC. As a result, the formulations are resistant to sugar or fat bloom.

5.2 Introduction

Cocoa butter on the one hand is the component in chocolate confectionery which allows for the sensational melt-in-the-mouth experience upon consumption, and plays a crucial role in the texture of chocolate.[1] On the other hand, cocoa butter (see figure 5.1) which predominantly consists of a mixture of triglyceride fats (the main fatty acids being palmitic acid, oleic acid, and stearic acid)[2] is an issue in today's attitude towards a healthy and balanced diet. In the UK, between 1993 and 2011, the adult population who are overweight and obese has risen from 58% to 65% in males and 49% to 58% in women.[3] A contributory factor towards this increase is the overconsumption of 'junk foods', with high quantities of fat, sugar and salt with little beneficial nutritional value. Chocolate falls into this category.

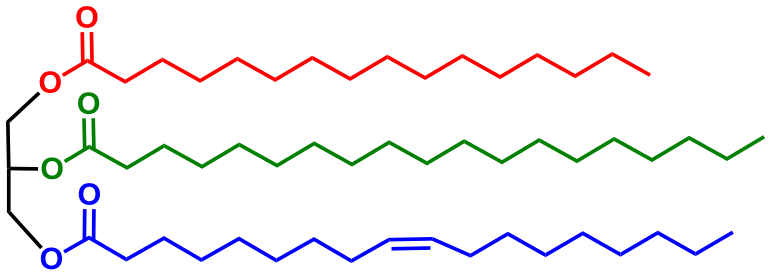

Figure 5.1 Structural formula of the main component of cocoa butter: triglyceride fat derived from palmitic (red), stearic (green) and oleic (blue) acids

Replacing a considerable relative volume of cocoa butter and other fats, such as milk and vegetable fats (mixtures of saturated and unsaturated triglycerides) from a confectionery formulation with a less calorie-rich alternative, therefore, is a high priority for chocolate manufacturers. A practiced method is to introduce air bubbles into the chocolate,[4] effectively lowering the bulk density of the candy, with commercialised products such as Aero or Bros (Nestlé), and Wispa (Cadburys/Kraft). The average bubble size is large in these aerated chocolate bars, thus from a tribological viewpoint these products are experienced by the consumer as porous, and therefore are marketed for their aerated texture. Lowering the average bubble size below the 'mouth-feel' threshold diameter results in the perception of a homogeneous and thus smooth chocolate product experience. The threshold size depends on the hardness and shape irregularity of the particulate matter, and is determined by human perception tests.[5] According to chocolate confectionery literature, the minimum particle size discernible is quoted as 30 μm diameter,[6] and if all particles reside below this value, the texture is considered to be of optimum smoothness.[7] However, the dispersion of sub 30 μm diameter bubbles into chocolate formulations is not feasible from a manufacturing perspective as Ostwald ripening leading to bubble coarsening in the molten chocolate state occurs on timescales

of minutes.[8] Although Ostwald ripening in bubbles can be arrested by a Pickering stabilisation strategy,[9] a "lightweight" chocolate bar may well be received in a dissatisfactory manner by the consumer. We therefore turned our attention towards dispersing liquids into chocolate formulations.

5.2.1 Fat reduction through emulsification

One strategy to reduce fat content is to replace part of the fat matrix with water droplets through emulsification. Water-in-oil emulsions allow the replacement of up to 80% by volume of the fat content without a discernible difference in 'fattiness texture' arising from the enrobed nature of the emulsion droplets. Water-in-oil emulsions containing up to 80% water exhibit a tribological response similar to pure oil. However, above this value gives unacceptable performance characteristics, as determined by ball and plate tribometer.[10] Well known examples of oil-in-water emulsions exist in the format of reduced fat margarine and mayonnaise, whereby matching the emulsion droplet size to the microstructure of the full fat product emulates a similar tribological experience.

As such, we aim to encapsulate water within the chocolate formulation and compartmentalise the water into droplets of which the droplet size distribution falls below the average 30 μm threshold value. Norton and co-workers prepared cocoa butter water-in-oil emulsions showing that up to 20 wt% of water droplets between 1-5 μm diameter could be embedded into the required polymorphic form for good eating qualities. Emulsions were created using both a high shear mixer and a thermally controlled laboratory scale margarine line, employing polyglycerol polyricinoleate (PGPR) and soy lecithin as emulsifying agents.[11] Our approach is to fabricate "stable" water-in-oil

emulsions, that is, fruit juice dispersed in molten chocolate with the aim to replace a significant quantity of the fat content in chocolate, comprising of cocoa butter and milk fats. By "stable" we mean not only that (1) coarsening and coalescence of individual droplets is restrained (ideally fully), but also that (2) settling of the droplets by gravity as a result of the higher density of aqueous dispersed phase is arrested effectively leading to a quiescent emulsion system.[12] The latter can warrant a homogeneous dispersion of the emulsion droplets throughout a molten chocolate matrix. Pickering stabilisation provides a viable route to fabricate emulsions that are not susceptible to coarsening and coalescence.

5.2.2 Pickering stabilisation

Pickering stabilisation was first observed by Ramsden[13] and Pickering[14] individually at the turn of the 20th century noting that stable oil in water emulsions could be generated by use of an inorganic particulate as a stabiliser. Finkle *et al.*[15] developed an initial theory describing how the solid stabiliser is partially wetted by both phases. In 1954, Wiley reported how freshly made emulsions incorporating a solid particulate could only partially coalesce to form a stable dispersion of oil in water droplets when 100% coverage of the droplets by solid particulate had been achieved.[16] However it was not until 1980 when Pieranski developed a comprehensive 2-D model of how a polystyrene sphere of radius *r*, vertically displaced *z* distance from its centre trapped at an air-water interface reduces overall interfacial energy[17] as depicted schematically in figure 5.2.

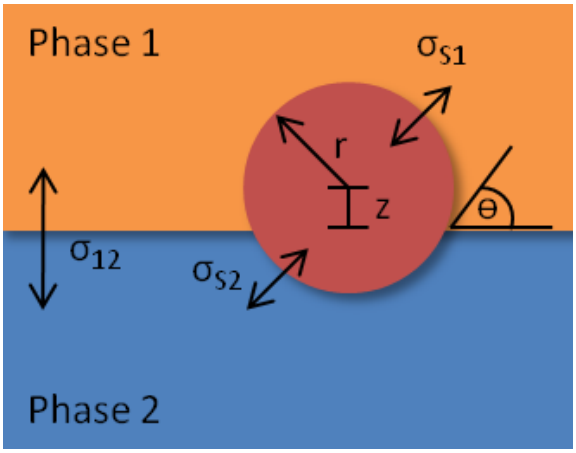

Figure 5.2 A schematic representation of a solid particle with radius r, vertically displaced z from the centre, trapped at the interface between phase 1 and 2. σ_{S1}, σ_{S2} and σ_{12} represent the surface tension between the solid and phase 1, solid and phase 2 and the surface tension between the two phases respectively. Θ represents the three phase contact angle

$$Z_0 = \frac{z}{r}$$

(1)

$$E_{S1} = \sigma_{S1} 2\pi r^2 (1 + Z_0) \quad (2)$$

$$E_{S2} = \sigma_{S2} 2\pi r^2 (1 - Z_0) \quad (3)$$

$$E_{12} = \sigma_{12} \pi r^2 (1 - {Z_0}^2) \quad (4)$$

$$E = E_{S1} + E_{S2} - E_{12} \quad (5)$$

Based on this model, the total energy is derived from the summation of the three surface tension components; the interfacial energy between the solid and phase 1 (equation 2), the solid and phase 2 (equation 3), and the loss of surface area between phase 1 and phase 2 arising from the presence of the particle (equation 4). The *z* displacement of the particle

between the two phases is accounted for by (equation 5). If the total interfacial energy is reduced by the presence of the solid particulate, i.e. $(E_{S1} + E_{S2}) < E_{12}$ the particle is irreversibly bound into a deep energy well.

When the total energy is scaled with $E_{unit} = \pi R^2 \sigma_{12}$ using (equation 6), a quadratic expression can be found (equation 7) where $a = \sigma_{S2}/\sigma_{12}$ and $b = \sigma_{S1}/\sigma_{12}$.

$$\tilde{E} = \frac{E}{E_{unit}} \tag{6}$$

$$\tilde{E} = Z_0^2 + 2(a-b)Z_0 + 2a + 2b - 1 \tag{7}$$

By plotting this expression, as depicted schematically in figure 5.3, it is possible to see a parabolic energy profile as a function of particle displacement from the interface, with an energy minimum at a particular z value. $\Delta\tilde{E}_1 = \tilde{E}_1 - \tilde{E}_{min}$ and $\Delta\tilde{E}_2 = \tilde{E}_2 - \tilde{E}_{min}$ represent the energy required to displace the particle from the interfacial minimum to phase 1 or phase 2 respectively. In the example given, the particle wettability slightly favours phase 1, hence the bias in z position and escape energy. In real terms, this energy can be in the magnitude of thousands of k_BT, effectively irreversibly binding the particle to the interface, unlike many molecular surfactants which can undergo spontaneous adsorption and desorption. As such Ostwald ripening,[18] or coarsening of droplets, can be retarded or even fully arrested in a Pickering system owing to the resistance to buckling upon a droplet shrinking arising from the inability for particle desorption.[19]

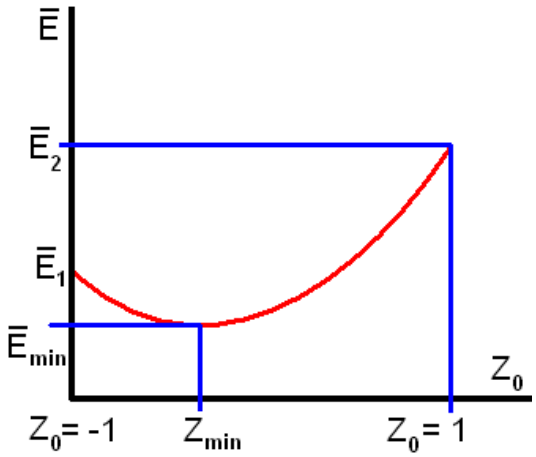

Figure 5.3 A potential energy profile of a particle as a function of Z position from particle centre. E_{min} represents the energy minimum at particle position Z_{min} the most thermodynamically favoured position. E_1 and E_2 denote the energy required for particle escape into phase 1 and phase 2 respectively

It is worth noting that this model is restricted to the gravity free regime i.e. one assumes to operate components of the system below the relative capillary length, the threshold below which interfacial forces dominate and the effect of gravity is negligible, as shown in equation 8. Where capillary length λ_c, is determined as a function of surface tension γ, medium viscosity ρ and gravitational force *g*.

$$\lambda_c = \sqrt{\frac{\gamma}{\rho g}} \tag{8}$$

Moreover the model fails to include two factors. Firstly line tension, the 1-D line at the three phase points of contact where the particle meets both phases, an energy contribution exists denoted as τL (with L in this case being a circumference). Aveyard and Chiot[20]

corrected the equation of Pieranski with this term. However, when the particle is a smooth spherical object one can often ignore the contribution to line tension of "larger" particles (approx. $r > 10$ nm), as its contribution scales with r, whereas the interfacial tension components scale with r^2. Secondly, a small activation energy may be required for the particle to actually breach the interface. Upon approaching the soft interface deformation and draining of the liquid phase in which the particle is dispersed is required, followed by dewetting so that the particle can sit at the interface. Theoretical work has demonstrated that even with the incorporation of line tension, there are discrepancies between theoretical and observed systems owing to the dynamic nature of a fluid-fluid interface. Despite the two phases being sharply defined, the interface is subject to perturbations which induce capillary waves. On approach to an interface, a particle can be 'pulled' to the interface if the capillary wave amplitude and frequency allow a transient reduction of distance between the particle and interface.[21] Although this has the effect of widening the potential energy well, the effect is only significant if the wave amplitude is of comparable length scale to the particle dimensions. For larger particles, this effect is negligible.

In recent years Pickering stabilisation has been exploited in a variety of colloidal systems such as emulsions,[22,23] foams,[24,25] High Internal Phase emulsions (HIPEs),[26,27] and for use as solid stabilisers, hereby replacing molecular surfactants, in emulsion polymerisation.[28] Furthermore, calcium carbonate particles with high aspect ratios have been shown to produce 'superstable'[29] and thermally responsive Pickering stabilised 'smart' foams.[30] Owing to the highly effective stabilising nature and versatility of

Pickering Stabilisation, we investigate the use of nanoparticle silicates as solid surfactants in creating robust water droplet dispersions in chocolate formulations.

5.2.3 Chitosan interfacial reinforcement

The mechanical robustness of Pickering stabilised emulsion droplets, sometimes referred to as armoured capsules or colloidosomes, can be further enhanced through scaffolding using a variety of methods[31] amongst which includes the (physi)sorption of macromolecules.

Velev first demonstrated the use of poly(L-lysine) as a 'sensitiser', adsorbing on to poly(styrene) microspheres. By adsorbing a cationic polyelectrolyte, the negative sulphate charge of the particles is mitigated, making adsorption on to a W/O interface more favourable. This allowed the formation of structured particle stabilised octanol droplets.[32] By adapting the technique, Weitz and co-workers showed how the Pickering stabiliser and polyelectrolyte 'sensitiser' could be dispersed in separate phases whilst still providing a synergistic effect. They fabricated reinforced supracolloidal structures through emulsifying a poly(L-lysine) aqueous solution into an organic dispersion of carboxylic acid functionalised polystyrene beads in toluene.[33]

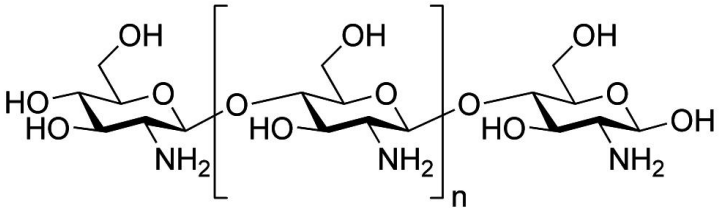

Figure 5.4 Structural formula of Chitosan. Note the primary amine which provides cationic charge in acidic conditions

Analogous to this we employed chitosan, a chitin derivative, as our macromolecule of choice. Chitin is the most abundant natural biopolymer on earth after cellulose and is synthesised in an enormous number of living organisms, serving many functions where strength and reinforcement are required, the exoskeletons of sea animals for instance. The seafood processing industry produces several million metric tonnes of shell-fish processing by-product wastes annually. In terms of management and commercialisation of this abundant type of "waste", production of value-added products such as chitin and chitosan are of utmost interest. Chitosan is a linear polysaccharide composed of (1 → 4)-linked 2-acetamido-2-deoxy-βD-glucopyranose (D-glucosamine) and 2-amino-2-deoxy-βD-glucopyranose (N-acetylglucosamine), and is manufactured by the partial deacetylation of chitin (polymeric N-acetylglucosamine). Chitosan salts are soluble in neutral and acidic aqueous solutions, the solubility being closely related to the degree of acetylation and the aqueous phase pH. It is a remarkable biopolymer with a broad range of potential applications in agriculture, food processing, cosmetics, pharmaceuticals and biotechnologies.[34,35] Some applications of this biodegradable, biocompatible and non-toxic polymer are its use as a fining agent for clarification and de-acidification of fruit juices, antimicrobial, chelating agent that selectively binds trace metals, food additive and/or quality enhancer owing to its hypocholesterolemic effect as well as pharmaceutical excipients.[36] However, most importantly, it has been reported as an effective emulsifier in food and non-food emulsions.[37,38] For this reason we investigate the use of chitosan as a sole surfactant and in conjunction with Pickering stabilisation in the role of promoting interfacial adsorption of particles to the droplet interface.

5.3. Results and discussion

Firstly, we will discuss our results on the preparation and characterisation of water-in-sunflower oil emulsions using chitosan, fumed silica, and a combination of both as stabiliser, after which cocoa butter model systems using water and fruit juices are discussed. To finish, our results on real chocolate systems, that is white, milk, and dark chocolate formulations are discussed.

5.3.1. Water-in-sunflower oil emulsions

We chose sunflower oil as it is a liquid at room temperature eliminating any effect of phase changing behaviour.

Chitosan as sole stabiliser

The first series of emulsions were prepared using chitosan as the sole stabiliser. In these systems, the stabilisation is both steric (due to the polymeric nature of the molecule) and electrostatic (due to the positive charges of the primary 2-amino group of its deacetylated units, which can become protonated). According to Del Blanco *et al*.,[39] the deacetylation degree of chitosan fall within 81–88% for optimum emulsification properties. 1 wt% of chitosan was dissolved in water in presence of an excess of acetic acid.[40,41] The pH of the resulting solution was equal to 3.2. This aqueous solution was then mixed with sunflower oil in a 1:1 ratio and subsequently emulsified using low shear (for example by hand shaking for 30 s). Very low volume W/O emulsions (this means considerable fractions of separate pure water and oil phases) with a broad droplet size polydispersity were obtained. Upon storage, these emulsions ripened and destabilised within several days,

hereby fusing droplets through coalescence.[42] This can be explained by the fact that molecular surfactants in general have a relatively low energy of attachment at the droplet interface.[19] More specifically, chitosan has been reported to only be a moderately efficient emulsifier, certainly due to its stiff polysaccharide nature.[38,39]

Silica as sole stabiliser

The second series of water-in-sunflower oil emulsions were prepared employing fumed silica particles of various hydrophobicities as Pickering stabilisers. Three commercial grades of fumed silica supplied by Wacker Chemie were used. Hydrophilic silica (HDK N20), prepared by flame hydrolysis, has a BET surface area between 175 – 225 m^2/g and contains 2 Si-OH groups/nm^2. Intermediate hydrophobic silica (HDK H20), of surface area between 170-230 m^2/g, is prepared by reacting hydrophilic silica (HDK N20) with dichlorodimethylsilane (DCDMS) in the presence of water giving a surface density of silanol groups of around 1 /nm^2, i.e., half of the surface contains silanol (Si−OH) groups and half contains $Si{-}O{-}Si(CH_3)_2$ groups. Hydrophobic silica (HDK H18), BET surface area of 170-230 nm^2/g is prepared analogous to HDK H20, with an increased quantity of DCDMS to render 25% silanol (0.5 /nm^2) and 75% dimethylsilane (1.5 /nm^2) surface groups.[43] The morphologies of the fumed silica particles were investigated by FEG-SEM, as seen in figure 5.5. The primary particles of fumed silica are approximately spherical, "pop-corn"-shaped particles, and possess diameters ranging from 5 nm to 30 nm. Owing to the production process (flame hydrolysis), these primary particles form larger agglomerates in the range of a 100–1000 nm.[44]

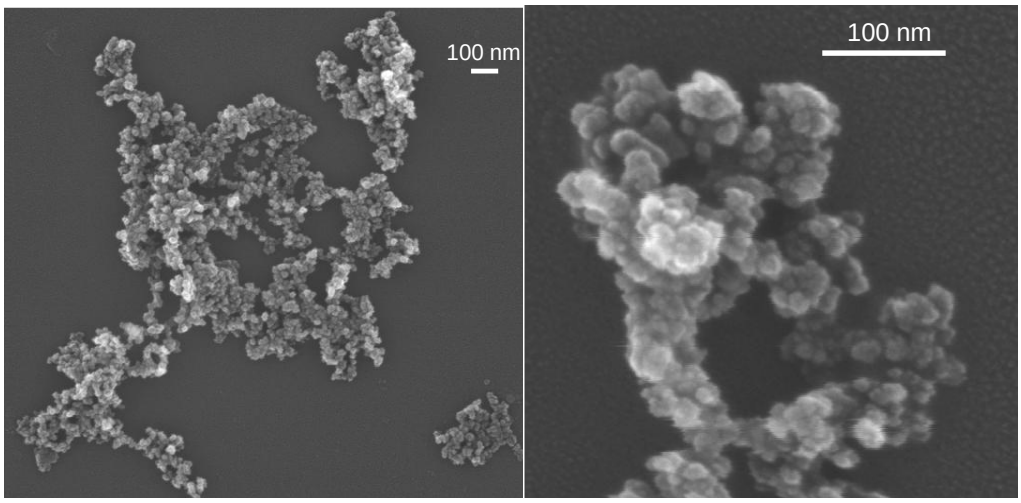

Figure 5.5 FEG-SEM micrographs of HDK-H20 fumed silica particles. Note the aggregation of primary particles into large clusters

W/O emulsions were obtained when HDK H18 and HDK H20 were dispersed into the oil phase prior to the addition of the water phase and subsequent emulsification. Typically, a 1:1 volume ratio mixture of deionised water and sunflower oil was emulsified at low shear (by hand shaking for 30 s) at room temperature, with various silica particle loadings. The amount of particles was varied being 0.6, 1.2, 2.0, 2.6 and 5.3 wt% with respect to the oil phase. Note that when HDK H20 particles were added to the water phase instead prior to emulsification, O/W emulsions were obtained. It has indeed been reported many times that the phase in which silica particles of intermediate hydrophobicity, such as HDK H20 silica particles, are dispersed first becomes the continuous phase of the emulsion prepared using them, in accordance to the 'Bancroft' rule.[45–48] Otherwise, the continuous phase of the emulsion is the one which shows the highest affinity/wettability for the particles, i.e. the oil phase (resp. water phase) for hydrophobic HDK H18 (resp. hydrophilic HDK N20) grades of silica nanoparticles.[49] Limited coalescence was observed upon storage by the appearance of larger droplets for

the emulsions prepared with either the hydrophilic (HDK N20) or the hydrophobic fumed silica (HDK H18). The most probable cause is a weaker adsorption of the silica particles at the oil–water interface (a relatively shallow energy well). On the contrary, the W/O emulsions prepared with the HDK H20 silica particles, which possess an intermediate wettability, were stable to coalescence, which is in agreement with the results obtained by Binks and coworkers.[48] We therefore decided to select the HDK H20 as our Pickering stabiliser of choice in our further studies.

Water and sunflower oil emulsions containing a range of loadings: 0.6, 1.3, 2.0, 2.6, 5.3 wt% of HDK H20 were generated by handshaking. For the highest two concentrations of HDK H20, i.e. 2.6 wt% and 5.3 wt% of silica particles, no distinct clear oil phase was observed after emulsification and storage overnight. It should be noted, however, that in all cases a distinct clear free water phase remained, which is undesirable as the end application requires complete dispersion of the aqueous phase.

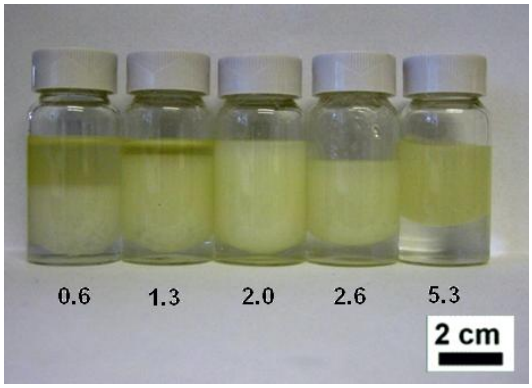

Figure 5.6 Emulsions prepared with a 1:1 water : oil (w/w), different HDK H20 silica particle concentrations (in wt% with respect to the oil phase). All pictures were taken 24 hours after preparation

An explanation for the free water phase can be accounted to the formation of a continuous colloidal silica matrix throughout the oil phase. The silica particles prefer this continuous phase network formation over stabilisation of water droplets, hereby limiting the maximum amount of water that can be dispersed. The emulsions prepared displayed excellent stability with respect to coalescence and Ostwald ripening for prolonged periods of time in excess of three months.

Silica and chitosan as synergistic stabilisers

In order to promote silica adsorption to the oil-water interface, a 1 wt% chitosan:1 wt% acetic acid aqueous solution at pH 3.2 was employed instead of water, resulting in the entire aqueous phase being adequately dispersed in all cases. Figure 5.7 displays the results after emulsification and storage for 24 hours for HDK H20 fumed silica particles at 0.6, 1.2, 2.0, 2.6 and 5.3 wt%. Interestingly the emulsion at the highest amount of silica particles did not flow under its own weight and therefore can be considered to be a gel under these conditions. The origin is a continuous network of colloidal flocs, which effectively renders the emulsion into a quiescent state, whereby the water droplets are dispersed into a solid like matrix, hereby counteracting settling. Such quiescent behaviour has previously been reported by Wiley *et al.*[12] Also noteworthy is the work by Raghavan and Khan [50] who demonstrated that flocculated dispersions of fumed silica in oil is gel-like, exhibiting a yield stress. Attempts to increase the aqueous volume fraction of the emulsions above 50 wt% using the optimum parameters described above proved to be unsuccessful owing to catastrophic phase inversion, thus forming oil in water emulsions.

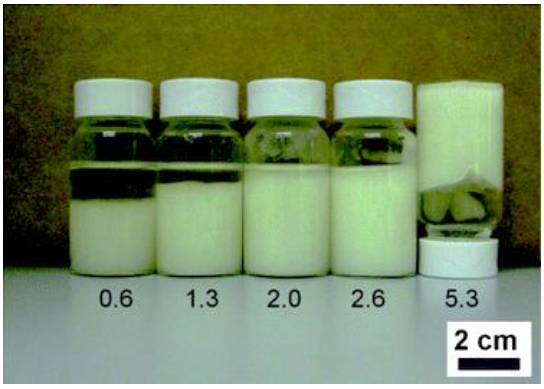

Figure 5.7 Emulsions prepared with a 1:1 water : oil (w/w), different HDK H20 silica particle concentrations (in wt% with respect to the oil phase), with a 1 wt% chitosan solution as water phase (pH of 3.2). All pictures were taken 24 hours after preparation

The effect of varying chitosan concentration in the aqueous phase on the emulsion viscosity was explored and is presented in figure 5.8. Using a Brookfield viscometer at set shear rate on 1:1 (v/v) aqueous phase : sunflower oil emulsions at a constant HDK H20 silica particle loading of 2 wt% with respect to the oil phase and different chitosan concentrations, viscosity was determined. The viscosity increases from 690 mPa s to approximately 2000 mPa s when the chitosan concentration increases from 0 to 1 wt%. At higher chitosan concentrations the values plateau at 2200–2300 mPa s. Varadhan and Watson showed that the viscosity of an emulsion is directly proportional/linked to the volume of dispersed phase of the system.[51] As such the viscosity increase observed upon chitosan concentration increase is directly related to the increase of the oil–water interface due to improvement of wetting properties of the silica particles by chitosan adsorption onto their surface. Nevertheless, from 1 wt% chitosan, it becomes less and less marked. The reason might be that the surface of the silica particles cannot accommodate more chitosan molecules (saturation of the surface).

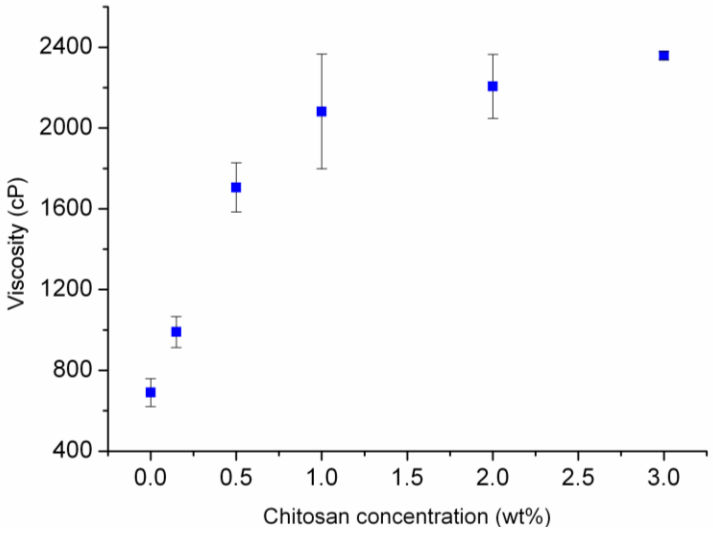

Figure 5.8 Viscosity of emulsions prepared with a constant silica particle concentration and an aqueous phase containing from 0 to 3 wt% chitosan (with respect to the weight of the aqueous phase). Measured by a Brookfield viscometer

Similarly to other systems made of negatively charged silica particles mixed with a cationic species,[52] we believe that synergistic action of silica particles and polymeric chitosan was responsible for this increase by promoting the adsorption of the silica particles at the droplet interface. Like other cationic/Ludox particle emulsifier systems described among others by Hassander, Binks and coworkers,[52–54] positively charged chitosan molecules certainly adsorb on the surface of the negatively charged silica particles, thanks to electrostatic interactions between chitosan and surface charges created by deprotonation of silanol groups, coupled to non-electrostatic interactions. Consequently, the wettability of the silica particles is modified. Macakova *et al.* reported that the absorbed amount of chitosan on a silica particle was of the range of 0.1 mg m^{-2}, i.e. about ten times as low as the amount that can adsorb on the surface of a highly charged mica surface.[55]

The addition of chitosan in the system promotes the silica to adsorb to the droplet interface favourably. It facilitates Pickering stabilised emulsion droplets being incorporated within the colloidal gel matrix, effectively resulting in a quiescent Pickering emulsion.

Now that we have established our conditions to generate quiescent Pickering water-in-sunflower oil emulsions, the next step is to transfer this to a technology platform for juice infused chocolate confectionery. For this we first replaced sunflower oil with cocoa butter.

5.3.2 Cocoa butter model systems

Quiescent Pickering emulsions of water containing 1.0 wt% of chitosan and 1 wt% of acetic acid (pH 3.2) were made as described above using a 50:50 wt/wt oil to water ratios, at an elevated temperature of 40 °C to warrant the cocoa butter to be in a liquid state. The minimum amount of silica HDK H20 required to ensure a complete emulsion phase, that is no pure aqueous and/or cocoa butter phases, was ca. 2.5 wt% based on cocoa butter. Rheological measurements using a Kinexus rheometer were conducted at 40 °C to further investigate state-of-matter.

Figure 5.9(l) shows repetitive measurements of viscosity as a function of increasing and decreasing shear rates, ranging from 0.1 to 1000 s^{-1}. Above a threshold value of 1.5 s^{-1} the system shows liquid-like shear thinning behaviour in all cases. Reversal of the shear rate after the initial run of the sample shows a clear hysteresis indicating that fabrication conditions of the Pickering emulsion influences the rheological data, in effect labelling its emulsification history. Indeed successive runs show reproducible behaviour. Below the

threshold shear rate of 1.5 s^{-1} the sample undergoes a transition to a gel-like state. This transition is clearer when we plot viscosity against stress, as depicted in figure 5.9(r)

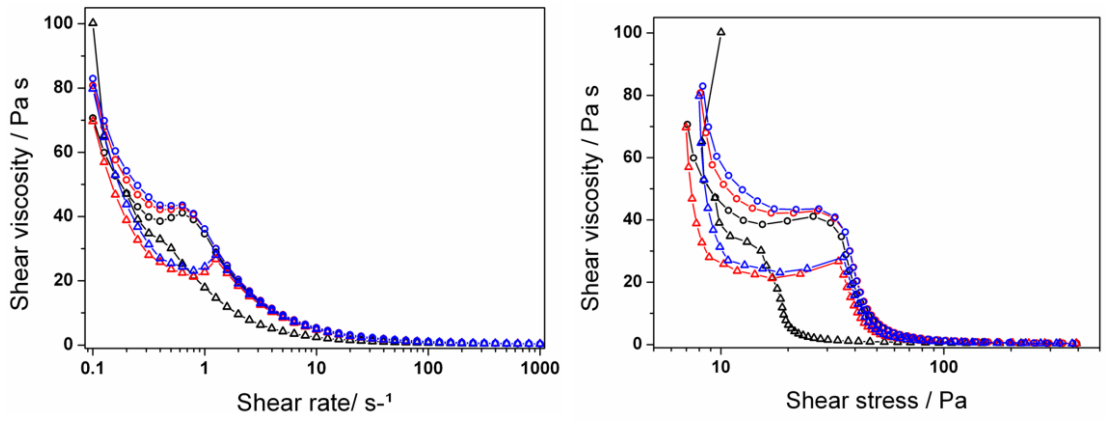

Figure. 5.9 Shear viscosity as a function of increasing and subsequent decreasing shear rates (l) and shear stress (r) for three cycles. Increasing profiles (Δ), decreasing profiles (○). First cycle (black), second cycle (red), and third cycle (blue)

From the data it is apparent that a yield stress, and thus a transition from a gel-like to a liquid-like state, exists at an applied shear stress of 35–40 Pa. Again, the exact value of the yield stress depends on the emulsification methodology of the sample, or in other words the amount of shear applied during emulsification, as evident from the hysteresis. Prior to rheological profiling, the emulsion droplet size is larger. The rheology measurement shears the sample in excess of the level achieved with handshaking. As a result, a smaller yield stress of 15–20 Pa is observed on the initial viscometry measurement compared with subsequent runs. We can therefore assume that a larger yield stress is attained with decreasing emulsion droplet size.

In order to obtain Pickering emulsion droplets of small enough diameter, that is below the mouth sensation threshold of 30 μm diameter, we used an ultraturrax at 11000 rpm for 120 s emulsification tool at 40 °C. We successfully managed to encapsulate 50% by

mass; cranberry juice, smooth orange juice, and decarbonated Cola soft drinks. Advantages are their acidic nature, which facilitates the dissolution of chitosan. The acidity, if necessary, can be tailored upon addition of small quantities of ascorbic acid (vitamin C) in order to maintain an aqueous phase pH in the range of 3.2–3.8.

The microstructure of our fruit juice infused cocoa butter systems was analysed by cryogenic scanning electron microscopy. Samples were prepared using a freeze-fracture method whereby the emulsions are frozen in slush nitrogen preserving the native structure of the emulsion. Figure 5.10 at relatively low magnification depicts droplets occupying approximately 50% visible surface area, as per the formulation. All droplets fall below the mouth sensation threshold of 30 μm diameter, with a mean average droplet diameter of 11.76 μm as measured by image analysis.

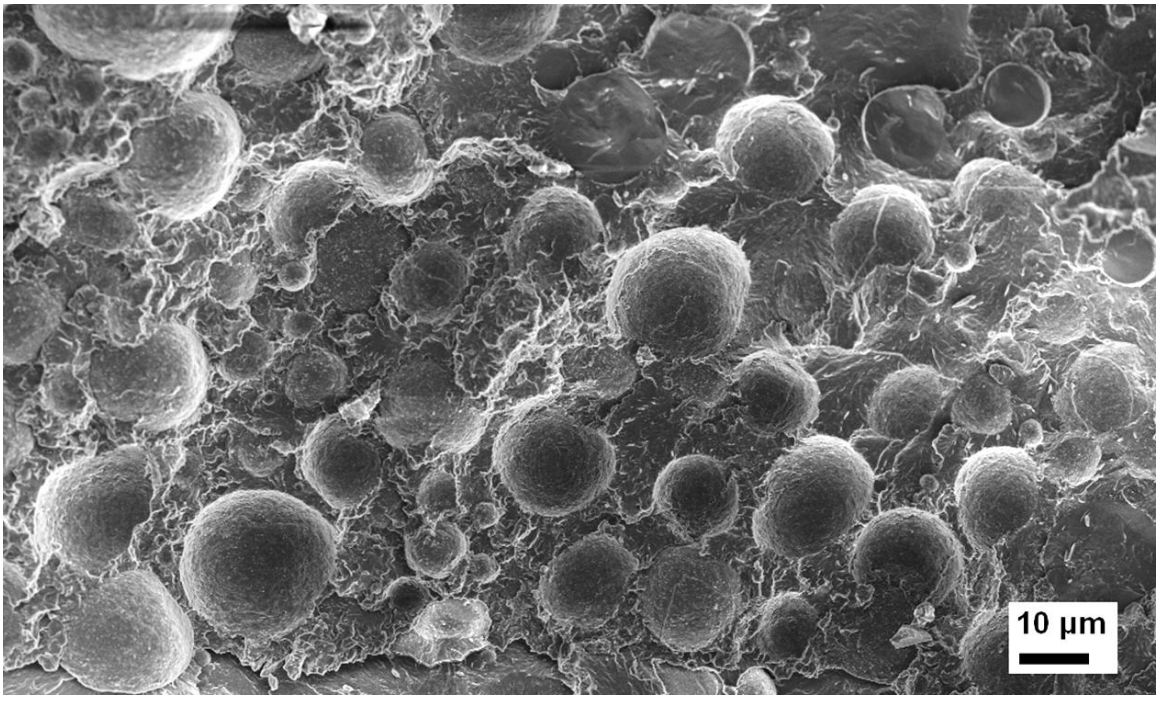

Figure. 5.10 Freeze-fractured cryogenic scanning electron micrograph of 50 vol% water-in-cocoa butter dispersions

Upon closer inspection of individual emulsion droplets (figure 5.11A and 5.11B), the fumed silica flocs are clearly visible at the interface of the droplet confirming their role as Pickering stabiliser to this system. Silica flocs are not present within the water droplets as depicted in figure 5.11B.

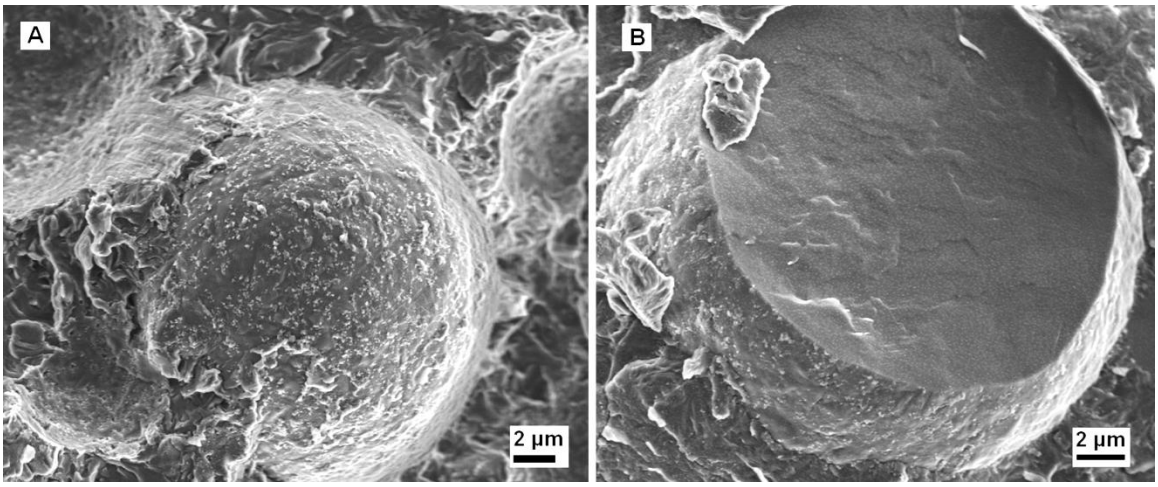

Figure. 5.11 (A) Cryogenic scanning electron micrographs depicting the surface and (B) cross-section of a droplet from 50 wt% water-in-cocoa butter emulsion

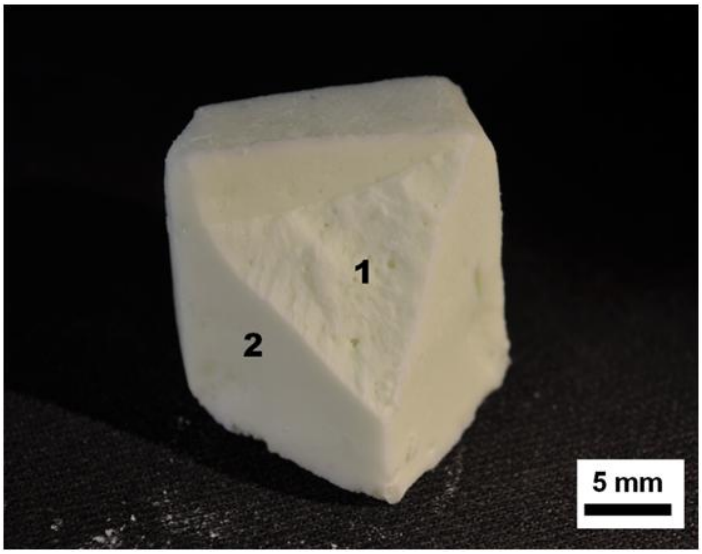

Figure. 5.12 A magnified image of the solidified 50 wt% water-in-cocoa butter emulsion. In (1) the product was cleaved apart revealing trapped emulsion microstructure, whereas in (2) the product sliced using sharp knife resulting in sheared emulsion droplets and a 'smooth' tribological texture

Figure 5.12 depicts a magnified image of the final cocoa butter product at room temperature, containing 50 wt% cranberry juice, dispersed as emulsion droplets. By cutting with a sharp knife, the emulsion yields and deforms analogous to 'real chocolate', offering a smooth mouth sensation. Upon cleaving the solid breaks along the weakest line exposing the emulsion surface. Note the small bubbles visible are an artefact of incident air bubbles trapped upon casting, and are not a result of emulsion ripening.

5.3.3 Real chocolate formulations

On the basis of our results obtained from the cocoa butter model systems, real chocolate formulations using commercially available white, milk and dark chocolate were explored. The use of chocolate builds a level of complexity as cocoa solids, milk fats and sugar content influence the properties of the final product. The weight percentage of aqueous phase, that is water or fruit juices, was adjusted to match the amount of fats present in the three types of chocolate. To be specific, the brand of white chocolate we used contains 33.5% total fat (milk and cocoa), milk chocolate contains 32.8%, and dark contains 28.8% cocoa butter only.

Cocoa butter has 6 polymorphic crystalline structures, with their melting points in a close range between 17.3 and 36.3 ℃. Polymorph V, with a melting point at 32–34 ℃ is the desired form which gives chocolate its gloss and firm snapping texture, whilst melting easily in the mouth with a smooth texture.[1] In order to maximise the content of polymorph V in chocolate, manufacturing processes involve a so-called tempering stage. The melting, cooling and precise heating to just above the melting temperature of form

IV leads to a maximum relative amount of the desired form V in the final product. Correctly tempered chocolate also prevents fat bloom, a phenomenon where fat diffuses to the surface as a result of the presence of lower melting point polymorphs, giving the chocolate surface an undesired grey/white coating. The addition of milk fat aids the suppression of fat bloom.[56] In addition to this sugar bloom may also occur, and is driven by exposure of the chocolate formulation to moisture. The dissolution of sugar from within the product and subsequent surface condensation and dehydration of the solution on the product surface renders a powdery white appearance, which again is undesirable.

We subjected the chocolate emulsion formulations to a tempering procedure immediately after emulsification by precisely manipulating temperature under low shear conditions. The final products are displayed in figure 5.13.

Figure. 5.13 Images of dark (left), milk (centre) and white (right) chocolate emulsion formulations in which 50 wt% of fat has been replaced with cranberry juice. Images were taken after 14 days storage at 5 °C

Differential Scanning Calorimetry measurements were conducted to determine the polymorphic structure of the confectionery. Samples were heated from 5–50 °C at a rate of 2 °Cmin^{-1}. Our model cocoa butter and dark chocolate formulations contain only cocoa butter as a source of fat. Figure 5.14(l) displays the DSC traces for our cocoa butter model formulation and the data for cocoa butter in itself as a reference. Comparison of

these two traces indicates similar melting properties with a bimodal distribution; the largest endothermic peak in both cases at approximately 35 °C corresponds to polymorph V. The smaller endothermic peak at ca. 30 °C indicates the presence of polymorph IV, which spontaneously reverts to form V during prolonged storage in cool conditions. In figure 5.14(r), the dark chocolate emulsion formulation is compared with dark chocolate as reference. Again we can observe that a large fraction of the cocoa butter has the desired polymorph crystal structure. In the latter case one can argue that a small relative reduction of the amount of cocoa butter in the correct polymorph is observed. Analyses of the milk (figure 5.15(l)) and white (figure 5.15(r)) chocolate formulations, revealed the prevalent polymorph V and IV peaks but also showed the appearance of an additional peak around 20 °C which can be ascribed to the milk fats present in these two types of chocolate. The exothermic peak in milk fat arises from the phase transition of α to β polymorphs and then direct crystallisation from amorphous to β once seeded.[57] All systems show considerable amounts of polymorph V, hereby providing the right chocolate structure to provide the desired tribological effect upon consumption.

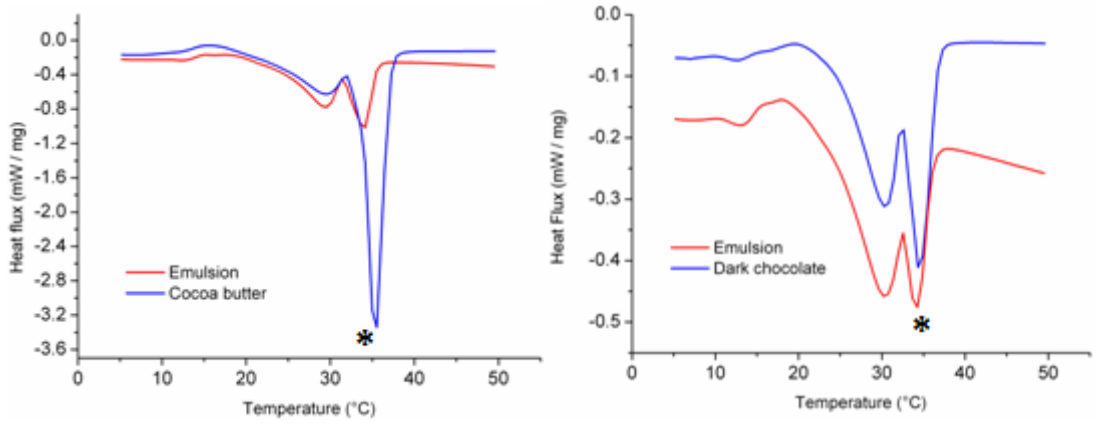

Figure. 5.14 DSC traces of the cocoa butter emulsion alongside pure cocoa butter (l) and dark chocolate emulsion alongside pure dark chocolate (r). Asterisk indicates peak for polymorph V

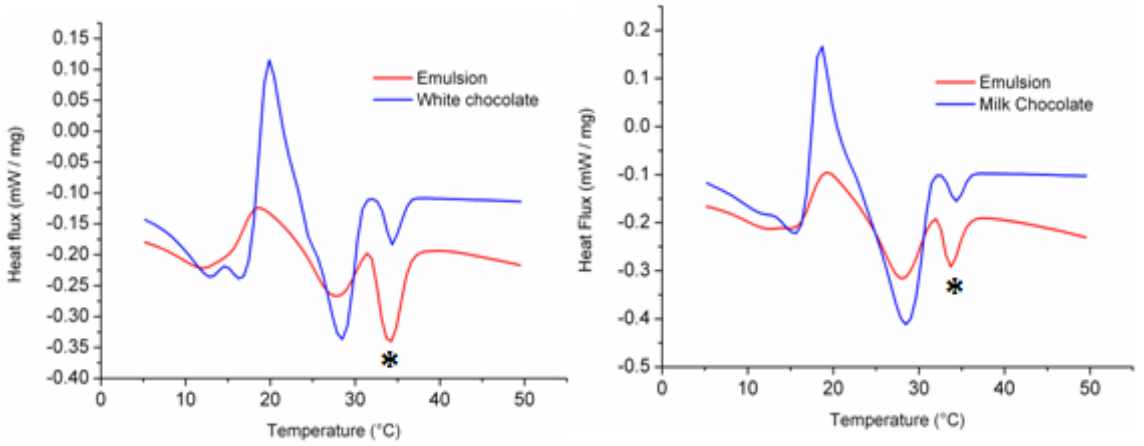

Figure. 5.15 DSC traces of the white chocolate emulsion alongside pure white chocolate (l) and milk chocolate emulsion alongside pure milk chocolate (r). Asterisk indicates peak for polymorph V

The relative large amounts of polymorph V in our chocolate formulations should arrest fat bloom. To investigate the extent of both fat and sugar bloom on our systems, chocolate formulations with a large exposed surface area were cast and left refrigerated uncovered at 5 ℃ for 14 days. Figure 5.16 shows an representative image of one of our white chocolate emulsion formulations with no evidence of fat or sugar bloom.

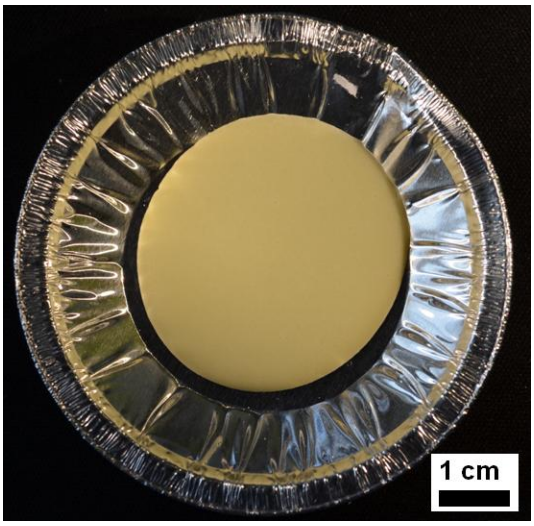

Figure. 5.16 A white chocolate emulsion formulation in which 50 wt% of the fat is replaced with cranberry juice after two weeks exposure at 5 °C

5.4 Conclusions

It has been demonstrated that preparation of emulsion based chocolate confectionaries in which 50% of the total fat content by weight (cocoa butter and milk fats) has been replaced with fruit juices using a quiescent Pickering emulsion as fabrication strategy. The combination of fumed silica particles and chitosan under acidic conditions (pH 3.2–3.8) was highly beneficial towards improvement of emulsion properties in terms of volume of dispersed phase and stability, in comparison to emulsions prepared with each compounds considered individually. Adsorption of the polycationic chitosan molecules onto the silica particles surface influenced the particle wettability making it an effective Pickering stabiliser. The formation of a colloidal gel in the continuous (molten) oil phase provided the system with a yield stress, hereby giving it a gel-like and thus quiescent behaviour under low shear conditions. This warrants a homogeneous distribution of emulsion droplets as settling through gravity upon storage under molten/liquid conditions is arrested. The emulsified confections were subsequently tempered with no fat or sugar bloom observed. All fruit-juice infused chocolate formulations exhibited the desired crystalline characteristics of chocolate. The technique is limited to 50% replacement of aqueous phase owing to catastrophic phase inversion. The use of a 'nanoparticle' additive, despite similar compounds being used in cosmetics and foodstuffs can be a sensitive issue to consumers. Additionally, chitosan is a non-vegetarian, non-kosher additive. However, despite these issues, we present a route to formulations with similar attributes to the full fat counterpart, and has the potential to be deployed in other food products such as ice cream and personal care formulations.

5.5 Experimental

5.5.1 Materials

Low and medium molecular weight chitosan 75–85% deacetylated, glacial acetic acid, L-ascorbic acid, (Sigma Aldrich corp.). Fumed silicate particles HDK-H2O, HDK-N20, HDK-H18 supplied by Wacker Chemie. Cocoa butter (RSSL, Reading, UK), sunflower oil (Tesco, UK), cranberry juice from concentrate (Ocean Spray), Pepsi Cola, smooth orange juice (Tropicana), white, milk and dark chocolate (ASDA, UK) were used as received.

5.5.2 Equipment

DSC measurements were performed on a Mettler Toledo TGA/DSC 1 thermogravimetric analyser. Samples were weighed out into aluminium pans on a 5 d.p. balance. Heat flux measurements were started at 5 ℃ increasing at a rate of 2 K/min and terminated at 50 °C under a flow of air.

Single shear viscosity measurements were conducted using a Brookfield DV-II+, spindle number 63 at 20 rpm.

Rheological measurements were carried out on a Kinexus Rheometer ultra (Malvern Instruments) with active heat exchanger and parallel plate geometries PU40 S0141 SS and PL40 C0007 SS. Pre-emulsified cocoa butter samples were heated to 40 ℃ and dispensed on to the heated 40.00 ℃ parallel plate geometry. Plate gap size was set at 1.00 mm. Sample temperature was monitored and allowed to equilibrate for 5 minutes prior to any measurement. Sunflower oil emulsions and separate components were dispensed

onto the plate geometry with a gap size of 1.00 mm. Samples were maintained at 25.00 °C with a 5 minute temperature equilibration prior to any measurement.

(Cryogenic) Scanning Electron Microscopy analyses were carried out using a Zeiss Supra 55-VP Field Emission Gun Scanning Electron Microscope with a Gatan Alto 2500 cryo transfer system and a Gatan C1002 Liquid Nitrogen cold stage. For analysis of the fumed silica particles the particles were deposited on to a double sided adhesive carbon black tab and attached to an aluminium stub. Following sputter coating with AuPd target (1.5 kV, 30 s, 15 mA), samples were imaged at a 10 kV accelerating voltage. Cryogenic FEG-SEM analyses of the cocoa butter confectionery were carried out as follows: molten emulsions at 40 °C were drawn into a brass rivet through capillary action and frozen in liquid nitrogen prior to scalpel fracturing to expose a clean internal structure. The sample was heated to −90 °C for 15 minutes to remove ice through sublimation followed by a platinum sputter target coating in an argon atmosphere (20 seconds, 10 mA). Imaging was undertaken at −125 °C using a 3 kV accelerating voltage with a gold anti-contaminator at −189 °C. Images were post-analysed using ImageJ computer software (NIH, US).

5.5.3 Protocols for preparation of the emulsions

Sunflower oil based emulsions

Chitosan was dissolved in 1% w/w glacial acetic acid solution. Separately, Wacker silicates were dispersed in oil via handshaking until visibly homogeneous. The two solutions were mixed and either hand shaken for 30 seconds or sheared with a rotor-stator mechanical shearer (ultra-turrax 11 000 rpm) for 120 seconds.

Cocoa butter emulsions

Silicates were dispersed in molten cocoa butter at 40 °C. Aqueous solutions of dissolved chitosan and acetic acid were also heated to 40 °C. The two warmed phases were mixed and sheared by handshaking or rotor-stator, prior to casting and cooling to RT or analysis at 40 °C.

Emulsions incorporating soft beverages

Where cranberry juice, smooth orange juice, or decarbonated Pepsi Cola, was used as aqueous phase, chitosan was added to the stirred beverage at 40 °C. Using L-ascorbic acid (vitamin C) the pH was continually adjusted to a native value between 3.2 and 3.8 to assist dissolution of the chitosan.

Real chocolate emulsions

Chocolate samples (milk, white and dark) and fruit juice containing 1.0 wt% chitosan were separately heated to 40 °C prior to mixing and emulsification by a rotor-stator mixer for 60 s. An equal ratio of aqueous phase with respect to fat content of the chocolate was used. Immediately after, formulations were cooled to 28 °C (dark chocolate and cocoa butter) or 26 °C (milk and white chocolate) prior to gradual re-heating whilst stirring to 33 °C (dark chocolate and cocoa butter) or 31.6 °C (milk and white chocolate) and holding at that temperature for 5 minutes. Samples were then refrigerated for a period of two weeks before DSC analysis.

5.6 References

(1) Beckett, S. T. *The Science of Chocolate*; 2nd ed.; RSC Publishing: Cambridge, 2008.

(2) Lipp, M.; Anklam, E. *Food Chemistry* **1998**, *62*, 73–97.

(3) Health and Social Care Information Centre Lifestyles Statistics. *Statistics on Obesity, Physical Activity and Diet*; London, 2013.

(4) Todd, J. W. Improved process for manufacturing articles of food or confectionery. G.B. Patent 459,583, November 7, 1937.

(5) Tyle, P. *Acta Psychologica* **1993**, *84*, 111–118.

(6) Hinton, C. L., Pratt, C. D., de Vadetsky, E., Landwill, K. E., McCloskey, K. E., Schuemann, H. W. *Twenty Years of Confectionery and Chocolate Progress*; 1st ed.; Avi Publishing Co.: Westport, 1970.

(7) Minifie, B. W. *Chocolate, Cocoa and Confectionery: Science and Technology*; 1st ed.; Springer: New York, 1989.

(8) Mezzenga, R.; Schurtenberger, P.; Burbidge, A.; Michel, M. *Nature Materials* **2005**, *4*, 729–740.

(9) Guevara, J. S.; Mejia, A. F.; Shuai, M.; Chang, Y.-W.; Mannan, M. S.; Cheng, Z. *Soft Matter* **2013**, *9*, 1327–1336.

(10) Le Révérend, B. J. D.; Norton, I. T.; Cox, P. W.; Spyropoulos, F. *Current Opinion in Colloid & Interface Science* **2010**, *15*, 84–89.

(11) Norton, J. E.; Fryer, P. J.; Parkinson, J.; Cox, P. W. *Journal of Food Engineering* **2009**, *95*, 172–178.

(12) Wiley, R. M. Quiescent suspension polymerisation. U.S. Patent 2,932,629, April 12, 1960.

(13) Ramsden, W. *Proceedings of the Royal Society of London* **1903**, *72*, 156–164.

(14) Pickering, S. U. *Journal of the Chemical Society, Transactions* **1907**, *91*, 2001–2021.

(15) Finkle, P.; Draper, H. D.; Hildebrand, J. H. *Journal of the American Chemical Society* **1923**, *45*, 2780–2788.

(16) Wiley, R. *Journal of Colloid Science* **1954**, *9*, 427–437.

(17) Pieranski, P. *Physical Review Letters* **1980**, *45*, 569–572.

(18) Ostwald, W. *Lehrbuch der Allgemeinen Chemie*; 2nd ed.; Engelmann: Leipzig, 1896.

(19) Binks, B. P. *Current Opinion in Colloid & Interface Scienceand Interface Science* **2002**, *7*, 21–41.

(20) Aveyard, R.; Clint, J. H. *Journal of the Chemical Society, Faraday Transactions* **1996**, *92*, 85–89.

(21) Cheung, D. L.; Bon, S. A. F. *Physical Review Letters* **2009**, *102*, 66103.

(22) Ashby, N. P.; Binks, B. P. *Physical Chemistry Chemical Physics* **2000**, *2*, 5640–5646.

(23) Giermanska-Kahn, J.; Schmitt, V.; Binks, B. P.; Leal-Calderon, F. *Langmuir* **2002**, *18*, 2515–2518.

(24) Wege, H. A.; Kim, S.; Paunov, V. N.; Zhong, Q.; Velev, O. D. *Langmuir* **2008**, *24*, 9245–9253.

(25) Wong, J. C. H.; Tervoort, E.; Busato, S.; Gonzenbach, U. T.; Studart, A. R.; Ermanni, P.; Gauckler, L. J. *Journal of Materials Chemistry* **2010**, *20*, 5628–5640.

(26) Claire Hermant, M.; Klumperman, B.; Koning, C. E. *Chemical communications* **2009**, 2738–2740.

(27) Colver, P. J.; Bon, S. A. F. *Chemistry of Materials* **2007**, *19*, 1537–1539.

(28) Colver, P. J.; Colard, C. a L.; Bon, S. A. F. *Journal of the American Chemical Society* **2008**, *130*, 16850–16851.

(29) Zhou, W.; Cao, J.; Liu, W.; Stoyanov, S. *Angewandte Chemie* **2009**, *48*, 378–81.

(30) Fameau, A.-L.; Saint-Jalmes, A.; Cousin, F.; Houinsou Houssou, B.; Novales, B.; Navailles, L.; Nallet, F.; Gaillard, C.; Boué, F.; Douliez, J.-P. *Angewandte Chemie* **2011**, *123*, 8414–8419.

(31) Bon, S. A. F.; Cauvin, S.; Colver, P. J. *Soft Matter* **2007**, *3*, 194–199.

(32) Velev, O. D.; Furusawa, K.; Nagayama, K. *Langmuir* **1996**, *12*, 2374–2384.

(33) Gordon, V. D.; Chen, X.; Hutchinson, J. W.; Bausch, A. R.; Marquez, M.; Weitz, D. A. *Journal of the American Chemical Society* **2004**, *126*, 14117–14122.

(34) Shahidi, F.; Arachchi, J. K. V.; Jeon, Y.-J. *Trends in Food Science & Technology* **1999**, *10*, 37–51.

(35) Ravi Kumar, M. N. V *Reactive and Functional Polymers* **2000**, *46*, 1–27.

(36) Ilium, L. *Pharmaceutical Research* **1998**, *15*, 1326–1331.

(37) Schulz, P. C.; Rodríguez, M. S.; Del Blanco, L. F.; Pistonesi, M.; Agulló, E. *Colloid & Polymer Science* **1998**, *276*, 1159–1165.

(38) Marie, E.; Landfester, K.; Antonietti, M. *Biomacromolecules* **2002**, *3*, 475–481.

(39) Del Blanco, L. F.; Rodriguez, M. S.; Schulz, P. C.; Agulló, E. *Colloid & Polymer Science* **1999**, *277*, 1087–1092.

(40) Rinaudo, M.; Pavlov, G.; Desbrières, J. *Polymer* **1999**, *40*, 7029–7032.

(41) Pa, J.-H.; Yu, T. L. *Macromolecular Chemistry and Physics* **2001**, *202*, 985–991.

(42) Deminiere, B.; Colin, A.; Leal-Calderon, F.; Muzy, J. F.; Bibette, J. *Physical Review Letters* **1999**, *82*, 229–232.

(43) *Perfect toners hide a secret: HDK – Pyrogenic Silica*; 6178-EN; Wacker Chemie, Munich, 2009.

(44) *HDK - Pyrogenic Silica*; 6180-EN; Wacker Chemie, Munich, 2009.

(45) Binks, B. P.; Lumsdon, S. O. *Physical Chemistry Chemical Physics* **2000**, *2*, 2959–2967.

(46) Binks, B. P.; Rodrigues, J. A. *Langmuir* **2003**, *19*, 4905–4912.

(47) Binks, B. P.; Philip, J.; Rodrigues, J. A. *Langmuir* **2005**, *21*, 3296–3302.

(48) Safouane, M.; Langevin, D.; Binks, B. P. *Langmuir* **2007**, *23*, 11546–11553.

(49) Binks, B. P.; Murakami, R. *Nature Materials* **2006**, *5*, 865–869.

(50) Raghavan, S. R.; Khan, S. A. *Journal of Rheology* **1995**, *39*, 1311–1325.

(51) Varadhan, C.; Watson, H. E. *Journal of the Indian Institute of Science* **1930**, *13*, 21–30.

(52) Binks, B. P.; Rodrigues, J. A.; Frith, W. J. *Langmuir* **2007**, *23*, 3626–3636.

(53) Hassander, H.; Johansson, B.; Törnell, B. *Colloids and Surfaces* **1989**, *40*, 93–105.

(54) Binks, B. P.; Desforges, A.; Duff, D. G. *Langmuir* **2006**, *23*, 1098–1106.

(55) Lundin, M.; Macakova, L.; Dedinaite, A.; Claesson, P. *Langmuir* **2008**, *24*, 3814–3827.

(56) Lohman, M.; Hartel, R. *Journal of the American Oil Chemists' Society* **1994**, *71*, 267–276 LA – English.

(57) Grotenhuis, E.; Aken, G. A.; Malssen, K. F.; Schenk, H. *Journal of the American Oil Chemists' Society* **1999**, *76*, 1031–1039.

Chapter 6

High internal phase agar hydrogel dispersions in confectionery formulations*

6.1 Abstract

The limitations encountered through the use of Pickering emulsion stabilisation led us to investigate an alternative strategy to reduce the fat content of chocolate through emulsification. The dispersion of hydrocolloid gel particles within a lipid continuous phase presents a viable route to produce chocolate formulations of up to 80 vol% aqueous phase, without the use of nanoparticles, and an improvement in stiffness. We exploit the

* Parts of this chapter have been published elsewhere: Thomas S. Skelhon, Patrik K. A. Olsson, Adam R. Morgan, and Stefan A. F. Bon, High internal phase Agar hydrogel dispersions in cocoa butter and chocolate as a route towards reducing fat content, *Food and Function*, **2013**, *4*, 1314-1321

use of agar, a natural biopolymer with a thermal hysteresis that allows the formation of sub mouthfeel threshold droplet emulsions in cocoa butter, dark, milk and white chocolate before gelation into discrete microgel particles as determined by cryogenic electron microscopy. Rheological profiling investigates the flow characteristics of microgel suspensions in oil and ultimately compares the flow performance of hydrocolloid gel dispersions to that of pure chocolate. Thermal analysis indicates how the favoured crystalline structure can be obtained in these dispersions. Finally, we demonstrate the ability to incorporate ethanol into the formulation without detriment to microgel stability.

6.2 Introduction

In the previous chapter we described a Pickering stabilised emulsion system that permitted the replacement of up to 50 vol% of the fat content in cocoa butter and chocolate with droplets of acidified water and fruit juice. This was achieved through the use of silicate nanoparticles coupled with the cationic biopolymer chitosan. Despite successfully dispersing droplets less than the mouthfeel threshold of 30 μm diameter, stable against coalescence and sedimentation, there are several areas which could be improved upon from a consumer, commercial and legislative perspective. Firstly, an EU directive exists regarding the disclosure of the use of 'nanomaterials' in food[1] and personal care products.[2] Any product which contains particulate matter of less than 100 nm diameter has to be clearly marked, and therefore can have negative connotations with consumers. Chitosan is a biopolymer derived from shellfish and can therefore limits use to non-vegetarians or consumers not restricted by faith. The Pickering system described

is limited to 50 vol% replacement of aqueous phase before catastrophic phase inversion. However, high quantities of dispersed water droplets will deteriorate the mechanical strength of the final product if higher aqueous phase loading were possible. Therefore exceeding dispersed volumes of water higher than the threshold value of 74% for high internal phase emulsions (HIPEs) whilst maintaining product stability throughout processing and storage without detriment to the chocolate eating qualities presents a significant challenge.

A solution to the abovementioned issues can be to turn the water droplets into hydrogels. There are many examples referring to the applied use of hydrogel particles in food formulations, including providing texture, structure[3] and encapsulation.[4] Particulate forms of gel are valued for their ease of processing in a flowable form, soft undetectable texture and ability to tune macroscopic properties by the control of particle size, shape and modulus. In addition, many hydrocolloids are derived from natural sources, and are therefore biocompatible.[5]

Dispersed hydrocolloid particles can also be used to mimic the texture of fat, and therefore used as a partial replacement to the fat content in processed food formulations. Brummel *et al.* demonstrate the use of several types of hydrocolloid particles as a replacement of fat in cheese spreads.[6] Gelation of a dispersed aqueous phase in cocoa butter, forming discrete microgels within the lipid matrix has been reported by Norton and coworkers.[7] They used gelatine, an animal derived biopolymer with a disintegration temperature (melting point) of 32 °C, allowing the microgels to melt at body temperature

emulating the phase transition of cocoa butter. At ambient temperatures the internal gel structure of the emulsified droplets imparts structural rigidity to the formulation. This elegant method stabilised up to 50% v/v aqueous phase with most droplets falling between 3-5 μm. Despite gelatine hydrocolloids melting at a convenient temperature, a drawback is that it is animal derived. Additionally, the product would not withstand storage at elevated temperatures above 32 ℃ as the gel phase would melt becoming liable to droplet coalescence and phase separation at elevated temperatures.

As such, there is scope for the development of low fat chocolate formulations by the dispersion of hydrogel particles in the continuous lipid phase. However, the use of a hydrocolloid that is more thermally resistant and vegetable derived is preferable. An alternative to gelatine is agar, an abundant biopolymer derived from red algae consisting of agarose and agaropectin.

6.2.1 Agarose hydrogels

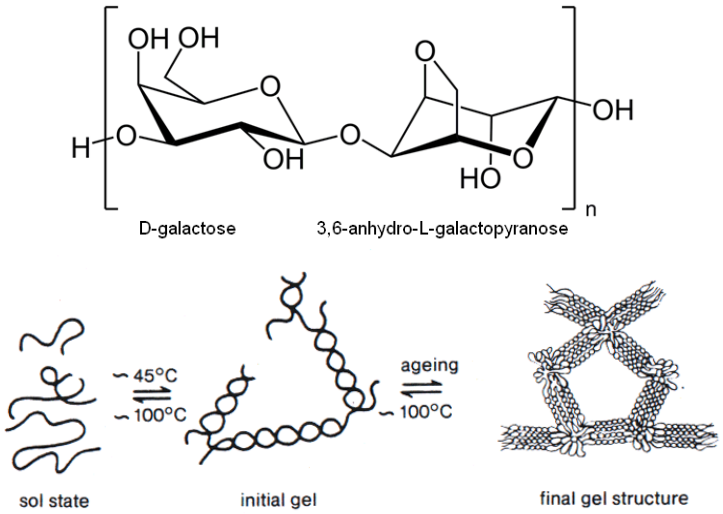

Figure 6.1 (Top) Structural formula of agarose biopolymer. (Bottom) Schematic of reversible thermally controlled gel formation[8]

Agar is a hydrocolloid derived from the Gelidium and Gracilaria species of red algae. The predominant component agarose consists of the alternating disaccharide D-galactose and 3,6-anhydro-L-galactopyranose of molecular weights exceeding 100,000 Daltons. The remainder, agaropectin, is a complex mixture of sulphate and pyruvate modified D-galactose and L-galactose disaccharide polymer chains, usually of lower molecular weight than agarose. The ratios between agarose and agaropectin vary between species of algae, however agarose is typically the major component, making up between 50-75 % by mass of the agar.[9] The mechanism of gelation relies upon the formation of double helixes of the agarose polymer chains in solution at the gelation temperature. These helixes aggregate thereby rapidly gelling the system which are then stable against thermal disintegration below 90 °C.[10] As such, agar exhibits a large gelling and melting

hysteresis, of 40 ℃ and 90 ℃ respectively (as seen in figure 6.2) which can be exploited in food processing, providing thermally stable physical gels.[11]

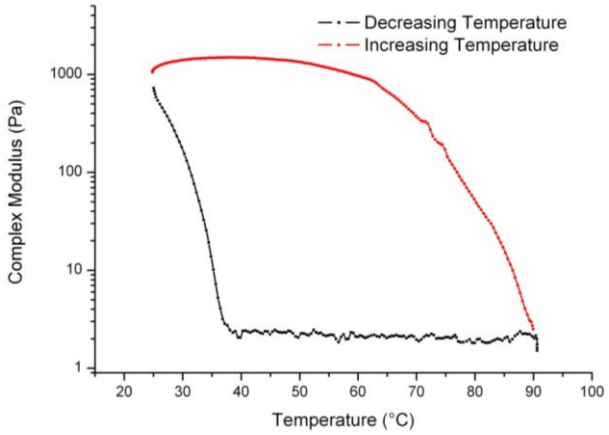

Figure 6.2 Oscillatory rheological profile of complex modulus (G*) as a function of decreasing before increasing temperature indicating a significant thermal hysteresis

From a nutritional viewpoint, the use of agar-based hydrogels to replace part of the fat matrix in confectionery has the additional benefit of agarose (80% of the agar) being classed as a dietary fibre serving as an appetite suppressant.[12]

An interesting feature of agar hydrogels is that once they have been formed, the gel matrix does not further swell in the presence of excess water.[13] Agar-based microgel particles, despite containing over 95% water are stable against coalescence due to the solid, non swellable mechanical properties they possess. This allows for the incorporation of high volume fractions of aqueous phase into oil based food formulations, exceeding levels which can be achieved using liquid droplets and conventional emulsifiers.

Dispersing agar microgels into an oil continuous phase significantly affects the rheological and mechanical properties of the overall formulation. Variation of the concentration of agar in the aqueous phase alters the gel particle modulus and together with varying the overall fraction of dispersed phase can increase the moduli over 3 orders of magnitude, and impart shear thinning behaviour.[14] At very high dispersed aqueous microgel fractions, the dispersion trends towards a 'jammed' regime imparting bulk gel-like, or even dilatant behaviour.[13] As such, the mechanical properties such as flowing characteristics and stiffness of the formulation can be tuned.

We therefore employ agar as the gelling agent in the formation of dispersed hydrocolloid particles in chocolate formulations.

6.2.2. Polyglycerol polyricinoleate stabiliser

Rather than employ the use of a Pickering stabiliser, we opted for the use of an FDA GRAS (generally recognised as safe)[15] approved food emulsifier and viscosity modifier[16] polyglycerol polyricinoleate (PGPR) as the sole surfactant to stabilise the liquid hydrogel emulsions before and during gelation period; the chemical structure of which can be seen in figure 6.3.

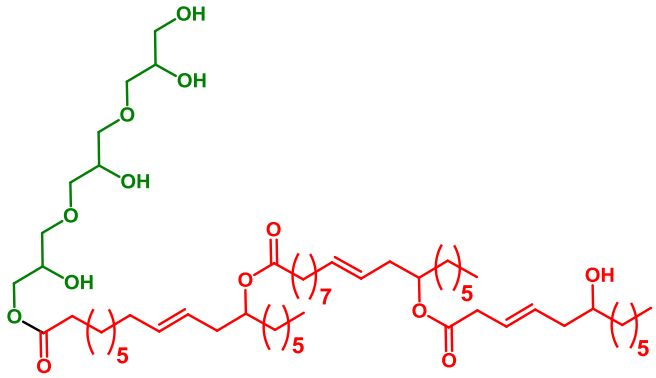

Figure 6.3 Structural formula of PGPR with hydrophilic and hydrophobic section marked in green and red respectively

PGPR is prepared by the esterification of condensed castor oil fatty acids with polyglycerol[17] and is most commonly used in chocolate formulations to reduce yield stress. This occurs by decreasing the frictional component between solid and crystalline components, facilitating moulding and entrained air release.[18] It has also been reported as an effective stabiliser, promoting the formation of water in oil emulsions owing to a very low hydrophilic-lipophilic balance (HLB) value of 1.5. The HLB of a surfactant is the degree of hydrophilicity/hydrophobicity it possesses as calculated theoretically by the contribution of different chemical groups on the molecule.[19,20] Normally, a compound of such lipophilicity would not perform well as an emulsifier. However similarities between surfactant and oil in terms of chain length and chemical composition contribute to maximise emulsion stability,[21] demonstrated in the case of PGPR and cocoa butter. As such Fryer *et al.*[22] reported the successful use of PGPR in stabilising 20 wt% water in cocoa butter formulations using a margarine line to achieve stable homogenous water in oil emulsions with droplet size below the mouthfeel threshold of 30 µm diameter.[23] Note that the maximum amount of PGPR which can be used in food is tightly regulated in the EU.[24] In chocolate products, the overall PGPR content should be less than 0.5 wt%. In

our studies we aim to stay below this upper threshold value, typically using 0.5 wt% in a formulation with 50 vol% aqueous phase, and 0.2 wt% in a formulation with 80 vol% aqueous phase.

6.3 Results and Discussion

Initially, water in sunflower oil emulsions were used as model systems and formulated to ascertain the optimum PGPR concentration for use in cocoa butter formulations. The liquid state of sunflower oil at ambient temperature provides a convenient analogue to molten cocoa butter. Values for interfacial tension (31 mNm^{-1}) and dynamic viscosity (50 mPa) for sunflower oil at 25 °C[25] and cocoa butter at 40 °C[26] are very similar.

Varying amounts of PGPR with respect to oil phase (0.5, 1.0, 2.0 and 5.0 wt%) were dispersed in the oil phase. The relative amounts of added water phase were varied and the systems were emulsified through handshaking the vials. Note that the aqueous phase was dyed with a small amount Rhodamine B, to simplify visual analysis of the emulsification process. The results after storing the emulsions for 24 hours are displayed in figure 6.4. From this it can be seen that 1.0 % w/w PGPR in the oil phase seemed optimum and could stabilise up to 60 vol% aqueous phase. Increasing the emulsifier concentration above this value resulted in an excess free water phase arising from the stabilisation of smaller droplets. The formation of smaller droplets upon increasing PGPR concentration is in agreement with results from studies of droplet sizes in lower dispersed phase volume (<25%) W/O emulsions.[27]

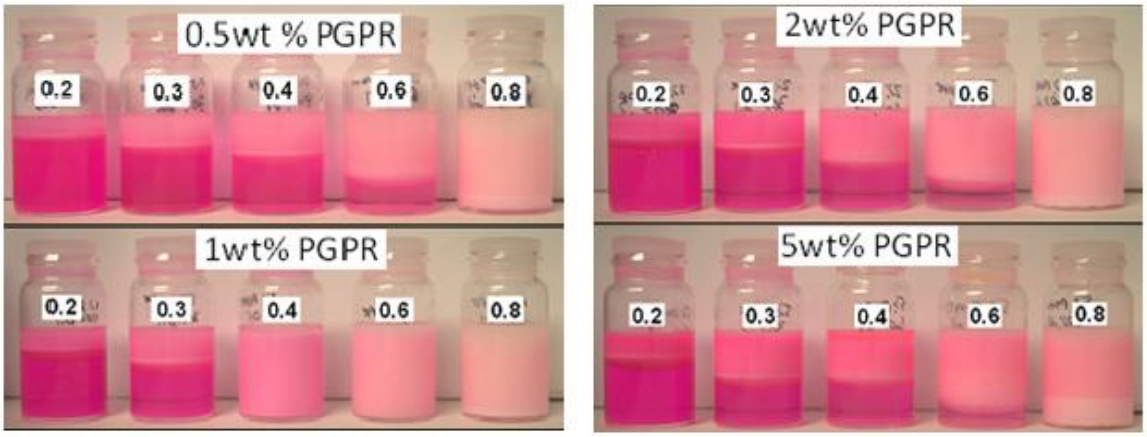

Figure 6.4 Hand shaken water in PGPR containing sunflower oil emulsions left standing for 24 hours. Each row represents a fixed PGPR content with respect to oil phase at a range of oil fractions, 0.2 to 0.8 from L to R respectively

6.3.1 Agar microgel dispersions in sunflower oil

The dispersion and gelation of agar solutions in sunflower oil was investigated. Based on the results above the concentration of PGPR was fixed at 1.0 wt% with respect to the oil phase. A 2.0 wt% agar solution in water was prepared at 90 ℃, and subsequently cooled to 50 ℃, keeping the temperature above its gelation point. Varying relative amounts of this aqueous phase was added to the PGPR containing sunflower oil at 50 ℃. The emulsification was carried out using ultraturrax, providing a high shear mixing environment. After emulsification for 60 seconds the emulsions were cooled to room temperature and left undisturbed. Following this strategy, stable emulsions containing up to 40% v/v aqueous phase were successfully made (see figure 6.5). Increased relative aqueous volumes resulted in catastrophic phase inversion upon cooling and gelation. A plausible reason for the maximum dispersed water phase only being 40 vol% when Agar was used, in comparison to 60 vol% in the reference system (see figure 6.4) is that part of

the PGPR molecules interact with the Agar, so that only a fraction of them can be used to stabilise the water-oil interface.

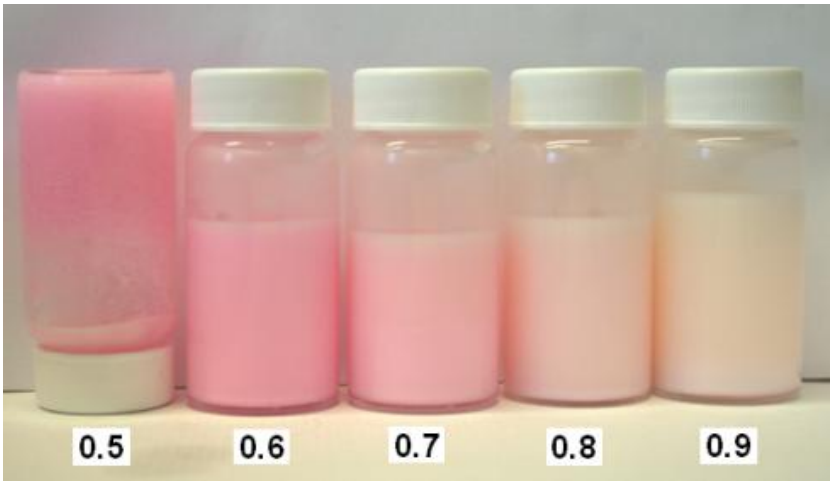

Figure 6.5 2.0 wt% Agar solutions emulsified into sunflower oil at 50 °C before cooling to room temperature. Oil volume fraction of dispersion is varied from 0.5 (L) to 0.9 (R). Note at an oil fraction of 0.5, the system phase inverts and gels

6.3.2 Two stage emulsification strategy

In order to prevent catastrophic phase inversion, and increase the overall fraction of dispersed water phase, we employed a two stage emulsification strategy exploiting the significant hysteresis agar gels exhibit (figure 6.2). In short the aqueous Agar containing phase was introduced into 2 steps, of equal proportion. In the first step, half of the water phase was emulsified at 50 ℃, and allowed to cool. This generates a set of dispersed hydrogel particles. Next, the system was re-heated to 50 ℃. Note that by doing this the gel particles are preserved as they are thermally stable up to 90 °C. The second half of the water phase is now introduced, whilst under shear, hereby generating a second batch of microgel particles upon cooling. This approach made it possible to increase the dispersed

phase up to 50 vol%. Higher relative amounts of water used (30 vol% + 30 vol%, and 35 vol% + 35vol%) again resulted in phase inversions (see figure 6.6).

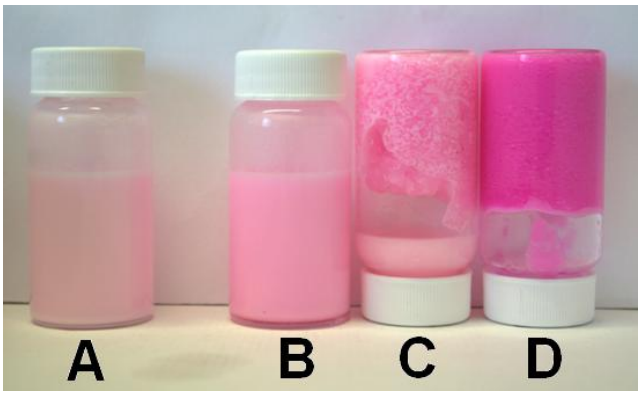

Figure 6.6 2.0 wt% Agar emulsified into sunflower oil following a two-stage emulsification strategy. A) 25 + 25 vol% agar phase after re-heating to 50 °C to demonstrate thermal stability of two-stage emulsion. B) 25 + 25 vol% agar phase. C) 30 + 30 vol% agar phase. D) 35 + 35vol% agar phase

An explanation for this instability can be as follows. Up to 50 vol% the formation of the Agar gel network is confined to the individual emulsified water droplets. Gel particles nucleate and either grow or coalesce within each droplet, resulting in discrete gel particles, templating the original emulsion droplet size. At higher aqueous phase volumes (>50 vol%), the gelation process is difficult to confine within the emulsified droplets. Bridging between droplets leading to coalescence extends the gel matrix, ultimately causing a phase inversion.

6.3.3 Shear cooling emulsification strategy

In order to further increase the dispersed gel phase content, an alternative strategy, that is the application of shear during the gelation process, was investigated. Agar solutions were emulsified into the PGPR containing sunflower oil at 50 °C (20, 30, 40, 50, 60, 70 and 80 vol% of Agar solution) using high shear emulsification. However, the cooling step

now involved exposing the samples to low shear by hand shaking instead of leaving them at rest. Deploying this strategy enabled the stable formation of up to 80 vol% dispersed gel phase in oil (see figure 6.7). Note that we tried to shred a macroscopic hydrogel into microgel parts by ultraturrax as a way to disperse gel particles in oil, but this was not successful.

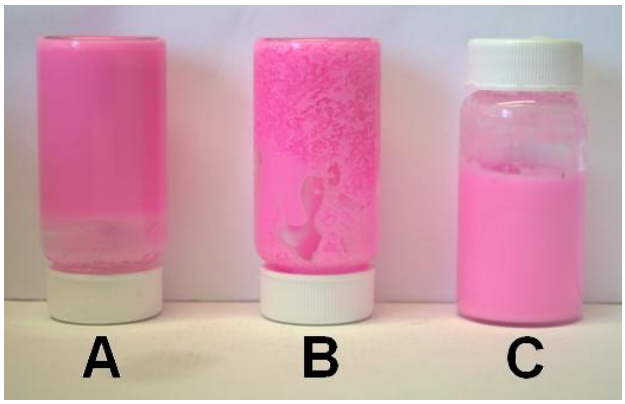

Figure 6.7 2.0 wt% Agar solutions emulsified into sunflower oil at 80 vol% aqueous fraction A) Emulsified at 50 °C, prior to quiescent cooling to room temperature. B) pre-gelled agar phase emulsified into oil phase at room temperature. C) Emulsified at 50 °C then sheared whilst cooling to room temperature. Note only sample C flows

Following the shear cooling regime, rather than generating quiescent gels confined to the original emulsion droplet size, large gel particles growing beyond the droplet phase which would normally cause phase inversion are sheared down into smaller gel particles, resulting in the desired 'fluid gel'. Fluid gel systems have been studied for their flexibility in reduced fat formulations. By altering the amount of agar used, shear rates and aqueous phase volume, the overall structure and properties of the final formulated can be tuned.[28] Furthermore, fluid gel microgel particles interact further in space than their spherical counterparts due to the non-spherical nature of sheared particles. As such, sheared gel suspensions have a more cohesive behaviour and contribute to the overall

modulus of the system. This has a knock-on effect of slowing down food break down and ultimately an increased sensation of satiety.[29]

6.3.4 Rheology of agar microgel in sunflower oil dispersions

Rheological properties of these agar microgel in sunflower oil dispersions were ascertained over a range of gel phase volumes. The shear viscosity was measured as a function of shear rate (see figure 6.8) and shear stress (see figure 6.9).

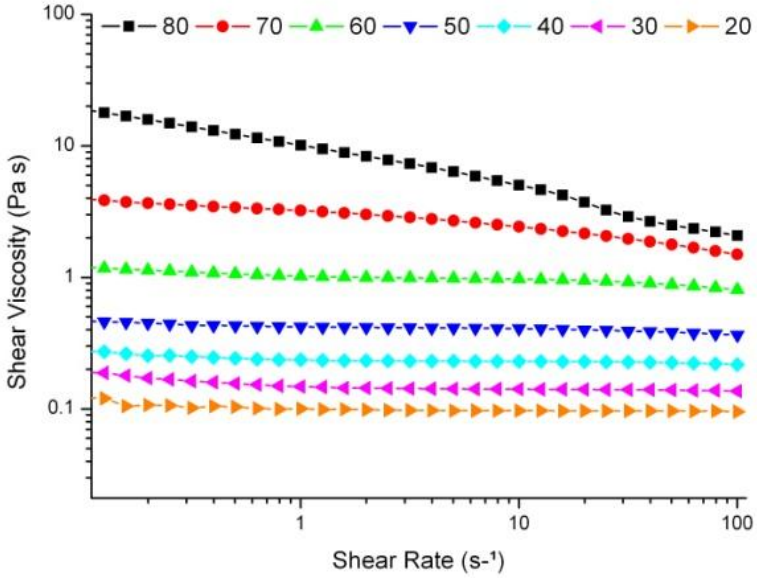

Figure 6.8 Viscosity as a function of shear rate for 2.0 wt% agar phase in sunflower oil dispersions over a range of aqueous phase fractions. Legend indicates percentage of aqueous agar phase in dispersion

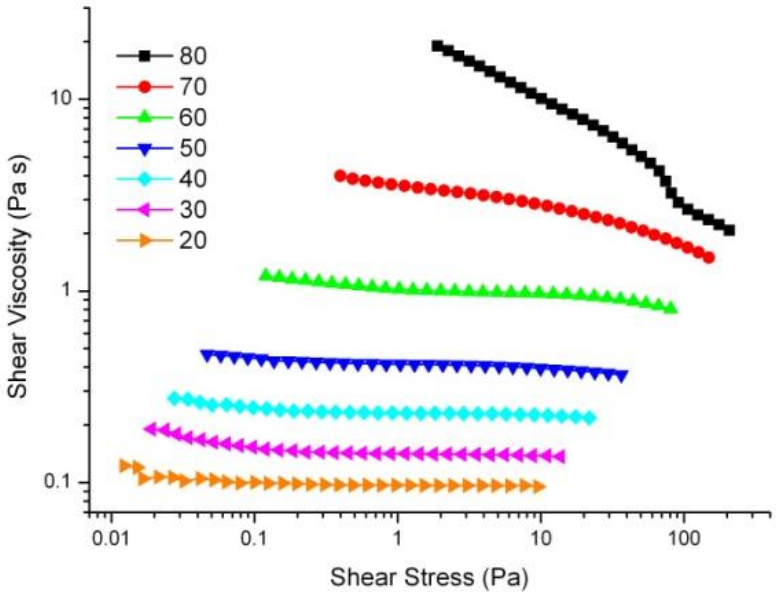

Figure 6.9 Viscosity as a function of shear stress for 2.0 wt% agar phase in sunflower oil dispersions over a range of aqueous phase fractions. Legend indicates percentage of aqueous agar phase in dispersion

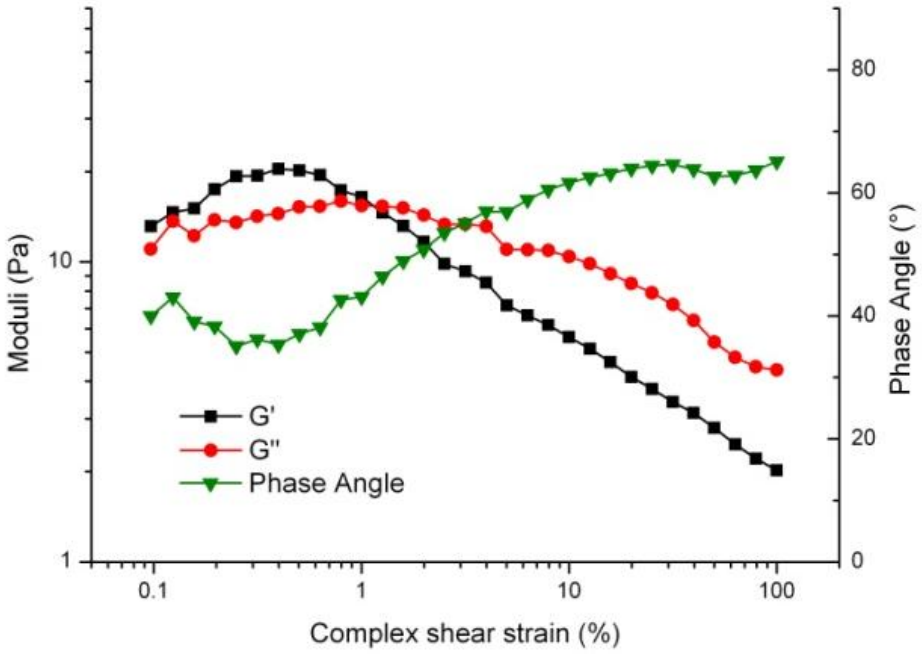

Figure 6.10 Oscillatory shear strain amplitude sweep at 1 Hz for an 80 vol% agar microgel dispersion in sunflower oil

The shear viscosities increase when higher amounts of hydrogel phase are dispersed within the continuous sunflower oil phase. This increase is non-linear as to be expected for soft colloidal systems. When the dispersed microgel phase exceeds 70 vol%, a marked increase in shear viscosity, together with the appearance of shear thinning behaviour, is observed. The latter indicates the plausibility of a yield stress, and thus a jammed morphology of the microgel particles. An amplitude sweep spectrum of the 80 vol% microgel dispersion at 1 Hz in figure 6.10 confirms this clearly. The storage modulus is higher than that of the loss modulus below 1% strain, confirming macroscopic gel-like behaviour attributed to the proximity and packing of the microgel particles into a jammed conformation. (Note that this confirms the observed behaviour for the right hand sample in figure 6.7, as the jammed-like gel structure collapses upon shear induced by gravitational force) At higher strains, fluid-like behaviour is observed showing shear thinning. The effect of shear thinning upon increasing strain is partially suppressed due to the soft nature of the Agar microgel particles and their polydisperse particle size distribution.

6.3.5 Electron microscopy of agar microgel in sunflower oil dispersions

Utilising cryogenic scanning electron microscopy (cryo-SEM), we visualised the microstructure of the 80 vol% Agar microgel dispersion in sunflower oil.

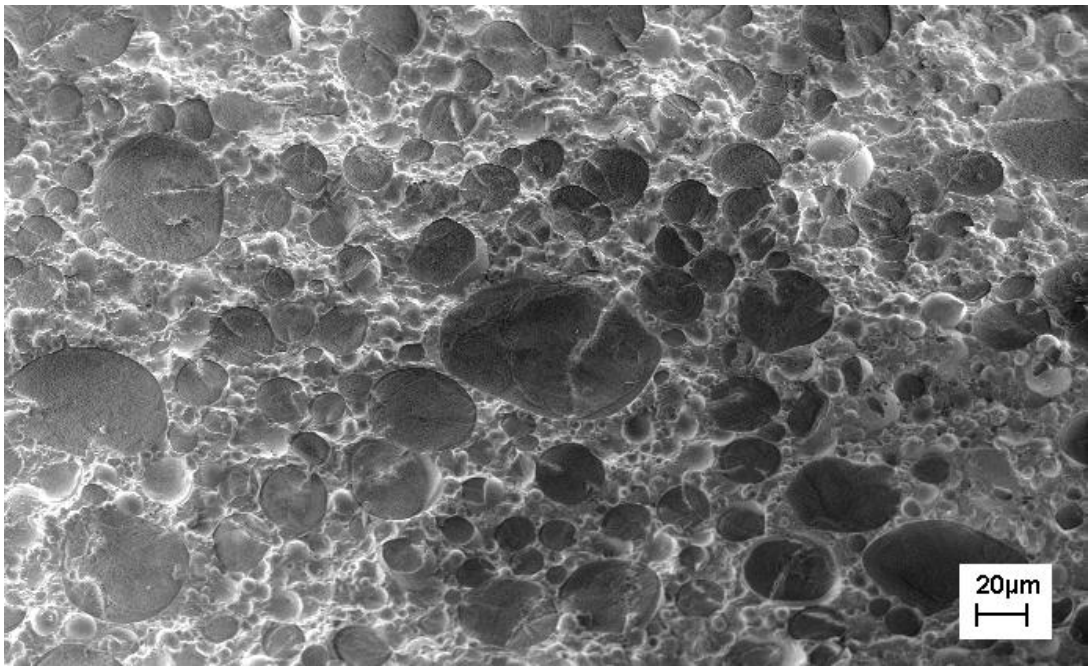

Figure 6.11 Cryo FEG-SEM image of an 80 vol% agar phase in sunflower oil dispersion

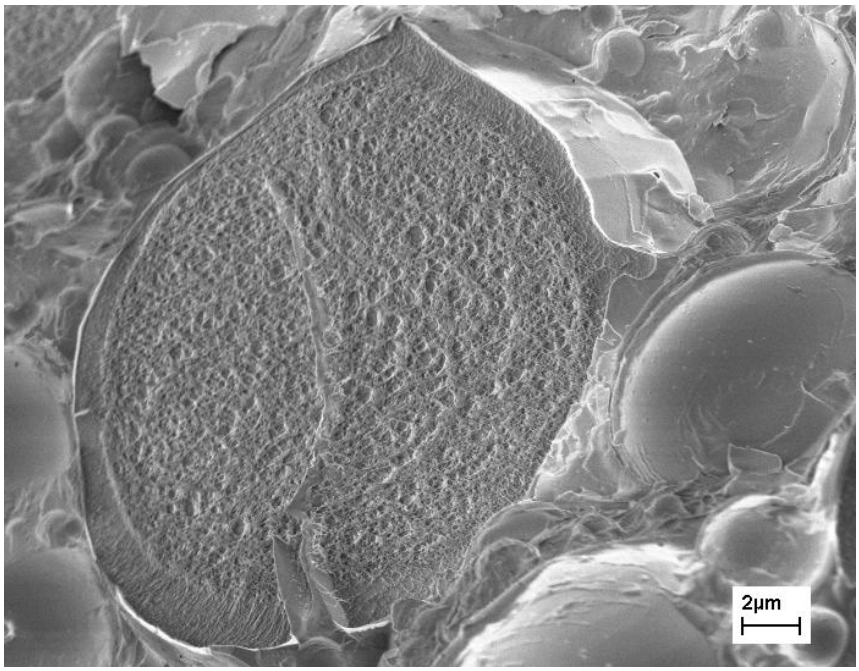

Figure 6.12 High magnification Cryo FEG-SEM image of a slice through an agar microgel particle from an 80 vol% agar phase in sunflower oil dispersion

From figure 6.11 it can be observed that indeed the microgel particles are dispersed into a continuous matrix of sunflower oil. Droplet size analysis indicates a polydisperse size distribution spanning from 1-2 μm up to 40-50 μm in diameter. Sublimation of the water phase from freeze-fractured microgel particles clearly reveals the agar gel polymer network (see figure 6.12) confined only to the droplets.

6.3.6 Agar microgel dispersions in cocoa butter

After developing a strategy to incorporate up to 80 vol% of microgel particles into a sunflower oil continuous phase, the process was translated for cocoa butter. Following the same formulation process as above, agar solutions were emulsified into the cocoa butter, and sheared whilst cooling to 40 ℃, below the gelation temperature, but above that of the cocoa butter melting point. Once formation of the microgel particles was complete (a few minutes), the emulsions were allowed to solidify at room temperature.

6.3.7 Electron microscopy of agar microgel dispersions in cocoa butter

Cryo-SEM analysis of 80 vol% agar microgel particles in cocoa butter revealed a similar morphology as for our sunflower oil model system (see figure 6.13).

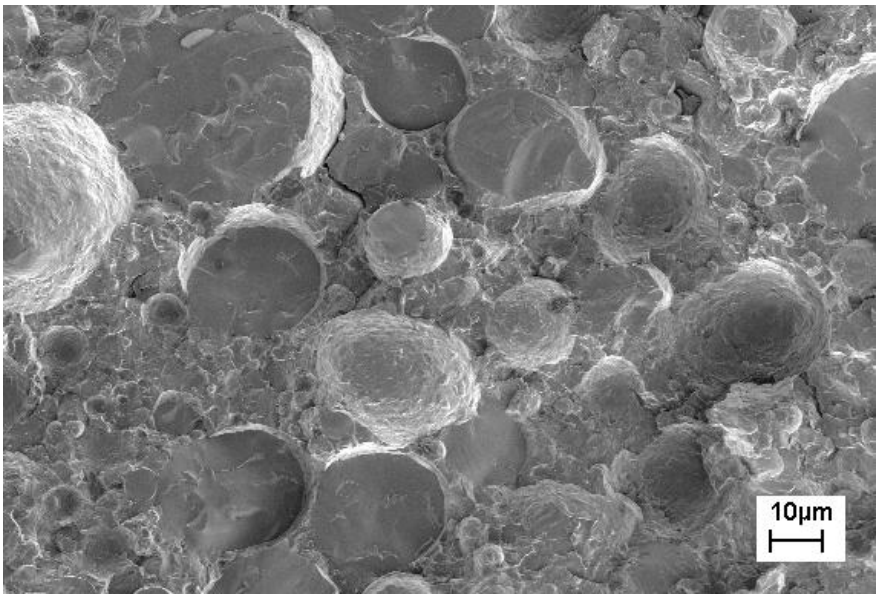

Figure 6.13 Cryo FEG-SEM image of 80 vol% agar phase in cocoa butter dispersion

Upon closer inspection of the larger microgel particles, it is possible to see a sub-domain of smaller gel particles trapped within. As mentioned earlier, gel particles generated in the primary high shear process are combined into larger ones during shear cooling, hereby creating W/W/O systems. Figure 6.14 depicts a cryo-SEM micrograph indicating smaller gel particles of approximately 1 µm diameter, trapped within a 10 µm gel particle.

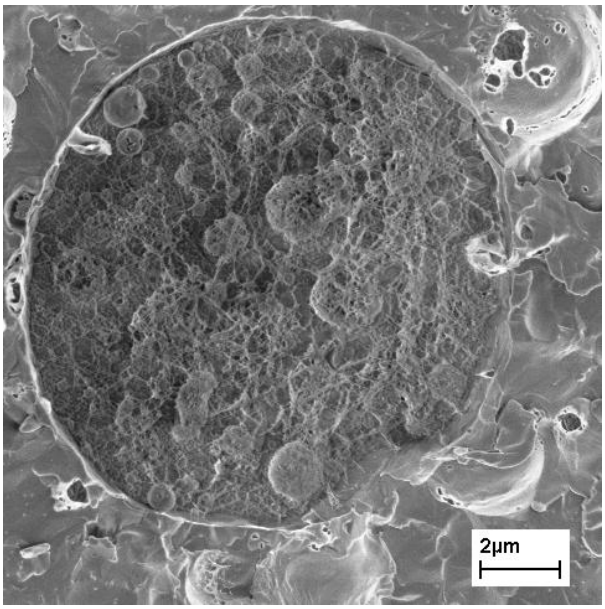

Figure. 6.14 High magnification Cryo FEG-SEM image of an agar microgel particle, from an 80 vol% agar phase in sunflower oil dispersion. Note the presence of smaller agar gel particles within

The microgel in cocoa butter process was carried out for different volume fractions of dispersed hydrogel phase (20, 30, 40 and 80 vol%) and particle size analysis by analysis of 70 microgel particles taken from cryo-SEM images. The cumulative distribution functions versus microgel diameter are given in figure 6.15. It is logical that at higher amounts of dispersed microgel phase the average particle size increases. The vast majority of microgels reside below the 30 µm diameter mouthfeel threshold for a homogenous tribological sensation.[23]

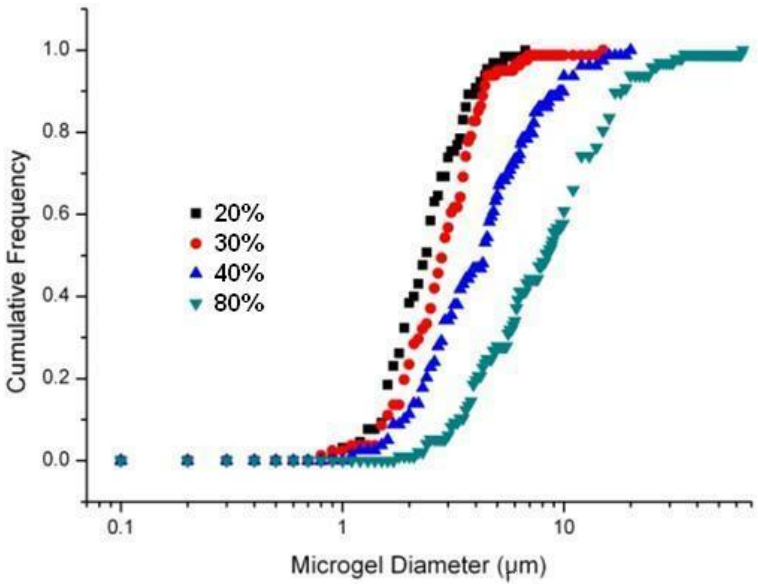

Figure. 6.15 Cumulative distribution function of microgel particle diameters for a range of aqueous agar phase volume fractions based on SEM image analysis. Legend indicates vol% of aqueous phase

6.3.8 Dispersing agar microgels in chocolate

Ultimately, agar solutions were dispersed into molten chocolate, an altogether more complex system than cocoa butter. Additional components including sugar, cocoa solids and non-cocoa fats significantly influence the properties of final product. 1.0 wt % PGPR was added with respect to the total fat content of the chocolate (33.5 wt% for white, 30.9 wt% for milk and 28.5 wt% for dark). 50 vol% agar phase was introduced and dispersed into the molten white, milk, and dark chocolate using the shear cooling process. After cooling to room temperature and subsequent refrigeration for 24 hours during storage, samples were imaged (see figure 6.16). A slice through the centre of the chocolate samples indicates a "homogenous" microstructure without visual presence of gel particles. As such, the emulsification and gelation of the chocolate formulations is not adversely affected by additional components present in three types of chocolate. On the contrary, the addition of up to 60% sucrose to an agar gel is reported to contribute toward

mechanical strength[30] which in our case re-enforces the gel component of the formulation.

Figure. 6.16 Photograph of milk, white and dark chocolate (L to R) with 50% w/w agar microgel content with respect to fat content of the chocolate

6.3.9 Rheology of chocolate based microgel dispersions

The rheological profiles of the milk, white and dark chocolate dispersions containing 50% aqueous phase, alongside that of pure chocolate and chocolate with 1 wt% PGPR (w/r to fat content) were measured to compare flow behaviour. A common rheological model used to characterise chocolate formulations is the Casson equation. Originally derived by Casson in 1957,[31,32] the model was derived to predict flow behaviour of pigment-oil suspensions, and quantifies the interactive behaviour between the solid and liquid components of a bi-phasic system. Components for both yield stress and shear thinning non-Newtonian viscosity are included. As such, it is an effective model for describing the flow of pseudoplastic materials such as blood and food products and can be mathematically expressed as shown in equation 1.[33]

$$\sqrt{\tau} = \sqrt{\tau_{CA}} + \sqrt{\eta_{CA}} \cdot \sqrt{\gamma} \qquad (1)$$

Where τ, τ_{CA}, η_{CA} and γ represent shear stress, Casson yield stress, Casson plastic viscosity and shear rate respectively.

Although superseded by improved models, the Casson equation is still widely used by the confectionery industry to characterise the flow behaviour of molten chocolate formulations.[34] We followed an ICA approved measurement protocol,[35] with some adaptations, namely the extension of the shear rate range from 2-50 s^{-1} to 0.1-100 s^{-1}. The Casson equation was fitted to the obtained data points (as seen in figure 6.17) and values for Casson Yield Stress (τ_{CA}) and Casson Plastic Viscosity (η_{CA}) were obtained, as seen in table 6.1. At low shear rates, the Casson model becomes unreliable in these confectionery systems,[36] as evidenced by the deviation of the model from the data points between 0.1-1 s^{-1}, hence why the industry recognised testing commences at 2 s^{-1}. The addition of 1 wt% PGPR has a considerable effect on Casson yield stress, as expected, for the primary use of PGPR in chocolate is to reduce the yield stress.[16] Upon dispersing 50 vol% aqueous phase into milk and white chocolate, the Casson Yield Stress increases by a factor of 2-3, which is logical due to the solid microgel particles providing a resistance to initiate flow. The dark chocolate microgel dispersion sees a slight reduction from a naturally high yield stress in pure dark chocolate, arising from the high quantities of cocoa solids in the product which have a more marked influence on the yield stress than the dispersed microgels. The Casson plastic viscosity values for both milk and white chocolate microgel dispersions are very similar to the pure chocolate counterparts. However, the dark chocolate microgel dispersion experiences a small reduction in Casson Plastic Viscosity, which could be due to exclusion of water from the dispersion,

lubricating the rheometer geometries and artificially lowering the viscosity. In terms of viability of the microgel dispersions as chocolate products, the recognised Casson parameters for chocolate have a τ_{CA} between 10-200 Pa and η_{CA} between 1-5 Pa•s.[34] All of the 50 vol% aqueous phase microgel dispersions that have been analysed fall within these parameters. The relatively high yield stress values for milk and white chocolate microgel dispersions also indicate their potential use in applications where shape retention and pattern holding is required such as the deposition of molten chocolate shapes, and the need for shape retention until setting.

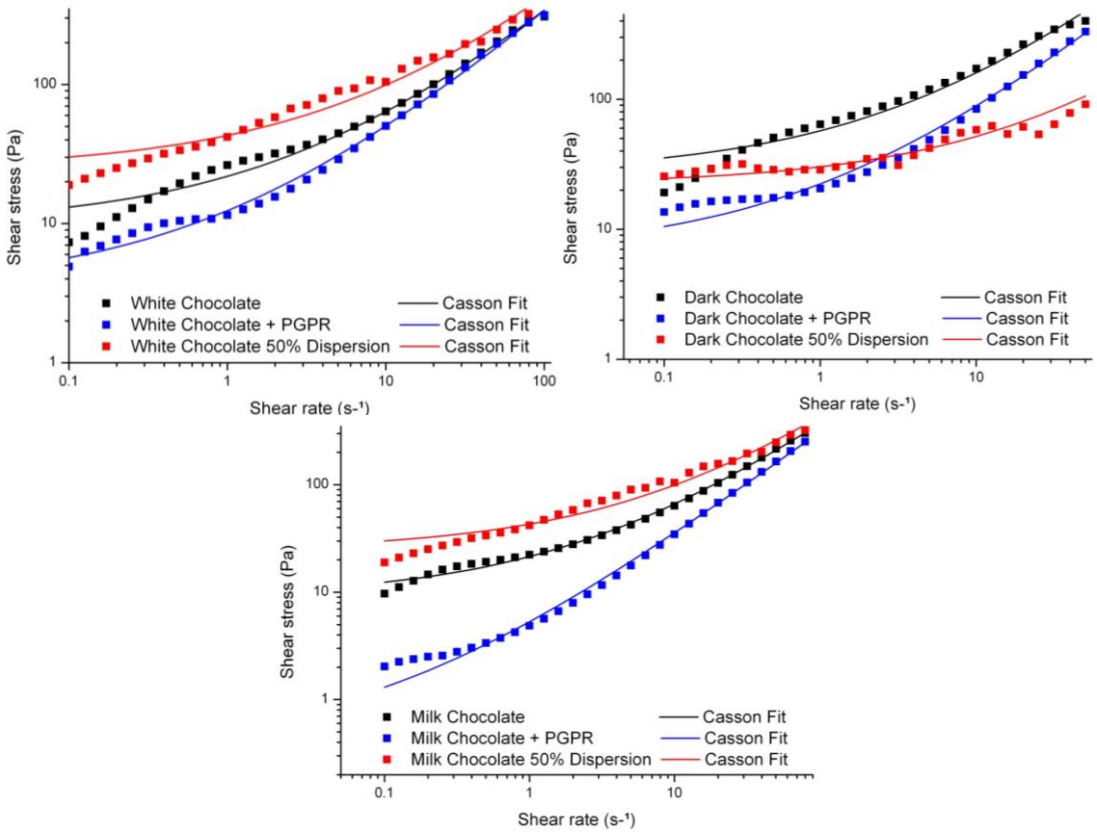

Figure. 6.17 Rheological flow profiles of molten chocolate formulations, each fitted by the Casson equation for (top left) white, (top right) dark and (bottom) milk chocolate

Sample	Yield Stress (Pa)		Plastic Viscosity (Pa·s)		R^2
	Value	Error	Value	Error	
White Chocolate	9.867	0.659	2.353	0.081	0.991
White Chocolate + 1% PGPR	3.453	0.240	2.755	0.054	0.997
White Choc 50% Dispersion	24.908	1.776	2.466	0.156	0.972
Milk Chocolate	9.057	0.264	2.630	0.040	0.998
Milk Chocolate + 1% PGPR	0.364	0.055	2.888	0.039	0.999
Milk Choc 50% Dispersion	24.908	1.776	2.466	0.156	0.972
Dark Chocolate	27.208	2.270	5.524	0.347	0.974
Dark Chocolate + 1% PGPR	6.507	0.533	4.753	0.154	0.993
Dark Choc 50% Dispersion	22.241	0.617	1.428	0.060	0.934

Table 6.1 Casson model Yield Stress (τ_{CA}) and Plastic Viscosity (η_{CA}) fitting parameters for chocolate formulations

6.3.10 Thermal analyses of chocolate microgel dispersions

Differential Scanning Calorimetry measurements of our hybrid agar microgel white, milk and dark chocolates were conducted after a simple thermal tempering process. DSC measurements were performed to measure the cocoa butter polymorphic composition of the final products (figure 6.18). In all cases, the major melting peak occurs at 32-34 °C, indicating considerable quantities of polymorph V, the most desired crystalline structure. Additional peaks appear in the 10-25 °C range for the milk and white chocolate samples which can be ascribed to the melting and crystallisation of the vegetable and milk fats present in the formulations. A further set of peaks present in all samples at 25-28 °C arises from the presence of polymorph IV, an unstable β' crystalline structure which reverts to the more stable polymorph V - β structure over prolonged storage in ambient conditions. Compared to the pure chocolate thermographs, the microgel dispersions show

a more pronounced heat flux in the polymorph V melting range. However the microgel dispersions have a slightly lower melting range of 2-3 °C compared with its pure chocolate counterpart.

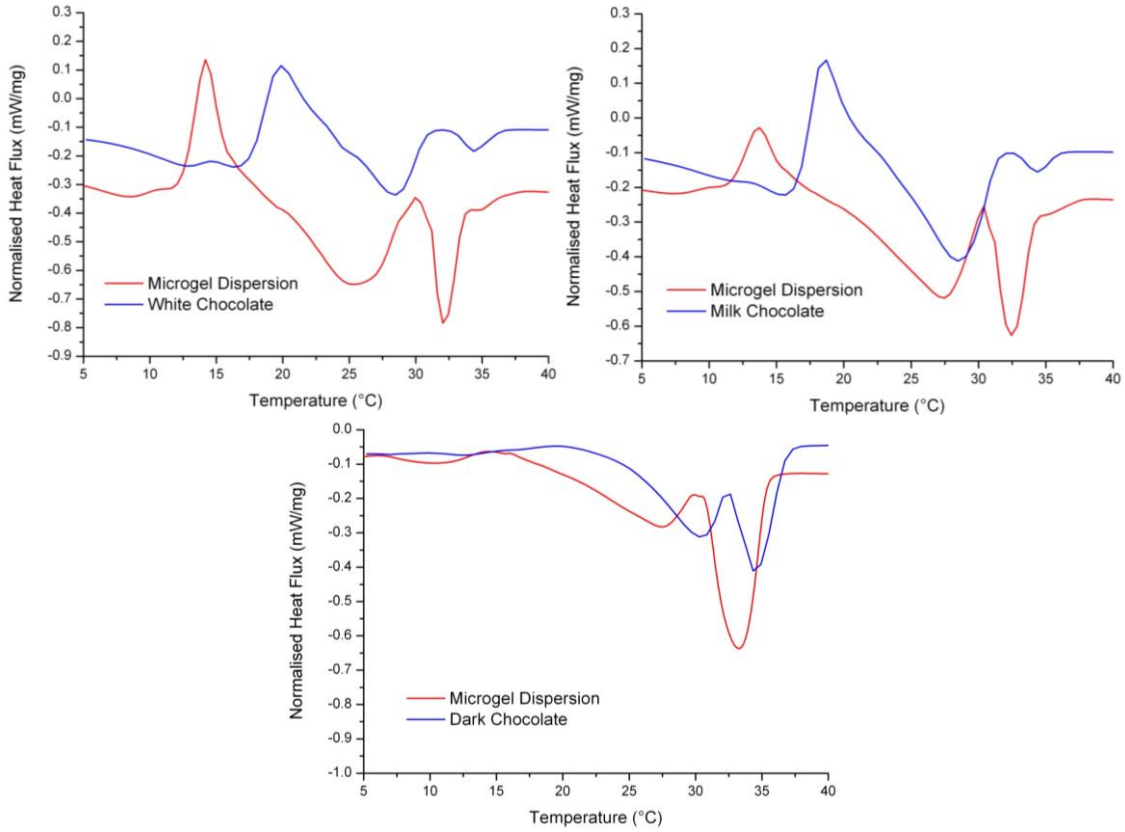

Figure 6.18 DSC thermographs of 50 vol% agar microgel dispersions in three types of chocolate; (top left) white ,(top right) dark and (bottom) milk

6.3.11 Incorporation of alcohol into the chocolate formulations

The addition of alcohol to chocolate based confectionery can be desired with the aim to impart the characteristic flavour of a beverage into the product. This commonly is deployed in the form of liquid centred chocolate 'liquors'. Emulsification of alcohol into chocolate formulations is challenging owing to the reduction of interfacial energy between the oil and aqueous phase induced by the presence of ethanol. For example, the

addition of ethanol to our fruit-juice containing chocolate formulations which were made with fumed silica particles serving as Pickering stabilisers, led to complete failure and destabilisation. However, our hybrid agar microgel formulations may offer a solution to this problem, as the gelation process is relatively unaffected by alcohol content. In a simple experiment, we replaced the aqueous agar phase in a milk chocolate and cocoa butter formulation with 60:40 water: ethanol agar solution to emulate the emulsification of a high strength alcoholic beverage (whisky or vodka for example). As can be seen in figure 6.19, chocolate formulations in which 50 vol% of the fat is replaced by microgel particles containing 40 vol% ethanol can easily be made.

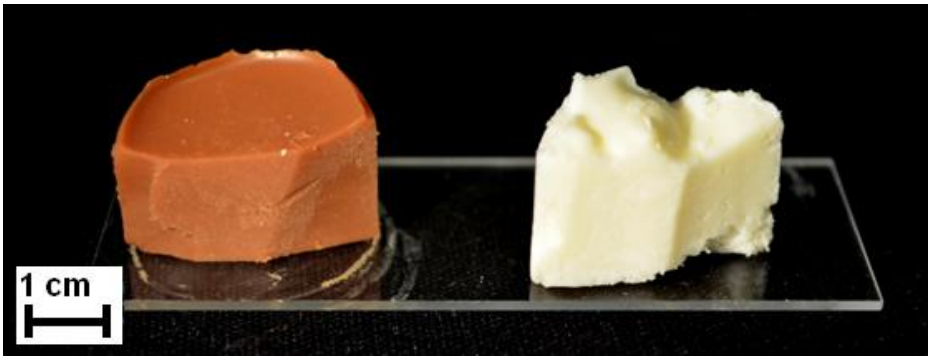

Figure 6.19 Milk chocolate (L) and Cocoa Butter (R) emulsions containing 40% ethanol as part of the 50% w/w aqueous gelled phase (based on fat content of the chocolate)

6.4 Conclusions

We have demonstrated that up to 50 vol% of aqueous agar solution can be emulsified into cocoa butter and chocolate in a simple shear, then gelation strategy. This can be increased to 80 vol% of aqueous agar solution by a shear cooling strategy. At this aqueous fraction, the microgel dispersion exhibits a yield stress, which aids the stability against sedimentation. The optimum PGPR concentration to stabilise this quantity of water phase

was tuned and kept below EU legislative limits. The developed strategy can be used to enrich chocolate confectionery with agar microgel particles, hereby reducing the overall fat content. These microgels can be swollen with water, or with alcohol containing liquids. Rheological profiling and comparison against industry recognised models indicates the suitability of these dispersions in commercial products. We believe that this technology can provide exciting avenues to be explored in new chocolate confectionery products.

6.5 Experimental

6.5.1 Materials

Agar-Agar White (Buenas, Gem Foods Int., Philippines), Polyglycerol polyricinoleate (PGPR-4150, Palsgaard, Denmark), Cocoa butter (VWR, UK), White chocolate, Dark chocolate, Milk chocolate (ASDA, UK), Sunflower oil (Costcutter, UK), Rhodamine B (Sigma Aldrich, UK), Ethanol (VWR, UK), were all used as received. Water was filtered and de-ionised to 18 $M\Omega cm^{-1}$

6.5.2 Equipment

Rheological measurements were carried out on a Kinexus Rheometer ultra (Malvern Instruments) with active heat exchanger and parallel plate geometries PU40 S0141 SS and PL40 C0007 SS. Pre-emulsified dispersions were dispensed on to the heated 40.00 °C parallel plate geometry. Plate gap size was set at 1.00 mm. Sample temperature was monitored and allowed to equilibrate for 5 minutes prior to any measurement. Chocolate formulation rheology included a 5 minute pre-shear step at 5 s^{-1} after thermal equilibrium

prior to a stepped shear rate/shear stress sequence from 0.1-100 s-1. Casson equation was fitted to the data using OriginPro 8 (OriginLab, USA).

Cryogenic Scanning Electron Microscopy analyses were carried out using a Zeiss Supra 55-VP Field Emission Gun Scanning Electron Microscope with a Gatan Alto 2500 cryo transfer system and a Gatan C1002 Liquid Nitrogen cold stage. Molten emulsions at 40 °C were drawn into a brass rivet through capillary action and frozen in liquid nitrogen prior to scalpel fracturing to expose a clean internal structure. The sample was heated to −90 °C for 10 minutes to remove ice through sublimation followed by a platinum sputter target coating in an argon atmosphere (20 seconds, 10 mA). Imaging was undertaken at −120 °C using a 3 kV accelerating voltage with a gold anti-contaminator at −189 °C. Images were post-analysed using ImageJ computer software (NIH, US).

Photographs were taken using a Nikon D5100 fitted with DX AF-S 18-55mm lens.

DSC measurements were performed on a Mettler Toledo TGA/DSC 1 thermogravimetric analyser. Chocolate microgel dispersions were thermally tempered by heating to 40 °C, cooling to 27 °C and gradually heating back up to 31 °C (dark chocolate) or 30 °C (milk and white chocolate) over a 10 minute period whilst under gentle stirring using a high accuracy Peltier heating stage. After which, tempered samples were weighed out into aluminium pans on a 5 d.p. balance. Heat flux measurements were started at 5 °C and terminated at 40 °C at a rate of 1 K/min under a flow of air. Heat flux was then normalised with respect to sample mass.

6.5.3 Emulsification protocols

Water in PGPR containing sunflower oil emulsions

PGPR was dissolved in oil, catalytic amounts of Rhodamine B was dispersed in water. At varying PGPR concentrations and aqueous phase volumes, the two solutions were hand shaken for 30 seconds and left to stand for 24 hours before imaging.

Agar microgel dispersions in sunflower oil, cocoa butter and chocolate

Agar polymer (2% w/w) and Rhodamine B (cat.) were dissolved in DI water at 95 °C. PGPR (1% w/w) was dissolved in oil phase (sunflower oil, molten cocoa butter or chocolate). Both solutions were equilibrated at 50 °C before homogenising by rotor stator (Ultra-turrax, 24,000rpm, 60 seconds). Samples were either cooled quiescently, or hand shaken to below gel point. Aqueous phase volume was adjusted against fat content in the chocolate emulsions. All samples were stored under sealed refrigerated conditions for at least two weeks prior to thermal analysis.

Incorporation of alcohol into the chocolate formulations

Chocolate and cocoa butter emulsions were generated in the manner described above, with the exception of using a 40/60 (v/v) ethanol: water mixture as the agar aqueous phase.

6.6 References

(1) *European Directive 1169/2011*.

(2) *European Directive 1223/2009*.

(3) Marcotte, M.; Taherian Hoshahili, A. R.; Ramaswamy, H. S. *Food Research International* **2001**, *34*, 695–703.

(4) Malone, M. E.; Appelqvist, I. A. *Journal of Controlled Release* **2003**, *90*, 227–241.

(5) Burey, P.; Bhandari, B. R.; Howes, T.; Gidley, M. J. *Critical Reviews in Food Science and Nutrition* **2008**, *48*, 361–377.

(6) Brummel, S. E.; Lee, K. *Journal of Food Science* **1990**, *55*, 1290–1292.

(7) Norton, J. E.; Fryer, P. J. *Journal of Food Engineering* **2012**, *113*, 329–336.

(8) Låås, T. *Agar Derivatives for Chromatography, Electrophoresis and Gel - Bound Enzymes*; 1st ed.; Almqvist & Wiksell: Stockholm, 1975.

(9) Tsuchiya, Y.; Hong, K. C. *Tohoku journal of agricultural research* **1965**, *16*, 141–146.

(10) Arnott, S.; Fulmer, A.; Scott, W. E.; Dea, I. C. M.; Moorhouse, R.; Rees, D. A. *Journal of Molecular Biology* **1974**, *90*, 269–284.

(11) Labropoulos, K. C.; Niesz, D. E.; Danforth, S. C.; Kevrekidis, P. G. *Carbohydrate Polymers* **2002**, *50*, 393–406.

(12) Maeda, H.; Yamamoto, R.; Hirao, K.; Tochikubo, O. *Diabetes, obesity & metabolism* **2005**, *7*, 40–46.

(13) Adams, S.; Frith, W. J.; Stokes, J. R. *Journal of Rheology* **2004**, *48*, 1195–1209.

(14) Suzawa, E.; Kaneda, I. *Journal of Biorheology* **2011**, *24*, 70–76.

(15) Food and Drug Administration *GRAS Notice no. GRN 000266*; 2009.

(16) Schantz, B.; Rohm, H. *LWT - Food Science and Technology* **2005**, *38*, 41–45.

(17) Wilson, R.; van Schie, B. J.; Howes, D. *Food and Chemical Toxicology* **1998**, *36*, 711–718.

(18) Banford, H. F.; Gardiner, K. J.; Howat, G. R.; Thomson, F. A. *Confectionery Production* **1970**, *36*, 359–365.

(19) Griffin, W. C. *Journal of Cosmetic Science* **1949**, *1*, 311–326.

(20) Davis, J. T. *Proceedings of the International Congress of Surface Activity* **1957**, 426–438.

(21) Korhonen, M.; Hirvonen, J.; Peltonen, L.; Antikainen, O.; Yrjänäinen, L.; Yliruusi, J. *International Journal of Pharmaceutics* **2004**, *269*, 227–239.

(22) Norton, J. E.; Fryer, P. J.; Parkinson, J.; Cox, P. W. *Journal of Food Engineering* **2009**, *95*, 172–178.

(23) Hinton, C. L., Pratt, C. D., de Vadetsky, E., Landwill, K. E.. McCloskey, K. E., Schuemann, H. W. *Twenty Years of Confectionery and Chocolate Progress*; 1st ed.; Avi Publishing Co.: Westport, 1970.

(24) *European Directive 95/2/EC*.

(25) Fisher, L. R.; MitchellL, E. E.; Parker, N. S. *Journal of Food Science* **1985**, *50*, 1201–1202.

(26) Altimiras, P.; Pyle, L.; Bouchon, P. *Journal of Food Engineering* **2007**, *80*, 600–610.

(27) Su, J.; Flanagan, J.; Hemar, Y.; Singh, H. *Food Hydrocolloids* **2006**, *20*, 261–268.

(28) Norton, I. T.; Jarvis, D. A.; Foster, T. J. *International Journal of Biological Macromolecules* **1999**, *26*, 255–261.

(29) Norton, I. T.; Frith, W. J.; Ablett, S. *Food Hydrocolloids* **2006**, *20*, 229–239.

(30) Nishinari, K.; Watase, K.; Miyoshi, E.; Tayaka, T.; Oakenfull, D. *Food Technology* **1995**, *49*, 92–96.

(31) Casson, N. In *Rheology of Dispersed Systems*; Mill, C. C., Ed.; Pergamon Press: New York, 1959; p. 84.

(32) Casson, N. *British Society of Rheology Bulletin* **1957**, *52*, 5–10.

(33) Kim, S. Ph.D. Thesis, Drexel University, 2002.

(34) Chevalley, J. *Journal of Texture Studies* **1975**, *6*, 177–196.

(35) International Confectionery Association. *Viscosity of chocolate and chocolate products.*; CAOBISCO, Belgium, 2000.

(36) Aeschilmann, J.-M.; Beckett, S. T. *Journal of Texture Studies* **2000**, *31*, 541–576.

Chapter 7

Conclusions and outlook

In this thesis we have explored two distinct areas in the field of soft matter, the first involving the synthesis, characterisation and application of Janus particles (chapters 2, 3 and 4), and the second; investigating emulsification strategies to disperse large quantities of water into chocolate confectionery (chapters 5 and 6). Although both parts of the work may seem worlds apart, we have in fact demonstrated how similar scientific principles in the field of soft matter can be applied to investigate these systems.

Chapter 2 described a simple optimised one pot procedure to render sub-micron amphiphilic Janus particles which demonstrate varied surface active behaviour, depending on their relative hydrophobic : hydrophilic lobe ratios. These particles exhibit anti-freeze properties, and owing to their non-toxic chemical properties, have the potential to be deployed in aqueous based products sensitive to low temperatures. Such applications include food stuffs, coatings formulations and organ preservation. *In order to develop this work into a viable product, investigations into upscaling the synthesis to permit high solids content of at least 40 wt% without the formation of higher order clusters is required. The anti-freeze mechanism on a microscopic level needs to be explored if we are to discover how these particles exhibit anti-freeze behaviour.*

Chapter 3 explored the synthesis of hard-soft Janus particles by seeded dispersion polymerisation, revealing a surface area dependence of the seed particles to render a

clean dispersion of hard-soft Janus particles. In addition, we demonstrated the ability to fabricate sub-micron hard-soft Janus particles. Such particles have potential in functional adhesive applications and in self assembly as demonstrated in chapter 4. *To improve the functional performance of these particles, future work into using separate reactive stabilisers or monomers to render anisotropic surface chemistry across the two hemispheres will improve interfacial selectivity. As we discovered the lower limit of required surface area, studies into the upper limit of surface area and hence highest solids content possible will define the optimal seed surface area envelope for synthesis In addition, seeded dispersion polymerisations from alternative PVP coated particles such as inorganic colloids can be investigated to demonstrate the versatility of this technique.*

Chapter 4 investigated the self assembly of hard-soft Janus particles as manufactured in chapter 3 into colloidal clusters and colloidosomes of controlled geometry. It was shown that upon desorption of PVP from the particle surface by dilution, the particles can aggregate into clusters of controlled geometry based on surface energy minimisation of the soft deformable phase. Hard-soft Janus particles were also shown to assemble over a 2-D planar interface to form textured colloidosomes. *A major improvement to this body of work involves the selective clustering of particles to allow only soft-soft interactions to occur. A potential strategy towards this aim includes anisotropic surface functionalisation of the particle hemispheres through the introduction of surface charge.*

.

Chapter 5 discussed the use of colloidal silica and cationic polyelectrolyte chitosan to manufacture water-in-oil emulsions for the purpose of reducing the fat content in chocolate. Up to 50% of the fat content could be replaced in cocoa butter, white, milk and dark chocolate, whilst retaining the desired physical characteristics of the confectionery. This technology is not limited to chocolate, but can also be developed for use in other foodstuffs and personal care products. *Although we present an improved methodology to reach the same overall aim in chapter 6, further increasing the water content without adversely affecting the desired physical characteristics would enhance the potential of this work. In addition, the ability to control formulation rheology by adjusting the emulsion microstructure would provide a major benefit to confectionery manufacturers without the use of additional emulsifiers.*

Chapter 6 presented an alternative strategy to reducing the fat content of chocolate through the emulsification of agar solutions into molten chocolate, resulting in microgel dispersions which replaced up to 80% of the fat content in chocolate formulations. Characterisation of the formulations demonstrate how the dispersions possess the necessary physical characteristics required of a chocolate product. *The ability to tune rheological properties of the formulation through emulsion microstructure, in terms of microgel size distribution and gel particle modulus would again prove a major advantage to manufacturers adopting this technique. Additionally, translating this methodology into other high fat containing foodstuffs, especially those at extremes of temperatures i.e. frozen and heated products would provide an exciting challenge that can test the boundaries of this technique.*

Appendix A

Characterisation of colloidal, interfacial and bulk properties

Throughout this thesis, a range of analytical methods have been employed to characterise the properties of the interfacial and colloidal systems described. This appendix details the theory of some of the techniques used.

A.1 Gravimetry

Gravimetry provides a simple method to follow total polymerisation conversion as a function of time. During a polymerisation, aliquots of reaction mixture are extracted at set time intervals and weighed immediately (M_{wet}) before complete drying and reweighing (M_{dry}). The drying procedure is assumed to evaporate water and remaining volatile monomer content. This calculated value is normalised against total theoretical solids content ($M_{monomer}$ / M_{total}) to yield conversion as expressed in equation 1.

$$X_M = \frac{M_{dry}}{M_{wet}} \cdot \frac{M_{total}}{M_{monomer}} \quad (1)$$

In the case of a seeded polymerisation containing a solid component from the beginning (M_{solid}), equation 2 is used.

$$X_M = \left(\frac{M_{dry}}{M_{wet}} - \frac{M_{solid}}{M_{total}}\right) \cdot \frac{M_{total}}{M_{monomer}} \quad (2)$$

A.2 Dynamic light scattering

Also known as photon correlation spectroscopy or quasi-electric light scattering, dynamic light scattering (DLS) calculates the hydrodynamic radii of sub-micron particulate dispersed in a continuous phase

Brownian motion is used to describe the random motion of particles influenced by collisions with solvent molecules. This velocity of translational motion is proportional to the size of the particle, temperature and viscosity of the medium. The larger the particle, the slower it diffuses through solution. DLS calculates particle size by measuring translational velocity arising from Brownian motion, using the Stokes-Einstein equation shown in equation 3.

$$d_z = \frac{kT}{3\pi\eta D} \quad (3)$$

Where d_z is hydrodynamic radius, k is Boltzmann's constant, T is temperature, η is viscosity, and D is diffusion co-efficient.

The measured value of hydrodynamic radius is dependent on how the particle interacts with the surrounding media. Therefore factors such as ionic strength of the media, surface functionality and particle morphology have a significant impact on the measurement.

This diffusion co-efficient is calculated by the scattering of an incident beam (He-Ne laser of wavelength λ = 633 nm for Malvern Zetasizer Nano ZS) by the particle

dispersion at an angle of 173°. The intensity fluctuations of the scattered light are measured as a function of time. Two light scattering theories are used to interpret intensity fluctuations. At diameters < (λ/10), i.e. ~60 nm in this case, the Rayleigh approximation assumes isotropic scattering and intensity is proportional to the diameter to the sixth power. However, larger particles with diameters equivalent to the wavelength of incident light are described by the Mie approximation, a complex function of maxima and minima with respect to angle, size and incident wavelength.

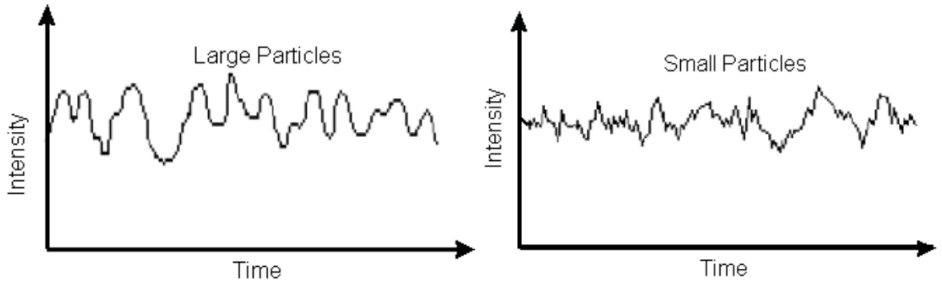

Figure A.1 Schematic indicating intensity fluctuations of backscattered incident laser beam as a function of time for a suspension containing large (left) and small (particles)

Intensity fluctuations are governed by the velocity of the particles and therefore the smaller the particles, the faster the intensity fluctuations as seen in figure A.1. The fluctuation signals are compared over a set of time intervals by use of a correlator which calculates an exponential decay correlation function $G(\tau) = A[1 + Be^{-2\Gamma\tau}]$. The smaller

the particles, the quicker the decay function due to the more rapid fluctuation of light intensity, indicated in figure A.2.

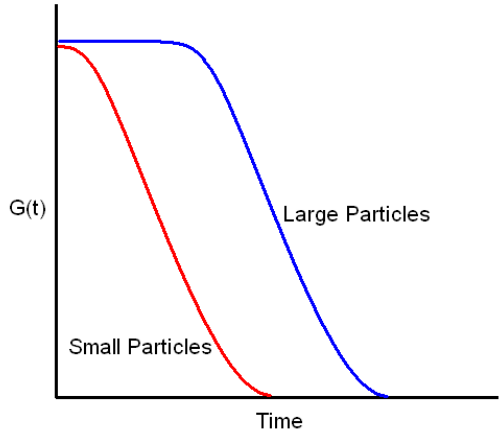

Figure A.2 Schematic of a correlation function depicting a more rapid exponential decay in scattering intensity for smaller particles

A.3 Electrophoretic light scattering

Electrophoretic light scattering measures the diffusion of particles suspended in a conductive continuous phase when under the influence of an applied electric field. Particulate matter possessing a surface charge will migrate toward the oppositely charged electrode in addition to the Brownian motion it experiences, so named electrophoretic mobility. This phenomenon is used to ascertain the zeta potential of a particle.

Particles with a net surface charge exist with a locally higher concentration of counter ions in their vicinity. This electrical double layer consists of two parts, an inner layer where counter ions are tightly bound to the particle surface – the Stern layer, and a more diffuse layer where ions are less associated with the particle. Within the diffuse layer there exists a notional boundary between ions that move with the particle, and those that remain in the bulk, known as the slipping plane as seen in Fig A.3.

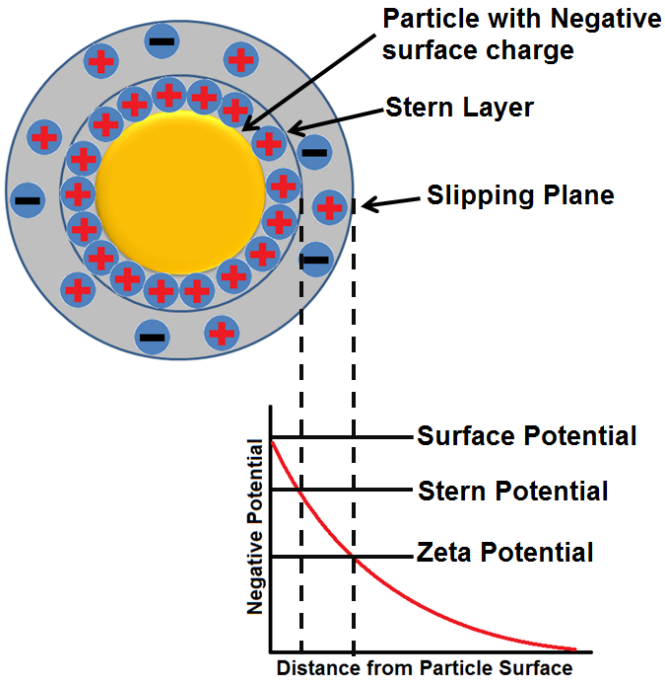

Figure A.3 Negative potential as a function of distance for a particle with an anionic surface charge in aqueous conditions. Zeta potential represents the negative potential at the border of the slipping plane with the bulk solution

The potential at this boundary is the zeta potential (ζ) and is related to electrophoretic mobility (U_E) by the Henry equation as expressed in equation 4.

$$U_E = \frac{2\varepsilon\zeta f(\kappa a)}{3\eta} \tag{4}$$

Where ε and η are dielectric constant and viscosity of the media respectively. $f(\kappa a)$ is the Henry function where κ^{-1} represents the thickness of the electric double layer (Debye length). Combined with a, particle radius, the function expresses the ratio between particle radius and electrical double layer. In aqueous polar media, $f(\kappa a)$ is taken as 1.5

from the Smoluchowski approximation, or as 1.0 in non-polar media from the Huckel approximation.

The value obtained for zeta potential gives an indication to the magnitude and polarity of colloidal stability of a particle possesses through electrostatic repulsion. Generally speaking, a zeta potential of < ±20mV is not colloidally stable and liable to flocculation, ± 20-50mV is moderately stable and > ±50mV is deemed very stable. However, zeta potential does not measure colloidal stability imparted by non-electrostatic means, such as steric stabilisation. Additionally, the zeta potential of a particle is sensitive to changes in pH and ionic strength and therefore permits the measurement of colloidal stability with respect to pH and salt concentrations. That being said, a zeta potential measurement without defining solution conditions is meaningless.

Laser doppler velocimetry is employed in the *Malvern Zetasizer nano ZS* to calculate zeta potential by measuring changes in light intensity fluctuations upon an applied electric field on the cell.

A.4 Electron microscopy

Resolution in a light microscope is limited to the visible wavelengths of light used, approximately 400 nm, for the case of a perfectly aligned system. Therefore in order to visualise objects smaller than this, electron microscopy provides a powerful solution.

Using a beam of electrons, wavelength is proportional to acceleration voltage and generates a far smaller wavelength than that of light microscopy. For instance an

acceleration voltage of 20 kV equates to a photon wavelength of 0.01 nm. Scanning electron microscopy was predominately used in this thesis.

Samples have to be coated in a conductive material typically carbon (by carbon evaporation) or sputter coated (by Au, AuPd or Pt target) to stop the accumulation of negative charge and deflection of the imaging beam. This however can alter the surface topology and give rise to erroneous EDX spectra,

The high vacuum environment and considerable thermal energy generated by the electron beam thereby causing beam damage limits the use of standard 'dry' SEM for systems with liquid or low T_g polymeric systems. Cryogenic electron microscopy provides a method of imaging in a less destructive environment. Particulate dispersions and emulsions in an aqueous environment are loaded into small metallic rivets and frozen in liquid nitrogen before being transferred into a preparation chamber. In a freeze fracture procedure, the top section of the ice layer is removed to yield a clean, uncontaminated cross section. The sample is then heated to -90 °C under vacuum to sublime a layer of ice, revealing the sample. After sputter coating the sample to provide conductivity, samples are typically imaged at -120 °C using acceleration voltages of 1-3 kV. Further cooling beyond this temperature risks contamination by ice recrystallisation on the sample surface. Higher acceleration voltages result in increased charging effects and beam damage. Artifacts in cryo-SEM imaging are common. Ice recrystallisation appears as uniform particles of 10-50 nm diameter over smooth sections of ice. Macro ice crystal growth from slow freezing presents as cellular structures especially in hydrogel samples. Structured systems may be disturbed by ice crystal growth, high vacuum and sublimation processes.

A.5 Rheology

Rheology is the science of *flow* and *deformation*. The flowing properties of a material can be characterised by viscosity, defined as a material's resistance (stress) to flow under an applied force (shear rate), expressed in equation 6.

$$Viscosity\ (\eta) = \frac{Shear\ Stress}{Shear\ Rate} = \frac{\tau}{\dot{\gamma}} \tag{6}$$

The flow profile of a material is defined by viscosity as a function of shear rate, of which there are three general regimes, graphically depicted in figure A.4.

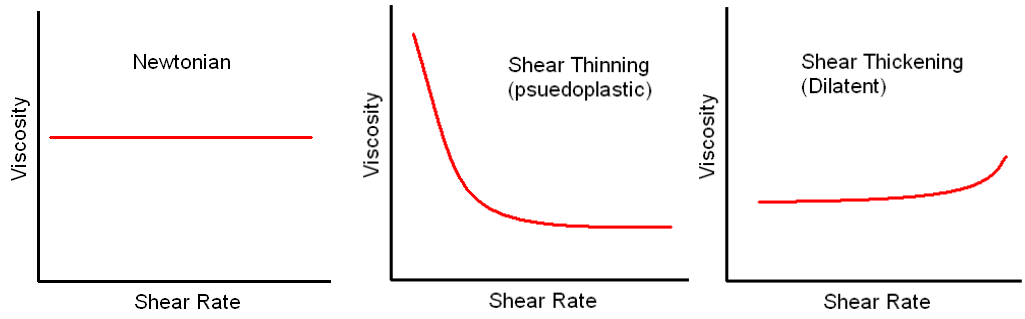

Figure A.4 Viscosity versus shear rate plots demonstrating 3 regimes of material behaviour whilst under an applied stress

Few colloidal systems exhibit Newtonian behaviour, and the majority of non-Newtonian systems tend to be shear thinning. Newtonian behavior shows no response with respect to shear rate. The flow profile of shear thinning behaviour can be further characterised to show two types of lower shear rate response. A material may have a yield stress, an ever

increasing viscosity as the shear rate tends towards zero, indicating a solid like behaviour at lower shear rates, i.e. storage and transit. A material may alternatively possess a zero shear viscosity, exhibiting a Newtonian plateau and therefore liquid like behaviour as shear rate tends towards zero. These two regimes are schematically represented in figure A.5.

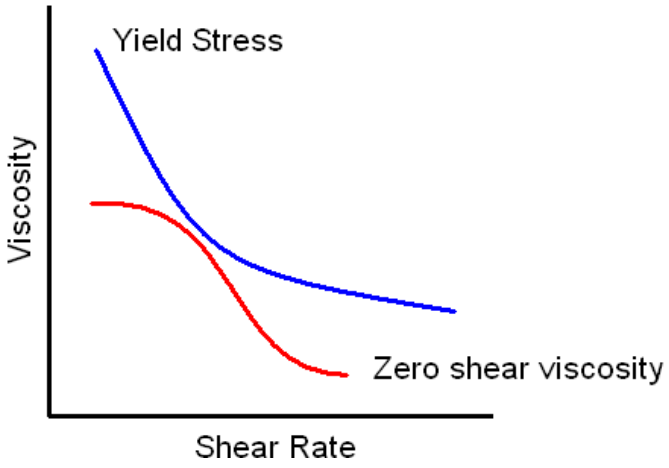

Figure A.5 Schematics of Viscosity response to an applied shear force in the case of a material with a yield stress or a zero shear viscosity

Material properties can also be analysed in the sense of deformation, i.e. their response to an applied force prior to flowing and therefore defines the *viscoelasticity*. Most materials are not completely 'solid' or 'liquid', but exhibit varying behaviour depending on the applied force.

Oscillatory analyses provide a route towards characterising viscoelastic behaviour by applying a sinusoidal force (shear stress) and measuring the displacement response (strain) as seen in figure A.6. Dividing these two components yields material stiffness (modulus) as seen in equation 6.

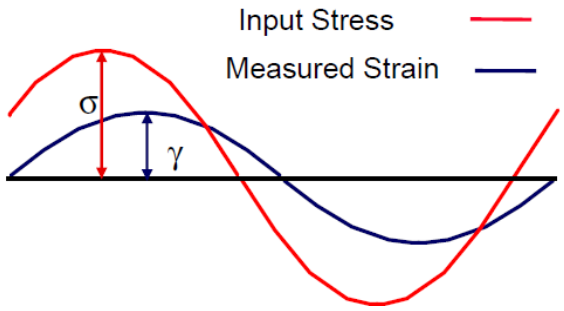

Figure A.6 Schematic indicating how viscoelastic behaviour is defined by the latency measured between an applied oscillating stress and its measured strain response. Diving these two components allows the calculation of complex modulus

$$Complex\ Modulus\ (G^*) = \frac{Shear\ Stress}{Shear\ Strain} = \frac{\sigma}{\gamma} \quad (6)$$

The phase angle is the temporal latency between applied stress and strain response and defines the viscous to elastic ratio of the material; I.e. liquid to solid behaviour. This is depicted in figure A.7.

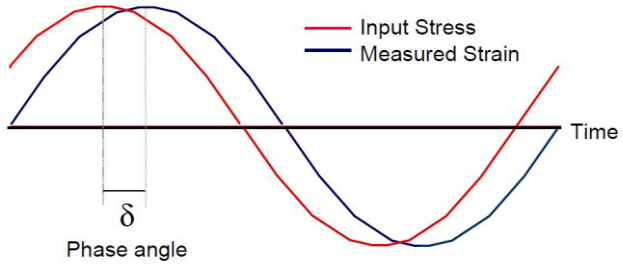

Figure A.7 The latency between input stress and measured strain is quantified by phase angle

A purely elastic material exhibits an instantaneous strain response to an applied stress giving rise to a phase angle of 0°. A purely viscous material however, exhibits a response $\frac{\pi}{2}$ out of phase with the applied stress, leading to a 90° phase angle. From this we can

extract the individual elastic (storage) and viscous (loss) modulus as expressed in equations 7 and 8 respectively. Purely elastic and viscous behaviour are depicted in figure A.8.

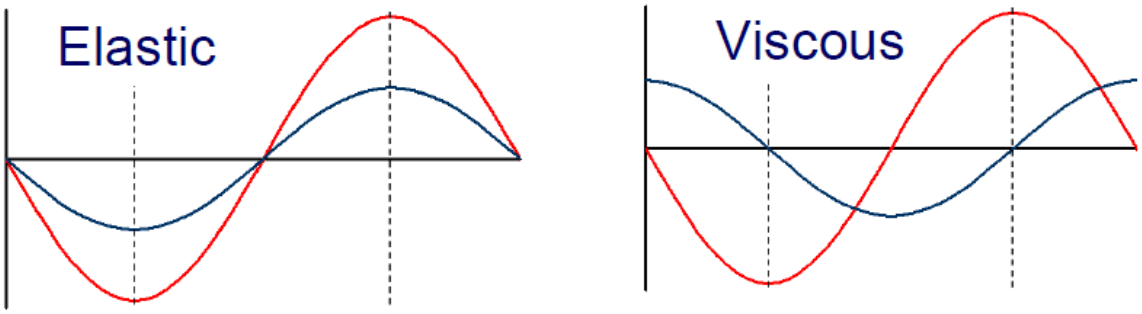

Figure A.8 Input stress (red) – measured strain responses (blue) for a purely elastic (left) and purely (viscous) material tested by oscillatory rheology

$$Elastic\ (Storage) Modulus = G' = \frac{\sigma}{\gamma} \cdot Sin\ \delta \quad (7)$$

$$Viscous\ (Loss) Modulus = G'' = \frac{\sigma}{\gamma} \cdot Cos\ \delta \quad (8)$$

If G' > G", i.e. $\delta < 45°$, Material is solid like

If G' < G", i.e. $\delta > 45°$ Material is liquid like

Oscillatory measurements are separated into frequency and amplitude dependent, referring to the applied stress. Amplitude sweep oscillatory measurements are used to determine the stability of a material suspension, i.e. emulsion or hydrogel before destructive breakdown into flow. This type of measurement is typically used to determine linear viscoelastic region (LVER), and therefore is used to ensure all subsequent tests are

conducted within the viscoelastic response domain. Frequency sweep analyses determine a fingerprint spectrum, classifying a material into one of three behaviours (figure A.9).

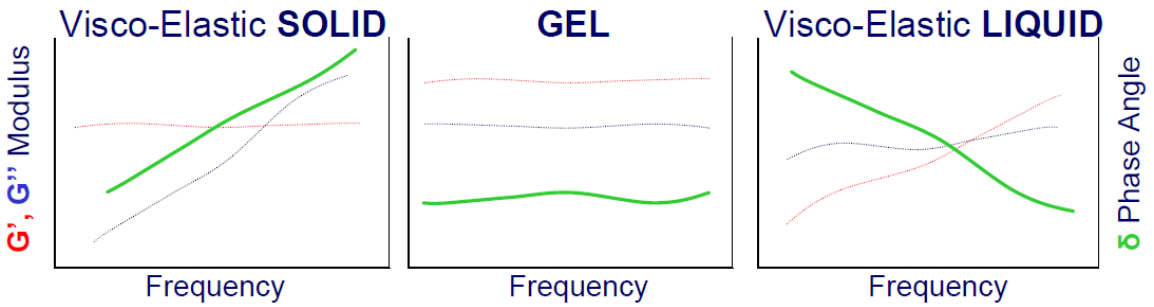

Figure A.9 Frequency sweep measurements at fixed amplitude can be used to characterise one of three main material behaviours, Viscoelastic solid, liquid and gel

A.6 Droplet shape analyser

The droplet shape analyser (DSA) provides a simple experimental setup to measure the contact angle and /or interfacial tension between two or more phases by optically measuring the profile of droplets and bubbles. For the experiments outlined in this thesis, the DSA was used in the pendant droplet mode whereby a liquid droplet of known volume is suspended in an immiscible liquid phase.

When in hydromechanical equilibrium, a droplet suspended in an environment phase will assume a characteristic shape based on its interaction with the environment phase and the influence of gravity from which interfacial tension can be determined. The Laplace pressure relates the internal pressure Δp of the droplet to the principle radii of curvature and interfacial tension σ based on the Laplace equation for capillarity (equation 9 and figure A.10).

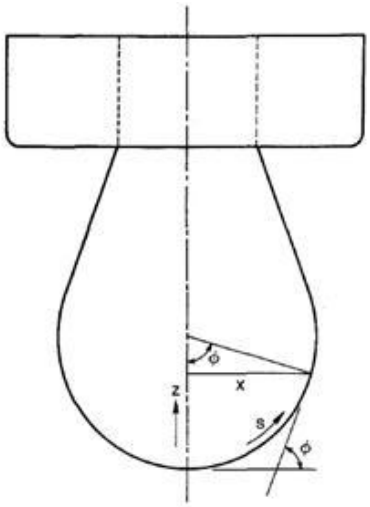

$$\Delta p = \sigma \cdot \left(\frac{1}{r_1} + \frac{1}{r_2}\right) \quad (9)$$

$$\Delta p = \Delta p_0 - \Delta \rho \cdot gz \quad (10)$$

Figure A.10 Schematic indicating the dimensions measured on a pendant droplet to ascertain interfacial tension

The equation represents a balance between two opposing forces, the surface tension attempting to minimise surface area and assume a spherical profile versus the influence of gravity elongating the droplet. Assuming only these two forces, the Laplace pressure Δp can also be expressed as a linear function of gravity g, difference in fluid density $\Delta \rho$, and vertical height z, from reference plane pressure $\Delta p_{0,}$ as expressed in equation 10.

In order to accurately calculate interfacial tension, the droplet curve function has to be mathematically derived. At the droplet apex, i.e $z = 0$, $R_1 = R_2 = b$, therefore $\Delta p_0 = \frac{2\sigma}{b}$

and since $R_2 = \frac{x}{\sin \varphi}$

$$\frac{1}{R_1} + \frac{\sin \varphi}{x} = \frac{\Delta \rho g z}{\sigma} + \frac{2}{b} \quad (11)$$

Φ is the angle between drop axis z and the normal of the surface where line intersects droplet. Based on equation 11, parameterisation and a set of first order differential equations are derived, from which the curve function can be numerically solved.[1]

A.7 References

(1) Yakhshi-Tafti, E.; Kumar, R.; Cho, H. J. *International Journal of Optomechatronics* **2011**, *5*, 393–403.

Appendix B

Additional data for Chapter 4

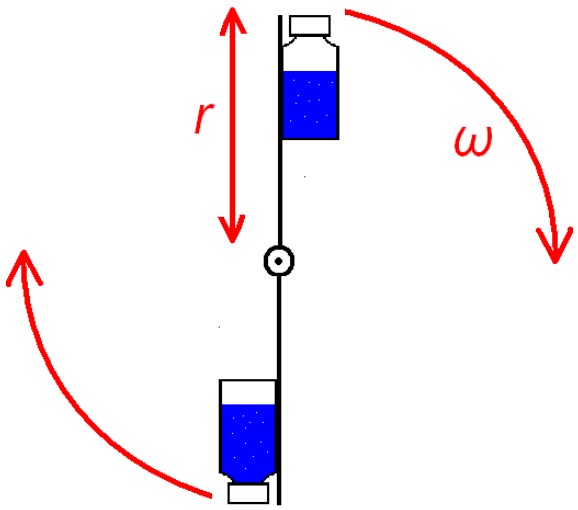

Figure B.1 Schematic of the experimental setup for the Janus particle turbidity measurements.

Figure B.1 indicates the experimental setup for the Janus particle turbidity measurements. The radius from the centre of the vial to the rotor centre was fixed at 20 cm. Angular velocity was varied from 22-72 rpm at fixed intervals.

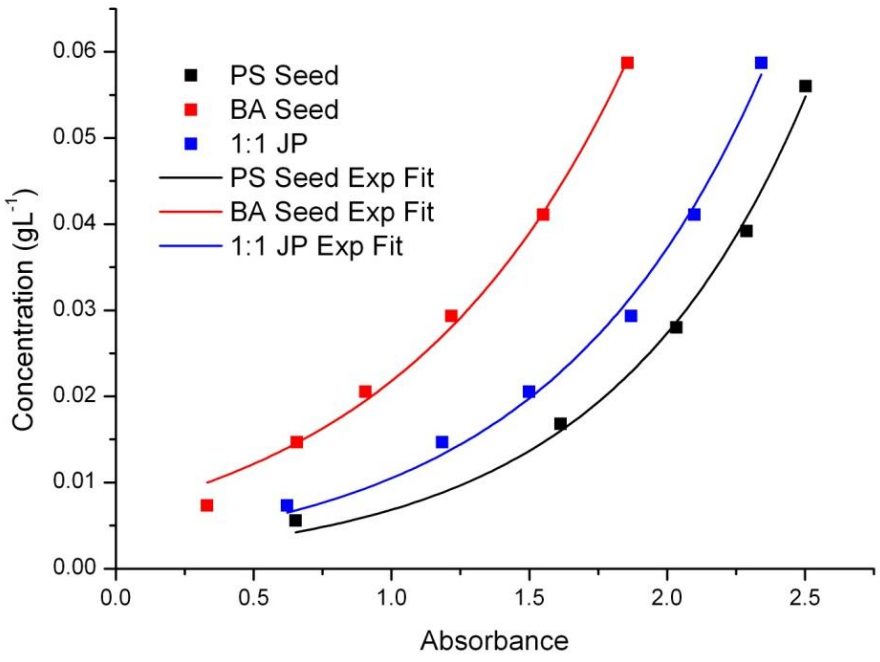

Figure B.2 Calibration curve used to back calculate absorbance to primary particle concentration

Absorbance measurements at 540 nm were taken for set concentrations of poly(styrene) particles (pSty seed), poly(butyl acrylate) particles (pBA seed) and 1:1 pSty:pBA Janus particles (1:1 JP) and plotted as seen in figure B.2. Evidently, the poly(styrene) seed absorbs and scatters more light than poly(butyl acrylate) beads, due to the higher refractive index of poly(styrene) compared with poly(butyl acrylate) (1.57 against 1.47 respectively). As expected, the Janus particle absorbance sits between these values, although biased towards the polystyrene value. This is due to the larger size and aspect ratio of the Janus particle as opposed to a sphere. A simple exponential function was fitted against these values, which was in turn was used to calculate concentration of singular particles from absorbance. We apply the assumption that particles, irrespective of size, scatter light equally, and that we may measure flocculation by the decrease in initial particle number.